ABSTRACT

Title of dissertation: FERROFLUIDS: MODELING, NUMERICAL ANALYSIS, AND SCIENTIFIC COMPUTATION

Ignacio Tomas, Doctor of Philosophy, 2015

Dissertation directed by: Professor Ricardo H. Nochetto
Department of Mathematics

This dissertation presents some developments in the Numerical Analysis of Partial Differential Equations (PDEs) describing the behavior of ferrofluids.

The most widely accepted PDE model for ferrofluids is the Micropolar model proposed by R.E. Rosensweig. The Micropolar Navier-Stokes Equations (MNSE) is a subsystem of PDEs within the Rosensweig model. Being a simplified version of the much bigger system of PDEs proposed by Rosensweig, the MNSE are a natural starting point of this thesis. The MNSE couple linear velocity $\mathbf{u}$, angular velocity $\mathbf{w}$, and pressure p. We propose and analyze a first-order semi-implicit fully-discrete scheme for the MNSE, which decouples the computation of the linear and angular velocities, is unconditionally stable and delivers optimal convergence rates under assumptions analogous to those used for the Navier-Stokes equations.

Moving onto the much more complex Rosensweig's model, we provide a definition (approximation) for the effective magnetizing field $\mathbf{h}$, and explain the assumptions behind this definition. Unlike previous definitions available in the literature,

this new definition is able to accommodate the effect of external magnetic fields. Using this definition we setup the system of PDEs coupling linear velocity $\mathbf{u}$, pressure p, angular velocity $\mathbf{w}$, magnetization $\mathbf{m}$, and magnetic potential φ. We show that this system is energy-stable and devise a numerical scheme that mimics the same stability property. We prove that solutions of the numerical scheme always exist and, under certain simplifying assumptions, that the discrete solutions converge. A notable outcome of the analysis of the numerical scheme for the Rosensweig's model is the choice of finite element spaces that allow the construction of an energy-stable scheme.

Finally, with the lessons learned from Rosensweig's model, we develop a diffuse-interface model describing the behavior of two-phase ferrofluid flows and present an energy-stable numerical scheme for this model. For a simplified version of this model and the corresponding numerical scheme we prove (in addition to stability) convergence and existence of solutions as by-product .

Throughout this dissertation, we will provide numerical experiments, not only to validate mathematical results, but also to help the reader gain a qualitative understanding of the PDE models analyzed in this dissertation (the MNSE, the Rosensweig's model, and the Two-phase model). In addition, we also provide computational experiments to illustrate the potential of these simple models and their ability to capture basic phenomenological features of ferrofluids, such as the Rosensweig instability for the case of the two-phase model. In this respect, we highlight the incisive numerical experiments with the two-phase model illustrating the critical role of the demagnetizing field to reproduce physically realistic behavior of ferrofluids.

FERROFLUIDS: MODELING, NUMERICAL ANALYSIS, AND SCIENTIFIC COMPUTATION

by

Ignacio Tomas

Dissertation submitted to the Faculty of the Graduate School of the
University of Maryland, College Park in partial fulfillment
of the requirements for the degree of
Doctor of Philosophy
2015

Advisory Committee:
Professor Ricardo H. Nochetto, Chair/Advisor
Professor Howard Elman
Professor Pierre-Emmanuel Jabin
Professor Benjamin Shapiro
Professor Konstantina Trivisa

"I think that there's a certain delusional quality that all successful people have to have. You have to believe that something different than what has happened for the past 50 million years of history, you have to believe that something different can happen.

Being realistic is the most commonly traveled road to mediocrity. Why would you be realistic? What's the point of being realistic? I'm gonna do it it's done, its already done, as soon as I decide it's done it's already done now we just gotta wait for y'all to see.

It's unrealistic to walk into a room and flick a switch and lights come on, fortunately Edison didn't think so. It's unrealistic to think you're gonna bend a piece of metal and fly people over an ocean in that metal. That's unrealistic. But fortunately the Wright brothers and others didn't believe that."

– Will Smith (Actor, Singer, Movie Producer)

Acknowledgments

Having read many theses, my feeling is that, acknowledgements sections are usually the most unfair part of a thesis. Who should I thank first, my advisor, who did a lot of things for my professional development, or my wife, who made many sacrifices in order to support my life choices? Well it is undoubtedly a difficult task, many people have done many things for me, but most of them have contributed in a different way. How do I make justice for their contribution? In which order should I acknowledge their contributions? Putting an order to them is equivalent to say that one contribution is more important than other. So I decided that I will let time do the ordering, by this I mean, I will acknowledge people in the chronological order in which their appeared in my life. Ranking their importance is left to the reader's discretion.

I will start with my early engineering training back in Argentina at UNMDP. It is not only clear for me that I had good professors and instructors, but also that a few of them truly inspired me to reach the point in which I am right now. I want to thank my physics professors Prof. Daniel Cortazar, Prof. Daniel Avalos, and Prof. Hilda Larrondo. Their lectures were truly inspirational. I can vividly remember a lecture of Prof. H. Larrondo on "Conserved Quantities in Physics" while discussing the basics of the wave equation. That was one of the first moments where I started the realize the unifying power of Partial Differential Equations (PDEs) to describe the physical world.

I want to thank Prof. Santiago Urquiza and his inspiring (also terrifying!)

"Fluid Dynamics" and "Introduction to Computational Fluid Mechanics" courses. If I had never taken his courses, most probably, I would have never wanted to pursue a PhD in Applied Mathematics.

I have to thank my wife Gaby, for coming with me to the American adventure in the northern hemisphere. Her constant love, care and support have been my most valuable treasures for the last 12 years.

I have to thank Prof. Adrian Cisilino from UNMDP, not only for his fantastic courses on "Rigid Body Mechanics", "Solid Mechanics" and "Computational Mechanics", but also for his invaluable friendship. After obtaining my engineering diploma, when I decided I wanted to study abroad, it was clear for me that I needed to stay in the academic environment for a couple of years more. Prof. Cisilino not only understood my intellectual needs, but also gave me a place where to do something useful. I also have to acknowledge the financial support Prof. P.M. Frontini during this period.

Undoubtedly, I have to thank Prof. Ricardo H. Nochetto, for accepting to be my doctoral advisor. He has invested a lot of time in my training, guiding me through material that I should learn, spending quite some time discussing mathematics with me in the blackboard, pushing me to be critical about what I do, pushing me to think critically about my (sometimes unclear) explanations in the blackboard, and pushing me to improve as a scientist and communicator. I also have to acknowledge his financial support during the last four years.

I have to thank my informal co-advisor Prof. Abner Salgado during his period as a postdoct at UMCP, for the many times we discussed ideas in the blackboard,

sometimes leading to sucessful results ... sometimes not ..., but on top of everything for giving me some time to discuss with him and for unselfishly sharing all his mathematical knowledge without imposing any air of intellectual superiority. I also have to thank Enrique Otarola, who was my first "math coach", and helped me survive my first years in the AMSC program.

I want to thank Prof. Konstantina Trivisa and Prof. Yanir Rubinstein for procuring the so much needed help when it was needed the most. I also owe a ton of moral support from Konstantina during the last years.

Last but not least, I was primarily supported through my advisor with the following NSF grants: DMS-0807811, DMS-1109325 and DMS-1411808. I also have acknowledge the generous support provided by the UMD Graduate School through the Ann G. Wylie Dissertation Fellowship.

I.T.

Table of Contents

List of Figures

List of Abbreviations

PDE	Partial Differential Equation
MNSE	Micropolar Navier Stokes Equation
Ω	physical domain
Γ	boundary of Ω
$d = 2$ or 3	space dimension
t_F	final/total time
$\Omega_{t_F} = \Omega \times (0, t_F)$	space time domain
$L^q(\Omega)$	Lebesgue space of q integrable scalar-valued functions
$\mathbf{L}^q(\Omega)$	Lebesgue space of q integrable vector-valued functions
$W_q^s(\Omega)$	Sobolev space of function with $s > 0$ weak derivatives (s not necessarily integer) in $L^q(\Omega)$
$\mathcal{C}_0^\infty(\Omega)$	smooth functions with compact support in Ω
K	number of time steps used to discretize the total interval of time $[0, t_F]$
k	integer index used to identify the time step number, i.e. $0 \leq k \leq K$.
τ	time discretization parameter, set to be $\tau := t_F/K$
t^k	k-th time step, $t^k := k\tau$
δ	backward difference operator
T	finite element, in general assumed to be a simplex, unless specified otherwise
$\mathcal{T}_h$	mesh/triangulation, that is, the set of all elements T
F	face of an element T, i.e $F \subset \partial T$.
h_T	diameter of the element T, i.e. $h_T := \operatorname{diam} T$
h	space discretization parameter, assumed to be $h := \max_{T \in \mathcal{T}_h} \operatorname{diam} T$
$\mathcal{F}^i$	the collection of internal faces F of $\mathcal{T}_h$, i.e. faces F that are not part of the boundary Γ
$\mathcal{F}^b$	the collection of faces F of $\mathcal{T}_h$ that are part of the boundary of Ω, that is $F \subset \Gamma$
$\boldsymbol{n}$	outwards unit normal vector of Γ
$\boldsymbol{n}_F$	arbitrary (pointing either in one of the two possible directions) normal vector to the face F
$u_t, \partial_t u, \frac{\partial u}{\partial t}$	equivalent notations for the partial derivative with respect to time t.
$u_x, \partial_x u, \frac{\partial u}{\partial x}$	equivalent notations for partial derivative with respect to the space coordinate x. Assume equivalent notations for the remaining spatial coordinates y and z.
∇	gradient operator, i.e. $\nabla\phi = \phi_x\hat{\imath} + \phi_y\hat{\jmath} + +\phi_z\hat{z}$
div	divergence operator, i.e. $div\,\mathbf{u} = \mathbf{u}_x^1 + \mathbf{u}_y^2 + \mathbf{u}_z^3$
Δ	laplacian operator, i.e. $\Delta\phi = \phi_{xx} + \phi_{yy} + \phi_{zz}$
$curl$	curl operator, i.e. $curl\,\mathbf{u} = (\mathbf{u}_y^3 - \mathbf{u}_z^2)\hat{\imath} + (\mathbf{u}_z^1 - \mathbf{u}_x^3)\hat{\jmath} + (\mathbf{u}_x^2 - \mathbf{u}_y^1)\hat{z}$
ℓ	constant used to define polynomial degree
$\mathcal{P}_\ell$	polynomials of total degree at most ℓ

$\mathcal{Q}_\ell$	polynomials of degree at most ℓ in each space variable
$\mathbf{u}$	linear velocity
p	pressure
$\mathbf{w}$	angular velocity
$\mathbf{m}$	magnetization
θ	phase
ψ	chemical potential
$\mathbf{h}$	total (effective) magnetizing field
$\mathbf{h}_a$	applied/external magnetizing field
$\mathbf{h}_d$	demagnetizing field (also called stray field)
φ	total (effective) magnetization potential
ϕ	magnetization potential associated to the applied magnetizing field $\mathbf{h}_a$
ψ	magnetization potential associated to the demagnetizing field $\mathbf{h}_d$
$\mathbf{U}^k$	approximation of the linear velocity $\mathbf{u}$ at time t^k
P^k	approximation of the pressure p at time t^k
$\mathbf{W}^k$	approximation of the angular velocity $\mathbf{w}$ at time t^k
$\mathbf{M}^k$	approximation of the magnetization $\mathbf{m}$ at time t^k
Θ^k	approximation of the phase at time t^k
Ψ^k	approximation of the chemical potential at time t^k
$\mathbf{H}^k$	approximation of the total (effective) magnetizing field at time t^k
Φ^k	approximation of the total (effective) magnetization potential
$\mathbb{U}$	finite element space used to approximate the velocity $\mathbf{U}^k$
$\mathbb{P}$	finite element space used to approximate the pressure P^k
$\mathbb{W}$	finite element space used to approximate the angular velocity $\mathbf{W}^k$
$\mathbb{M}$	finite element space used to approximate the magnetization $\mathbf{M}^k$
$\mathbb{G}$	finite element space used to approximate the phase Θ^k
$\mathbb{Y}$	finite element space used to approximate the chemical potential Ψ^k
$\mathbb{X}$	finite element space used to approximate the magnetization potential Φ^k
$\{\Pi_s\mathbf{u}, \pi_s p\}$	Stokes projection of $\{\mathbf{u}, p\}$, where $\{\Pi_s\mathbf{u}, \pi_s p\} \in \mathbb{U} \times \mathbb{P}$

Chapter 1: Introduction

1.1 Background

A ferrofluid is a liquid which becomes strongly magnetized in the presence of applied magnetic fields. It is a colloid made of nanoscale monodomain ferromagnetic particles suspended in a carrier fluid (water, oil, or other organic solvent). These particles are suspended by Brownian motion and will not precipitate nor clump under normal conditions. Ferrofluids are dielectric (non conducting) and paramagnetic (they are attracted by magnetic fields, and do not retain magnetization in the absence of an applied field); see [1].

Ferrofluids can be controlled by means of external magnetic fields, which gives rise to many control-based applications. They were developed in the 1960's to pump fuel in spacecrafts without mechanical action [2]. Recent interest in ferrofluids is related to technical applications such as instrumentation, vacuum technology, lubrication, vibration damping, radar absorbing materials, and acoustics [3, 4, 5]. For instance, they are used as liquid seals for the drive shafts of hard disks, for vibration control and damping in vehicles and enhanced heat transfer of electronics. Other potential applications are in micro/nanoelectromechanical systems: magnetic manipulation of microchannel flows, particle separation, nanomotors, micro electrical

generators, and nanopumps [6, 7, 8, 9, 10]. One of the most promising applications are in the field of medicine, where targeted (magnetically guided) chemotherapy and radiotherapy, hyperthermia treatments, and magnetic resonance imaging contrast enhancement are very active areas of research [11, 12, 13]. An interesting potential application of ferrofluids under current research is the construction of adaptive deformable mirrors [14, 15, 16].

The applications mentioned above justify the development of mathematical models describing the physical behavior of ferrofluids. At the time of this writing there are two well established PDE models describing the behavior of ferrofluids which we will call by the name of their developers: the Rosensweig model and the Shliomis model (cf. [17, 18]). On the other hand, rigorous mathematical work on the mathematical analysis (existence of global weak solutions and local existence of strong solutions) for the Rosensweig and the Shliomis models is very recent (cf. [19, 20, 21, 22]).

Mathematical models for ferrofluids and their scope of validity have been areas of active research (cf. [23, 24]). Most ferrofluid flows have so far been studied using exact and approximate analytical solutions of the Rosensweig model (see for instance [25]) contrasted with experimental data. However, these flows are analytically tractable in a very limited number of cases [25, 26], and as shown for instance in [27] satisfactory model calibration/validation is beyond the current capabilities of analytic (asymptotic and perturbation) methods. Clearly, there is significant room for interdisciplinary work at the interface between model development, numerical analysis, and experimentation.

Mathematical modeling of ferrofluids may have some points in common with magnetohydrodynamics (MHD), micromagnetism and liquid crystals, but generally speaking it uses significantly different ideas. For instance, the equations of MHD deal with nonmagnetizable but electrically conducting fluids, which is in sharp constrast to ferrofluids. The dominant body force in MHD is the Lorentz force, whereas for ferrofluids the Kelvin force is the most important one, leading to different kinds of nonlinearities. The Landau-Lifshitz-Gilbert equations of micromagnetism use rigid director fields as they model saturated *magnetically hard* materials: they have a high coercive force, are difficult to magnetize and demagnetize, but are capable of retaining a significant residual magnetization. If the magnetization $\mathbf{m}$ satisfies $|\mathbf{m}| = m_s$, with m_s the saturation magnetization, we can factor out m_s and include it into the constitutive parameters, thus obtaining an equation for unitary director fields. On the other hand, ferrofluids are *magnetically soft*: They are easy to magnetize, yet they retain very little or no residual magnetization in the absence of an external magnetic field and they usually exhibit a high saturation value [1]. Therefore, rigid director fields are not suitable to describe the magnetization of a ferrofluid.

The micropolar continuum mechanics theory proposed independently by Eringen and Scriven (cf.[28, 29, 30, 31]) is a natural extension from classical continuum mechanics when we want to consider continuum media subject to distributed couples (non-symmetric stress tensors). On the other hand, non-symmetric stresses are natural when we consider interaction between electromagnetic fields and polarizable/magnetizable media, since the Maxwell's stress tensor turns out to be, in general, not symmetric. Micropolar continuum mechanics is directly related to PDE

models for ferrofluids, as the Rosensweig model is built on top of this theory. Therefore, a reasonable starting point of my research program was the development and analysis of a numerical scheme for the Micropolar Navier-Stokes equations (MNSE), which consists of a set of coupled PDEs for the linear velocity $\mathbf{u}$, pressure p, and angular velocity $\mathbf{w}$; see *Chapter 2*. Yet, it is important to point out that micropolar continuum mechanics is an ambitious theory which covers much more than just non-symmetric stresses, as it is reflected in the massive monographs [31, 32, 33, 34], which attempt to develop a general theory for continuum media with microstructure, and continuum media interacting with electromagnetic fields.

Having gained some experience with the MNSE, we proceed to focus on the Rosensweig model (*Chapter 3*) which includes all the inherent difficulties of the simpler Shliomis model. Our key interest is around boundary conditions and discretization techniques leading to energy-stable continuum and discrete systems. This task becomes particularly complicated if we want to include the effects of non-trivial applied magnetizing fields, an issue which so far has not been properly addressed in the literature. For this purpose we will need to revisit the theory of magnetostatics and typical boundary value problems associated with it. Finally, we feel compelled to remark that, to the best of our knowledge, this is the first work presenting a stable numerical scheme for the Rosensweig model fully coupled with the (simplified) magnetostatics equations accounting for the effect of the demagnetizing field.

Both the Rosensweig and Shliomis models deal with one-phase flows, which is the case of many technological applications. However, some applications arise naturally in the form of a two-phase flow: one of the phases has magnetic properties

and the other one does not (e.g. magnetic manipulation of microchannel flows, microvalves, magnetically guided transport, etc). There has been a major effort in order to develop physically reasonable interfacial conditions of two-phase flows in the sharp interface regime within the micropolar theory (see [35, 36]), yet we are far from saying that we have at our disposal a mathematically and physically sound PDE model for two-phase ferrofluid flows.

There are not well established PDE models describing the behavior of two-phase ferrofluid flows. On the other hand, systematic derivation of a two-phase model from first principles, using energy-variational techniques in the spirit of Onsager's principle as in [37, 38, 39, 40, 41], would be highly desirable, but most probably too premature, given the current state of the art.

In this context, numerical analysis and scientific computation have a lot to offer, where carefully crafted computational experiments can help understand much better the limits of the current models and assist the development of new ones. Ad-hoc development (trial and error) of new models and numerical evaluation does not replace a proper mathematical derivation, but it can clearly help to find a reasonable starting point. In this spirit, in *Chapter 4* we present a simple two-phase PDE model for ferrofluids. The model is not derived, but rather assembled using components of already existing models and high-level (as opposite to deep) understanding of the physics of ferrofluids. The model attempts to retain only the essential features and mathematical difficulties that might appear in much more sophisticated models. To the best of our knowledge this contribution is the first modeling/numerical work in the direction of time-dependent behavior of two-phase ferrofluid flows together with

energy-stable and/ or convergent schemes.

1.2 Preliminaries and Notation

1.2.1 Function spaces

In this dissertation we shall consider evolutionary PDEs in a open, bounded, polygonal and convex domain $\Omega \subset \mathbb{R}^d$ (d equal to either 2 or 3), for a finite interval of time $(0, t_F)$, and we will denote $\Omega_{t_F} = \Omega \times (0, t_F)$. The boundary of Ω will be denoted as Γ. We use the standard Sobolev spaces $W_q^s(\Omega)$ for $0 \leq s \leq \infty$ and $1 \leq q \leq \infty$ that consist of functions $f \in L^q(\Omega)$ whose distributional derivatives of order up to s are also in $L^q(\Omega)$. To simplify notation, we set $H^s(\Omega) = W_2^s(\Omega)$, and denote the closure of $\mathcal{C}_0^\infty(\Omega)$ in $H^1(\Omega)$ by $H_0^1(\Omega)$.

We denote with bold characters vector-valued functions and their spaces, that is, for instance, $u : \Omega \to \mathbb{R}$ will denote a scalar-valued function, while $\mathbf{u} : \Omega \to \mathbb{R}^d$ will denote a vector-valued function. Similarly, $L^2(\Omega)$ is the space of scalar-valued square-integrable functions in Ω, while $\mathbf{L}^2(\Omega)$ denotes the space of vector-valued square-integrable functions in Ω. Yet, the inner products in $L^2(\Omega)$ and $\mathbf{L}^2(\Omega)$ are indistinctly denoted by $(\cdot, \cdot)$. If the domain in which we consider the inner product is any other than Ω, say for instance $T \subset \Omega$, for the sake of clarity we will overload the notation by writing $(\cdot, \cdot)_T$ to denote that the domain of integration is just T. The subspace of functions in $L^2(\Omega)$ with zero mean is denoted by $L_0^2(\Omega)$. Whenever it is convenient, for reasons of space, the usual notation $L^2(\Omega)$, $\mathbf{L}^2(\Omega)$, $H^1(\Omega)$, $\mathbf{H}_0^1(\Omega)$, $\mathcal{C}_0^\infty(\Omega)$, etc, will be replaced by the more compact notation L^2, $\mathbf{L}^2$, H^1, $\mathbf{H}_0^1$, $\mathcal{C}_0^\infty$,

which omits the domain of integration Ω in order to shorten long expressions.

Whenever E is a normed space, we denote by $\|\cdot\|_E$ its norm. The space of functions $\varrho : [0,T] \to E$ such that the map $(0,t_F) \ni t \mapsto \|\varrho(t)\|_E \in \mathbb{R}$ satisfies

$$\int_0^{t_F} \|\varrho(s)\|_E^q \, ds < \infty \,,$$

is denoted by $L^q(0,t_F;E)$, or simply by the shorthand notation $L^q(E)$.

We shall make repeated use of the following integration by parts formula for the *curl* operator:

$$(curl\,\mathbf{w},\mathbf{u}) = (\mathbf{w},curl\,\mathbf{u}) \quad \forall \mathbf{u},\mathbf{w} \in \mathbf{H}_0^1(\Omega). \tag{1.1}$$

We recall the following identity for vector-valued functions in the space $\mathbf{H}_0^1(\Omega)$

$$\|\nabla \mathbf{u}\|_{\mathbf{L}^2}^2 = \|curl\,\mathbf{u}\|_{\mathbf{L}^2}^2 + \|div\,\mathbf{u}\|_{\mathbf{L}^2}^2 \,, \forall \mathbf{u} \in \mathbf{H}_0^1(\Omega) \tag{1.2}$$

which holds true provided Ω is bounded and simply connected (see for instance [42]), and straightforwardly implies

$$\|curl\,\mathbf{u}\|_{\mathbf{L}^2}^2 \le \|\nabla \mathbf{u}\|_{\mathbf{L}^2}^2 \quad \forall \mathbf{u} \in \mathbf{H}_0^1(\Omega). \tag{1.3}$$

Let $\boldsymbol{\mathcal{H}}$ and $\boldsymbol{\mathcal{V}}$ denote the classical spaces of divergence-free functions (see for instance [43])

$$\begin{aligned} \boldsymbol{\mathcal{H}} &= \left\{ \mathbf{v} \in \mathbf{L}^2(\Omega) \,|\, div\,\mathbf{v} = 0 \text{ in } \Omega \text{ and } \mathbf{v}\cdot n = 0 \text{ on } \Gamma \right\}, \\ \boldsymbol{\mathcal{V}} &= \left\{ \mathbf{v} \in \mathbf{H}_0^1(\Omega) \,|\, div\,\mathbf{v} = 0 \,\text{in}\, \Omega \right\} = \mathbf{H}_0^1(\Omega) \cap \boldsymbol{\mathcal{H}} \,, \end{aligned} \tag{1.4}$$

and the space $\boldsymbol{\mathcal{M}}$

$$\boldsymbol{\mathcal{M}} = \left\{ \mathbf{z} \in \mathbf{L}^2(\Omega) \;|\; div\,\mathbf{z} \in L^2(\Omega),\; curl\,\mathbf{z} \in \mathbf{L}^2(\Omega) \right\} = \mathbf{H}(curl,\Omega) \cap \mathbf{H}(div,\Omega) \,.$$

where

$$\mathbf{H}(curl,\Omega) = \left\{\mathbf{z} \in \mathbf{L}^2(\Omega) |\ curl\, \mathbf{z} \in L^2(\Omega)\right\}\ ,$$

$$\mathbf{H}(div,\Omega) = \left\{\mathbf{z} \in \mathbf{L}^2(\Omega) |\ div\, \mathbf{z} \in L^2(\Omega)\right\}\ ,$$

more details about these spaces and the characterization of their traces can be found in [44, 42].

Henceforth c denotes a generic constant, whose value might change at each occurrence. This constant might depend on the data of our problem and, when discussing discretization, its exact solution, but it does not depend on the discretization parameters h and τ or the numerical solution. We denote by c_p the best constant in the Poincaré inequality, i.e.,

$$\|\mathbf{u}\|_{\mathbf{L}^2} \leq c_p \|\nabla \mathbf{u}\|_{\mathbf{L}^2} \quad \forall \mathbf{u} \in \mathbf{H}_0^1(\Omega), \qquad c_p \approx diam(\Omega).$$

We define the trilinear form $b(\cdot,\cdot,\cdot)$

$$b(\mathbf{u},\mathbf{v},\mathbf{w}) = \sum_{i,j=1}^{d} \int_\Omega \mathbf{u}^i\, \mathbf{v}^j_{x_i} \mathbf{w}^j\, dx\,, \tag{1.5}$$

which, as it is well known (cf. [43]), is skew-symmetric with respect to the last two arguments whenever the first argument $\mathbf{u}$ is divergence-free and has vanishing normal trace ($\mathbf{u}\cdot\boldsymbol{n} = 0$). In addition, we shall use the following, also well known, inequalities (see [45]):

$$b(\mathbf{u},\mathbf{v},\mathbf{w}) \leq c\, \|\nabla \mathbf{u}\|_{\mathbf{L}^2} \|\nabla \mathbf{v}\|_{\mathbf{L}^2} \|\nabla \mathbf{w}\|_{\mathbf{L}^2},\ \forall \mathbf{u},\mathbf{v},\mathbf{w} \in \mathbf{H}_0^1(\Omega), \tag{1.6}$$

$$b(\mathbf{u},\mathbf{v},\mathbf{w}) \leq c\, \|\mathbf{u}\|_{\mathbf{L}^\infty} \|\nabla \mathbf{v}\|_{\mathbf{L}^2} \|\mathbf{w}\|_{\mathbf{L}^2},\ \forall \mathbf{u} \in H^2(\Omega), \mathbf{v} \in \mathbf{H}_0^1(\Omega), \mathbf{w} \in \mathbf{L}^2(\Omega), \tag{1.7}$$

$$b(\mathbf{u},\mathbf{v},\mathbf{w}) \leq c\, \|\mathbf{u}\|_{\mathbf{L}^2} \|\nabla \mathbf{v}\|_{\mathbf{L}^2} \|\mathbf{w}\|_{\mathbf{L}^\infty},\ \forall \mathbf{u} \in \mathbf{L}^2(\Omega), \mathbf{v} \in \mathbf{H}_0^1(\Omega), \mathbf{w} \in \mathbf{H}^2(\Omega), \tag{1.8}$$

$$b(\mathbf{u},\mathbf{v},\mathbf{w}) \leq c\, \|\mathbf{u}\|_{\mathbf{L}^2} \|\mathbf{v}\|_{\mathbf{H}^2} \|\nabla \mathbf{w}\|_{\mathbf{L}^2},\ \forall \mathbf{u} \in \mathbf{L}^2(\Omega), \mathbf{v} \in H^2(\Omega), \mathbf{w} \in \mathbf{H}_0^1(\Omega). \tag{1.9}$$

In this dissertation the classical Aubin-Lions lemma will be used to establish the relative compactness of some families of parametrized functions (cf.[46])

Lemma 1.2.1 (Aubin-Lions)**.** *Let B_0, B and B_1 denote three Banach spaces such that*

$$B_0 \subset B \subset B_1$$

with B_0 and B_1 being reflexive, and $B_0 \subset\subset B$. We define the space W

$$W = \left\{ w \,\middle|\, w \in L^{p_0}(0, t_F; B_0),\ w_t \in L^{p_1}(0, t_F; B_1) \right\}$$

with $1 < p_0, p_1 < \infty$, endowed with the following norm

$$\|w\|_W = \|w\|_{L^{p_0}(0,t_F;B_0)} + \|w_t\|_{L^{p_1}(0,t_F;B_1)}\,.$$

Then, the space W is compactly embedded in $L^{p_0}(0, t_F; B)$.

Remark 1.2.1. Lemma 1.2.1 allows us to establish the relative $L^{p_0}(0, t_F; B)$ compactness for a family of functions by just showing that they are uniformly bounded in the W-norm. The above version of the celebrated Aubin-Lions lemma is perhaps the most popular one, somehow restrictive, but user friendly. There are much more general variants of this result, in particular the reflexivity hypothesis might be removed, the compact embedding $B_0 \subset\subset B$ might be replaced by a simple embedding, the assumption on the exponents weakened to $1 \leq p_i < \infty$, and even the space W modified by not requiring w_t to be defined. The reader can consult [45, 47, 48] for other ways to establish the relative $L^{p_0}(0, t_F; B)$ compactness of a family functions other than establishing bounds in the W-norm.

1.2.2 Time discretization

We introduce $K > 0$ to denote the total number of steps, define the time step as $\tau = t_F/K > 0$ and set $t^k = k\tau$ for $0 \le k \le K$. For $\varrho : [0, t_F] \to E$, where E is a normed space, we set

$$\varrho^k = \varrho(t^k)\,.$$

A sequence will be denoted by $\varrho^\tau = \left\{\varrho^k\right\}_{k=0}^K$ and we introduce the following norms:

$$\|\varrho^\tau\|_{\ell^\infty(E)} = \max_{0\le k\le K} \|\varrho^k\|_E, \qquad \|\varrho^\tau\|_{\ell^r(E)} = \left(\sum_{k=0}^K \tau \|\varrho^k\|_E^r\right)^{1/r}\,,\ r \in [1,\infty).$$

We also define the backward difference operator δ:

$$\delta\varrho^k = \varrho^k - \varrho^{k-1}. \tag{1.10}$$

so that $\delta^2\varrho^k := \delta(\delta\varrho^k) = \varrho^k - 2\varrho^{k-1} + \varrho^{k-2}$.

The following identity will be used repeatedly

$$2(a, a-b) = |a|^2 - |b|^2 + |a-b|^2\,. \tag{1.11}$$

Similarly, the following "summation by parts" formula (also called Abel's transformation) will be used in this dissertation:

$$\sum_{k=1}^K a^k\,\delta b^k = a^K b^K - a^0 b^0 - \sum_{k=1}^{K-1} b^k\,\delta a^{k+1} \tag{1.12}$$

The following Discrete Grönwall's lemma will be particularly useful in the context of stability analysis (and a priori error estimates) of nonlinear parabolic partial differential equations:

Lemma 1.2.2 (Discrete Grönwall)**.** *Let a^τ, b^τ, c^τ and γ^τ be sequences of nonnegative numbers such that $\tau\gamma_k < 1$ for all k, and let $g_0 \geq 0$ be so that the following inequality holds:*

$$a_K + \tau \sum_{k=0}^{K} b_k \leq \tau \sum_{k=0}^{K} \gamma_k a_k + \tau \sum_{k=0}^{K} c_k + g_0.$$

Then

$$a_K + \tau \sum_{k=0}^{K} b_k \leq \left(\tau \sum_{k=0}^{K} c_k + g_0 \right) \exp\left(\tau \sum_{k=0}^{K} \sigma_k \gamma_k \right),$$

where $\sigma_k = (1 - \tau\gamma_k)^{-1}$.

Proof. See [49, 50]. □

1.2.3 Space Discretization

Space discretization will be carried out using polynomial-based finite elements, both of the continuous and discontinuous type. We assume that $\mathcal{T}_h$ is a shape regular triangulation of the polygonal domain Ω, made of open disjoint elements T such that $\overline{\Omega} = \bigcup_{T \in \mathcal{T}_h} \overline{T}$.

Elements T, are assumed to be simplices (triangles in 2d and tetrahedrons in 3d) unless specified otherwise. The mesh $\mathcal{T}_h$ will be assumed to be quasi-uniform for all theoretical purposes, but some computations will be carried using adaptive meshes (which violates the quasi-uniformity condition). For additional details about finite element spaces the reader can consult standard literature (cf.[42, 51, 52]).

When using discontinuous finite elements spaces it will be assumed that they contain a continuous subspace, that is, let $\mathbb{A}$ be a generic finite element space, we

will assume that $\mathbb{A} \cap \mathcal{C}(\Omega) \neq \emptyset$. More generally, for any finite element space $\mathbb{A}$, either continuous or discontinuous, we will assume that there exist an interpolation operator $\mathrm{I}_{\mathbb{A}} : \mathcal{C}^0(\overline{\Omega}) \to \mathbb{A} \cap \mathcal{C}(\Omega)$ which is capable of delivering optimal convergence rates:

$$\begin{aligned} \|\mathrm{I}_{\mathbb{A}}\lambda - \lambda\|_{L^2} + h\|\nabla(\mathrm{I}_{\mathbb{A}}\lambda - \lambda)\|_{L^2} &\leq c\, h^{\ell+1}|\lambda|_{H^{\ell+1}(\Omega)} \quad \forall \lambda \in H^{\ell+1}(\Omega)\,, \\ \|\mathrm{I}_{\mathbb{A}}\lambda - \lambda\|_{L^\infty} + h\|\nabla(\mathrm{I}_{\mathbb{A}}\lambda - \lambda)\|_{L^\infty} &\leq c\, h^{\ell+1}|\lambda|_{W^{\ell+1}_\infty(\Omega)} \quad \forall \lambda \in W^{\ell+1}_\infty(\Omega)\,, \end{aligned} \tag{1.13}$$

where ℓ is the polynomial degree of the finite element space $\mathbb{A}$, and $h = \max_{T\in\mathcal{T}_h} \mathrm{diam}(T)$. The construction of these interpolation operators can be found in [42, 51, 52, 53] and references therein.

Let $\mathbb{U} \subset \mathbf{H}^1_0(\Omega)$ be a vector-valued finite element space, and $\mathbb{P} \subset L^2(\Omega)$ a scalar-valued finite element space, such that the pair $\{\mathbb{U}, \mathbb{P}\}$ satisfies the uniform inf-sup compatibility condition (also called LBB compatibility condition):

$$\inf_{0\neq \mathrm{Q}\in\mathbb{P}} \sup_{0\neq \mathbf{V}\in\mathbb{U}} \frac{(div\,\mathbf{V}, \mathrm{Q})}{\|\mathrm{Q}\|_{\mathbf{L}^2}\|\nabla\mathbf{V}\|_{\mathbf{L}^2}} \geq \beta^*, \tag{1.14}$$

with β^* independent of the discretization parameter h. Specific construction and examples of finite element spaces satisfying this condition can be found in [42, 53].

Definition 1.2.1 (Fortin operator)**.** We say that $\Pi_f : \mathbf{H}^1_0(\Omega) \longrightarrow \mathbb{U}$ is a divergence-preserving operator if

$$(div\,\Pi_f\mathbf{v} - div\,\mathbf{v}, \mathrm{Q}) = 0 \;\; \forall \mathbf{v} \in \mathbf{H}^1_0(\Omega)\,,\; \forall \mathrm{Q} \in \mathbb{P}\,. \tag{1.15}$$

If the following additional stability property holds true

$$\|\Pi_f\mathbf{v}\|_{\mathbf{H}^1_0(\Omega)} \leq c\|\mathbf{v}\|_{\mathbf{H}^1_0(\Omega)}\,, \tag{1.16}$$

we will call Π_f a Fortin operator. Given a finite element pair $\{\mathbb{U}, \mathbb{P}\}$: existence of an operator Π_f satisfying (1.15) and (1.16) is necessary and sufficient condition for $\{\mathbb{U}, \mathbb{P}\}$ to satisfy the LBB compatibily condition (1.14) (cf.[42, 53]).

Definition 1.2.2 (Stokes projector)**.** The Stokes projection of $(\mathbf{w}, r) \in \mathbf{H}_0^1(\Omega) \times L^2(\Omega)$ is the pair $(\Pi_s \mathbf{w}, \pi_s r) \in \mathbb{U} \times \mathbb{P}$ that solves

$$\begin{cases} (\nabla \Pi_s \mathbf{w}, \nabla \mathbf{V}) - (\pi_s r, div\, \mathbf{V}) = (\nabla \mathbf{w}, \nabla \mathrm{Q}) - (r, div\, \mathbf{V}) & \forall \mathbf{V} \in \mathbb{U} \\ (div\, \Pi_s \mathbf{w}, \mathrm{Q}) = (div\, \mathbf{w}, \mathrm{Q}) & \forall \mathrm{Q} \in \mathbb{P}\,. \end{cases} \tag{1.17}$$

We will assume that the Stokes projection $(\Pi_s \mathbf{w}, \pi_s r)$ satisfies the following approximation properties (see for instance [42, 50, 54])

$$\begin{aligned} &\|\mathbf{w} - \Pi_s \mathbf{w}\|_{\mathbf{L}^2} + h\|\mathbf{w} - \Pi_s \mathbf{w}\|_{\mathbf{H}_0^1} \\ &\qquad + h\|r - \pi_s r\|_{L^2} \le c\, h^{\ell+1} \left(\|\mathbf{w}\|_{\mathbf{H}^{\ell+1}} + \|r\|_{H^\ell} \right), \end{aligned} \tag{1.18}$$

for all $(\mathbf{w}, r) \in \mathbf{H}^{\ell+1}(\Omega) \cap \mathbf{H}_0^1(\Omega) \times H^\ell(\Omega)$, with c independent of h, $\mathbf{w}$ and r, as well as the following stability property

$$\|\Pi_s \mathbf{w}\|_{\mathbf{L}^\infty \cap \mathbf{W}_3^1} + \|\pi_s r\|_{H^1} \le c \left(\|\mathbf{w}\|_{\mathbf{H}^2} + \|r\|_{H^1} \right), \tag{1.19}$$

for all $\mathbf{w} \in \mathbf{H}^2(\Omega)$ and $r \in H^1(\Omega)$.

If $d = 2$, we will also assume that the Stokes Projector (1.17) satisfies the following estimate in L^∞-norm (see [55, p. 73])

$$\begin{aligned} &(h|\log h|)^{-1} \|\mathbf{w} - \Pi_s \mathbf{w}\|_{\mathbf{L}^\infty} + \|\nabla(\mathbf{w} - \Pi_s \mathbf{w})\|_{\mathbf{L}^\infty} + |\log h|^{-\frac{1}{2}} \|r - \pi_s r\|_{L^\infty} \\ &\qquad \le c\, |\log h|^2 \inf_{(\mathbf{V}, \mathrm{Q}) \in \mathbb{U} \times \mathbb{P}} \left(\|\nabla(\mathbf{w} - \mathbf{V})\|_{\mathbf{L}^\infty} + \|r - \mathrm{Q}\|_{L^\infty} \right). \end{aligned} \tag{1.20}$$

Estimate (1.20) cannot be taken for granted for any arbitrary choice of finite element spaces $\{\mathbb{U}, \mathbb{P}\}$ and mesh $\mathcal{T}_h$. A partial list of finite element pairs $\{\mathbb{U}, \mathbb{P}\}$ and the

requirements on the triangulation $\mathcal{T}_h$ such that (1.20) holds true can be found in [55]. For results similar to (1.20) valid in three dimensions see Remark 1.2.2.

We will denote $\mathbb{V} \subset \mathbb{U}$ to be the following space of discretely divergence-free functions:

$$\mathbb{V} = \{\mathbf{V} \in \mathbb{U} \mid (\mathrm{Q}, div\, \mathbf{V}) = 0 \ \forall\, \mathrm{Q} \in \mathbb{P}\} \ .$$

Let $\Pi_{\mathbb{V}} : \mathbf{L}^2(\Omega) \longrightarrow \mathbb{V}$ denote the $\mathbf{L}^2(\Omega)$ projection onto the space $\mathbb{V}$:

$$(\Pi_{\mathbb{V}}\mathbf{v}, \mathbf{V}) = (\mathbf{v}, \mathbf{V}) \ \ \forall\, \mathbf{V} \in \mathbb{V}\,. \tag{1.21}$$

We will assume that the projector $\Pi_{\mathbb{V}}$, defined in (1.21), is $\mathbf{H}_0^1(\Omega)$-stable, namely

$$\|\nabla \Pi_{\mathbb{V}}\mathbf{v}\|_{\mathbf{L}^2} \leq c\, \|\mathbf{v}\|_{\mathbf{H}_0^1} \ \ \forall\, \mathbf{v} \in \boldsymbol{\mathcal{V}}\,, \tag{1.22}$$

with c independent of h and $\mathbf{v}$. The most common approach to prove this property is by establishing the existence of a Fortin operator $\Pi_f : \mathbf{H}_0^1(\Omega) \longrightarrow \mathbb{U}$ with optimal approximation properties in $\mathbf{L}^2(\Omega)$ as detailed in the following proposition.

Proposition 1.2.1. *If the finite element pair* $\{\mathbb{U}, \mathbb{P}\}$ *admits a Fortin operator (see definition 1.2.1) satisfying*

$$\|\Pi_f\mathbf{v} - \mathbf{v}\|_{\mathbf{L}^2} \leq c\, h \|\mathbf{v}\|_{\mathbf{H}_0^1} \ \ \forall\, \mathbf{v} \in \mathbf{H}_0^1(\Omega)\,, \tag{1.23}$$

then (1.22) *holds true.*

Proof. Assume that $\mathbf{v} \in \boldsymbol{\mathcal{V}}$, we start with the triangle inequality

$$\|\nabla \Pi_{\mathbb{V}}\mathbf{v}\|_{\mathbf{L}^2} \leq \|\nabla \Pi_{\mathbb{V}}\mathbf{v} - \nabla \Pi_f\mathbf{v}\|_{\mathbf{L}^2} + \|\nabla \Pi_f\mathbf{v}\|_{\mathbf{L}^2}\,, \tag{1.24}$$

where the second term in the right-hand side of (1.24) already satisfies the bound $\|\nabla\Pi_f\mathbf{v}\|_{\mathbf{L}^2} \leq c\|\nabla\mathbf{v}\|_{\mathbf{L}^2}$ because of (1.16). On the other hand, for the first term in the right-hand side of (1.24), using an inverse inequality and triangle inequality we get:

$$\begin{aligned}\|\nabla\Pi_{\mathbb{V}}\mathbf{v} - \nabla\Pi_f\mathbf{v}\|_{\mathbf{L}^2} &\leq ch^{-1}\|\Pi_{\mathbb{V}}\mathbf{v} - \Pi_f\mathbf{v}\|_{\mathbf{L}^2} \\ &\leq ch^{-1}\big(\|\Pi_{\mathbb{V}}\mathbf{v} - \mathbf{v}\|_{\mathbf{L}^2} + \|\mathbf{v} - \Pi_f\mathbf{v}\|_{\mathbf{L}^2}\big)\,.\end{aligned} \tag{1.25}$$

Since $\Pi_{\mathbb{V}}\mathbf{v}$ is the best $\mathbf{L}^2(\Omega)$ approximation of $\mathbf{v}$ in the finite dimensional space $\mathbb{V}$, and $\Pi_f\mathbf{v} \in \mathbb{V}$, we naturally have that

$$\|\Pi_{\mathbb{V}}\mathbf{v} - \mathbf{v}\|_{\mathbf{L}^2} \leq \|\Pi_f\mathbf{v} - \mathbf{v}\|_{\mathbf{L}^2}\,. \tag{1.26}$$

Using this inequality and approximation property (1.23) into (1.25) we conclude that:

$$\|\nabla\Pi_{\mathbb{V}}\mathbf{v} - \nabla\Pi_f\mathbf{v}\|_{\mathbf{L}^2} \leq ch^{-1}\|\Pi_f\mathbf{v} - \mathbf{v}\|_{\mathbf{L}^2} \leq c\|\mathbf{v}\|_{\mathbf{H}^1_0}\,. \tag{1.27}$$

This concludes the proof of the proposition. □

Existence of a Fortin operator satisfying (1.23) was originally known to be true for a large class finite element pairs $\{\mathbb{U}, \mathbb{P}\}$, including some of the most popular finite element pairs used in practice (cf.[42, 50] and references therein). In [56] the authors provide explicit construction of operators Π_f satisfying (1.23) which is applicable the vast majority of well-known LBB stable pairs $\{\mathbb{U}, \mathbb{P}\}$. Finally, in [57, p. 226] it was proved that existence of a Fortin operator Π_f satisfying (1.23) holds true for every LBB stable pair, provided that Ω is convex or of class $\mathcal{C}^{1,1}$.

Remark 1.2.2 (L^∞ estimates for the Stokes projector for $d = 3$)**.** Estimates analogous to (1.20) valid in three dimensions are very recent (cf.[58, 59, 60, 61]), and are limited to a handful of finite element pairs $\{\mathbb{U}, \mathbb{P}\}$, such as the second and third order Taylor-Hood element, and the lowest order Bernardi-Raugel element. All the L^∞-norm estimates reported in [58, 59, 60, 61] use finite element pairs $\{\mathbb{U}, \mathbb{P}\}$ with continuous velocities combined with continuous pressures, or discontinuous pressures of order zero (piecewise constants), which turns out to be not enough for some particular problems like those presented in this thesis. At the time of this writing, there are no L^∞ estimates (analogous to (1.20)) for finite element pairs $\{\mathbb{U}, \mathbb{P}\}$ using continuous velocities $\mathbb{U}$ and higher-order (at least first-order) discontinuous pressures $\mathbb{P}$.

Chapter 2: The Micropolar Navier Stokes Equation (MNSE)

2.1 Background, Motivations, and Outline of the chapter

Let us briefly describe the derivation of the MNSE. The mathematical modeling of the laws governing the motion of a fluid begins with a description of the conservation of mass, linear and angular momentum, which can be written as (see [31] or [62]):

$$\begin{aligned} \frac{D\rho}{Dt} &= 0, \\ \rho\frac{D\mathbf{u}}{Dt} &= div\,\boldsymbol{\sigma} + \rho\mathbf{f}, \qquad (2.1) \\ \rho\frac{D}{Dt}\left(\ell + \mathbf{x}\times\mathbf{u}\right) &= \rho\mathbf{t} + \rho\mathbf{x}\times\mathbf{f} + div\,\Sigma + \mathbf{x}\times div\,\boldsymbol{\sigma} + \boldsymbol{\sigma}_{\times}, \qquad (2.2) \end{aligned}$$

where ρ is the density; $\mathbf{u}$ is the linear velocity; $\boldsymbol{\sigma} \in \mathbb{R}^{3\times 3}$ is the Cauchy stress tensor; $\mathbf{f}$ is the density of external body forces per unit mass; ℓ is the angular momentum per unit mass; $\Sigma \in \mathbb{R}^{3\times 3}$ is the moment stress tensor; $\mathbf{t}$ represents a body source of moments; and $(\boldsymbol{\sigma}_{\times})_i = \epsilon_{ijk}\boldsymbol{\sigma}_{jk}$, where ϵ_{ijk} is the Levi-Civita symbol, i.e., $\epsilon_{ijk} = \frac{1}{2}(i-j)(j-k)(k-i)$. As usual, we denote by D/Dt the material derivative. The physical meaning of the moment stress tensor Σ is analogous to that one of the stress tensor $\boldsymbol{\sigma}$. In other words, given a plane with normal ν, the vector $\mathbf{m} = \Sigma\cdot\nu$ is the moment vector per unit area acting on that plane.

Take the cross product of $\mathbf{x}$ and (2.1) and subtract the result from (2.2) to

obtain a simplified version of the conservation of angular momentum, namely

$$\rho \frac{D\ell}{Dt} = \rho \mathbf{t} + div\, \Sigma + \boldsymbol{\sigma}_{\times}. \tag{2.3}$$

Expressions (2.2) and (2.3) are usually attributed to Dahler and Scriven (see [28] and [29]) and have been extensively used by Eringen (see [31] and [32]) to develop a general theory of continuum media with director fields or, more generally, continuum media with microstructure.

In classical continuum mechanics it is usually assumed that the microconstituents do not possess angular momentum and there are no distributed couples. In other words, $\ell = 0$, $\Sigma = 0$ and $\mathbf{t} = 0$. Under these assumptions, (2.3) implies that the stress tensor $\boldsymbol{\sigma}$ is symmetric, which is the situation generally considered in the literature. These assumptions are appropriate for most practical applications. However, this approach is not satisfactory (nor even physical) when, for instance, the orientability of the microconstituents plays a major role in the physical process of interest. Classical examples are anisotropic fluids, liquid polymers, fluids with rod-like particles, ferrofluids, liquid crystals and polarizable media in general. In these cases a precise description of the moments and rotations associated to the microconstituents of the material is necessary.

In the situation described above, the conservation of angular momentum (2.3) needs to be taken explicitly into account which, among other things, means that it is necessary to propose constitutive relations for $\boldsymbol{\sigma}$, ℓ and Σ. Eringen proposed the following (cf. [30, 32, 62]):

$$\ell = \mathbb{I}\mathbf{w},$$

where $\mathbb{I} \in \mathbb{R}^{3\times 3}$ is the so-called microinertia density tensor;

$$\boldsymbol{\sigma} = (-p + \lambda div\, \mathbf{u})\mathbf{I} + \mu(\nabla \mathbf{u} + \nabla \mathbf{u}^T) + \mu_r(\nabla \mathbf{u} - \nabla \mathbf{u}^T) - 2\mu_r \mathbf{w}_\times,$$

where p is the pressure, $\mathbf{I} \in \mathbb{R}^{3\times 3}$ is the identity tensor, and $(\mathbf{w}_\times)_{ij} = \varepsilon_{kij}\mathbf{w}_k$; and

$$\Sigma = \gamma_0\, div\, \mathbf{w}\, \mathbf{I} + \gamma_d(\nabla \mathbf{w} + \nabla \mathbf{w}^T) + \gamma_a(\nabla \mathbf{w} - \nabla \mathbf{w}^T).$$

To further simplify the model we will assume that $\mathbb{I}$ is isotropic, so that it can be replaced by a scalar $\jmath$, the so-called inertia density. To guarantee that the constitutive relationships do not violate the Clausius-Duhem inequality (see [62]), the material constants μ, μ_r, γ_0, γ_a and γ_d are required to satisfy the following relations:

$$\begin{gathered} 3\lambda + 2\mu \geq 0, \quad \mu \geq 0, \quad \mu_r \geq 0, \quad \gamma_d \geq 0, \quad \gamma_a + \gamma_d \geq 0, \\ 3\gamma_0 + 2\gamma_d \geq 0, \quad -(\gamma_a + \gamma_d) \leq \gamma_d - \gamma_a \leq (\gamma_a + \gamma_d). \end{gathered} \tag{2.4}$$

As a final simplification, we will assume that the fluid is incompressible and has constant density.

Let $\Omega \subset \mathbb{R}^d$ with $d = 2$ or 3 be the domain occupied by the fluid. Replacing these constitutive relationships into (2.1) and (2.3), we arrive at the MNSE,

$$\begin{cases} \mathbf{u}_t - (\nu + \nu_r)\Delta \mathbf{u} + (\mathbf{u} \cdot \nabla)\mathbf{u} + \nabla p = 2\nu_r\, curl\, \mathbf{w} + \mathbf{f}, \\ \qquad\qquad div\, \mathbf{u} = 0, \\ \jmath \mathbf{w}_t - (c_a + c_d)\Delta \mathbf{w} + \jmath(\mathbf{u} \cdot \nabla)\mathbf{w} \\ \quad -(c_0 + c_d - c_a)\nabla div\, \mathbf{w} + 4\nu_r \mathbf{w} = 2\nu_r\, curl\, \mathbf{u} + \mathbf{t}\ , \end{cases} \tag{2.5}$$

where we implicitly redefined the pressure as $\rho^{-1}p$, and the constants ν, ν_r, c_a, c_d and c_0 are the kinematic viscosities (i.e. μ, μ_r, γ_a, γ_d and γ_0, respectively) divided by

ρ. This system is supplemented with the following initial and boundary conditions

$$\begin{aligned} &\mathbf{u}|_{t=0} = \mathbf{u}_0, \qquad \mathbf{w}|_{t=0} = \mathbf{w}_0, \\ &\mathbf{u}|_{\Gamma\times(0,T)} = 0, \quad \mathbf{w}|_{\Gamma\times(0,T)} = 0. \end{aligned} \tag{2.6}$$

The reader is referred to [62] for questions regarding existence, uniqueness and regularity of solutions to (2.5)-(2.6) and related models. The purpose of our work is to propose and analyze numerical techniques for this problem. To simplify notation, in what follows we will set

$$\widehat{\nu} = \nu + \nu_r, \quad c_1 = c_a + c_d, \quad c_2 = c_0 + c_d - c_a, \tag{2.7}$$

and we will assume that $c_1, c_2 > 0$ (see for instance [62]) which is consistent with the thermodynamical constraints (2.4).

The MNSE can be regarded as a building block of models that describe the physics of polarizable media. For instance, Rosensweig (see [17]) described the behavior of ferrofluids subject to a magnetizing field $\mathbf{h}$ with the MNSE and

$$\begin{cases} \mathbf{f} = \mu_0(\mathbf{m}\cdot\nabla)\mathbf{h}, \quad \mathbf{t} = \mu_0\mathbf{m}\times\mathbf{h}, \\ \mathbf{m}_t - \sigma\Delta\mathbf{m} + (\mathbf{u}\cdot\nabla)\mathbf{m} = \mathbf{w}\times\mathbf{m} - \frac{1}{\mathscr{T}}(\mathbf{m} - \varkappa_0\mathbf{h}) \quad \text{in } \Omega, \end{cases} \tag{2.8}$$

where $\mathbf{m}$ denotes the magnetization field and $\mathscr{T} > 0$, $\sigma \geq 0$, $\varkappa_0 > 0$ are material constants. The magnetizing field $\mathbf{h}$ is assumed to obey the Maxwell equations. The reader is referred to [22, 21] for an analysis of this model. The system (2.5)-(2.8) will eventually be (later in *Chapter 3*) the focus of our attention.

In addition to applications in smart fluids and polarizable media, there has been a growing interest on the MNSE in other areas. For instance, they have been

used to describe granular flows, where the size of the microconstituents is comparable to the macroscopic scale ([63]) and the frictional interaction between particles is not properly modeled by the classical equations of hydrodynamics. Another application is the modeling of micro and nano flows ([64]), where again the size of the microconstituents is comparable to the "macroscopic" scale and the rotational effects cannot be neglected.

The key points of this chapter (*Chapter 2*) are organized as follows. Section 2.1.1 introduces a very simple experiment (ferrofluid pumping) as a motivation for the analysis and numerical implementation of the MNSE. In §2.1.2 we recall the basic energy estimates and existence theory for the MNSE. In addition to the general notation defined in §1.2, in §2.1.3 we introduce specific notation and basic tools for this chapter, required for the analysis of the numerical scheme proposed later in §2.2. Error estimates for the linear and angular velocities are derived in §2.3.1, and error estimates for the pressure are derived in §2.3.3. We also present a formally second-order scheme in §2.4, and show that it is almost unconditionally stable, i.e. it is stable provided the time step is smaller than a constant dependent on the material parameters, but not on the space discretization parameter; see (2.48) for details. Finally, in §2.5, we provide numerical validation of the error estimates derived earlier.

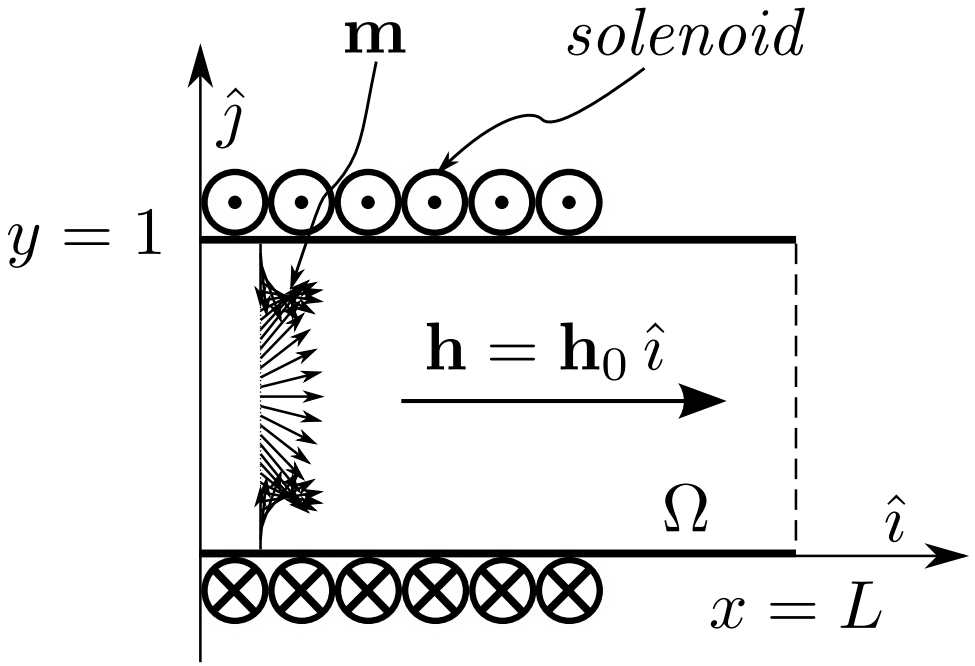

Figure 2.1: **MNSE pumping experiment: idealized configuration of a pumping experiment.** A planar duct with a solenoid that generates a uniform magnetizing field $\mathbf{h} = h_0\hat{\imath}$. Since, $\mathbf{t} = \mu_0\mathbf{m}\times\mathbf{h}$ (see (2.8)), it will produce torque in the regions where $\mathbf{h}$ and $\mathbf{m}$ are not collinear. In a real ferrofluid the magnetization vector field $\mathbf{m}$ would evolve through the channel satisfying the evolution equation (2.8) and will try to align with the magnetizing field. However, and as part of an idealized setting, we will assume that the magnetization profile $\mathbf{m}$ depends only on the y-direction.

2.1.1 Potential Application: Ferrofluid Pumping by Magnetic Induction

To illustrate the differences between the MNSE and the classical Navier-Stokes equations here we propose a setting by means of which it is possible, at least theoretically, to generate fluid motion via a well designed forcing term in the equation of angular momentum. This example is inspired by [26], where a ferrofluid is pumped by the actuation of a spatially-uniform sinusoidally time-varying magnetizing field. Another pumping strategy, this time based on a magnetizing field that is varying in space and time, is proposed in [65].

The idealized setting that we shall consider is depicted in Figure 2.1. We assume that our domain is a planar duct of unit height and length $L \geq 1$, which is wrapped by a solenoid that generates a uniform magnetizing field $\mathbf{h} = h_0\,\hat{\imath}$, where h_0 is just a positive constant. From (2.8) we infer that $\mathbf{f} = 0$, since the magnetizing field is constant in space. As part of our idealized setting, we disregard the evolution equation in (2.8) for the magnetization field, and set $\mathbf{m}$ to be constant in time and depend only on the vertical variable y, i.e.,

$$\mathbf{m} = m_0(\cos\theta\hat{\imath} + \sin\theta\hat{\jmath}),$$

where m_0 is just a positive constant, and $\theta = \theta(y)$. Using (2.8) we get:

$$\mathbf{t} = -\mu_0 m_0 h_0 \sin\theta(y)\,\hat{\kappa}. \tag{2.9}$$

As reference configuration we will consider a linear interpolation between the

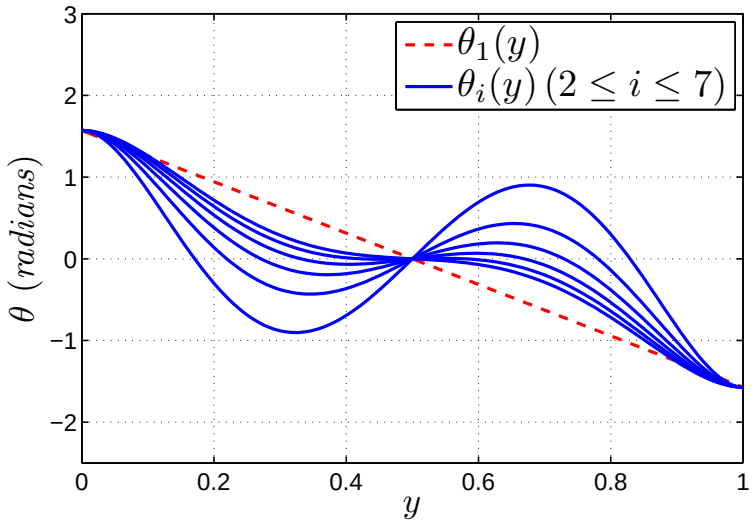

Figure 2.2: **MNSE pumping experiment: forcing functions.** Plot of the function $\theta_1(y)$ (dotted line), and the family of functions $\{\theta_i(y)\}_{i=2}^{7}$ (solid lines). These are used to induce a force in the angular momentum equation. The function θ_1 is a linear interpolation between $\pm\pi/2$ and θ_i, for $i = 2, \ldots, 7$ are small perturbations of it.

points $(0, \pi/2)$ and $(1, -\pi/2)$, that is

$$\theta_1(y) = -\pi \left(y - \tfrac{1}{2}\right).$$

As perturbations from this reference case we consider, for $i = 2, \ldots, 7$,

$$\theta_i(y) = -\frac{1}{2(i^2 + 10i - 35)} \big(\pi(480x^5 - 1200x^4 - 4x^3(i^2 + 10i - 275) \\ +6x^2(i^2 + 10i - 75) - i^2 - 5(2i - 7))\big).$$

A plot of these functions is provided in Figure 2.2. Notice that they all satisfy $\theta_i(0) = \pi/2$, $\theta_i(1/2) = 0$ and $\theta_i(1) = -\pi/2$ which we require to model a magnetization field that is perfectly aligned with the magnetizing field at the center of the channel, but is perpendicular to it at the top and bottom walls.

We assume the fluid is initially at rest, the boundary conditions for the upper and lower part of the duct are no slip, and for the left and right sides of the duct we consider open boundary conditions. We apply the magnetizing field linearly in time, that is we set $\mathbf{h} = h_0(t/T)\hat{\imath}$. We let $L = 1$, and the material constants be $\nu = \nu_r = 1$, $c_a = c_d = c_0 = 1$, and $\jmath = 1$. We use a Taylor-Hood finite element discretization of 40 elements in the horizontal and vertical directions, and a time-step $\tau = 1/50$. The numerical scheme used for this example is the first-order method discussed and analyzed in this work. Figure 2.3 shows the velocity profiles at time $t = T$ and $x = 1$ obtained by setting $\mathbf{t}$ as in (2.9). These results are stable (in the sense that they do not change) with respect to the spatial and temporal discretizations, and length of the channel. However, as it would happen with any physical model, these results can be sensitive to changes in the constitutive parameters. A discussion about the

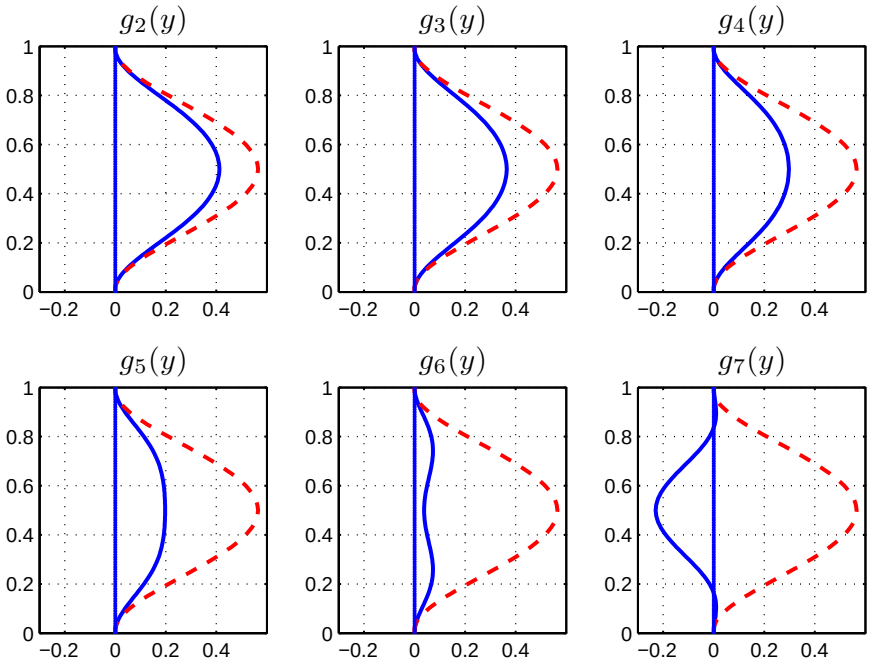

Figure 2.3: **MNSE pumping experiment: velocity profiles.** Velocity profiles obtained with the forcing terms $\{\mathbf{t}_i\}_{i=2}^{7}$ (solid lines). For comparison the velocity profile obtained by using $\mathbf{t}_1$ is also shown (dotted line). The figures show that it is possible to generate linear velocity via appropriate actuation in the angular momentum equation. Notice that, although it is not dramatically different from the others, the forcing term $\mathbf{t}_7$ induces motion in the opposite direction.

possible influence of the constitutive parameters on the pumping phenomena goes beyond the scope of this paper (see for instance [25]).

The results in Figure 2.3 give an idea about the kind of forces that are necessary in a real ferrohydrodynamic setting, in particular in the case of a spatially uniform and sinusoidal in time magnetizing field as in [26]. The main observation here is that small variations of the forcing term can yield quite different flow regimes, including flow in the opposite direction; this feature is observed in experiments (cf. [26]). Finally, the reader should be reminded that this is just an idealized setting which illustrates the main pumping mechanism. In real ferrohydrodynamics we cannot set the value of magnetization $\mathbf{m}$ as we please because $\mathbf{m}$ is actually determined by the evolution law in (2.8).

2.1.2 Energy Estimates and Existence Theorems

The stability and error analysis of the scheme that will be proposed in §2.2 is based on energy arguments. Therefore, to gain intuition, let us briefly describe the basic formal energy estimates that can be obtained from (2.5). Multiply the linear momentum equation by $\mathbf{u}$ and the angular momentum equation by $\mathbf{w}$ and integrate in Ω. Adding both ensuing equations, we obtain

$$\begin{aligned}\tfrac{1}{2}\tfrac{d}{dt}\big(\|\mathbf{u}\|^2_{\mathbf{L}^2}+\jmath\|\mathbf{w}\|^2_{\mathbf{L}^2}\big)+\widehat{\nu}\,\|\nabla\mathbf{u}\|^2_{\mathbf{L}^2}+c_1\,\|\nabla\mathbf{w}\|^2_{\mathbf{L}^2}+c_2\,\|div\,\mathbf{w}\|^2_{\mathbf{L}^2}+4\nu_r\,\|\mathbf{w}\|^2_{\mathbf{L}^2}\\ =4\nu_r\big(curl\,\mathbf{u},\mathbf{w}\big)+\big(\mathbf{f},\mathbf{u}\big)+\big(\mathbf{t},\mathbf{w}\big),\end{aligned}$$

where the parameters $\widehat{\nu}$, c_1 and c_2 were defined in (2.7). Repeated applications of Young's and Poincaré's inequalities yield, after integration in time,

$$\begin{aligned}\|\mathbf{u}(t)\|^2_{\mathbf{L}^2} + \jmath\,\|\mathbf{w}(t)\|^2_{\mathbf{L}^2} + \nu\int_0^t \|\nabla\mathbf{u}(s)\|^2_{\mathbf{L}^2}\,ds + c_1\int_0^t \|\nabla\mathbf{w}(s)\|^2_{\mathbf{L}^2}\,ds \\ + c_2\int_0^t \|div\,\mathbf{w}\|^2_{\mathbf{L}^2}\,ds \leq c_p^2\int_0^T \left(\tfrac{1}{\nu}\|\mathbf{f}(s)\|^2_{\mathbf{L}^2} + \tfrac{1}{c_1}\|\mathbf{t}(s)\|^2_{\mathbf{L}^2}\right)ds \\ + \|\mathbf{u}_0\|^2_{\mathbf{L}^2} + \jmath\,\|\mathbf{w}_0\|^2_{\mathbf{L}^2} \quad \forall t \leq T\,.\end{aligned} \tag{2.10}$$

This formal energy estimate suggests that solutions to (2.5) are such that

$$\mathbf{u} \in L^\infty(\boldsymbol{\mathcal{H}}) \cap L^2(\boldsymbol{\mathcal{V}}), \qquad \mathbf{w} \in L^\infty(\mathbf{L}^2(\Omega)) \cap L^2(\mathbf{H}^1_0(\Omega)). \tag{2.11}$$

where $\boldsymbol{\mathcal{H}}$ and $\boldsymbol{\mathcal{V}}$ where defined in (1.4). To obtain an estimate on the pressure, we use a well-known estimate on the right inverse of the divergence operator (cf. [42, 66]), i.e.,

$$\beta\|q\|_{L^2} \leq \sup_{\mathbf{v}\in\mathbf{H}^1_0} \frac{(q, div\,\mathbf{v})}{\|\mathbf{v}\|_{\mathbf{H}^1_0}}, \quad \forall q \in L^2_0(\Omega). \tag{2.12}$$

From (2.12) and the linear momentum equation in (2.5) we get

$$\begin{aligned}\int_0^T \|p(s)\|^2_{L^2} ds \leq c\int_0^T \Big(\|\mathbf{u}_t(s)\|^2_{\mathbf{L}^2} + \|\nabla\mathbf{u}(s)\|^2_{\mathbf{L}^2} \\ + \|\nabla\mathbf{u}(s)\|^4_{\mathbf{L}^2} + \|\nabla\mathbf{w}(s)\|^2_{\mathbf{L}^2} + \|\mathbf{f}\|^2_{\mathbf{L}^2}\Big)\,ds,\end{aligned}$$

so that, to obtain an estimate on the pressure, we must assume $\mathbf{u} \in L^4(\mathbf{H}^1_0(\Omega))$ and, in addition, we need an estimate on the time derivative of the linear velocity at least in $L^2(\mathbf{L}^2(\Omega))$. This is standard for the Navier-Stokes equations. To obtain it we differentiate with respect to time the equations of conservation of linear and angular momentum. Repeating the steps used to obtain (2.10) we arrive at the desired estimate.

The existence of weak solutions can be summarized as follows.

Theorem 2.1.1 (Existence of weak solutions)**.** *Let* $\mathbf{f}, \mathbf{t} \in L^2(\mathbf{L}^2(\Omega))$*,* $\mathbf{u}_0 \in \boldsymbol{\mathcal{H}}$ *and* $\mathbf{w}_0 \in \mathbf{L}^2(\Omega)$*. Then there exist* $(\mathbf{u}, \mathbf{w}, p) \in L^\infty(\boldsymbol{\mathcal{H}}) \times L^\infty(\mathbf{L}^2(\Omega)) \times \mathcal{D}'(\Omega_T)$ *satisfying* (2.5) *in the sense of distributions. Moreover,* $\mathbf{u}$ *and* $\mathbf{w}$ *satisfy the energy estimate* (2.10)*.*

Proof. see Theorem 1.6.1 of [62]. □

Just like for the Navier-Stokes equations, uniqueness of solutions of the MNSE is an open issue.

2.1.3 Space Discretization

To construct an approximation to the solution of (2.5) via Galerkin techniques we introduce three families of finite dimensional spaces: $\mathbb{U} \subset \mathbf{H}_0^1(\Omega)$, $\mathbb{P} \subset H^1(\Omega) \cap L_0^2(\Omega)$, and $\mathbb{W} \subset \mathbf{H}_0^1(\Omega)$. The spaces $\mathbb{U}$ and $\mathbb{P}$ will be used to approximate the linear velocity $\mathbf{u}$ and pressure p respectively, and the space $\mathbb{W}$ will be used to approximate the angular velocity $\mathbf{w}$. We will assume that these spaces have optimal approximation properties in the sense of (1.13). We require the spaces $\mathbb{U}$ and $\mathbb{P}$ to be LBB compatible, meaning that they satisfy (1.14). To simplify the presentation we will assume that $\mathbb{U} = \mathbb{W}$ throughout this chapter, but this is not strictly necessary from a mathematical point of view.

Lastly, we assume that the velocity space $\mathbb{U}$ (also the space $\mathbb{W}$) satisfies the following inverse inequality:

$$\|\mathbf{U}\|_{\mathbf{L}^\infty} \leq c\,\psi(h)\|\mathbf{U}\|_{\mathbf{H}_0^1} \quad \forall \mathbf{U} \in \mathbb{U}, \tag{2.13}$$

where $\psi(h) = (1 + |\log h|)^{\frac{1}{2}}$ if $d = 2$ and $\psi(h) = h^{-\frac{1}{2}}$ if $d = 3$. References [53, 42] provide a comprehensive list of suitable choices for these spaces.

In addition to the Stokes projection (see (1.17) and (1.18)), for a.e. $t \in [0, T]$ we define an elliptic-like projection of $\mathbf{w}(t)$ as the function $\Pi_w \mathbf{w}(t) \in \mathbb{W}$ that solves

$$\begin{aligned} c_1(\nabla \Pi_w \mathbf{w}, \nabla \mathbf{X}) + c_2(div\, \Pi_w \mathbf{w}, div\, \mathbf{X}) + 4\nu_r(\Pi_w \mathbf{w}, \mathbf{X}) = \\ = c_1(\nabla \mathbf{w}, \nabla \mathbf{X}) + c_2(div\, \mathbf{w}, div\, \mathbf{X}) + 4\nu_r(\mathbf{w}, \mathbf{X}) \quad \forall \mathbf{X} \in \mathbb{W}\,. \end{aligned} \tag{2.14}$$

The properties of the Stokes projector are summarized in (1.17) and (1.18), and the properties of the elliptic-like projector are summarized as follows:

Lemma 2.1.1 (Properties of the elliptic projector $\Pi_w \mathbf{w}$)**.** *If* $\mathbf{w} \in L^\infty(\mathbf{H}^{\ell+1}(\Omega) \cap \mathbf{H}_0^1(\Omega))$*, then the elliptic-projection satisfies the following approximation properties:*

$$\|\mathbf{w} - \Pi_w \mathbf{w}\|_{L^\infty(\mathbf{L}^2)} + h\|\mathbf{w} - \Pi_w \mathbf{w}\|_{L^\infty(\mathbf{H}_0^1)} \leq c\, h^{\ell+1} \|\mathbf{w}\|_{L^\infty(\mathbf{H}^{\ell+1})}, \tag{2.15}$$

If $\mathbf{w} \in L^\infty(\mathbf{H}^2(\Omega) \cap \mathbf{H}_0^1(\Omega))$, then the elliptic projection $\Pi_w \mathbf{w}$ is stable in the $\mathbf{L}^\infty(\Omega)$ and $\mathbf{W}_3^1(\Omega)$ norms in dimension $d \leq 3$, i.e.,

$$\|\Pi_w \mathbf{w}\|_{L^\infty(\mathbf{L}^\infty \cap \mathbf{W}_3^1)} \leq c\, \|\mathbf{w}\|_{L^\infty(\mathbf{H}^2)}\,.$$

Proof. The proof is standard and follows by classical duality arguments for general elliptic operators; see for instance [52, 53]. □

We introduce a discretization of the trilinear form $b(\cdot, \cdot, \cdot)$ in the equations for the linear and angular velocities:

$$b_h(\cdot, \cdot, \cdot) : \mathbb{U} \times (\mathbb{U} + \mathbb{W}) \times (\mathbb{U} + \mathbb{W}) \to \mathbb{R}.$$

more precisely (see for instance [43])

$$b_h(\mathbf{U},\mathbf{V},\mathbf{W}) := b(\mathbf{U},\mathbf{V},\mathbf{W}) + \tfrac{1}{2}(div\,\mathbf{U},\mathbf{V}\cdot\mathbf{W}), \forall \mathbf{U}\in\mathbb{U},\mathbf{V},\mathbf{W}\in(\mathbb{U}+\mathbb{W}), \quad (2.16)$$

and recall that it is consistent, i.e. $b_h(\mathbf{u},\mathbf{v},\mathbf{w}) = b(\mathbf{u},\mathbf{v},\mathbf{w})$ whenever $\mathbf{u}\in\boldsymbol{\mathcal{V}}$, and skew-symmetric with respect to its last two arguments, i.e.

$$b_h(\mathbf{U},\mathbf{V},\mathbf{W}) = -\,b_h(\mathbf{U},\mathbf{W},\mathbf{V}), \quad \forall\,\mathbf{U}\in\mathbb{U};\ \mathbf{V},\mathbf{W}\in(\mathbb{U}+\mathbb{W}) \tag{2.17}$$

This form satisfies estimates similar to (1.6)–(1.9), namely

$$\begin{aligned} b_h(\mathbf{U},\mathbf{V},\mathbf{W}) &\le c\,\|\nabla\mathbf{U}\|_{\mathbf{L}^2}\|\nabla\mathbf{V}\|_{\mathbf{L}^2}\|\nabla\mathbf{W}\|_{\mathbf{L}^2}, \quad \forall\mathbf{U},\mathbf{V},\mathbf{W}\in\mathbb{U},\\ b_h(\mathbf{U},\mathbf{v},\mathbf{W}) &\le c\,\|\mathbf{U}\|_{\mathbf{L}^2}\|\mathbf{v}\|_{\mathbf{H}^2}\|\nabla\mathbf{W}\|_{\mathbf{L}^2}, \quad \forall\mathbf{U},\mathbf{W}\in\mathbb{U},\mathbf{v}\in H^2(\Omega), \end{aligned} \tag{2.18}$$

and

$$b_h(\mathbf{U},\mathbf{V},\mathbf{W}) \le c\,\|\mathbf{U}\|_{\mathbf{L}^2}\|\mathbf{V}\|_{\mathbf{L}^\infty\cap\mathbf{W}^1_3}\|\nabla\mathbf{W}\|_{\mathbf{L}^2}, \quad \forall\mathbf{U},\mathbf{V},\mathbf{W}\in\mathbb{U}. \tag{2.19}$$

Since, by assumption, the space $\mathbb{U}$ satisfies the inverse inequality (2.13), then for $d=3$ we also have

$$\begin{aligned} b_h(\mathbf{U},\mathbf{V},\mathbf{W}) &\le c\,h^{-\frac{1}{2}}\|\mathbf{U}\|_{\mathbf{L}^2}\|\nabla\mathbf{V}\|_{\mathbf{L}^2}\|\nabla\mathbf{W}\|_{\mathbf{L}^2} \qquad \forall\mathbf{U},\mathbf{V},\mathbf{W}\in\mathbb{U}\\ b_h(\mathbf{U},\mathbf{V},\mathbf{W}) &\le c\,h^{-\frac{1}{2}}\,\|\nabla\mathbf{U}\|_{\mathbf{L}^2}\|\nabla\mathbf{V}\|_{\mathbf{L}^2}\|\mathbf{W}\|_{\mathbf{L}^2} \qquad \forall\mathbf{U},\mathbf{V},\mathbf{W}\in\mathbb{U} \end{aligned} \tag{2.20}$$

2.2 Description of the first-order scheme

To the best of our knowledge, the only work that is concerned with the construction and analysis of a scheme for the MNSE is [67], where a fully discrete penalty projection method for this system is developed and analyzed, and suboptimal convergence rates are derived. Our scheme instead possesses optimal approximation properties

and requires the solution of a saddle point problem at each time step, which can be done efficiently (cf.[68]). However, it can be easily modified to decouple the linear velocity and pressure via an incremental projection method, while maintaining optimal orders of convergence. For brevity this will not be included.

Let us now describe the scheme. The scheme computes $\{\mathbf{U}^\tau, \mathbf{W}^\tau, P^\tau\} \subset \mathbb{U} \times \mathbb{W} \times \mathbb{P}$ meant to approximate, at each time step, the linear and angular velocities and the pressure. We initialize the scheme by setting

$$(\mathbf{U}^0, P^0) = (\Pi_s \mathbf{u}^0, \pi_s p^0), \qquad \mathbf{W}^0 = \Pi_w \mathbf{w}^0, \tag{2.21}$$

that is, we compute the Stokes and elliptic-like projections of the initial data.

Remark 2.2.1 (Initialization)**.** The initialization step (2.21) requires that the initial data is regular enough so that the projections are well defined, which from now on we will assume. If this is not the case, (2.21) must be modified, say for instance, taking L^2-projections. The analysis below must be accordingly adjusted to take this into account (cf. [50]).

After initialization, for $k = 1, \ldots, K$, we march in time in two steps:

Linear Momentum: Compute $(\mathbf{U}^k, P^k) \in \mathbb{U} \times \mathbb{P}$, solution of

$$\begin{aligned} \Big(\tfrac{\delta \mathbf{U}^k}{\tau}, \mathbf{V}\Big) + \widehat{\nu}\big(\nabla \mathbf{U}^k, \nabla \mathbf{V}\big) + b_h\big(\mathbf{U}^{k-1}, \mathbf{U}^k, \mathbf{V}\big) - \big(P^k, div\, \mathbf{V}\big) \\ = 2\nu_r \big(curl\, \mathbf{W}^{k-1}, \mathbf{V}\big) + \big(\mathbf{f}^k, \mathbf{V}\big)\,, \end{aligned} \tag{2.22a}$$

$$\big(\mathrm{Q}, div\, \mathbf{U}^k\big) = 0\,, \tag{2.22b}$$

for all $\mathbf{V} \in \mathbb{U}$, $\mathrm{Q} \in \mathbb{P}$. Recall that the backward difference operator δ was defined in (1.10).

Angular Momentum: Find $\mathbf{W}^k \in \mathbb{U}$ that solves

$$\begin{aligned} \jmath\left(\frac{\delta \mathbf{W}^k}{\tau}, \mathbf{X}\right) + c_1\big(\nabla \mathbf{W}^k, \nabla \mathbf{X}\big) + \jmath\, b_h\big(\mathbf{U}^k, \mathbf{W}^k, \mathbf{X}\big) + c_2\big(div\, \mathbf{W}^k, div\, \mathbf{X}\big) \\ + 4\nu_r\big(\mathbf{W}^k, \mathbf{X}\big) = 2\nu_r\big(curl\, \mathbf{U}^k, \mathbf{X}\big) + \big(\mathbf{t}^k, \mathbf{X}\big)\,, \end{aligned} \tag{2.23}$$

for all $\mathbf{X} \in \mathbb{W}$.

Notice that we have decoupled the linear and angular momentum equations by time-lagging of the variables. This scheme is unconditionally stable, as the following result shows.

Proposition 2.2.1 (Unconditional stability of the first-order scheme)**.** *The sequence* $\{\mathbf{U}^\tau, \mathbf{W}^\tau, P^\tau\} \subset \mathbb{U} \times \mathbb{W} \times \mathbb{P}$*, solution of* (2.22)–(2.23)*, satisfies*

$$\begin{aligned} &\|\mathbf{U}^K\|^2_{\mathbf{L}^2} + (\jmath + 4\nu_r\tau)\|\mathbf{W}^K\|^2_{\mathbf{L}^2} + \sum_{k=1}^{K}\left(\|\delta\mathbf{U}^k\|^2_{\mathbf{L}^2} + \jmath\|\delta\mathbf{W}^k\|^2_{\mathbf{L}^2}\right) \\ &\qquad + \sum_{k=1}^{K}\tau\left(\nu\|\nabla\mathbf{U}^k\|^2_{\mathbf{L}^2} + \tau c_1\|\nabla\mathbf{W}^k\|^2_{\mathbf{L}^2}\right) + 2\sum_{k=1}^{K}\tau c_2\|div\,\mathbf{W}^k\|^2_{\mathbf{L}^2} \\ &\qquad \le \sum_{k=1}^{K}\tau\left(\tfrac{c_p^2\nu_r}{\nu}\|\mathbf{f}^k\|^2_{\mathbf{L}^2} + \tfrac{c_p^2\nu_r}{c_1}\|\mathbf{t}^k\|^2_{\mathbf{L}^2}\right) + \|\mathbf{U}^0\|^2_{\mathbf{L}^2} + (\jmath + 4\nu_r\tau)\|\mathbf{W}^0\|^2_{\mathbf{L}^2}\,. \end{aligned} \tag{2.24}$$

Proof. Set $\mathbf{V} = 2\tau\mathbf{U}^k$ in (2.22) and $\mathbf{X} = 2\tau\mathbf{W}^k$ in (2.23), respectively, and add the results. Using identity (1.11), the integration by parts formula (1.1), $\widehat{\nu} = \nu + \nu_r$ (see (2.7)), estimate (1.3) and Young's inequality to obtain

$$\begin{aligned} &\|\mathbf{U}^k\|^2_{\mathbf{L}^2} + (\jmath + 4\nu_r\tau)\|\mathbf{W}^k\|^2_{\mathbf{L}^2} + \|\delta\mathbf{U}^k\|^2_{\mathbf{L}^2} + \jmath\|\delta\mathbf{W}^k\|^2_{\mathbf{L}^2} \\ &\qquad + \tau\nu\|\nabla\mathbf{U}^k\|^2_{\mathbf{L}^2} + \tau c_1\|\nabla\mathbf{W}^k\|^2_{\mathbf{L}^2} + 2\tau c_2\|div\,\mathbf{W}^k\|^2_{\mathbf{L}^2} \\ &\qquad \le \tfrac{c_p^2\nu_r\tau}{\nu}\|\mathbf{f}^k\|^2_{\mathbf{L}^2} + \tfrac{c_p^2\nu_r\tau}{c_1}\|\mathbf{t}^k\|^2_{\mathbf{L}^2} + \|\mathbf{U}^{k-1}\|^2_{\mathbf{L}^2} + (\jmath + 4\nu_r\tau)\|\mathbf{W}^{k-1}\|^2_{\mathbf{L}^2}\,. \end{aligned}$$

Adding over k we obtain the desired estimate (2.24). □

2.3 A Priori Error Analysis

Here we perform an error analysis of scheme (2.22)–(2.23) and show that this method has optimal convergence properties. The analysis is based on energy arguments and hinges on the unconditional stability result of Proposition 2.2.1. The arguments used are rather standard for the Navier-Stokes equations, the main novelty and difficulty being the coupling with the angular momentum equation, which requires lengthy and careful computations.

We shall assume, for the sake of simplicity, that the solution to (2.5)–(2.6) satisfies:

$$\mathbf{u}, \mathbf{w} \in \mathcal{C}^1([0,T], \mathbf{H}^{\ell+1}(\Omega)) \quad \text{and} \quad \mathbf{u}_{tt}, \mathbf{w}_{tt} \in L^2([0,T], \mathbf{L}^2(\Omega)). \tag{2.25}$$

These assumptions will be enough to derive optimal convergence rates for the linear and angular velocities. If we want to do the same with the pressure we will require the additional regularity:

$$\mathbf{u}_{tt}, \mathbf{w}_{tt} \in \mathcal{C}([0,T], \mathbf{H}^{\ell+1}(\Omega)). \tag{2.26}$$

These assumptions are standard in the error analysis of incompressible flows (cf. [45]).

The first step in the error analysis is to analyze the consistency of the method. To do so, we proceed as it is customary in the analysis of evolutionary problems

(cf. [49]) and split the errors

$$\mathbf{E}^k = \mathbf{u}^k - \mathbf{U}^k, \qquad \mathcal{E}^k = \mathbf{w}^k - \mathbf{W}^k, \qquad e^k = p^k - P_h^k,$$

into the so-called interpolation and approximation errors via the Stokes and elliptic projections (see (1.17) and (2.14)) i.e.,

$$\begin{aligned} &\mathbf{S}^k = \mathbf{u}^k - \Pi_s \mathbf{u}^k, \qquad \mathbf{R}^k = \mathbf{w}^k - \Pi_w \mathbf{w}^k, \quad r^k = p^k - \pi_s p^k, \\ &\mathbf{E}_h^k = \Pi_s \mathbf{u}^k - \mathbf{U}^k, \quad \mathcal{E}_h^k = \Pi_w \mathbf{w}^k - \mathbf{W}^k, \quad e_h^k = \pi_s p^k - P^k. \end{aligned} \tag{2.27}$$

The interpolation errors $(\mathbf{S}^\tau, \mathbf{R}^\tau, r^\tau)$ are controlled by means of (1.18) and (2.15), so that the next step is to derive an energy estimate for the approximation errors $(\mathbf{E}_h^\tau, \mathcal{E}_h^\tau, e_h^\tau)$ which is a slight variation of that one obtained for $(\mathbf{U}^\tau, \mathbf{W}^\tau, P^\tau)$ in (2.24).

2.3.1 Error estimates for the Linear and Angular Velocities

The approximation errors $(\mathbf{E}_h^\tau, \mathcal{E}_h^\tau, e_h^\tau)$ satisfy the following energy identity:

$$\begin{aligned} &\|\mathbf{E}_h^k\|_{\mathbf{L}^2}^2 + (\jmath + 8\tau\nu_r)\|\mathcal{E}_h^k\|_{\mathbf{L}^2}^2 - \|\mathbf{E}_h^{k-1}\|_{\mathbf{L}^2}^2 - \jmath\|\mathcal{E}_h^{k-1}\|_{\mathbf{L}^2}^2 + 2\tau\widehat{\nu}\|\nabla\mathbf{E}_h^k\|_{\mathbf{L}^2}^2 \\ &\qquad + 2\tau c_1\|\nabla\mathcal{E}_h^k\|_{\mathbf{L}^2}^2 + \|\delta\mathbf{E}_h^k\|_{\mathbf{L}^2}^2 + \|\delta\mathcal{E}_h^k\|_{\mathbf{L}^2}^2 + 2\tau c_2\|div\,\mathcal{E}_h^k\|_{\mathbf{L}^2}^2 = \sum_{i=1}^{6} A_i \end{aligned} \tag{2.28}$$

with

$$A_1 = 2\tau\, b_h\big(\mathbf{U}^{k-1}, \mathbf{U}^k, \mathbf{E}_h^k\big) - 2\tau\, b_h\big(\mathbf{u}^k, \mathbf{u}^k, \mathbf{E}_h^k\big)\,,$$

$$A_2 = 2\jmath\tau\, b_h\big(\mathbf{U}^k, \mathbf{W}^k, \mathcal{E}_h^k\big) - 2\jmath\tau\, b_h\big(\mathbf{u}^k, \mathbf{w}^k, \mathcal{E}_h^k\big)\,,$$

$$A_3 = 4\tau\nu_r\big(curl\,\mathbf{w}^k - curl\,\mathbf{W}^{k-1}, \mathbf{E}_h^k\big)\,,$$

$$A_4 = 4\tau\nu_r\big(curl\,\mathbf{E}^k, \mathcal{E}_h^k\big)\,,$$

$$A_5 = -2\big(\delta\mathbf{S}^k, \mathbf{E}_h^k\big) - 2\jmath\big(\delta\mathbf{R}^k, \mathcal{E}_h^k\big)\,,$$

$$A_6 = 2\tau\big(\mathcal{R}_{\mathbf{u}}^k, \mathbf{E}_h^k\big) + 2\jmath\tau\big(\mathcal{R}_{\mathbf{w}}^k, \mathcal{E}_h^k\big)\,,$$

where $\mathcal{R}_{\mathbf{u}}^k$ and $\mathcal{R}_{\mathbf{w}}^k$ are integral representations of Taylor remainders (see for instance [45]), i.e.

$$\mathcal{R}_{\mathbf{u}}^k = \frac{1}{\tau}\int_{t^{k-1}}^{t^k} (t^{k-1}-s)\mathbf{u}_{tt}(s)\,ds \quad \text{and} \quad \mathcal{R}_{\mathbf{w}}^k = \frac{1}{\tau}\int_{t^{k-1}}^{t^k} (t^{k-1}-s)\mathbf{w}_{tt}(s)\,ds. \tag{2.29}$$

The main difficulty, and our focus from now on, is to estimate the residual terms A_i for $i = 1, \ldots, 6$.

Theorem 2.3.1 (Error estimate on velocities)**.** *Assume* (2.25)*, then*

$$\|\mathbf{E}_h^\tau\|_{\ell^\infty(\mathbf{L}^2)} + \|\mathcal{E}_h^\tau\|_{\ell^\infty(\mathbf{L}^2)} + h\left(\|\nabla\mathbf{E}_h^\tau\|_{\ell^2(\mathbf{L}^2)} + \|\nabla\mathcal{E}_h^\tau\|_{\ell^2(\mathbf{L}^2)}\right) \le c\,(\tau + h^{\ell+1}) \tag{2.30}$$

whenever

$$\tau \le \frac{1}{K} \quad \textit{with} \quad K \simeq \ \max\left\{\frac{M}{\nu_0}, \frac{\mathcal{M}\jmath^2}{c_1}, \frac{M\jmath^2}{c_1}, \frac{\nu_r^2}{c_1}, \frac{\nu_r^2}{\nu_0}\right\}, \tag{2.31}$$

where M and $\mathcal{M}$ satisfy

$$\begin{aligned} \sup_{t\in(0,t_F]} \left(\|\nabla\Pi_s\mathbf{u}\|_{\mathbf{L}^3} + \|\Pi_s\mathbf{u}\|_{\mathbf{L}^\infty}\right)^2 + \sup_{\Omega_{t_F}} |\mathbf{u}|^2 \le M < \infty, \\ \sup_{t\in(0,t_F]} \left(\|\nabla\Pi_w\mathbf{w}\|_{\mathbf{L}^3} + \|\Pi_w\mathbf{w}\|_{\mathbf{L}^\infty}\right)^2 + \sup_{\Omega_{t_F}} |\mathbf{w}|^2 \le \mathcal{M} < \infty. \end{aligned} \tag{2.32}$$

Proof. It suffices to provide bounds for the terms A_i above and employ the discrete Grönwall lemma 1.2.2. To begin with, notice that

$$\begin{aligned} b_h(\mathbf{U}^{k-1},\mathbf{U}^k,\mathbf{V}) - b_h(\mathbf{u}^k,\mathbf{u}^k,\mathbf{V}) &= -b_h(\delta\mathbf{u}^k,\mathbf{u}^k,\mathbf{V}) - b_h(\mathbf{u}^{k-1},\mathbf{S}^k,\mathbf{V}) \\ &\quad - b_h(\mathbf{S}^{k-1},\Pi_s\mathbf{u}^k,\mathbf{V}) - b_h(\mathbf{E}^{k-1},\Pi_s\mathbf{u}^k,\mathbf{V}) \\ &\quad + b_h(\mathbf{E}_h^{k-1},\mathbf{E}_h^k,\mathbf{V}) - b_h(\Pi_s\mathbf{u}^{k-1},\mathbf{E}_h^k,\mathbf{V}), \quad \forall\mathbf{V}\in\mathbb{U}, \end{aligned} \tag{2.33}$$

and

$$\begin{aligned} b_h\big(\mathbf{U}^k,\mathbf{W}^k,\mathbf{X}\big) - b_h\big(\mathbf{u}^k,\mathbf{w}^k,\mathbf{X}\big) &= -b_h\big(\mathbf{u}^k,\mathbf{R}^k,\mathbf{X}\big) + b_h\big(\mathbf{E}_h^k,\mathcal{E}_h^k,\mathbf{X}\big) \\ - b_h\big(\mathbf{E}_h^k,\Pi_w\mathbf{w}^k,\mathbf{X}\big) - b_h\big(\mathbf{S}^k,\Pi_w\mathbf{w}^k,\mathbf{X}\big) - b_h\big(\Pi_s\mathbf{u}^k,\mathcal{E}_h^k,\mathbf{X}\big), &\quad \forall\mathbf{X}\in\mathbb{U}. \end{aligned} \tag{2.34}$$

Set $\mathbf{V}=2\tau\mathbf{E}_h^k$ in (2.33). Since $b_h(\cdot,\cdot,\cdot)$ is skew-symmetric the last two terms vanish, and we can rewrite A_1 as:

$$\begin{aligned} A_1 &= -2\tau\, b_h\big(\delta\mathbf{u}^k,\mathbf{u}^k,\mathbf{E}_h^k\big) - 2\tau\, b_h\big(\mathbf{u}^{k-1},\mathbf{S}^k,\mathbf{E}_h^k\big) - 2\tau\, b_h(\mathbf{S}^{k-1},\Pi_s\mathbf{u}^k,\mathbf{E}_h^k) \\ &\quad - 2\tau\, b_h(\mathbf{E}_h^{k-1},\Pi_s\mathbf{u}^k,\mathbf{E}_h^k) \\ &= A_{11}+A_{12}+A_{13}+A_{14}. \end{aligned}$$

The functions $\delta\mathbf{u}^k$ and $\mathbf{u}^{k-1}$ are solenoidal so that the consistency of b_h yields control on A_{11} and A_{12}:

$$\begin{aligned} A_{11} &= 2\tau\, b_h\big(\delta\mathbf{u}^k,\mathbf{E}_h^k,\mathbf{u}^k\big) \le 2\tau\|\delta\mathbf{u}^k\|_{\mathbf{L}^2}\|\nabla\mathbf{E}_h^k\|_{\mathbf{L}^2}\|\mathbf{u}^k\|_{\mathbf{L}^\infty} \\ &\le \tfrac{\widehat{\nu}\tau}{9}\|\nabla\mathbf{E}_h^k\|_{\mathbf{L}^2}^2 + \tfrac{9M\tau}{\widehat{\nu}}\|\delta\mathbf{u}^k\|_{\mathbf{L}^2}^2 \\ A_{12} &= -2\tau\, b_h\big(\mathbf{u}^{k-1},\mathbf{S}^k,\mathbf{E}_h^k\big) \le 2\tau\ \|\mathbf{u}^{k-1}\|_{\mathbf{L}^\infty}\|\nabla\mathbf{E}_h^k\|_{\mathbf{L}^2}\|\mathbf{S}^k\|_{\mathbf{L}^2} \\ &\le \tfrac{\widehat{\nu}\tau}{9}\|\nabla\mathbf{E}_h^k\|_{\mathbf{L}^2}^2 + \tfrac{9M\tau}{\widehat{\nu}}\|\mathbf{S}^k\|_{\mathbf{L}^2}^2, \end{aligned}$$

where we have used (1.8) and (1.7). By (2.25), we deduce

$$\|\delta\mathbf{u}^k\|_{\mathbf{L}^2}^2 \le \tau\int_{t_{k-1}}^{t_k}\|\mathbf{u}_t\|_{\mathbf{L}^2}^2\,dt. \tag{2.35}$$

The terms A_{13} and A_{14} can be estimated via (2.19) as follows:

$$A_{13} + A_{14} \leq \tfrac{2\widehat{\nu}\tau}{9}\|\nabla \mathbf{E}_h^k\|_{\mathbf{L}^2}^2 + \tfrac{9M\tau^2}{\widehat{\nu}}\|\mathbf{S}^{k-1}\|_{\mathbf{L}^2}^2 + \tfrac{9M\tau^2}{\widehat{\nu}}\|\mathbf{E}_h^{k-1}\|_{\mathbf{L}^2}^2.$$

Set $\mathbf{X} = 2\tau\mathcal{E}_h^k$ in (2.34). We rewrite A_2 as

$$\begin{aligned} A_2 &= -2\jmath\tau\, b_h\big(\mathbf{u}^k, \mathbf{R}^k, \mathcal{E}_h^k\big) - 2\tau\jmath\, b_h\big(\mathbf{E}_h^k, \Pi_w\mathbf{w}^k, \mathcal{E}_h^k\big) - 2\tau\jmath\, b_h\big(\mathbf{S}^k, \Pi_w\mathbf{w}^k, \mathcal{E}_h^k\big) \\ &= A_{21} + A_{22} + A_{23}. \end{aligned}$$

Since $\mathbf{u}^k$ is solenoidal the bound on A_{21} proceeds as that of A_{12}, whereas (2.19) gives control on A_{22} and A_{23}:

$$A_2 \leq \tfrac{3c_1\tau}{7}\|\nabla\mathcal{E}_h^k\|_{\mathbf{L}^2}^2 + \tfrac{7M\jmath^2\tau}{c_1}\left(\|\mathbf{R}^k\|_{\mathbf{L}^2}^2 + \|\mathbf{E}_h^k\|_{\mathbf{L}^2}^2 + \|\mathbf{S}^k\|_{\mathbf{L}^2}^2\right).$$

The bound on A_3 begins by noticing that $\mathbf{w}^k - \mathbf{W}^{k-1} = \delta\mathbf{w}^k + \mathbf{R}^{k-1} + \mathcal{E}_h^{k-1}$. The integration by parts formula (1.1) then yields

$$A_3 = 4\tau\nu_r\big(\delta\mathbf{w}^k, curl\,\mathbf{E}_h^k\big) + 4\tau\nu_r\big(\mathbf{R}^{k-1}, curl\,\mathbf{E}_h^k\big) + 4\tau\nu_r\big(\mathcal{E}_h^{k-1}, curl\,\mathbf{E}_h^k\big),$$

whence

$$\begin{aligned} A_3 &\leq 4\tau\nu_r\|\delta\mathbf{w}^k\|_{\mathbf{L}^2}\|\nabla\mathbf{E}_h^k\|_{\mathbf{L}^2} + 4\tau\nu_r\|\mathbf{R}^{k-1}\|_{\mathbf{L}^2}\|\nabla\mathbf{E}_h^k\| + 4\tau\nu_r\|\mathcal{E}_h^{k-1}\|_{\mathbf{L}^2}\|\nabla\mathbf{E}_h^k\|_{\mathbf{L}^2} \\ &\leq \tfrac{\widehat{\nu}\tau}{3}\|\nabla\mathbf{E}_h^k\|_{\mathbf{L}^2}^2 + \tfrac{36\nu_r^2\tau}{\widehat{\nu}}\|\delta\mathbf{w}^k\|_{\mathbf{L}^2}^2 + \tfrac{36\nu_r^2\tau}{\widehat{\nu}}\|\mathbf{R}^{k-1}\|_{\mathbf{L}^2}^2 + \tfrac{36\nu_r^2\tau}{\widehat{\nu}}\|\mathcal{E}_h^{k-1}\|_{\mathbf{L}^2}^2. \end{aligned}$$

The term $\|\delta\mathbf{w}^k\|_{\mathbf{L}^2}^2$ can be bounded similarly to (2.35).

The bound on A_4 follows along the same lines as those of A_3:

$$\begin{aligned} A_4 &= 4\tau\nu_r\big(\mathbf{S}^k, curl\,\mathcal{E}_h^k\big) + 4\tau\nu_r\big(\mathbf{E}_h^k, curl\,\mathcal{E}_h^k\big) \\ &\leq \tfrac{2c_1\tau}{7}\|\nabla\mathcal{E}_h^k\|_{\mathbf{L}^2}^2 + \tfrac{28\nu_r^2\tau}{c_1}\|\mathbf{S}^k\|_{\mathbf{L}^2}^2 + \tfrac{28\nu_r^2\tau}{c_1}\|\mathbf{E}_h^k\|_{\mathbf{L}^2}^2. \end{aligned}$$

The last two terms A_5 and A_6 can be easily bounded as follows

$$A_5 = -2\big(\delta\mathbf{S}^k, \mathbf{E}_h^k\big) - 2\jmath\big(\delta\mathbf{R}^k, \mathcal{E}_h^k\big) \le \tfrac{\widehat{\nu}\tau}{9}\|\nabla\mathbf{E}_h^k\|_{\mathbf{L}^2}^2 + \tfrac{9c_p^2}{\widehat{\nu}\tau}\|\delta\mathbf{S}^k\|_{\mathbf{L}^2}^2 + \tfrac{c_1\tau}{7}\|\nabla\mathcal{E}_h^k\|_{\mathbf{L}^2}^2 + \tfrac{7c_p^2\jmath^2}{c_1\tau}\|\delta\mathbf{R}^k\|_{\mathbf{L}^2}^2,$$

and

$$A_6 = 2\tau\big(\mathcal{R}_{\mathbf{u}}^k, \mathbf{E}_h^k\big) + 2\tau\jmath\big(\mathcal{R}_{\mathbf{w}}^k, \mathcal{E}_h^k\big) \le \tfrac{\widehat{\nu}\tau}{9}\|\nabla\mathbf{E}_h^k\|_{\mathbf{L}^2}^2 + \tfrac{9c_p^2\tau}{\widehat{\nu}}\|\mathcal{R}_{\mathbf{u}}^k\|_{\mathbf{L}^2}^2 + \tfrac{c_1\tau}{7}\|\nabla\mathcal{E}_h^k\|_{\mathbf{L}^2}^2 + \tfrac{7c_p^2\jmath^2\tau}{c_1}\|\mathcal{R}_{\mathbf{w}}^k\|_{\mathbf{L}^2}^2.$$

The interpolation errors are bounded by (1.18) and (2.15) which, in conjunction with (2.25), also implies

$$\begin{aligned}\|\delta\mathbf{S}^k\|_{\mathbf{L}^2} + h\|\delta\nabla\mathbf{S}^k\|_{\mathbf{L}^2} &\le c\,\tau\,h^{\ell+1}\big(\|\mathbf{u}_t\|_{L^\infty(\mathbf{H}^{\ell+1})} + \|p_t\|_{L^\infty(H^\ell)}\big)\\ \|\delta\mathbf{R}^k\|_{\mathbf{L}^2} + h\|\delta\nabla\mathbf{R}^k\|_{\mathbf{L}^2} &\le c\,\tau\,h^{\ell+1}\|\mathbf{w}_t\|_{L^\infty(\mathbf{H}^{\ell+1})}\end{aligned} \tag{2.36}$$

Assumption (2.25) also gives an estimate on the truncation errors $\mathcal{R}_{\mathbf{u}}^k$ and $\mathcal{R}_{\mathbf{w}}^k$,

$$\|\mathcal{R}_{\mathbf{u}}^k\|_{\mathbf{L}^2}^2 \le \frac{\tau}{3}\int_{t^{k-1}}^{t^k}\|\mathbf{u}_{tt}\|_{\mathbf{L}^2}^2\,dt \quad , \quad \|\mathcal{R}_{\mathbf{w}}^k\|_{\mathbf{L}^2}^2 \le \frac{\tau}{3}\int_{t^{k-1}}^{t^k}\|\mathbf{w}_{tt}\|_{\mathbf{L}^2}^2\,dt. \tag{2.37}$$

Inserting the estimates above for A_i, $1 \le i \le 6$, into (2.28), summing in k and applying Grönwall's lemma 1.2.2 concludes the proof. □

Remark 2.3.1 (Smallness assumption on τ)**.** Condition (2.31) does not depend on the space discretization parameter h. It does depend, however, on the constants M and $\mathcal{M}$ defined in (2.32); this is standard for Navier-Stokes. In addition, this estimate depends on the quotients $\nu_r^2/\widehat{\nu}$ and ν_r^2/c_1, which gives an indication of how strong the coupling between linear and angular momentum is.

2.3.2 Error Estimates for the Discrete Time Derivative

When dealing with the Navier-Stokes equations, it is well-known (see, for instance, [54]) that in order to derive optimal error estimates for the pressure in $\ell^2(L^2(\Omega))$ one must first obtain estimates on the discrete time derivative of the velocity, which is the main reason for the additional regularity requested in (2.26). Our analysis is no exception, and this is additionally complicated by the fact that we must obtain error estimates for the derivatives of the linear and angular velocities.

Applying the increment operator δ, defined in (1.10), to the equations that govern the approximation errors and proceeding as in the proof of Proposition 2.2.1 we conclude that the discrete time derivatives $\tau^{-1}\delta\mathbf{E}_h^\tau$ and $\tau^{-1}\delta\mathcal{E}_h^\tau$ satisfy an energy identity similar to (2.28), namely,

$$\begin{aligned}
&\|\tau^{-1}\delta\mathbf{E}_h^k\|_{\mathbf{L}^2}^2 + (\jmath + 8\nu_r\tau)\|\tau^{-1}\delta\mathcal{E}_h^k\|_{\mathbf{L}^2}^2 - \|\tau^{-1}\delta\mathbf{E}_h^{k-1}\|_{\mathbf{L}^2}^2 - \jmath\|\tau^{-1}\delta\mathcal{E}_h^{k-1}\|_{\mathbf{L}^2}^2 \\
&\qquad + 2\widehat{\nu}\tau\|\tau^{-1}\delta\nabla\mathbf{E}_h^k\|_{\mathbf{L}^2}^2 + 2c_1\tau\|\tau^{-1}\delta\nabla\mathcal{E}_h^k\|^2 + \|\tau^{-1}\delta^2\mathbf{E}_h^k\|_{\mathbf{L}^2}^2 \\
&\qquad + \jmath\|\tau^{-1}\delta^2\mathcal{E}_h^k\|_{\mathbf{L}^2}^2 + 2c_2\tau\|\tau^{-1}div\,\delta\mathcal{E}_h^k\|_{\mathbf{L}^2}^2 = \sum_{i=1}^{5} F_i
\end{aligned} \tag{2.38}$$

where

$$\begin{aligned}
F_1 &= 2\,b_h\big(\mathbf{U}^{k-1},\mathbf{U}^k,\tau^{-1}\delta\mathbf{E}_h^k\big) - 2\,b_h\big(\mathbf{u}^k,\mathbf{u}^k,\tau^{-1}\delta\mathbf{E}_h^k\big) \\
&\quad - 2\,b_h\big(\mathbf{U}^{k-2},\mathbf{U}^{k-1},\tau^{-1}\delta\mathbf{E}_h^k\big) + 2\,b_h\big(\mathbf{u}^{k-1},\mathbf{u}^{k-1},\tau^{-1}\delta\mathbf{E}_h^k\big)\,, \\
F_2 &= 2\jmath\,b_h\big(\mathbf{U}^k,\mathbf{W}^k,\tau^{-1}\delta\mathcal{E}_h^k\big) - 2\jmath\,b_h\big(\mathbf{u}^k,\mathbf{w}^k,\tau^{-1}\delta\mathcal{E}_h^k\big)\,, \\
&\quad - 2\jmath\,b_h\big(\mathbf{U}^{k-1},\mathbf{W}^{k-1},\tau^{-1}\delta\mathcal{E}_h^k\big) + 2\jmath\,b_h\big(\mathbf{u}^{k-1},\mathbf{w}^{k-1},\tau^{-1}\delta\mathcal{E}_h^k\big)\,, \\
F_3 &= 4\nu_r\big(curl\,\delta\mathbf{w}^k - curl\,\delta\mathbf{W}^{k-1},\tau^{-1}\delta\mathbf{E}_h^k\big) + 4\nu_r\big(curl\,\delta\mathbf{u}^k - curl\,\delta\mathbf{U}^k,\tau^{-1}\delta\mathcal{E}_h^k\big)\,, \\
F_4 &= -2\tau^{-1}\big(\delta^2\mathbf{S}^k,\tau^{-1}\delta\mathbf{E}_h^k\big) - 2\jmath\tau^{-1}\big(\delta^2\mathbf{R}^k,\tau^{-1}\delta\mathcal{E}_h^k\big)\,,
\end{aligned}$$

$$F_5 = 2\big(\delta\mathcal{R}^k_{\mathbf{u}}, \tau^{-1}\delta\mathbf{E}^k_h\big) + 2\jmath\big(\delta\mathcal{R}^k_{\mathbf{w}}, \tau^{-1}\delta\mathcal{E}^k_h\big).$$

A bound on these terms then yields a bound on the discrete time derivatives. This is the content of the following result.

Theorem 2.3.2 (Error estimate for the discrete time derivatives)**.** *Assume* (2.26)*, if*

$$h^{-1/2}\|\mathbf{E}^\tau_h\|_{\ell^\infty(\mathbf{L}^2)} \qquad \textit{and} \qquad h^{-1/2}\|\mathcal{E}^\tau_h\|_{\ell^\infty(\mathbf{L}^2)} \tag{2.39}$$

are sufficiently small, then

$$\left\|\tfrac{\delta\mathbf{E}^\tau_h}{\tau}\right\|_{\ell^\infty(\mathbf{L}^2)} + \left\|\tfrac{\delta\mathcal{E}^\tau_h}{\tau}\right\|_{\ell^\infty(\mathbf{L}^2)} \leq c\,(\tau + h^\ell). \tag{2.40}$$

Proof. In analogy to Theorem 2.3.1, it suffices to bound the residual terms $\{F_i\}_{i=1}^5$. The proof is rather technical and tedious, and consists of careful manipulations of these five terms. Take the difference of (2.33) for two consecutive time-steps, which allows us to write F_1 as the sum of six terms $\{F_{1i}\}_{i=1}^6$:

$$\begin{aligned}
F_{11} &= -2\,b(\delta\mathbf{u}^k, \mathbf{u}^k, \tau^{-1}\delta\mathbf{E}^k_h) + 2\,b(\delta\mathbf{u}^{k-1}, \mathbf{u}^{k-1}, \tau^{-1}\delta\mathbf{E}^k_h)\,,\\
F_{12} &= -2\,b(\mathbf{u}^{k-1}, \mathbf{S}^k, \tau^{-1}\delta\mathbf{E}^k_h) + 2\,b(\mathbf{u}^{k-2}, \mathbf{S}^{k-1}, \tau^{-1}\delta\mathbf{E}^k_h)\,,\\
F_{13} &= -2\,b_h(\mathbf{S}^{k-1}, \Pi_s\mathbf{u}^k, \tau^{-1}\delta\mathbf{E}^k_h) + 2\,b_h(\mathbf{S}^{k-2}, \Pi_s\mathbf{u}^{k-1}, \tau^{-1}\delta\mathbf{E}^k_h)\,,\\
F_{14} &= -2\,b_h(\mathbf{E}^{k-1}_h, \Pi_s\mathbf{u}^k, \tau^{-1}\delta\mathbf{E}^k_h) + 2\,b_h(\mathbf{E}^{k-2}_h, \Pi_s\mathbf{u}^{k-1}, \tau^{-1}\delta\mathbf{E}^k_h)\,,\\
F_{15} &= 2\,b_h(\mathbf{E}^{k-1}_h, \mathbf{E}^k_h, \tau^{-1}\delta\mathbf{E}^k_h) - 2\,b_h(\mathbf{E}^{k-2}_h, \mathbf{E}^{k-1}_h, \tau^{-1}\delta\mathbf{E}^k_h)\,,\\
F_{16} &= -2\,b_h(\Pi_s\mathbf{u}^{k-1}, \mathbf{E}^k_h, \tau^{-1}\delta\mathbf{E}^k_h) + 2\,b_h(\Pi_s\mathbf{u}^{k-2}, \mathbf{E}^{k-1}_h, \tau^{-1}\delta\mathbf{E}^k_h).
\end{aligned}$$

Using the linearity and skew-symmetry of the trilinear form, these six terms can be appropriately rewritten and bounded using (1.6)-(1.8) and (2.18)-(2.20) to get

$$
\begin{aligned}
F_{11} &= 2\,b(\delta\mathbf{u}^k, \tau^{-1}\delta\mathbf{E}_h^k, \delta\mathbf{u}^k) + 2\,b(\delta^2\mathbf{u}^k, \tau^{-1}\delta\mathbf{E}_h^k, \mathbf{u}^{k-1}) \\
&\le \tfrac{\widehat{\nu}_\tau}{14}\|\tau^{-1}\delta\nabla\mathbf{E}_h^k\|_{\mathbf{L}^2}^2 + \tfrac{c}{\widehat{\nu}_\tau}\|\delta\nabla\mathbf{u}^k\|_{\mathbf{L}^2}^4 + \tfrac{\widehat{\nu}_\tau}{14}\|\tau^{-1}\delta\nabla\mathbf{E}_h^k\|_{\mathbf{L}^2} + \tfrac{M}{\widehat{\nu}_\tau}\|\delta^2\mathbf{u}^k\|_{\mathbf{L}^2}^2, \\
F_{12} &= 2\,b(\mathbf{u}^{k-1}, \tau^{-1}\delta\mathbf{E}_h^k, \delta\mathbf{S}^k) + 2\,b(\delta\mathbf{u}^{k-1}, \tau^{-1}\delta\mathbf{E}_h^k, \mathbf{S}^{k-1}) \\
&\le \tfrac{\widehat{\nu}_\tau}{14}\|\tau^{-1}\delta\nabla\mathbf{E}_h^k\|_{\mathbf{L}^2}^2 + \tfrac{M}{\widehat{\nu}_\tau}\|\delta\mathbf{S}^k\|_{\mathbf{L}^2}^2 + \tfrac{\widehat{\nu}_\tau}{14}\|\tau^{-1}\delta\nabla\mathbf{E}_h^k\|_{\mathbf{L}^2}^2 \\
&\quad + \tfrac{c}{\widehat{\nu}_\tau}\|\delta\nabla\mathbf{u}^{k-1}\|_{\mathbf{L}^2}^2\|\nabla\mathbf{S}^{k-1}\|_{\mathbf{L}^2}^2, \\
F_{13} &= -2\,b_h(\delta\mathbf{S}^{k-1}, \Pi_s\mathbf{u}^k, \tau^{-1}\delta\mathbf{E}_h^k) - 2\,b_h(\mathbf{S}^{k-2}, \delta\Pi_s\mathbf{u}^{k-1}, \tau^{-1}\delta\mathbf{E}_h^k) \\
&\le \tfrac{\widehat{\nu}_\tau}{14}\|\tau^{-1}\delta\nabla\mathbf{E}_h^k\|_{\mathbf{L}^2}^2 + \tfrac{M}{\widehat{\nu}_\tau}\|\delta\mathbf{S}^{k-1}\|_{\mathbf{L}^2}^2 + \tfrac{\widehat{\nu}_\tau}{14}\|\tau^{-1}\delta\nabla\mathbf{E}_h^k\|_{\mathbf{L}^2}^2 \\
&\quad + \tfrac{c}{\widehat{\nu}_\tau}\|\delta\nabla\Pi_s\mathbf{u}^{k-1}\|_{\mathbf{L}^2}^2\|\nabla\mathbf{S}^{k-2}\|_{\mathbf{L}^2}^2, \\
F_{14} &= -2\tau\,b_h(\tau^{-1}\delta\mathbf{E}_h^{k-1}, \Pi_s\mathbf{u}^k, \tau^{-1}\delta\mathbf{E}_h^k) - 2\,b_h(\mathbf{E}_h^{k-2}, \delta\Pi_s\mathbf{u}^k, \tau^{-1}\delta\mathbf{E}_h^k) \\
&\le \tfrac{\widehat{\nu}_\tau}{14}\|\tau^{-1}\delta\nabla\mathbf{E}_h^k\|_{\mathbf{L}^2}^2 + \tfrac{M\tau^2}{\widehat{\nu}_\tau}\|\tau^{-1}\delta\mathbf{E}_h^{k-1}\|_{\mathbf{L}^2}^2 + \tfrac{\widehat{\nu}_\tau}{14}\|\tau^{-1}\delta\nabla\mathbf{E}_h^k\|_{\mathbf{L}^2}^2 \\
&\quad + \tfrac{c}{\widehat{\nu}_\tau}\|\delta\nabla\Pi_s\mathbf{u}^k\|_{\mathbf{L}^2}^2\|\nabla\mathbf{E}_h^{k-2}\|_{\mathbf{L}^2}^2, \\
F_{15} &= 2\tau\,b_h(\tau^{-1}\delta\mathbf{E}_h^{k-1}, \mathbf{E}_h^{k-1}, \tau^{-1}\delta\mathbf{E}_h^k) \\
&\le \tfrac{c\|\mathbf{E}_h^{k-1}\|_{\mathbf{L}^2}}{h^{1/2}}\tau\left(\|\tau^{-1}\delta\nabla\mathbf{E}_h^{k-1}\|_{\mathbf{L}^2}^2 + \|\tau^{-1}\delta\nabla\mathbf{E}_h^k\|_{\mathbf{L}^2}^2\right), \\
F_{16} &= -2\,b_h(\delta\Pi_s\mathbf{u}^{k-1}, \mathbf{E}_h^k, \tau^{-1}\delta\mathbf{E}_h^k) \le \tfrac{\widehat{\nu}_\tau}{14}\|\tau^{-1}\delta\nabla\mathbf{E}_h^k\|_{\mathbf{L}^2}^2 \\
&\quad + \tfrac{c}{\widehat{\nu}_\tau}\|\delta\nabla\Pi_s\mathbf{u}^{k-1}\|_{\mathbf{L}^2}^2\|\nabla\mathbf{E}_h^k\|_{\mathbf{L}^2}^2\,.
\end{aligned}
$$

Similarly, applying δ to (2.34), F_2 can be expressed as the sum of five terms $\{F_{2i}\}_{i=1}^5$:

$$
\begin{aligned}
F_{21} &= -2\jmath\,b_h\big(\mathbf{u}^k, \mathbf{R}^k, \tau^{-1}\delta\mathcal{E}_h^k\big) + 2\jmath\,b_h\big(\mathbf{u}^{k-1}, \mathbf{R}^{k-1}, \tau^{-1}\delta\mathcal{E}_h^k\big), \\
F_{22} &= 2\jmath\,b_h\big(\mathbf{E}_h^k, \mathcal{E}_h^k, \tau^{-1}\delta\mathcal{E}_h^k\big) - 2\jmath\,b_h\big(\mathbf{E}_h^{k-1}, \mathcal{E}_h^{k-1}, \tau^{-1}\delta\mathcal{E}_h^k\big), \\
F_{23} &= -2\jmath\,b_h\big(\mathbf{E}_h^k, \Pi_w\mathbf{w}^k, \tau^{-1}\delta\mathcal{E}_h^k\big) + 2\jmath\,b_h\big(\mathbf{E}_h^{k-1}, \Pi_w\mathbf{w}^{k-1}, \tau^{-1}\delta\mathcal{E}_h^k\big), \\
F_{24} &= -2\jmath\,b_h\big(\mathbf{S}^k, \Pi_w\mathbf{w}^k, \tau^{-1}\delta\mathcal{E}_h^k\big) + 2\jmath\,b_h\big(\mathbf{S}^{k-1}, \Pi_w\mathbf{w}^{k-1}, \tau^{-1}\delta\mathcal{E}_h^k\big),
\end{aligned}
$$

$$F_{25} = -2\jmath\, b_h\big(\Pi_s \mathbf{u}^k, \mathcal{E}_h^k, \tau^{-1}\delta\mathcal{E}_h^k\big) + 2\jmath\, b_h\big(\Pi_s \mathbf{u}^{k-1}, \mathcal{E}_h^{k-1}, \tau^{-1}\delta\mathcal{E}_h^k\big).$$

We now bound each of these terms separately

$$\begin{aligned}
F_{21} &= -2\jmath\, b_h\big(\delta\mathbf{u}^k, \mathbf{R}^k, \tau^{-1}\delta\mathcal{E}_h^k\big) + 2\jmath\, b_h\big(\mathbf{u}^{k-1}, \delta\mathbf{R}^k, \tau^{-1}\delta\mathcal{E}_h^k\big)\\
&\le \tfrac{c_1\tau}{12}\|\tau^{-1}\delta\nabla\mathcal{E}_h^k\|_{\mathbf{L}^2}^2 + \tfrac{c\jmath^2}{c_1\tau}\|\delta\nabla\mathbf{u}^k\|_{\mathbf{L}^2}^2\|\nabla\mathbf{R}^k\|_{\mathbf{L}^2}^2 + \tfrac{c_1\tau}{12}\|\tau^{-1}\delta\nabla\mathcal{E}_h^k\|_{\mathbf{L}^2}^2\\
&\quad + \tfrac{M\jmath^2}{c_1\tau}\|\delta\mathbf{R}^k\|_{\mathbf{L}^2}^2,\\
F_{22} &= 2\jmath\tau\, b_h\big(\tau^{-1}\delta\mathbf{E}_h^k, \mathcal{E}_h^k, \tau^{-1}\delta\mathcal{E}_h^k\big)\\
&\le \tfrac{c\|\mathcal{E}_h^k\|_{\mathbf{L}^2}}{h^{1/2}}\jmath\tau\left(\|\tau^{-1}\delta\nabla\mathbf{E}_h^k\|_{\mathbf{L}^2}^2 + \|\tau^{-1}\delta\nabla\mathcal{E}_h^k\|_{\mathbf{L}^2}^2\right),\\
F_{23} &= -2\jmath\, b_h\big(\mathbf{E}_h^k, \delta\Pi_w\mathbf{w}^k, \tau^{-1}\delta\mathcal{E}_h^k\big) + 2\jmath\tau\, b_h\big(\tau^{-1}\delta\mathbf{E}_h^k, \Pi_w\mathbf{w}^{k-1}, \tau^{-1}\delta\mathcal{E}_h^k\big)\\
&\le \tfrac{c_1\tau}{12}\|\tau^{-1}\delta\nabla\mathcal{E}_h^k\|_{\mathbf{L}^2}^2 + \tfrac{c\jmath^2}{c_1\tau}\|\delta\nabla\mathbf{w}_h^k\|_{\mathbf{L}^2}^2\|\nabla\mathbf{E}_h^k\|_{\mathbf{L}^2}^2 + \tfrac{c_1\tau}{12}\|\tau^{-1}\delta\nabla\mathcal{E}_h^k\|_{\mathbf{L}^2}^2\\
&\quad + \tfrac{\mathcal{M}\jmath^2\tau^2}{c_1\tau}\|\tau^{-1}\delta\mathbf{E}_h^k\|_{\mathbf{L}^2}^2,\\
F_{24} &= -2\jmath\, b_h\big(\delta\mathbf{S}^k, \Pi_w\mathbf{w}^k, \tau^{-1}\delta\mathcal{E}_h^k\big) - 2\jmath\, b_h\big(\mathbf{S}^{k-1}, \delta\Pi_w\mathbf{w}^k, \tau^{-1}\delta\mathcal{E}_h^k\big)\\
&\le \tfrac{c_1\tau}{12}\|\tau^{-1}\delta\nabla\mathcal{E}_h^k\|_{\mathbf{L}^2}^2 + \tfrac{\mathcal{M}\jmath^2}{\varepsilon_2}\|\delta\mathbf{S}^k\|_{\mathbf{L}^2}^2 + \tfrac{c_1\tau}{12}\|\tau^{-1}\delta\nabla\mathcal{E}_h^k\|_{\mathbf{L}^2}^2\\
&\quad + \tfrac{c\jmath^2}{c_1\tau}\|\delta\nabla\mathbf{w}_h^k\|_{\mathbf{L}^2}^2\|\nabla\mathbf{S}^{k-1}\|_{\mathbf{L}^2}^2,\\
F_{25} &= -2\jmath\, b_h\big(\delta\Pi_s\mathbf{u}^k, \mathcal{E}_h^k, \tau^{-1}\delta\mathcal{E}_h^k\big) - 2\jmath\, b_h\big(\Pi_s\mathbf{u}^{k-1}, \delta\mathcal{E}_h^k, \tau^{-1}\delta\mathcal{E}_h^k\big)\\
&\le \tfrac{c_1\tau}{12}\|\tau^{-1}\delta\nabla\mathcal{E}_h^k\|_{\mathbf{L}^2}^2 + \tfrac{c\jmath^2}{c_1\tau}\|\delta\nabla\mathbf{u}_h^k\|_{\mathbf{L}^2}^2\|\nabla\mathcal{E}_h^k\|_{\mathbf{L}^2}^2 + \tfrac{c_1\tau}{12}\|\tau^{-1}\delta\nabla\mathcal{E}_h^k\|_{\mathbf{L}^2}^2\\
&\quad + \tfrac{M\jmath^2}{c_1\tau}\|\delta\mathcal{E}_h^k\|_{\mathbf{L}^2}^2.
\end{aligned}$$

By virtue of (1.1), F_3 can be estimated as follows:

$$\begin{aligned}
F_3 &= 4\nu_r\big(\delta^2\mathbf{w}^k + \delta\mathbf{R}^{k-1} + \delta\mathcal{E}_h^{k-1}, \tau^{-1}curl\,\delta\mathbf{E}_h^k\big) + 4\nu_r\big(\delta\mathbf{S}^k + \delta\mathbf{E}_h^k, \tau^{-1}curl\,\delta\mathcal{E}_h^k\big)\\
&\le \tfrac{3}{14}\widehat{\nu}\tau\|\tau^{-1}\delta\nabla\mathbf{E}_h^k\|_{\mathbf{L}^2}^2 + \tfrac{56\nu_r^2}{\tau\widehat{\nu}}\left(\|\delta^2\mathbf{w}^k\|_{\mathbf{L}^2}^2 + \|\delta\mathbf{R}^{k-1}\|_{\mathbf{L}^2}^2 + \|\delta\mathcal{E}_h^{k-1}\|_{\mathbf{L}^2}^2\right)\\
&\quad + \tfrac{c_1\tau}{6}\|\delta\nabla\mathcal{E}_h^k\|_{\mathbf{L}^2} + \tfrac{48\nu_r^2}{\tau c_1}\left(\|\delta\mathbf{S}^k\|_{\mathbf{L}^2}^2 + \|\delta\mathbf{E}_h^k\|_{\mathbf{L}^2}^2\right).
\end{aligned}$$

The last two terms F_4 and F_5 require no further manipulation and result in

$$F_4 \leq \tfrac{\widehat{\nu}\tau}{14}\|\tau^{-1}\delta\nabla\mathbf{E}_h^k\|_{\mathbf{L}^2}^2 + \tfrac{14c_p^2\tau^{-2}}{\widehat{\nu}\tau}\|\delta^2\mathbf{S}^k\|_{\mathbf{L}^2}^2 + \tfrac{c_1\tau}{12}\|\tau^{-1}\delta\nabla\mathcal{E}_h^k\|_{\mathbf{L}^2}^2$$
$$+ \tfrac{12c_p^2\tau^{-3}\jmath^2}{c_1}\|\delta^2\mathbf{R}^k\|_{\mathbf{L}^2}^2,$$
$$F_5 \leq \tfrac{\widehat{\nu}\tau}{14}\|\tau^{-1}\delta\nabla\mathbf{E}_h^k\|_{\mathbf{L}^2}^2 + \tfrac{14c_p^2}{\widehat{\nu}\tau}\|\delta\mathcal{R}_{\mathbf{u}}^k\|_{\mathbf{L}^2}^2 + \tfrac{c_1\tau}{12}\|\tau^{-1}\delta\nabla\mathcal{E}_h^k\|_{\mathbf{L}^2}^2 + \tfrac{12c_p^2\jmath^2}{c_1\tau}\|\delta\mathcal{R}_{\mathbf{w}}^k\|_{\mathbf{L}^2}^2.$$

Collecting all the estimates for $\|\tau^{-1}\delta\nabla\mathbf{E}_h^k\|_{\mathbf{L}^2}^2$ and $\|\tau^{-1}\delta\nabla\mathcal{E}_h^k\|_{\mathbf{L}^2}^2$, and using assumption (2.39), we get

$$\tfrac{2C\|\mathbf{E}_h^k\|_{\mathbf{L}^2}}{h^{1/2}}\tau + \tfrac{C\jmath\|\mathcal{E}_h^k\|_{\mathbf{L}^2}}{h^{1/2}}\tau \leq \widehat{\nu}\tau \qquad \tfrac{2C\jmath\|\mathcal{E}_h^k\|_{\mathbf{L}^2}}{h^{1/2}}\tau \leq c_1\tau.$$

These conditions allow for cancellation of the problematic terms F_{15} and F_{22} with the fifth and sixth terms on the left hand side of (2.38). Finally, summation of the energy identity (2.38) and application of discrete Grönwall's lemma lead to (2.40). □

Remark 2.3.2 (Smallness assumption)**.** The error estimates of Theorem 2.3.2 hinge on the smallness assumption (2.39) which, in light of (2.30), can be recast as

$$\tau h^{-1/2} \leq c_s \tag{2.41}$$

for a small enough constant c_s. This requirement is not a special characteristic of our method but rather a recurrent feature in the analysis of schemes for the Navier-Stokes equations. See, for instance [54, 50].

2.3.3 Error Estimates for the Pressure

The control on the derivatives of the velocities provided by Theorem 2.3.2 enables us to obtain error estimates for the pressure. To do so, it is crucial that the discrete

spaces are compatible in the sense of (1.14). This is the idea behind the following result.

Theorem 2.3.3 (Error estimate for the pressure)**.** *If* (2.26) *and* (2.40) *are valid, then the following estimate holds*

$$\|e_h^\tau\|_{\ell^2(L^2)} \leq c\left(\tau + h^\ell\right). \tag{2.42}$$

Proof. As already mentioned, the approximation errors $\mathbf{E}_h^\tau$ and e_h^τ are actually solutions to (2.22) with a special right hand side composed of consistency terms. Condition (1.14) then allows us to write

$$\beta^* \|e_h^k\|_{L^2(\Omega)} \leq \sup_{\mathbf{V}\in\mathbb{U}} \frac{(e_h^k, div\,\mathbf{V})}{\|\mathbf{V}\|_{\mathbf{H}_0^1}} \leq \sum_{i=1}^{6} B_i, \tag{2.43}$$

where

$$\begin{aligned}
B_1 &= \sup_{\mathbf{V}\in\mathbb{U}} \frac{\tau^{-1}\big(\delta\mathbf{E}_h^k, \mathbf{V}\big)}{\|\mathbf{V}\|_{\mathbf{H}_0^1}},\\
B_2 &= \widehat{\nu} \sup_{\mathbf{V}\in\mathbb{U}} \frac{\big(\nabla\mathbf{E}_h^k, \nabla\mathbf{V}\big)}{\|\mathbf{V}\|_{\mathbf{H}_0^1}},\\
B_3 &= \sup_{\mathbf{V}\in\mathbb{U}} \frac{b_h(\mathbf{u}^k, \mathbf{u}^k, \mathbf{V}) - b_h(\mathbf{U}^{k-1}, \mathbf{U}^k, \mathbf{V})}{\|\mathbf{V}\|_{\mathbf{H}_0^1}},\\
B_4 &= 2\nu_r \sup_{\mathbf{V}\in\mathbb{U}} \frac{(curl\,\mathbf{W}^{k-1} - curl\,\mathbf{w}^k, \mathbf{V})}{\|\mathbf{V}\|_{\mathbf{H}_0^1}},\\
B_5 &= \sup_{\mathbf{V}\in\mathbb{U}} \frac{\tau^{-1}\big(\delta\mathbf{S}^k, \mathbf{V}\big)}{\|\mathbf{V}\|_{\mathbf{H}_0^1}},\\
B_6 &= \sup_{\mathbf{V}\in\mathbb{U}} \frac{(\mathcal{R}_{\mathbf{u}}^k, \mathbf{V})}{\|\mathbf{V}\|_{\mathbf{H}_0^1}}.
\end{aligned}$$

So that it suffices to provide suitable bounds for each one of these terms.

We readily have, for B_1 and B_2, that

$$B_1 = \sup_{\mathbf{V}\in\mathbb{U}} \frac{\tau^{-1}\big(\delta\mathbf{E}_h^k, \mathbf{V}\big)}{\|\mathbf{V}\|_{\mathbf{H}_0^1}} \lesssim \left\|\tau^{-1}\delta\mathbf{E}_h^k\right\|_{\mathbf{L}^2}, \quad B_2 \lesssim \|\nabla\mathbf{E}_h^k\|_{\mathbf{L}^2}.$$

Identity (2.33) can be used to express the numerator of B_3 as

$$B_3 \leq \sup_{\mathbf{V}\in\mathbb{U}} \frac{b_h(\delta\mathbf{u}^k, \mathbf{u}^k, \mathbf{V})}{\|\mathbf{V}\|_{\mathbf{H}_0^1}} + \sup_{\mathbf{V}\in\mathbb{U}} \frac{b_h(\mathbf{u}^{k-1}, \mathbf{S}^k, \mathbf{V})}{\|\mathbf{V}\|_{\mathbf{H}_0^1}} + \sup_{\mathbf{V}\in\mathbb{U}} \frac{b_h(\mathbf{E}^{k-1}, \Pi_s\mathbf{u}^k, \mathbf{V})}{\|\mathbf{V}\|_{\mathbf{H}_0^1}}$$
$$+ \sup_{\mathbf{V}\in\mathbb{U}} \frac{b_h(\mathbf{E}_h^{k-1}, \mathbf{E}_h^k, \mathbf{V})}{\|\mathbf{V}\|_{\mathbf{H}_0^1}} + \sup_{\mathbf{V}\in\mathbb{U}} \frac{b_h(\Pi_s\mathbf{u}^{k-1}, \mathbf{E}_h^k, \mathbf{V})}{\|\mathbf{V}\|_{\mathbf{H}_0^1}} = \sum_{i=1}^{5} B_{3i}.$$

Inequality (1.9) and the regularity assumptions (2.25) imply

$$B_{31} = \sup_{\mathbf{V}\in\mathbb{U}} \frac{b_h(\delta\mathbf{u}^k, \mathbf{u}^k, \mathbf{V})}{\|\mathbf{V}\|_{\mathbf{H}_0^1}} \lesssim \|\mathbf{u}^k\|_{\mathbf{H}^2}\|\delta\mathbf{u}^k\|_{\mathbf{L}^2} \lesssim \|\delta\mathbf{u}^k\|_{\mathbf{L}^2}.$$

To bound B_{32}, B_{33} and B_{35} we use inequality (2.18), the stability (1.19) of the projectors and the regularity assumptions (2.25),

$$B_{32} = \sup_{\mathbf{V}\in\mathbb{U}} \frac{b_h(\mathbf{u}^{k-1}, \mathbf{S}^k, \mathbf{V})}{\|\mathbf{V}\|_{\mathbf{H}_0^1}} \lesssim \|\nabla\mathbf{u}^{k-1}\|_{\mathbf{L}^2}\|\nabla\mathbf{S}^k\|_{\mathbf{L}^2} \lesssim \|\nabla\mathbf{S}^k\|_{\mathbf{L}^2},$$
$$B_{33} = \sup_{\mathbf{V}\in\mathbb{U}} \frac{b_h(\mathbf{E}^{k-1}, \Pi_s\mathbf{u}^k, \mathbf{V})}{\|\mathbf{V}\|_{\mathbf{H}_0^1}} \lesssim \|\nabla\mathbf{E}^{k-1}\|_{\mathbf{L}^2}\|\nabla\Pi_s\mathbf{u}^k\|_{\mathbf{L}^2} \lesssim \|\nabla\mathbf{E}^{k-1}\|_{\mathbf{L}^2},$$
$$B_{35} = \sup_{\mathbf{V}\in\mathbb{U}} \frac{b_h(\Pi_s\mathbf{u}^{k-1}, \mathbf{E}_h^k, \mathbf{V})}{\|\mathbf{V}\|_{\mathbf{H}_0^1}} \lesssim \|\nabla\Pi_s\mathbf{u}^{k-1}\|_{\mathbf{L}^2}\|\nabla\mathbf{E}_h^k\|_{\mathbf{L}^2} \lesssim \|\nabla\mathbf{E}_h^k\|_{\mathbf{L}^2}.$$

The first inequality in (2.20) yields

$$B_{34} = \sup_{\mathbf{V}\in\mathbb{U}} \frac{b_h(\mathbf{E}_h^{k-1}, \mathbf{E}_h^k, \mathbf{V})}{\|\mathbf{V}\|_{\mathbf{H}_0^1}} \lesssim h^{-1/2}\|\mathbf{E}_h^{k-1}\|_{\mathbf{L}^2}\|\nabla\mathbf{E}_h^k\|_{\mathbf{L}^2}.$$

In conclusion, we have proved the bound

$$|B_3| \lesssim \|\delta\mathbf{u}^k\|_{\mathbf{L}^2} + \|\nabla\mathbf{S}^k\|_{\mathbf{L}^2} + \|\nabla\mathbf{S}^{k-1}\|_{\mathbf{L}^2} + \|\nabla\mathbf{E}_h^{k-1}\|_{\mathbf{L}^2}$$
$$+ h^{-1/2}\,\|\mathbf{E}_h^{k-1}\|_{\mathbf{L}^2}\|\nabla\mathbf{E}_h^k\|_{\mathbf{L}^2} + \|\nabla\mathbf{E}_h^k\|_{\mathbf{L}^2}.$$

Integrating by parts as in (1.1), we infer that

$$B_4 = 2\nu_r \sup_{\mathbf{V}\in\mathbb{U}} \frac{(curl\,\mathbf{W}^{k-1} - curl\,\mathbf{w}^k, \mathbf{V})}{\|\mathbf{V}\|_{\mathbf{H}_0^1}} = \sup_{\mathbf{V}\in\mathbf{H}_0^1(\Omega)} \frac{(\delta\mathbf{w}^k + \mathcal{E}^{k-1}, curl\,\mathbf{V})}{\|\mathbf{V}\|_{\mathbf{H}_0^1}}$$

$$\lesssim \|\delta\mathbf{w}^k\|_{\mathbf{L}^2} + \|\mathcal{E}^{k-1}\|_{\mathbf{L}^2}.$$

Finally, we see that

$$B_5 = \sup_{\mathbf{V}\in\mathbb{U}} \frac{\tau^{-1}\big(\delta\mathbf{S}^k, \mathbf{V}\big)}{\|\mathbf{V}\|_{\mathbf{H}_0^1}} \lesssim \tau^{-1}\|\delta\mathbf{S}^k\|_{\mathbf{L}^2} \ , \quad B_6 = \sup_{\mathbf{V}\in\mathbf{H}_0^1(\Omega)} \frac{(\mathcal{R}_{\mathbf{u}}^k, \mathbf{V})}{\|\mathbf{V}\|_{\mathbf{H}_0^1}} \lesssim \|\mathcal{R}_{\mathbf{u}}^k\|_{\mathbf{L}^2}.$$

It suffices now to realize that all the bounds involve consistency, interpolation or approximation errors and that they all have the right order. This concludes the proof. □

2.4 A Second Order Scheme

Let us present a second order scheme for the solution of (2.5) and show its stability properties. We first recall a three-term recursion inequality originally shown in [69], which is instrumental to show stability.

Proposition 2.4.1 (Three-term recursion)**.** *The three-term recursion equation*

$$3x^{k+1} - 4x^k + x^{k-1} = g^{k+1}, \quad \forall k \geq 1, \tag{2.44}$$

has the following general solution

$$x^\nu = c_1 + \frac{c_2}{3^\nu} + \sum_{l=2}^{\nu} \frac{1}{3^{\nu+1-l}} \sum_{s=2}^{l} g^s, \qquad c_1,\ c_2 \in \mathbb{R}.$$

Let $\{y^k\}_{k\geq 0}$ be the solution to the three-term recursion inequality

$$3y^{k+1} - 4y^k + y^{k-1} \leq g^{k+1}, \quad \forall k \geq 1,$$

with initial data y^0 and y^1. If $\{x^k\}_{k\geq 0}$ is the solution to (2.44) *with initial data $x^0 = y^0$ and $x^1 = y^1$, then the following estimate holds*

$$y^\nu \leq x^\nu, \quad \forall \nu \geq 0.$$

Proof. See [69]. □

For $\{y^k\}_{k\geq 0}$ let $\delta_-^2 y^k$ denote the second-order backward difference, i.e.

$$\delta_-^2 y^k = \tfrac{1}{2}(3y^{k+1} - 4y^k + y^{k-2}) \quad \forall k \geq 2.$$

Let us now describe the scheme. We begin with an initialization step, in which we set

$$\left(\mathbf{U}^k, P^k, \mathbf{W}^k\right) = \left(\Pi_s \mathbf{u}^k, \pi_s p^k, \Pi_w \mathbf{w}^k\right), \quad k = 0, 1.$$

In other words, we compute the Stokes and elliptic-like projections of the initial data and the solution on the first time step. This initialization is only for ease of presentation as it clearly requires knowledge of the exact solution. In practice one can compute the projection of the initial data and then perform one step with the first-order scheme of § 2.2.

We march in time, for $k = 2, \ldots, K$, as follows:

Linear Momentum: Find $(\mathbf{U}^k, P^k) \in \mathbb{U} \times \mathbb{P}$ that solves

$$\begin{aligned}\left(\frac{\delta_-^2 \mathbf{U}^k}{\tau}, \mathbf{V}\right) + \widehat{\nu}\left(\nabla \mathbf{U}^k, \nabla \mathbf{V}\right) + b_h\left(\mathbf{U}^{k,\star}, \mathbf{U}^k, \mathbf{V}\right) - \left(P^k, div\, \mathbf{V}\right) \\ = 2\nu_r\left(curl\, \mathbf{W}^{k,\star}, \mathbf{V}\right) + \left(\mathbf{f}^k, \mathbf{V}\right),\end{aligned} \tag{2.45a}$$

$$\left(\mathrm{Q}, div\, \mathbf{U}^k\right) = 0, \tag{2.45b}$$

for all $\mathbf{V} \in \mathbb{U}$, $\mathrm{Q} \in \mathbb{P}$, where, for a time-discrete function ϕ^τ, we introduce the second-order extrapolation

$$\phi^{k,\star} = 2\phi^{k-1} - \phi^{k-2}. \tag{2.46}$$

Angular Momentum: Compute $\mathbf{W}^k \in \mathbb{W}$, solution of

$$\begin{aligned} &\jmath\left(\frac{\delta_-^2 \mathbf{W}^k}{\tau}, \mathbf{X}\right) + c_1\big(\nabla \mathbf{W}^k, \nabla \mathbf{X}\big) + \jmath\, b_h\big(\mathbf{U}^k, \mathbf{W}^k, \mathbf{X}\big) + \\ &\quad + c_2\big(div\, \mathbf{W}^k, div\, \mathbf{X}\big) + 4\nu_r\big(\mathbf{W}^k, \mathbf{X}\big) = 2\nu_r\big(curl\, \mathbf{U}^k, \mathbf{X}\big) + \big(\mathbf{t}^k, \mathbf{X}\big)\,, \end{aligned} \tag{2.47}$$

for all $\mathbf{X} \in \mathbb{W}$.

This scheme turns out to be almost unconditionally stable, as shown in the following result. To avoid irrelevant technicalities, we assume that $\mathbf{f}^\tau = \mathbf{t}^\tau = 0$.

Theorem 2.4.1 (Stability of second-order scheme)**.** *Assume that the time step satisfies*

$$\tau \le \frac{\jmath\nu}{8\nu_r^2}. \tag{2.48}$$

Then, the sequence $\{\mathbf{U}^\tau, \mathbf{W}^\tau, P^\tau\} \subset \mathbb{U} \times \mathbb{W} \times \mathbb{P}$*, solution of* (2.45a)–(2.47)*, satisfies*

$$\|\mathbf{U}^\tau\|_{\ell^\infty(\mathbf{L}^2)} + \|\mathbf{W}^\tau\|_{\ell^\infty(\mathbf{L}^2)} + \|\nabla \mathbf{U}^\tau\|_{\ell^2(\mathbf{L}^2)} + \|\nabla \mathbf{W}^\tau\|_{\ell^2(\mathbf{L}^2)} \le c\,,$$

where the constant c *depends on the material parameters and the values of* $\{\mathbf{U}^k, \mathbf{W}^k, P^k\}$ *for* $k = 0, 1$*, but does not depend on the discretization parameters.*

Proof. We combine the techniques used to prove Proposition 2.2.1 and Theorem 5.1 of [69]. We begin by setting $\mathbf{V} = 4\tau \mathbf{U}^k$ in (2.45a) and $\mathbf{X} = 4\tau \mathbf{W}^k$ in (2.47) and adding the result. Using (2.45b), we obtain

$$\begin{aligned} &3y^k - 4y^{k-1} + y^{k-2} + 2\delta\left(\|\delta \mathbf{U}^k\|_{\mathbf{L^2}}^2 + \jmath\|\delta \mathbf{W}^k\|_{\mathbf{L^2}}^2\right) + \|\delta^2 \mathbf{U}^k\|_{\mathbf{L^2}}^2 + \jmath\|\delta^2 \mathbf{W}^k\|_{\mathbf{L^2}}^2 \\ &\quad + 4\tau\left(\widehat{\nu}\|\nabla \mathbf{U}^k\|_{\mathbf{L^2}}^2 + c_1\|\nabla \mathbf{W}^k\|_{\mathbf{L^2}}^2\right) + 4c_2\tau\|div\, \mathbf{W}^k\|_{\mathbf{L^2}}^2 + 16\nu_r\tau\|\mathbf{W}^k\|_{\mathbf{L^2}}^2 \\ &\quad = 8\nu_r\tau\big(curl\, \mathbf{U}^k, 2\mathbf{W}^k - \delta^2 \mathbf{W}^k\big), \end{aligned}$$

where

$$y^k = \|\mathbf{U}^k\|_{\mathbf{L^2}}^2 + \jmath\|\mathbf{W}^k\|_{\mathbf{L^2}}^2\,.$$

Here we used the identity

$$2a^k(3a^k - 4a^{k-1} + a^{k-2}) = 3|a^k|^2 - 4|a^{k-1}|^2 + |a^{k-2}|^2 + 2\delta|\delta a^k|^2 + |\delta^2 a^k|^2.$$

and, to produce the right hand side, we integrated by parts using (1.1) and employed the equality

$$\phi^k + \phi^{\star,k} = \phi^k + 2\phi^{k-1} - \phi^{k-2} = 2\phi^k - \delta^2\phi^k,$$

which is a consequence of (2.46). Using (1.3) we obtain

$$8\nu_r\tau\big(curl\,\mathbf{U}^k, 2\mathbf{W}^k - \delta^2\mathbf{W}^k\big) \leq 16\nu_r\tau\|\mathbf{W}^k\|^2_{\mathbf{L^2}} + 4\nu_r\tau\|\nabla\mathbf{U}^k\|^2_{\mathbf{L^2}} + \jmath\|\delta^2\mathbf{W}^k\|^2_{\mathbf{L^2}} + \frac{16\nu_r^2\tau^2}{\jmath}\|\nabla\mathbf{U}^k\|^2_{\mathbf{L^2}}\,.$$

Since $\widehat{\nu} = \nu + \nu_r$ assumption (2.48) yields

$$4\nu\tau - \frac{16\nu_r^2\tau^2}{\jmath} = 4\nu\tau\left(1 - \frac{4\nu_r^2\tau}{\jmath\nu}\right) \geq 2\nu\tau.$$

The estimates of Proposition 2.4.1 imply the assertion. □

Remark 2.4.1 (time step constraint)**.** Notice that the constraint on the time step (2.48), necessary for stability, is meaningful. First of all, the quantity on the right hand side has units of time. In addition, it is consistent with the fact that, for the classical Navier-Stokes equations (that is $\nu_r = 0$) no constraints are necessary for the stability of a second order semi-implicit discretization.

2.5 Numerical Validation

We now present a numerical validation of our error estimates. The implementation has been carried out with the help of the `deal.II` library, see [70, 71]. We use the

lowest order Taylor-Hood elements, that is $\mathcal{Q}_2/\mathcal{Q}_1$, so that $\ell = 2$. The arising linear systems have been solved with the direct solver UMFPACK©.

Consider a square domain $\Omega = (0,1)^2 \subset \mathbb{R}^2$, and a smooth divergence-free linear velocity, pressure, and angular velocity defined by

$$\mathbf{u}(x,y,t) = (\sin(2\pi x + t)\,\sin(2\pi y + t), \cos(2\pi x + t)\,\cos(2\pi y + t))^{\intercal},$$

$$p(x,y,t) = \sin(2\pi(x-y) + t),$$

$$\mathbf{w}(x,y,t) = \sin(2\pi x + t)\,\sin(2\pi y + t).$$

To verify the $\ell^2(\mathbf{H}^1(\Omega))$ error for the velocity and the $\ell^2(L^2(\Omega))$ error for the pressure we fix the relationship $\tau = h^2$, and consider a sequence of meshes with $h = 2^{-i}$ for $2 \leq i \leq 6$. The corresponding errors are displayed in Figure 2.4, thereby showing clearly the predicted convergence rates.

To validate the $\ell^\infty(\mathbf{L}^2(\Omega))$ error of the velocities we fix the relationship $\tau = h^3$, and consider the same sequence of meshes. The corresponding errors are depicted in Figure 2.5 and exhibit the expected optimal rates.

2.6 Conclusions

We have presented a first-order, fully discrete semi-implicit scheme for the MNSE which is unconditionally stable and possesses optimal convergence rates in time and space. The scheme is semi-implicit, therefore it only involves, at every time-step, the solution of linear systems. In addition, the equations of linear and angular momentum are decoupled, which makes the implementation simpler and the scheme more efficient. To further decouple the unknowns, fractional time-stepping techniques

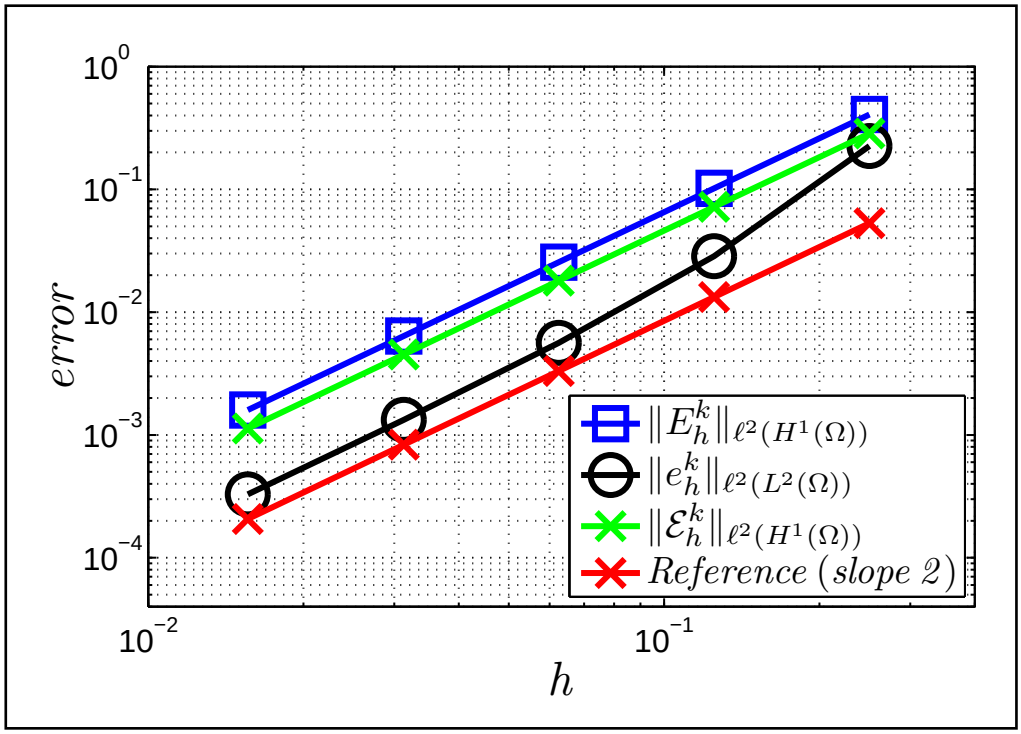

Figure 2.4: $\ell^2(\mathbf{H}^1(\Omega))$ error of the velocities and $\ell^2(L^2(\Omega))$ error of the pressure with respect to mesh size. The axes are in logarithmic scale.

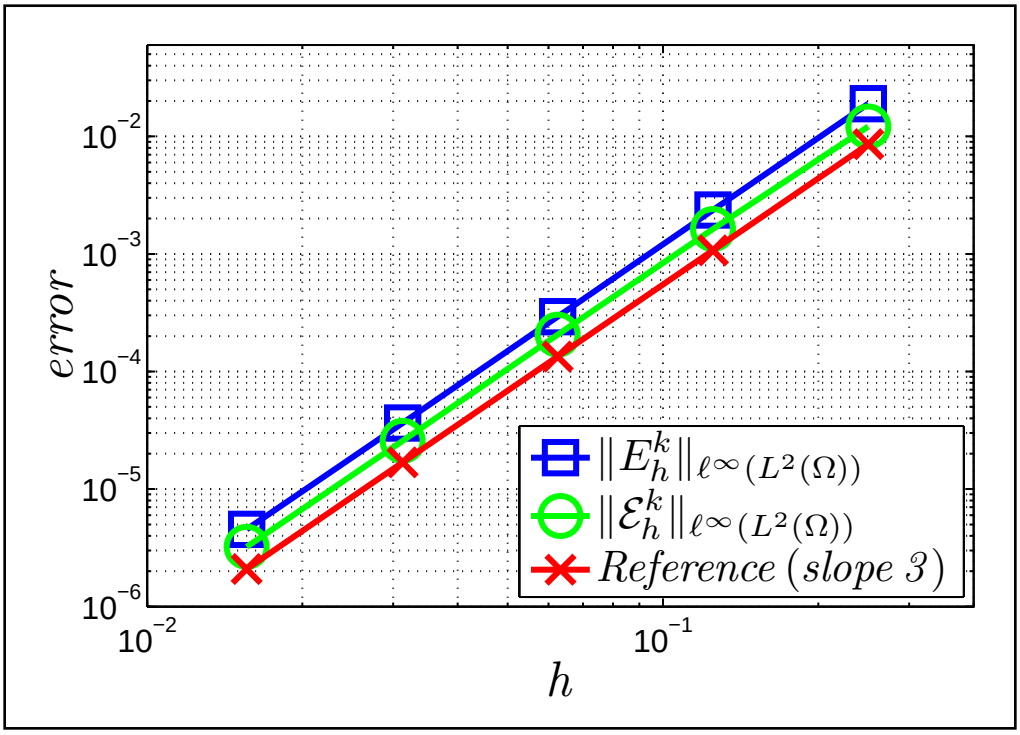

Figure 2.5: $\ell^\infty(\mathbf{L}^2(\Omega))$ error of the linear and angular velocities with respect to mesh size. The axes are in logarithmic scale.

can be incorporated, and we believe that their analysis shall not present difficulties beyond those already encountered in this work.

We have also presented a formally second order scheme which is almost unconditionally stable and shares similar properties to the first-order scheme, i.e., it is semi-implicit, decouples the linear and angular velocities and it can be easily simplified further with fractional time stepping techniques.

The idea of pumping micropolar fluid through excitation of the spin equation was explored by testing a simple family of forcing terms $\mathbf{t}$ (distributed torque). It was observed computationally that the regimes of effective pumping and reverse pumping regimes are not well separated. In other words, very similar forcing terms $\mathbf{t}$ can induce very different effects in the velocity profile, or even opposite effects (reverse direction of the net flow).

The most challenging extension of this work is towards the solution of the equations of ferrohydrodynamics: the MNSE coupled with the magnetic equations (2.8). The design, analysis and implementation of a scheme for this problem is the main topic of the next chapter.

Chapter 3: Rosensweig's model

3.1 Introduction

There are currently two generally accepted ferrofluid models which we will call by the name of their developers: the Rosensweig [17] and Shliomis [18] models. Rigorous work on the analysis (existence of global weak solutions and local existence of strong solutions) for these models is very recent [19, 20, 21, 22]. In this chapter we will concentrate on the Rosensweig model which includes all the inherent difficulties of the simpler Shliomis model.

Our key interest is around boundary conditions and discretization techniques leading to energy-stable continuum and discrete systems. This task becomes particularly complicated if we want to include the effects of non-trivial applied magnetizing fields, which so far has not been properly addressed in the literature. For this purpose we will need to revisit the theory of magnetostatics and typical boundary value problems associated with it. At this stage most manipulations are formal, but they are still able to shed light into very important issues such as space discretization techniques. Finally, we feel compelled to remark that, to the best of our knowledge, this is the first work presenting a stable numerical scheme for the Rosensweig model fully coupled with the magnetostatics equations accounting for the effect of

the demagnetizing field.

Our presentation is organized as follows: in §3.2 we present the Rosensweig model, we elaborate on several issues related to boundary conditions in §3.2.1–§3.2.3. In §3.3.1 we derive a formal energy estimate which constitutes the main guideline to devise a numerical scheme. We introduce the numerical method in §3.4, show that this scheme is energy-stable, and that solutions always exist. In §3.5 we consider a simplified model, and devise a scheme for this model for which we show (in addition to stability) convergence. In §3.6 we validate the scheme using prefabricated solutions, and finally in §3.7 we show a series of numerical examples which illustrate the potential of the scheme in the context of real applications.

3.2 The Rosensweig model of ferrohydrodynamics

Consider a mass of homogeneous, incompressible micropolar ferrofluid with linear velocity $\mathbf{u}$ and angular velocity $\mathbf{w}$ contained in a bounded simply connected domain $\Omega \subset \mathbb{R}^3$, subject to a smooth harmonic (curl-free and div-free) applied magnetizing field $\mathbf{h}_a$ inducing a magnetization field $\mathbf{m}$ and a demagnetizing (stray) field $\mathbf{h}_d$. The evolution of such fluid is described (see for instance [17, 72], and Remark 3.2.1):

$$\mathbf{u}_t + (\mathbf{u}\cdot\nabla)\mathbf{u} - \widehat{\nu}\Delta\mathbf{u} + \nabla p = 2\nu_r \mathit{curl}\,\mathbf{w} + \mu_0(\mathbf{m}\cdot\nabla)\mathbf{h} \tag{3.1a}$$

$$\mathit{div}\,\mathbf{u} = 0 \tag{3.1b}$$

$$\jmath\mathbf{w}_t + \jmath(\mathbf{u}\cdot\nabla)\mathbf{w} - c_1\Delta\mathbf{w} - c_2\nabla \mathit{div}\,\mathbf{w} + 4\nu_r\mathbf{w} = 2\nu_r \mathit{curl}\,\mathbf{u} + \mu_0\mathbf{m}\times\mathbf{h} \tag{3.1c}$$

$$\mathbf{m}_t + (\mathbf{u}\cdot\nabla)\mathbf{m} - \sigma\Delta\mathbf{m} = \mathbf{w}\times\mathbf{m} - \tfrac{1}{\mathscr{T}}(\mathbf{m} - \varkappa_0\mathbf{h}) \tag{3.1d}$$

in Ω for every $t \in [0, t_F]$, where

$$\mathbf{h} = \mathbf{h}_a + \mathbf{h}_d \tag{3.2}$$

is the effective magnetizing field; see Remark 3.2.2 below. The material constants $\widehat{\nu}$, ν_r, c_1 c_2, and $\jmath$ where defined in (2.7), and the new constants μ_0, σ, $\mathscr{T}$, and $\varkappa_0$ are assumed nonnegative. Expression (3.1a) represents the conservation of linear momentum, (3.1b) corresponds to the conservation of mass, (3.1c) corresponds to the conservation of angular momentum, and (3.1d) corresponds to the evolution of the magnetization. The forcing term $\mu_0(\mathbf{m} \cdot \nabla)\mathbf{h}$ in the linear momentum equation is the so-called Kelvin force.

The magnetic diffusion σ was introduced in [22] as a regularization mechanism in order to prove global existence of weak solutions; but its physical grounds have been called into question [73], σ is negligibly small or zero. Therefore, we will primarily focus on the case $\sigma = 0$. If $\sigma > 0$ the boundary conditions associated with the vector Laplacian $\Delta\mathbf{m}$ allow us to introduce additional modeling features. Thus, in this case, we will propose energy-stable boundary conditions.

The constant $\varkappa_0$ is dimensionless; it is the magnetic susceptibility, the product $\mu_0(1+\varkappa_0)$ is what is usually called the magnetic permeability of the material (cf.[74]). For oil-based ferrofluids [25] we have $\varkappa_0 \in [0.3, 4.3]$, and for water-based ferrofluid $\varkappa_0$ is generally smaller than the unity. If $\varkappa_0 = 0$ the medium is not magnetizable, so there is no ferrohydrodynamic phenomena: magnetic fields cannot exert any force or torque on the fluid. The quantity $\varkappa_0\mathbf{h}$ is usually called the *equilibrium magnetization*: if $\sigma \equiv 0$, $\mathbf{u} \equiv 0$ and $\mathbf{w} \equiv 0$ in the magnetization

equation (3.1d), and $\mathbf{h}$ is given, then we get

$$\mathbf{m}_t + \tfrac{1}{\mathscr{T}}\mathbf{m} = \tfrac{\varkappa_0}{\mathscr{T}}\mathbf{h}\,, \tag{3.3}$$

so that $\mathbf{m} \approx \varkappa_0 \mathbf{h}$ when close to equilibrium. The core dynamics of the magnetization equation in (3.1d) is dominated by the reaction terms for most flows of interest (see for instance [75, 25] for the dimensional analysis of the Rosensweig model). Essentially, this is the case because the relaxation time $\mathscr{T}$ of commercial grade ferrofluids is in the range of 10^{-5} to 10^{-9} seconds (see for instance [75, 18]), which makes $\frac{1}{\mathscr{T}}$ a very large constant.

System (3.1) is supplemented with initial conditions for the linear velocity, the angular velocity, and the magnetization

$$\mathbf{u}|_{t=0} = \mathbf{u}_0, \quad \mathbf{w}|_{t=0} = \mathbf{w}_0, \quad \mathbf{m}|_{t=0} = \mathbf{m}_0, \tag{3.4}$$

as well as boundary conditions for the linear and angular velocities

$$\mathbf{u}|_{\Gamma\times(0,t_F)} = 0, \quad \mathbf{w}|_{\Gamma\times(0,t_F)} = 0. \tag{3.5}$$

The quantities $\mathbf{h}$ and $\mathbf{m}$ are subordinate to Maxwell's equations, which hold in the whole space $\mathbb{R}^3$. Truncating $\mathbf{h}$ to Ω and choosing suitable boundary conditions necessarily compromises the nature of the original magnetostatic problem, yet it can provide a reasonable starting point to develop and understand an energy-stable PDE system. We will reduce the magnetostatic problem to a single a scalar potential in §3.2.1, and in §3.2.2 we discuss the information that is lost in this process, derive the (approximate) boundary value problem (BVP) that $\mathbf{h}_d$ satisfies, the boundary conditions that can be applied to $\mathbf{h}_d$ and $\mathbf{m}$, and discuss how physically realistic they

are. We will also comment on the requirements for $\mathbf{h}_a$ to be a physically reasonable magnetizing field.

Remark 3.2.1 (Assumptions underlying the derivation of the Rosensweig model)**.** A ferrofluid is a colloidal suspension of ferromagnetic particles in a carrier fluid. The limitations of model (3.1) can be traced back to the assumptions made on these particles at the time of its derivation. It is important to point out that model (3.1) was derived (see for instance [72]) under the following quite restrictive assumptions:

- ◇ The ferromagnetic particles are spherical.
- ◇ The ferrofluid is a monodisperse mixture, meaning that the ferromagnetic particles are of the same mass/size.
- ◇ The density of ferromagnetic particles (number of particles per unit volume) in the carrier liquid is considered to be homogeneous.
- ◇ No agglomeration, clumping, anisotropic behavior (e.g. formation of chains), and/or particle-to-particle interactions are considered.
- ◇ The induced fields (e.g. $\mathbf{m}$ and $\mathbf{h}_d$) are unable to perturb the applied magnetic field $\mathbf{h}_a$.

These assumptions might restrict the applicability of the Rosensweig model for some physical situations, see [17, 24] for more details.

Remark 3.2.2 (Effective magnetizing field)**.** The effective magnetizing field is defined by (3.2). In other models the effective magnetizing field can be more complicated and include, as in micromagnetics, terms due to the exchange of energy and

anisotropy [76]. Most analytic computations for the Rosensweig model are usually derived assuming that $\varkappa_0 << 1$ so that $\mathbf{h}_d$ and the equations of magnetostatics can be disregarded, thus setting $\mathbf{h} := \mathbf{h}_a$. In §3.5 we will consider this definition and provide some arguments to justify this simplification. Finally, the only available existence results for the Rosensweig model [21, 22] define the effective magnetizing field in a way that leads to $\mathbf{h} = \mathbf{h}_d$, which is equivalent to considering the unforced case (relaxation to equilibrium).

3.2.1 Modeling the magnetic field: The scalar potential approach

One of the main difficulties in the analysis and approximation of (3.1) lies in the fact that the magnetic field $\mathbf{h}$ is governed by Maxwell's equations which are naturally defined in $\mathbb{R}^3$. Under reasonable assumptions these can be further simplified to the equations of magnetostatics

$$curl\,\mathbf{h} = 0\,,\ div\,\mathbf{b} = 0 \ \text{ in } \mathbb{R}^3, \tag{3.6}$$

which imply the transmission conditions

$$[\![\mathbf{h}]\!] \times \boldsymbol{n} = 0\,,\ [\![\mathbf{b}]\!] \cdot \boldsymbol{n} = 0 \text{ on } \Gamma\,, \tag{3.7}$$

over any surface $\Gamma \subset \mathbb{R}^3$; hereafter $\boldsymbol{n}$ denotes the outward unit normal to Γ, the boundary of Ω, and $[\![q]\!]$ the jump of the quantity q over Γ. The magnetic induction $\mathbf{b}$ is defined as

$$\mathbf{b} = \mu_0\,(\mathbf{h} + \mathbf{1}_\Omega \mathbf{m})\,, \tag{3.8}$$

where $\mathbf{1}_\Omega$ is the characteristic function of Ω. Definitions (3.2) and (3.8), together with (3.6) and (3.7), and assuming that $\mathbf{h}_a$ is a smooth harmonic (curl-free and div-free, see Remark 3.2.3) vector field in $\mathbb{R}^3$, yield the following constraints for $\mathbf{h}_d$:

$$curl\,\mathbf{h}_d = 0 \text{ in } \mathbb{R}^3\,,\ div\,\mathbf{h}_d = -div\,\mathbf{m} \text{ in } \Omega\,,\ div\,\mathbf{h}_d = 0 \text{ in } \mathbb{R}^3 \setminus \Omega\,, \tag{3.9}$$

supplemented with (assuming that $[\![\mathbf{h}_a]\!] = 0$ on Γ):

$$\boldsymbol{n} \times \mathbf{h}_d = \boldsymbol{n} \times \mathbf{h}_d^{\text{out}}, \quad \mathbf{h}_d \cdot \boldsymbol{n} = (\mathbf{h}_d^{\text{out}} - \mathbf{m}) \cdot \boldsymbol{n} \quad \text{on } \Gamma, \tag{3.10}$$

where we use the superscript "out" to denote values in $\mathbb{R}^3 \setminus \Omega$. The problem defined by (3.9) and (3.10) is the most physical approach to compute $\mathbf{h}_d$; see for instance [76, Chapter 3] in the context of micromagnetism. This approach, however, entails a major difficulty: we have to deal with an exterior problem. This may not be an issue from the point of view of analysis but, from the numerical point of view this would require highly specialized techniques for our (already) quite complex ferro-hydrodynamics problem. There are just a few references actually solving problem (3.9)-(3.10) (see for instance [77, 78]), but most generally (see for instance [79] in the context of micromagnetics) some form of truncation is favored. Following [20, 21] we will truncate the support of $\mathbf{h}_d$, i.e. we will assume that $\mathbf{h}_d^{\text{out}} = 0$, which yields the BVP:

$$\begin{gathered} curl\,\mathbf{h}_d = 0 \text{ in } \Omega,\ div\,\mathbf{h}_d = -div\,\mathbf{m} \text{ in } \Omega, \\ \mathbf{h}_d \cdot \boldsymbol{n} = -\mathbf{m} \cdot \boldsymbol{n},\ \boldsymbol{n} \times \mathbf{h}_d = 0 \text{ on } \Gamma. \end{gathered} \tag{3.11}$$

The simplification that leads to (3.11) is not necessarily physically faithful (unless $\mathbf{h}_d^{\text{out}} \approx 0$), yet it is widely used in practice [80, 81, 82, 83]. We can approximate

problem (3.11) by using a scalar potential approach [80], that is we set $\mathbf{h}_d = \nabla\psi$ where ψ solves either

$$-\Delta\psi = div\,\mathbf{m} \ \text{ in } \Omega, \quad \frac{\partial\psi}{\partial\boldsymbol{n}} = -\mathbf{m}\cdot\boldsymbol{n} \ \text{ on } \Gamma \tag{3.12}$$

or

$$-\Delta\psi = div\,\mathbf{m} \ \text{ in } \Omega, \quad \psi = 0 \ \text{ on } \Gamma. \tag{3.13}$$

This approach, however, does not retain all the boundary conditions of (3.11). The Neumann BVP (3.12) retains $\mathbf{h}_d \cdot \boldsymbol{n} = -\mathbf{m}\cdot\boldsymbol{n}$, while the tangential condition $\boldsymbol{n}\times\mathbf{h}_d = 0$ results from $\psi = 0$ of the Dirichlet BVP (3.13).

Further simplified problems are used in practice for $\mathbf{h}_d$. The homogeneous Neumann problem

$$-\Delta\psi = div\,\mathbf{m} \quad \text{in } \Omega, \qquad \frac{\partial\psi}{\partial\boldsymbol{n}} = 0 \quad \text{on } \Gamma, \tag{3.14}$$

is also used [22, 82, 80, 81] to approximate the demagnetizing field. Problem (3.14), however, can only be justified if $\mathbf{m}\cdot\boldsymbol{n}$ is very small.

Starting from the Maxwell's equations (3.6) we arrived to the Neumann problem (3.14) for the scalar potential. This encompasses a series of simplifying assumptions, rarely explained in the scientific literature, here made explicit. These simplifications compromise the nature of the original magnetostatic problem, but for the time being, the simplified problem (3.14) will keep the spirit of the demagnetizing field alive. Finally, it is worth mentioning that so far only (3.12) and (3.14) have been used for the construction of an energy-stable system and the analysis of

the Rosensweig model [22, 20, 21]. In this chapter, we will use (3.12), giving us control of the normal condition on $\mathbf{h}_d$ but not on the tangential component.

Remark 3.2.3 (Physical requirements on $\mathbf{h}_a$)**.** It is not difficult to see that $\mathbf{h}_a$ must be harmonic. If ω is a control volume and there is no magnetizable media inside ω we have that $\mathbf{m} \equiv 0$ and $\mathbf{h}_d \equiv 0$ in ω. By Maxwell's equations then $curl\,\mathbf{h} = curl\,\mathbf{h}_a = 0$ and $div\,\mathbf{b} = \mu_0 div\,\mathbf{h}_a = 0$ in ω. Since ω is arbitrary $\mathbf{h}_a$ is harmonic.

Remark 3.2.4 (Variational problems for the magnetizing fields)**.** Multiply (3.12) by a sufficiently smooth test function χ. Integrating by parts, and using $\frac{\partial \psi}{\partial \boldsymbol{n}} = -\mathbf{m}\cdot\boldsymbol{n}$ yields

$$\int_\Omega \nabla\psi \cdot \nabla\chi \, dx = -\int_\Omega \mathbf{m} \cdot \nabla\chi \, dx \quad \forall\, \chi \in H^1(\Omega)\,. \tag{3.15}$$

Since $curl\,\mathbf{h}_a = 0$, there exists a scalar potential ϕ such that $\mathbf{h}_a = \nabla\phi$, then

$$\int_\Omega \nabla\phi \cdot \nabla\chi \, dx = \int_\Omega \mathbf{h}_a \cdot \nabla\chi \, dx \quad \forall\, \chi \in H^1(\Omega). \tag{3.16}$$

It will be useful (primarily, to simplify the presentation) to set $\mathbf{h} = \nabla\varphi$ with $\varphi = \psi + \phi$, so that φ satisfies

$$\int_\Omega \nabla\varphi \cdot \nabla\chi \, dx = \int_\Omega (\mathbf{h}_a - \mathbf{m}) \cdot \nabla\chi \, dx \quad \forall\, \chi \in H^1(\Omega)\,, \tag{3.17}$$

which is the variational form of the BVP

$$-\Delta\varphi = div\,\mathbf{m} \quad \text{in } \Omega, \qquad \frac{\partial\varphi}{\partial\boldsymbol{n}} = (\mathbf{h}_a - \mathbf{m})\cdot\boldsymbol{n} \quad \text{on } \Gamma, \tag{3.18}$$

where the term $-div\,\mathbf{h}_a$ on the right-hand side of the PDE has been omitted since $\mathbf{h}_a$ is solenoidal.

3.2.2 Boundary conditions for $\mathbf{m}$ and their coupling with $\mathbf{h}_d$

For the magnetization $\mathbf{m}$ we consider both $\sigma = 0$ and $\sigma > 0$ in (3.1). Since $\mathbf{u} \cdot \boldsymbol{n} = 0$ on Γ, no boundary conditions for $\mathbf{m}$ are needed when $\sigma = 0$, because the PDE for $\mathbf{m}$ is a transport equation. If $\sigma > 0$, on the contrary, we must impose boundary conditions that are compatible with the convection-diffusion equation for $\mathbf{m}$. For the magnetizing field $\mathbf{h}$, Maxwell's equations dictated our choice. For $\mathbf{m}$, however, suitable boundary conditions are rarely discussed in the literature. For this reason, our selection criterion for boundary conditions is whether they lead to an energy law.

The boundary conditions that can be applied to the magnetization $\mathbf{m}$ are those of the vector Laplacian. Since $-\Delta\mathbf{m} = curl^2\mathbf{m} - \nabla div\,\mathbf{m}$, integration by parts yields

$$\begin{aligned}\int_\Omega -\Delta\mathbf{m}\cdot\mathbf{z}\,dx = &\int_\Omega curl\,\mathbf{m}\cdot curl\,\mathbf{z} + div\,\mathbf{m}\,div\,\mathbf{z}\,dx \\ &- \int_\Gamma (curl\,\mathbf{m}\times\boldsymbol{n})\cdot\mathbf{z}\,dS \; - \int_\Gamma div\,\mathbf{m}(\mathbf{z}\cdot\boldsymbol{n})\,dS\,,\end{aligned} \tag{3.19}$$

so that we can consider:

- ◇ Magnetic boundary conditions (cf.[22])

$$\mathbf{m}\cdot\boldsymbol{n} = g\,,\; curl\,\mathbf{m}\times\boldsymbol{n} = \mathbf{r} \text{ on } \Gamma\,, \tag{3.20}$$

  where g and $\mathbf{r}$ are the boundary data. The condition $curl\,\mathbf{m}\times\boldsymbol{n} = \mathbf{r}$ is natural, while $\mathbf{m}\cdot\boldsymbol{n} = g$ is essential.

- ◇ Electric boundary conditions (cf.[84])

$$div\,\mathbf{m} = q\,,\; \mathbf{m}\times\boldsymbol{n} = \mathbf{y} \text{ on } \Gamma\,, \tag{3.21}$$

where the first condition is natural, the second is essential, and the data $\mathbf{y}$ only has tangential component.

◇ Robin-like boundary conditions

$$\begin{aligned} curl\,\mathbf{m}\times\boldsymbol{n}+\gamma_1(\mathbf{m}-(\mathbf{m}\cdot\boldsymbol{n})\boldsymbol{n}-\mathbf{y})=\mathbf{r} \quad \text{on } \Gamma\,, \\ div\,\mathbf{m}+\gamma_2(\mathbf{m}\cdot\boldsymbol{n}-g)=q \quad \text{on } \Gamma\,. \end{aligned} \tag{3.22}$$

Since $|\boldsymbol{n}|=1$ we have that $(\mathbf{u}-(\mathbf{u}\cdot\boldsymbol{n})\boldsymbol{n})\cdot\mathbf{w}=(\mathbf{u}\times\boldsymbol{n})\cdot(\mathbf{w}\times\boldsymbol{n})$, then we get from (3.19) the following variational formulation of $-\Delta\mathbf{m}=\mathbf{f}$: find $\mathbf{m}\in\boldsymbol{\mathcal{M}}$ such that

$$\begin{aligned} &\int_\Omega curl\,\mathbf{m}\cdot curl\,\mathbf{v}+div\,\mathbf{m}\,div\,\mathbf{v}\,dx+\gamma_1\int_\Gamma(\mathbf{m}\times\boldsymbol{n})\cdot(\mathbf{v}\times\boldsymbol{n})\,dS \\ &+\gamma_2\int_\Gamma(\mathbf{m}\cdot\boldsymbol{n})(\mathbf{v}\cdot\boldsymbol{n})\,dS=\int_\Omega\mathbf{f}\cdot\mathbf{v}\,dx+\int_\Gamma\mathbf{r}\cdot\mathbf{v}\,dS \\ &+\int_\Gamma q(\mathbf{v}\cdot\boldsymbol{n})\,dS+\gamma_1\int_\Gamma(\mathbf{y}\times\boldsymbol{n})\cdot(\mathbf{v}\times\boldsymbol{n})\,dS+\gamma_2\int_\Gamma g(\mathbf{v}\cdot\boldsymbol{n})\,dS \quad \forall\,\mathbf{v}\in\boldsymbol{\mathcal{M}}. \end{aligned}$$

The following asymptotic cases are if interest: for $\gamma_1=0$, $\gamma_2\to\infty$, (3.22) tends to the magnetic boundary conditions (3.20), while if $\gamma_2=0$, $\gamma_1\to\infty$, (3.22) tends to the electric boundary conditions (3.21).

◇ Natural boundary conditions

$$curl\,\mathbf{m}\times\boldsymbol{n}=0, \quad div\,\mathbf{m}=0 \qquad \text{on } \Gamma\,, \tag{3.23}$$

which lead to an energy-stable system. We will mainly use these conditions to explain the main ideas behind the development of an energy estimate for (3.1).

3.2.3 Problems to be considered

In this chapter we will consider the simplified Initial Boundary Value Problem (IVBP) of ferrohydrodynamics: given a smooth harmonic vector field $\mathbf{h}_a = \mathbf{h}_a(x,t)$, find $\{\mathbf{u}, p, \mathbf{w}, \mathbf{m}, \mathbf{h}\}$ satisfying the equations (3.1) in $\Omega \times [0, t_F]$, where $\mathbf{u}$ and $\mathbf{w}$ satisfy the boundary conditions (3.5), $\mathbf{h} = \nabla\varphi$ where φ solves (3.18), and the equation for $\mathbf{m}$ in (3.1) is supplemented with one of the following boundary conditions:

1. $\sigma = 0$, with no boundary conditions for $\mathbf{m}$.

2. $\sigma > 0$ with the natural boundary conditions (3.23).

3. $\sigma > 0$ with the following variant of (3.22):

$$\begin{aligned} \mathit{curl}\,\mathbf{m} \times \boldsymbol{n} + \gamma\big(\mathbf{m} - (\mathbf{m}\cdot\boldsymbol{n})\boldsymbol{n} - \varkappa_0(\mathbf{h} - (\mathbf{h}\cdot\boldsymbol{n})\boldsymbol{n})\big) = 0 \ \text{ on } \Gamma\,, \\ \mathit{div}\,\mathbf{m} + \gamma\big(\mathbf{m}\cdot\boldsymbol{n} - \varkappa_0\mathbf{h}\cdot\boldsymbol{n}\big) = 0 \ \text{ on } \Gamma\,, \end{aligned} \tag{3.24}$$

   which is obtained by setting $\gamma_1 = \gamma$, $\mathbf{y} = \varkappa_0(\mathbf{h} - (\mathbf{h}\cdot\boldsymbol{n})\boldsymbol{n})$, $\mathbf{r} = 0$, $\gamma_2 = \gamma$, $g = \varkappa_0\mathbf{h}\cdot\boldsymbol{n}$, and $q = 0$ in (3.22), with γ being a material constant that characterizes the magnetization dynamics on the surface of the ferrofluid.

Remark 3.2.5 (Boundary dynamics)**.** A possible physical explanation for (3.24) is that, on the boundary, $\mathbf{m}$ will attempt to reach equilibrium $\mathbf{m} = \varkappa_0\mathbf{h}$ according to (3.3), but it will lag behind since $\mathbf{m}$ can only change at a finite rate limited by the characteristic dynamics of the magnetization. This is consistent with the no-slip and no-spin boundary conditions, so the behavior of $\mathbf{m}$ on the boundary is solely controlled by a magnetic relaxation time as in (3.3).

3.3 A priori estimates and existence

Let us review the available existence results for the problems under consideration. We shall first provide some formal a priori energy estimates, which serve as basis for the existence results that will be discussed later and, more importantly, will guide us in the development of stable numerical schemes, see §3.4.

3.3.1 A priori energy estimates

Let us obtain an energy estimate for Case 2 of §3.2.3. Setting $\sigma = 0$ in the final estimate we get the corresponding estimate for Case 1 of §3.2.3. The energy estimate for Case 3, is outlined in Remark 3.3.1. We begin by showing two crucial identities that make possible the energy estimate.

Lemma 3.3.1 (Identities for the magnetization and magnetic field)**.** *Let* $\mathbf{m}$ *and* $\mathbf{h}$ *denote the magnetization and effective magnetizing field, respectively. If they are sufficiently smooth we have*

$$-(\Delta\mathbf{m},\mathbf{h}) = -\|div\,\mathbf{h}\|^2_{\mathbf{L}^2} - \int_\Gamma (curl\,\mathbf{m}\times\boldsymbol{n})\cdot\mathbf{h}\,dS - \int_\Gamma div\,\mathbf{m}\,(\mathbf{h}\cdot\boldsymbol{n})\,dS\,, \quad (3.25)$$

and, for every smooth vector field $\mathbf{v}$*, such that* $div\,\mathbf{v} = 0$ *in* Ω *and* $\mathbf{v}\cdot\boldsymbol{n} = 0$ *on* Γ

$$b(\mathbf{v},\mathbf{m},\mathbf{h}) = -\,b(\mathbf{m},\mathbf{h},\mathbf{v})\,, \quad (3.26)$$

where the trilinear form $b(\cdot,\cdot,\cdot)$ *was defined in* (1.5)*.*

Proof. To obtain (3.25), we first take $\mathbf{z} := \mathbf{h}$ in (3.19) and recall that $curl\,\mathbf{h} = 0$. Upon multiplying (3.18) by $div\,\mathbf{h} = \Delta\varphi$ and integrating, we deduce $(div\,\mathbf{m}, div\,\mathbf{h}) = -\|div\,\mathbf{h}\|^2_{\mathbf{L}^2}$, which substituted in (3.19) yields (3.25).

Since $\mathbf{h}$ is curl-free we have that $\mathbf{h}^j_{x_i} = \mathbf{h}^i_{x_j}$. Integration by parts then yields

$$\begin{aligned} b(\mathbf{m},\mathbf{h},\mathbf{v}) &= \sum_{i,j=1}^{d} \int_\Omega \mathbf{m}^i \mathbf{h}^j_{x_i} \mathbf{v}^j \, dx = \sum_{i,j=1}^{d} \int_\Omega \mathbf{m}^i \mathbf{h}^i_{x_j} \mathbf{v}^j \, dx \\ &= \sum_{i,j=1}^{d} \int_\Omega \big((\mathbf{m}^i \mathbf{h}^i)_{x_j} - \mathbf{m}^i_{x_j} \mathbf{h}^i \big) \mathbf{v}^j \, dx \\ &= \sum_{i,j=1}^{d} \int_\Omega -(\mathbf{m}^i \mathbf{h}^i) \mathbf{v}^j_{x_j} - \mathbf{m}^i_{x_j} \mathbf{h}^i \mathbf{v}^j \, dx + \int_\Gamma (\mathbf{m}^i \mathbf{h}^i) \mathbf{v}^j \boldsymbol{n}^j \, dS \\ &= -\int_\Omega (\mathbf{m} \cdot \mathbf{h}) \, div\, \mathbf{v} \, dx - \, b(\mathbf{v},\mathbf{m},\mathbf{h}) + \int_\Gamma (\mathbf{m} \cdot \mathbf{h}) \mathbf{v} \cdot \boldsymbol{n} \, dS \end{aligned} \tag{3.27}$$

The fact that $\mathbf{v}$ is solenoidal and has zero normal trace on the boundary yields (3.26).

□

With these identities at hand we obtain a formal energy estimate. To shorten the exposition we denote

$$\mathscr{E} = \mathscr{E}(\mathbf{u},\mathbf{w},\mathbf{m},\mathbf{h};s) = \tfrac{1}{2}\left(\|\mathbf{u}(s)\|^2_{\mathbf{L}^2} + \jmath \|\mathbf{w}(s)\|^2_{\mathbf{L}^2} + \mu_0 \|\mathbf{m}(s)\|^2_{\mathbf{L}^2} + \mu_0 \|\mathbf{h}(s)\|^2_{\mathbf{L}^2} \right),$$

$$\begin{aligned} \mathscr{D} = \mathscr{D}(\mathbf{u},\mathbf{w},\mathbf{m},\mathbf{h};s) &= \nu \|\nabla \mathbf{u}(s)\|^2_{\mathbf{L}^2} + c_1 \|\nabla \mathbf{w}(s)\|^2_{\mathbf{L}^2} + \sigma\mu_0 \|curl\, \mathbf{m}(s)\|^2_{\mathbf{L}^2} \\ &\quad + \sigma\mu_0 \|div\, \mathbf{m}(s)\|^2_{\mathbf{L}^2} + \sigma\mu_0 \|div\, \mathbf{h}(s)\|^2_{\mathbf{L}^2} + c_2 \|div\, \mathbf{w}(s)\|^2_{\mathbf{L}^2} \\ &\quad + \nu_r \|(curl\, \mathbf{u} - 2\mathbf{w})(s)\|^2_{\mathbf{L}^2} + \tfrac{\mu_0}{\mathscr{T}} \|\mathbf{m}(s)\|^2_{\mathbf{L}^2} + \tfrac{\mu_0}{2\mathscr{T}} \big(\tfrac{1}{2} + 3\varkappa_0 \big) \|\mathbf{h}(s)\|^2_{\mathbf{L}^2}, \end{aligned}$$

$$\mathscr{F} = \mathscr{F}(\mathbf{h}_a;s) = \mathscr{T}\mu_0 \|\partial_t \mathbf{h}_a(s)\|^2_{\mathbf{L}^2} + \tfrac{\mu_0}{2\mathscr{T}}(1+\varkappa_0) \|\mathbf{h}_a(s)\|^2_{\mathbf{L}^2}.$$

Proposition 3.3.1 (Formal energy estimate)**.** *The solution* $\{\mathbf{u}, p, \mathbf{w}, \mathbf{m}, \mathbf{h}\}$ *of problem* (3.1), (3.4), (3.5) *and* (3.18) *satisfies*

$$\begin{aligned} \mathscr{E}(\mathbf{u},\mathbf{w},\mathbf{m},\mathbf{h};t_F) + \int_0^{t_F} \mathscr{D}(\mathbf{u},\mathbf{w},\mathbf{m},\mathbf{h};s) \, ds \\ \leq \int_0^{t_F} \mathscr{F}(\mathbf{h}_a;s) \, ds + \mathscr{E}(\mathbf{u},\mathbf{w},\mathbf{m},\mathbf{h};0). \end{aligned} \tag{3.28}$$

Proof. The main ideas of this estimate come from [85, 22, 19], but we now use (3.17) for the scalar potential associated to the magnetizing field instead. We multiply (3.1a) by $\mathbf{u}$, (3.1c) by $\mathbf{w}$, (3.1d) by $\mu_0\mathbf{m}$, and integrate by parts. Setting $\chi = \frac{\varkappa_0\mu_0}{\mathscr{T}}\varphi$ in (3.17) and adding the ensuing identities yields

$$\begin{aligned}\tfrac{d}{dt}\left(\mathscr{E} - \tfrac{\mu_0}{2}\|\mathbf{h}\|^2_{\mathbf{L}^2}\right) + \mathscr{D} - \sigma\mu_0\|div\,\mathbf{h}\|^2_{\mathbf{L}^2} - \tfrac{\mu_0}{2\mathscr{T}}\left(\tfrac{1}{2}+\varkappa_0\right)\|\mathbf{h}\|^2_{\mathbf{L}^2} \\ = \mu_0\, b(\mathbf{m},\mathbf{h},\mathbf{u}) + \mu_0(\mathbf{m}\times\mathbf{h},\mathbf{w}) + \tfrac{\varkappa_0\mu_0}{\mathscr{T}}(\mathbf{h}_a,\nabla\varphi) \\ + \sigma\mu_0\int_\Gamma (curl\,\mathbf{m}\times\boldsymbol{n})\cdot\mathbf{m}\,dS + \sigma\mu_0\int_\Gamma div\,\mathbf{m}\,(\mathbf{m}\cdot\boldsymbol{n})\,dS.\end{aligned} \tag{3.29}$$

Note that to form the term $\|curl\,\mathbf{u} - 2\mathbf{w}\|^2_{\mathbf{L}^2}$ in $\mathscr{D}$ we have used (1.2) on $\|\nabla\mathbf{u}\|^2_{\mathbf{L}^2}$ and (2.7). Multiply the magnetization equation (3.1d) by $\mu_0\mathbf{h}$. Identities (3.25) and (3.26) yield

$$\begin{aligned}\sigma\mu_0\|div\,\mathbf{h}\|^2_{\mathbf{L}^2} + \tfrac{\varkappa_0\mu_0}{\mathscr{T}}\|\mathbf{h}\|^2_{\mathbf{L}^2} = -\mu_0\, b(\mathbf{m},\mathbf{h},\mathbf{u}) - \mu_0(\mathbf{m}\times\mathbf{h},\mathbf{w}) + \mu_0(\mathbf{m}_t,\mathbf{h}) \\ + \tfrac{\mu_0}{\mathscr{T}}(\mathbf{m},\mathbf{h}) - \sigma\mu_0\int_\Gamma (curl\,\mathbf{m}\times\boldsymbol{n})\cdot\mathbf{h}\,dS \\ - \sigma\mu_0\int_\Gamma div\,\mathbf{m}\,(\mathbf{h}\cdot\boldsymbol{n})\,dS\,.\end{aligned}$$

Adding this expression to (3.29) we get

$$\begin{aligned}\tfrac{d}{dt}\left(\mathscr{E} - \tfrac{\mu_0}{2}\|\mathbf{h}\|^2_{\mathbf{L}^2}\right) + \mathscr{D} - \tfrac{\mu_0}{2\mathscr{T}}\left(\tfrac{1}{2}-\varkappa_0\right)\|\mathbf{h}\|^2_{\mathbf{L}^2} = \mu_0(\mathbf{m}_t,\mathbf{h}) + \tfrac{\mu_0}{\mathscr{T}}(\mathbf{m},\mathbf{h}) \\ + \tfrac{\varkappa_0\mu_0}{\mathscr{T}}(\mathbf{h}_a,\nabla\varphi) + \sigma\mu_0\int_\Gamma (curl\,\mathbf{m}\times\boldsymbol{n})\cdot(\mathbf{m}-\mathbf{h})\,dS \\ + \sigma\mu_0\int_\Gamma div\,\mathbf{m}\,(\mathbf{m}-\mathbf{h})\cdot\boldsymbol{n}\,dS\,.\end{aligned} \tag{3.30}$$

Set $\chi = \nabla\varphi$ in (3.17) to obtain

$$\|\nabla\varphi\|^2_{\mathbf{L}^2} = (\mathbf{h}_a - \mathbf{m}, \nabla\varphi). \tag{3.31}$$

Differentiate (3.17) with respect to time and set $\chi = \varphi$. This implies

$$\tfrac{1}{2}\tfrac{d}{dt}\|\nabla\varphi\|^2_{\mathbf{L}^2} = (\partial_t \mathbf{h}_a - \partial_t \mathbf{m}, \nabla\varphi). \tag{3.32}$$

Insert these two identities in (3.30), and use that $\mathbf{h} = \nabla\varphi$, to get

$$\begin{aligned}
&\tfrac{d}{dt}\mathscr{E}(\mathbf{u},\mathbf{w},\mathbf{m},\mathbf{h};t) + \mathscr{D}(\mathbf{u},\mathbf{w},\mathbf{m},\mathbf{h};t) + \tfrac{\mu_0}{4\mathscr{T}}(3+2\varkappa_0)\|\nabla\varphi\|^2_{\mathbf{L}^2} \\
&\qquad = \mu_0(\partial_t\mathbf{h}_a, \nabla\varphi) + \tfrac{\mu_0}{\mathscr{T}}(1+\varkappa_0)(\mathbf{h}_a, \nabla\varphi) \\
&\qquad + \sigma\mu_0 \int_\Gamma (curl\,\mathbf{m}\times\boldsymbol{n})\cdot(\mathbf{m}-\mathbf{h})\,dS \\
&\qquad + \sigma\mu_0 \int_\Gamma div\,\mathbf{m}\,(\mathbf{m}-\mathbf{h})\cdot\boldsymbol{n}\,dS\,.
\end{aligned} \tag{3.33}$$

Notice that all the boundary integrals that appear on the right hand side of (3.33) are multiplied by σ, so that this is already the sought energy estimate for Case 1 of §3.2.3. For Case 2, the boundary conditions (3.23) imply that the boundary integrals in (3.33), whence

$$\begin{aligned}
&\tfrac{d}{dt}\mathscr{E}(\mathbf{u},\mathbf{w},\mathbf{m},\mathbf{h};t) + \mathscr{D}(\mathbf{u},\mathbf{w},\mathbf{m},\mathbf{h};t) + \tfrac{\mu_0}{4\mathscr{T}}(3+2\varkappa_0)\|\nabla\varphi\|^2_{\mathbf{L}^2} \\
&\qquad = \mu_0(\partial_t\mathbf{h}_a, \nabla\varphi) + \tfrac{\mu_0}{\mathscr{T}}(1+\varkappa_0)(\mathbf{h}_a, \nabla\varphi)\,.
\end{aligned}$$

After suitably bounding the terms on the right hand side, integration in time yields the desired estimate (3.28). □

Notice that (3.28) suggests that the natural spaces to search for a solution are

$$\begin{aligned}
\mathbf{u} &\in L^\infty(0,t_F,\boldsymbol{\mathcal{H}}) \cap L^2(0,t_F,\boldsymbol{\mathcal{V}}) \\
\mathbf{w} &\in L^\infty(0,t_F,\mathbf{L}^2(\Omega)) \cap L^2(0,t_F,\mathbf{H}^1_0(\Omega)) \\
\mathbf{m},\ \mathbf{h} &\in L^\infty(0,t_F,\mathbf{L}^2(\Omega)) \cap L^2(0,t_F,\boldsymbol{\mathcal{M}})\,.
\end{aligned} \tag{3.34}$$

Remark 3.3.1 (Energy stability using Robin boundary conditions)**.** Multiplying (3.1a), (3.1c) and (3.1d) by $\varkappa_0\mathbf{u}$, $\varkappa_0\mathbf{w}$ and $\varkappa_0\mu_0\mathbf{h}$, respectively, and following the arguments of Proposition 3.3.1 we obtain

$$\begin{aligned}
&\tfrac{d}{dt}\big(\tfrac{\varkappa_0}{2}\|\mathbf{u}\|^2_{\mathbf{L}^2}+\tfrac{\varkappa_0 J}{2}\|\mathbf{w}\|^2_{\mathbf{L}^2}+\tfrac{\mu_0}{2}\|\mathbf{m}\|^2_{\mathbf{L}^2}\big)+\varkappa_0\nu\|\nabla\mathbf{u}\|^2_{\mathbf{L}^2}+\varkappa_0 c_1\|\nabla\mathbf{w}\|^2_{\mathbf{L}^2}\\
&\qquad+\sigma\mu_0\|curl\,\mathbf{m}\|^2_{\mathbf{L}^2}+\sigma\mu_0(1+\varkappa_0)\|div\,\mathbf{m}\|^2_{\mathbf{L}^2}+\varkappa_0 c_2\|div\,\mathbf{w}\|^2_{\mathbf{L}^2}\\
&\qquad+\varkappa_0\nu_r\|curl\,\mathbf{u}-2\mathbf{w}\|^2_{\mathbf{L}^2}+\tfrac{\mu_0}{\mathscr{J}}\|\mathbf{m}\|^2_{\mathbf{L}^2}+\tfrac{\mu_0\varkappa_0}{\mathscr{J}}(1+\varkappa_0)\|\nabla\varphi\|^2_{\mathbf{L}^2}\\
&\qquad=\varkappa_0\mu_0(\mathbf{m}_t,\mathbf{h})+\tfrac{\varkappa_0\mu_0}{\mathscr{J}}(\mathbf{m},\mathbf{h})+\tfrac{\varkappa_0\mu_0}{\mathscr{J}}(\mathbf{h}_a,\nabla\varphi)\\
&\qquad+\sigma\mu_0\int_\Gamma(curl\,\mathbf{m}\times\boldsymbol{n})\cdot(\mathbf{m}-\varkappa_0\mathbf{h})\,dS\\
&\qquad+\sigma\mu_0\int_\Gamma div\,\mathbf{m}\,(\mathbf{m}-\varkappa_0\mathbf{h})\cdot\boldsymbol{n}\,dS\,.
\end{aligned}\tag{3.35}$$

The Robin-type boundary conditions (3.24) and identities (3.31) and (3.32) yield

$$\begin{aligned}
&\tfrac{d}{dt}\big(\tfrac{\varkappa_0}{2}\|\mathbf{u}\|^2_{\mathbf{L}^2}+\tfrac{\varkappa_0 J}{2}\|\mathbf{w}\|^2_{\mathbf{L}^2}+\tfrac{\mu_0}{2}\|\mathbf{m}\|^2_{\mathbf{L}^2}+\tfrac{\varkappa_0\mu_0}{2}\|\nabla\varphi\|^2_{\mathbf{L}^2}\big)+\varkappa_0\widehat{\nu}\|\nabla\mathbf{u}\|^2_{\mathbf{L}^2}\\
&\qquad+\varkappa_0 c_1\|\nabla\mathbf{w}\|^2_{\mathbf{L}^2}+\sigma\mu_0\|curl\,\mathbf{m}\|^2_{\mathbf{L}^2}+\sigma\mu_0(1+\varkappa_0)\|div\,\mathbf{m}\|^2_{\mathbf{L}^2}\\
&\qquad+\varkappa_0 c_2\|div\,\mathbf{w}\|^2_{\mathbf{L}^2}+\varkappa_0\nu_r\|curl\,\mathbf{u}-2\mathbf{w}\|^2_{\mathbf{L}^2}+\tfrac{\mu_0}{\mathscr{J}}\|\mathbf{m}\|^2_{\mathbf{L}^2}\\
&\qquad+\tfrac{\mu_0\varkappa_0}{\mathscr{J}}(2+\varkappa_0)\|\nabla\varphi\|^2_{\mathbf{L}^2}+\sigma\mu_0\gamma\int_\Gamma|(\mathbf{m}-\varkappa_0\mathbf{h})\times\boldsymbol{n}|^2\,dS+\\
&\qquad+\sigma\mu_0\gamma\int_\Gamma|(\mathbf{m}-\varkappa_0\mathbf{h})\cdot\boldsymbol{n}|^2\,dS\\
&\qquad=\varkappa_0\mu_0(\partial_t\mathbf{h}_a,\nabla\varphi)+\tfrac{2\varkappa_0\mu_0}{\mathscr{J}}(\mathbf{h}_a,\nabla\varphi).
\end{aligned}\tag{3.36}$$

A trivial application of the Cauchy-Schwarz inequality shows that the system is energy-stable with the boundary conditions (3.24). Note that we also have control of additional boundary terms.

Remark 3.3.2 (Neumann boundary conditions)**.** If we were to supplement the system with the boundary conditions $\mathbf{m}\cdot\boldsymbol{n}=\mathbf{h}_d\cdot\boldsymbol{n}=0$ we would not be able

to obtain, at least with the present techniques, an energy estimate. This relates to (3.13).

3.3.2 Existence results

To date, the results concerning existence of solutions for the equations of ferrohydrodynamics (3.1) available in the literature are as follows:

1. **Local strong solution [21].** Let $\sigma = 0$ and $\mathbf{h} = \nabla\vartheta$, where ϑ solves

$$-\Delta\vartheta = div\,(\mathbf{m} - \mathbf{h}_a) \quad \text{in } \Omega, \qquad \frac{\partial\vartheta}{\partial \boldsymbol{n}} = -\mathbf{m}\cdot\boldsymbol{n} \quad \text{on } \Gamma\,, \tag{3.37}$$

then, for $q > 3$ and $r = \min\{q, 6\}$, there exists a time $T^* > 0$ for which problem (3.1) has a unique strong solution $\{\mathbf{u}, p, \mathbf{w}, \mathbf{m}, \mathbf{h}\}$ such that

$$\mathbf{u} \in L^\infty(0, T^*, \mathbf{H}^2(\Omega)\cap\boldsymbol{\mathcal{V}}) \cap W^1_\infty(0, T^*, \boldsymbol{\mathcal{H}}) \cap L^2(0, T^*, \mathbf{W}^2_r(\Omega))$$

$$p \in L^2(0, T^*, W^1_r(\Omega))$$

$$\mathbf{w} \in L^\infty(0, T^*, \mathbf{H}^2(\Omega)\cap\mathbf{H}^1_0(\Omega)) \cap W^1_\infty(0, T^*, \mathbf{L}^2(\Omega)) \cap L^2(0, T^*, \mathbf{H}^3(\Omega))$$

$$\mathbf{m}, \mathbf{h} \in L^\infty(0, T^*, \mathbf{W}^1_\infty(\Omega)) \cap W^1_\infty(0, T^*, \mathbf{L}^q(\Omega)),$$

provided that the data $\{\mathbf{u}_0, \mathbf{w}_0, \mathbf{m}_0, \mathbf{h}_a\}$ are sufficiently small and regular, i.e.

$$\mathbf{u}_0 \in \mathbf{H}^2(\Omega)\cap\boldsymbol{\mathcal{V}}\ ,\ \mathbf{w}_0 \in \mathbf{H}^2(\Omega)\cap\mathbf{H}^1_0(\Omega)\ ,\ \mathbf{m}_0 \in W^1_q(\Omega)\ ,\ div\,\mathbf{h}_a \in W^1_\infty(0, T^*, L^q(\Omega)).$$

2. **Global weak solutions [22].** Let $\sigma > 0$ and $\mathbf{h} = \nabla\vartheta$, where ϑ solves

$$-\Delta\vartheta = div\,(\mathbf{m} - \mathbf{h}_a) \quad \text{in } \Omega, \qquad \frac{\partial\vartheta}{\partial \boldsymbol{n}} = 0 \quad \text{on } \Gamma\,, \tag{3.38}$$

and consider the magnetic boundary conditions $curl\,\mathbf{m} \times \boldsymbol{n} = 0$ and $\mathbf{m} \cdot \boldsymbol{n} = 0$ for $\mathbf{m}$. Then for every set of data $\{\mathbf{u}_0, \mathbf{w}_0, \mathbf{m}_0, \mathbf{h}_a\}$ that satisfies

$$\mathbf{u}_0 \in \boldsymbol{\mathcal{H}}\ ,\quad \mathbf{w}_0 \in \mathbf{L}^2(\Omega)\ ,\quad \mathbf{m}_0 \in \mathbf{L}^2(\Omega)\ ,\quad div\,\mathbf{h}_a \in H^1(0, t_F, L^2(\Omega))\,.$$

there is a global in time weak solution $\{\mathbf{u}, p, \mathbf{w}, \mathbf{m}, \mathbf{h}\}$ of problem (3.1) such that

$$\mathbf{u} \in L^\infty(0, t_F, \boldsymbol{\mathcal{H}}) \cap L^2(0, t_F, \boldsymbol{\mathcal{V}}) \cap \mathcal{C}_w([0, t_F], \boldsymbol{\mathcal{H}})$$

$$\mathbf{w} \in L^\infty(0, t_F, \mathbf{L}^2(\Omega)) \cap L^2(0, t_F, \mathbf{H}_0^1(\Omega)) \cap \mathcal{C}_w([0, t_F], \mathbf{L}^2(\Omega))$$

$$\mathbf{m} \in L^\infty(0, t_F, \mathbf{L}^2(\Omega)) \cap L^2(0, t_F, \boldsymbol{\mathcal{M}}) \cap \mathcal{C}_w([0, t_F], \mathbf{L}^2(\Omega))$$

$$\mathbf{h} \in L^\infty(0, t_F, \mathbf{L}^2(\Omega)) \cap L^2(0, t_F, \mathbf{H}^1(\Omega)),$$

where for a Hilbert space $\mathcal{H}$ we denote by $\mathcal{C}_w([0, t_F], \mathcal{H})$ the space of functions $f : [0, t_F] \to \mathcal{H}$ that are continuous in the weak topology of $\mathcal{H}$.

These two existence results only hold for a smooth domain. Note that the BVPs for the magnetic potential (3.37) and (3.38) are different from the one proposed in (3.18). The BVPs (3.37) and (3.38) are not appropriate to capture the effects of an external magnetic field $\mathbf{h}_a$. In fact, if $\mathbf{h}_a$ is divergence-free (a physically reasonable $\mathbf{h}_a$ in the context of dielectric media should be divergence-free, see Remark 3.2.3), the BVPs (3.37) and (3.38) would yield $\mathbf{h} = \mathbf{h}_d$, with no effect from $\mathbf{h}_a$, so that the behavior of the system would reduce to relaxation to equilibrium. In this sense, the BVP proposed in (3.18) is a much more physically realistic approximation to the effective magnetic field than (3.37) or (3.38).

3.4 Ideal space discretization

For the space discretization we introduce finite dimensional subspaces $\mathbb{U} \subset \mathbf{H}_0^1(\Omega)$, $\mathbb{P} \subset L^2(\Omega)$, $\mathbb{W} \subset \mathbf{H}_0^1(\Omega)$, $\mathbb{M} \subset \mathbf{L}^2(\Omega)$ and $\mathbb{X} \subset H^1(\Omega)$, where we will approximate the linear velocity, pressure, angular velocity, magnetization and magnetic potential, respectively. About the pair of spaces $(\mathbb{U}, \mathbb{P})$ we assume that they are LBB stable (see (1.14) in *Chapter 1*). To be able to focus on the fundamental difficulties in the design of an energy-stable scheme we will first describe the scheme without being specific on the particular structure of these spaces. As we will see, their choice shall come naturally from this analysis.

The discretization of the trilinear form $b(\cdot,\cdot,\cdot)$ follows the same definition as in (2.16) and (2.17). Similarly, we will also need another discretization for the trilinear form associated to the Kelvin force $\mu_0(\mathbf{m}\cdot\nabla)\mathbf{h}$, and the convective term of the magnetization equation $(\mathbf{u}\cdot\nabla)\mathbf{m}$

$$b_h^m(\cdot,\cdot,\cdot) : \mathbb{U}\times\mathbb{M}\times\mathbb{M} \to \mathbb{R}\,, \tag{3.39}$$

and we will also assume that it is skew-symmetric with respect to its last two arguments

$$b_h^m(\mathbf{U},\mathbf{V},\mathbf{W}) = -\,b_h^m(\mathbf{U},\mathbf{W},\mathbf{V}), \quad \forall\,\mathbf{U}\in\mathbb{U};\ \mathbf{V},\mathbf{W}\in\mathbb{M}. \tag{3.40}$$

Finally, we introduce a consistent discretization of the vector Laplacian

$$a_h(\cdot,\cdot) : \mathbb{M}\times\mathbb{M} \to \mathbb{R},$$

which we assume is coercive, that is

$$a_h(\mathbf{M},\mathbf{M}) \geq c_{\text{stab}}|\mathbf{M}|_a^2 \quad \forall\, \mathbf{M} \in \mathbb{M}, \tag{3.41}$$

for a discrete semi-norm $|\cdot|_a$ to be specified later.

Let $\mathrm{I}_{\mathbb{U}}$, $\mathrm{I}_{\mathbb{W}}$ and $\mathrm{I}_{\mathbb{M}}$ denote the usual nodal interpolants

$$\mathrm{I}_{\mathbb{U}} : \boldsymbol{\mathcal{C}}^0(\overline{\Omega}) \to \mathbb{U}\ , \quad \mathrm{I}_{\mathbb{W}} : \boldsymbol{\mathcal{C}}^0(\overline{\Omega}) \to \mathbb{W}\ , \quad \mathrm{I}_{\mathbb{M}} : \boldsymbol{\mathcal{C}}^0(\overline{\Omega}) \to \mathbb{M} \cap \boldsymbol{\mathcal{C}}^0(\overline{\Omega})\ , \tag{3.42}$$

with optimal approximation properties in the sense of (1.13).

More notation and details about the space discretization will be provided in §3.4.2. Here we confine ourselves to mention that the interpolation operators $\mathrm{I}_{\mathbb{U}}$, $\mathrm{I}_{\mathbb{W}}$ and $\mathrm{I}_{\mathbb{M}}$ can be easily constructed using finite elements (see for instance [52, 53]).

Now we present a fully discrete scheme and show that it is unconditionally stable. This result will, in a sense, reproduce the formal energy estimate of Proposition 3.3.1. In addition, it will serve as the basis for a proof of existence of discrete solutions in §3.4.3, as well as for a proof of convergence towards weak solutions in a simplified case in §3.5.4.

3.4.1 Scheme

In order to avoid unnecessary technicalities, assume that the initial data is smooth and initialize the scheme as follows:

$$\mathbf{U}^0 = \mathrm{I}_{\mathbb{U}}[\mathbf{u}(0)]\ , \quad \mathbf{W}^0 = \mathrm{I}_{\mathbb{W}}[\mathbf{w}(0)]\ , \quad \mathbf{M}^0 = \mathrm{I}_{\mathbb{M}}[\mathbf{m}(0)]\ , \tag{3.43}$$

after that, for every $k \in \{1, \ldots, K\}$ we compute $\{\mathbf{U}^k, P^k, \mathbf{W}^k, \mathbf{M}^k, \Phi^k\} \in \mathbb{U} \times \mathbb{P} \times \mathbb{W} \times \mathbb{M} \times \mathbb{X}$ that solves

$$\begin{aligned}\Big(\tfrac{\delta \mathbf{U}^k}{\tau}, \mathbf{V}\Big) + b_h\big(\mathbf{U}^k, \mathbf{U}^k, \mathbf{V}\big) + \widehat{\nu}\big(\nabla \mathbf{U}^k, \nabla \mathbf{V}\big) - \big(P^k, div\, \mathbf{V}\big) \\ = 2\nu_r\big(curl\, \mathbf{W}^k, \mathbf{V}\big) + \mu_0\, b_h^m\big(\mathbf{V}, \mathbf{H}^k, \mathbf{M}^k\big)\,,\end{aligned} \tag{3.44a}$$

$$\big(\mathrm{Q}, div\, \mathbf{U}^k\big) = 0, \tag{3.44b}$$

$$\begin{aligned}\jmath\Big(\tfrac{\delta \mathbf{W}^k}{\tau}, \mathbf{X}\Big) + \jmath\, b_h\big(\mathbf{U}^k, \mathbf{W}^k, \mathbf{X}\big) + c_1\big(\nabla \mathbf{W}^k, \nabla \mathbf{X}\big) + c_2\big(div\, \mathbf{W}^k, div\, \mathbf{X}\big) \\ + 4\nu_r\big(\mathbf{W}^k, \mathbf{X}\big) = 2\nu_r\big(curl\, \mathbf{U}^k, \mathbf{X}\big) + \mu_0\big(\mathbf{M}^k \times \mathbf{H}^k, \mathbf{X}\big)\,,\end{aligned} \tag{3.44c}$$

$$\begin{aligned}\Big(\tfrac{\delta \mathbf{M}^k}{\tau}, \mathbf{Z}\Big) - b_h^m\big(\mathbf{U}^k, \mathbf{Z}, \mathbf{M}^k\big) + \sigma\, a_h(\mathbf{M}^k, \mathbf{Z}) + \big(\mathbf{M}^k \times \mathbf{W}^k, \mathbf{Z}\big) \\ + \tfrac{1}{\mathscr{T}}\big(\mathbf{M}^k, \mathbf{Z}\big) + \sigma\gamma(\mathbf{M}^k \times \boldsymbol{n}, \mathbf{Z} \times \boldsymbol{n})_\Gamma + \sigma\gamma(\mathbf{M}^k \cdot \boldsymbol{n}, \mathbf{Z} \cdot \boldsymbol{n})_\Gamma \\ = \tfrac{1}{\mathscr{T}}\big(\varkappa_0 \mathbf{H}^k, \mathbf{Z}\big) + \sigma\gamma(\varkappa_0 \mathbf{H}^k \times \boldsymbol{n}, \mathbf{Z} \times \boldsymbol{n})_\Gamma \\ + \sigma\gamma(\varkappa_0 \mathbf{H}^k \cdot \boldsymbol{n}, \mathbf{Z} \cdot \boldsymbol{n})_\Gamma\,,\end{aligned} \tag{3.44d}$$

$$(\nabla \Phi^k, \nabla \mathrm{X}) = (\mathbf{h}_a^k - \mathbf{M}^k, \nabla \mathrm{X}), \tag{3.44e}$$

for all $\mathbf{V} \in \mathbb{U}$, $\mathbf{X} \in \mathbb{W}$, $\mathbf{Z} \in \mathbb{M}$, $\mathrm{X} \in \mathbb{X}$, where $\mathbf{H}^k := \nabla \Phi^k$.

Notice that a discrete analogue of (3.26) is built into the scheme because of the term $\mu_0\, b_h^m\big(\mathbf{V}, \mathbf{H}^k, \mathbf{M}^k\big)$ in the right hand side of (3.44a). The initialization proposed in (3.43) is the simplest choice and it is used because of that reason. From the point of view of convergence to strong solutions (a priori error estimates) it is suboptimal (cf. [86, 49, 53, 87]). However, the choice of initialization has no effect on the stability of the scheme; it only affects the regularity assumed on the initial data.

We now present the stability of scheme (3.44). To shorten the presentation we denote

$$\begin{aligned}
\mathscr{E}^k_{h,\tau}(\mathbf{U}^\tau,\mathbf{W}^\tau,\mathbf{M}^\tau,\mathbf{H}^\tau) &= \tfrac{1}{2}\big(\|\mathbf{U}^k\|^2_{\mathbf{L}^2} + \jmath\|\mathbf{W}^k\|^2_{\mathbf{L}^2} + \mu_0\|\mathbf{M}^k\|^2_{\mathbf{L}^2} \\
&\quad + \mu_0\|\mathbf{H}^k\|^2_{\mathbf{L}^2}\big), \\
\mathscr{I}^k_{h,\tau}(\mathbf{U}^\tau,\mathbf{W}^\tau,\mathbf{M}^\tau,\mathbf{H}^\tau) &= \mathscr{E}^k_{h,\tau}(\delta\mathbf{U}^\tau,\delta\mathbf{W}^\tau,\delta\mathbf{M}^\tau,\delta\mathbf{H}^\tau), \\
\mathscr{D}^k_{h,\tau}(\mathbf{U}^\tau,\mathbf{W}^\tau,\mathbf{M}^\tau,\mathbf{H}^\tau) &= \nu\|\nabla\mathbf{U}^k\|^2_{\mathbf{L}^2} + c_1\|\nabla\mathbf{W}^k\|^2_{\mathbf{L}^2} + \nu_r\|div\,\mathbf{U}^k\|^2_{\mathbf{L}^2} \\
&\quad + c_2\|div\,\mathbf{W}^k\|^2_{\mathbf{L}^2} + \nu_r\|curl\,\mathbf{U}^k - 2\mathbf{W}^k\|^2_{\mathbf{L}^2} \\
&\quad + \tfrac{\mu_0}{\mathscr{T}}\|\mathbf{M}^k\|^2_{\mathbf{L}^2} + \tfrac{\mu_0}{2\mathscr{T}}\left(\tfrac{1}{2} + 3\varkappa_0\right)\|\mathbf{H}^k\|^2_{\mathbf{L}^2}, \\
\mathscr{F}^k(\mathbf{h}_a) &= \tfrac{\mathscr{T}\mu_0}{\tau}\int_{t^{k-1}}^{t^k}\|\partial_t\mathbf{h}_a(s)\|^2_{\mathbf{L}^2}\,ds + \tfrac{\mu_0}{2\mathscr{T}}(1+\varkappa_0)\|\mathbf{h}^k_a\|^2_{\mathbf{L}^2}.
\end{aligned}$$

Proposition 3.4.1 (Discrete stability)**.** *Let* $\sigma = 0$*, and* $\{\mathbf{U}^\tau, P^\tau, \mathbf{W}^\tau, \mathbf{M}^\tau, \Phi^\tau\} \subset \mathbb{U}\times\mathbb{P}\times\mathbb{W}\times\mathbb{M}\times\mathbb{X}$ *solve* (3.44)*. If* $\nabla\mathbb{X}\subset\mathbb{M}$*,* (2.17) *and* (3.40) *hold, then we have the following estimate*

$$\mathscr{E}^K_{h,\tau} + \tau^{-1}\left\|\mathscr{I}^\tau_{h,\tau}\right\|_{\ell^1} + \left\|\mathscr{D}^\tau_{h,\tau}\right\|_{\ell^1} \le \|\mathscr{F}^\tau\|_{\ell^1} + \mathscr{E}^0_{h,\tau}\,,$$

where $\mathscr{E}^k_{h,\tau} := \mathscr{E}^k_{h,\tau}(\mathbf{U}^\tau,\mathbf{W}^\tau,\mathbf{M}^\tau,\mathbf{H}^\tau)$*,* $\mathscr{I}^k_{h,\tau} := \mathscr{I}^k_{h,\tau}(\mathbf{U}^\tau,\mathbf{W}^\tau,\mathbf{M}^\tau,\mathbf{H}^\tau)$*,* $\mathscr{D}^k_{h,\tau} := \mathscr{D}^k_{h,\tau}(\mathbf{U}^\tau,\mathbf{W}^\tau,\mathbf{M}^\tau,\mathbf{H}^\tau)$ *and* $\mathscr{F}^k_{h,\tau} := \mathscr{F}^k(\mathbf{h}_a)$*.*

Proof. Set $\mathbf{V} = 2\tau\mathbf{U}^k$, $\mathbf{X} = 2\tau\mathbf{W}^k$, $\mathbf{Z} = 2\tau\mu_0\mathbf{M}^k$, $\nabla\mathrm{X} = \frac{2\tau\varkappa_0\mu_0}{\mathscr{T}}\nabla\Phi^k$ in (3.44) and

add the results. Using (1.2) and the identity (1.11), we get

$$\begin{aligned} 2\delta\mathscr{E}^k_{h,\tau} - \mu_0\delta\|\mathbf{H}^k\|^2_{\mathbf{L}^2} + 2\mathscr{I}^k_{h,\tau} - \mu_0\|\delta\mathbf{H}^k\|^2_{\mathbf{L}^2} + 2\tau\mathscr{D}^k_{h,\tau} \\ - \tfrac{\mu_0\tau}{\mathscr{T}}\left(\tfrac{1}{2} + \varkappa_0\right)\|\nabla\Phi^k\|^2_{\mathbf{L}^2} = 2\mu_0\tau\, b^m_h\big(\mathbf{U}^k, \mathbf{H}^k, \mathbf{M}^k\big) \\ + 2\mu_0\tau(\mathbf{M}^k \times \mathbf{H}^k, \mathbf{W}^k) + \tfrac{2\mu_0\varkappa_0\tau}{\mathscr{T}}(\mathbf{h}^k_a, \nabla\Phi^k). \end{aligned} \tag{3.46}$$

As in the proof of Proposition 3.3.1, to deal with the trilinear terms $2\mu_0\tau\, b^m_h\big(\mathbf{U}^k, \mathbf{H}^k, \mathbf{M}^k\big)$ and $2\mu_0\tau(\mathbf{M}^k \times \mathbf{H}^k, \mathbf{W}^k)$ we set $\mathbf{Z} = 2\mu_0\tau\mathbf{H}^k$. Notice that $\mathbf{H}^k = \nabla\Phi^k$ is, by assumption, a valid test function. In doing so we obtain

$$\begin{aligned} \tfrac{2\mu_0\tau\varkappa_0}{\mathscr{T}}\|\nabla\Phi^k\|^2_{\mathbf{L}^2} = -2\mu_0\tau\, b^m_h\big(\mathbf{U}^k, \mathbf{H}^k, \mathbf{M}^k\big) - 2\mu_0\tau\big(\mathbf{M}^k \times \mathbf{H}^k, \mathbf{W}^k\big) \\ + 2\mu_0\left(\delta\mathbf{M}^k, \nabla\Phi^k\right) + \tfrac{2\mu_0\tau}{\mathscr{T}}\big(\mathbf{M}^k, \nabla\Phi^k\big). \end{aligned} \tag{3.47}$$

Adding (3.47) to (3.46) we obtain

$$\begin{aligned} 2\delta\mathscr{E}^k_{h,\tau} - \mu_0\delta\|\mathbf{H}^k\|^2_{\mathbf{L}^2} + 2\mathscr{I}^k_{h,\tau} - \mu_0\|\delta\mathbf{H}^k\|^2_{\mathbf{L}^2} + 2\tau\mathscr{D}^k_{h,\tau} \\ + \tfrac{\mu_0\tau}{\mathscr{T}}\left(\varkappa_0 - \tfrac{1}{2}\right)\|\nabla\Phi^k\|^2_{\mathbf{L}^2} = 2\mu_0\left(\delta\mathbf{M}^k, \nabla\Phi^k\right) \\ + \tfrac{2\mu_0\tau}{\mathscr{T}}\big(\mathbf{M}^k, \nabla\Phi^k\big) + \tfrac{2\mu_0\varkappa_0\tau}{\mathscr{T}}(\mathbf{h}^k_a, \nabla\Phi^k). \end{aligned} \tag{3.48}$$

We now must obtain discrete analogues of (3.31) and (3.32). To do so, we set $\mathrm{X} = \Phi^k$ to obtain

$$\|\nabla\Phi^k\|^2_{\mathbf{L}^2} = (\mathbf{h}^k_a - \mathbf{M}^k, \nabla\Phi^k). \tag{3.49}$$

Taking increments on (3.44e) and setting $\mathrm{X} = \Phi^k$ yields

$$(\delta\nabla\Phi^k, \nabla\Phi^k) = (\delta\mathbf{h}^k_a - \delta\mathbf{M}^k, \nabla\Phi^k). \tag{3.50}$$

Adding suitable multiples of (3.49) and (3.50) to (3.48), and dividing everything by

2, we obtain

$$\mathscr{E}^k_{h,\tau} + \mathscr{I}^k_{h,\tau} + \tau\mathscr{D}^k_{h,\tau} + \tfrac{\mu_0\tau}{2\mathscr{T}}\left(\tfrac{3}{2}+\varkappa_0\right)\|\nabla\Phi^k\|^2_{\mathbf{L}^2} = \mathscr{E}^{k-1}_{h,\tau} + \mu_0\left(\delta\mathbf{h}^k_a, \nabla\Phi^k\right) + \tfrac{\mu_0\tau}{\mathscr{T}}(1+\varkappa_0)\left(\mathbf{h}^k_a, \nabla\Phi^k\right). \tag{3.51}$$

Adding over k, using the trivial identity $\|\delta\mathbf{h}^k_a\|^2_{\mathbf{L}^2} = \tau^2\left\|\frac{\delta\mathbf{h}^k_a}{\tau}\right\|^2_{\mathbf{L}^2}$ and the estimate

$$\left\|\tfrac{\delta\mathbf{h}^k_a}{\tau}\right\|^2_{\mathbf{L}^2} \le \tfrac{1}{\tau}\int_{t^{k-1}}^{t^k}\|\partial_t\mathbf{h}_a(s)\|^2_{\mathbf{L}^2}ds\,,$$

to control $\tau^{-1}\left\|\delta\mathbf{h}^k_a\right\|_{\mathbf{L}^2}$, yields the asserted estimate. □

3.4.2 Practical space discretization

Having understood what is required from scheme (3.44) to achieve stability we will now specify our choices using finite elements. We assume that we have at hand a conforming and shape regular triangulation $\mathcal{T}_h$ of the polygonal domain Ω, made of open disjoint elements T such that $\overline{\Omega} = \bigcup_{T\in\mathcal{T}_h}\overline{T}$. We will denote by $\mathcal{F}^i$ the collection of internal faces F of $\mathcal{T}_h$. As Proposition 3.4.1 shows, to gain stability it is convenient to have $\nabla\mathbb{X}\subset\mathbb{M}$. Since the space $\mathbb{X}$ is used to approximate the solution of an elliptic problem with Neumann boundary conditions, the simplest choice for $\mathbb{X}$ is a finite element space of continuous functions

$$\mathbb{X} = \left\{\mathrm{X}\in\mathcal{C}^0\left(\overline{\Omega}\right) \mid \mathrm{X}|_T\in\mathcal{P}_\ell(T)\,,\forall T\in\mathcal{T}_h\right\}\subset H^1(\Omega). \tag{3.52}$$

To achieve $\nabla\mathbb{X}\subset\mathbb{M}$ we allow $\mathbb{M}$ to be a space of discontinuous functions

$$\mathbb{M} = \left\{\mathbf{M}\in\mathbf{L}^2(\Omega) \mid \mathbf{M}|_T\in[\mathcal{P}_{\ell-1}(T)]^d\,,\forall\,T\in\mathcal{T}_h\right\}, \tag{3.53}$$

and, consequently, the forms $b_h^m(\cdot,\cdot,\cdot)$ and $a_h(\cdot,\cdot)$ must be defined accordingly. Here $\mathcal{P}_\ell$ denotes the space of polynomials of total degree at most ℓ, usually associated to simplicial elements.

The trilinear form b_h^m is defined by

$$\begin{aligned} b_h^m(\mathbf{U},\mathbf{V},\mathbf{W}) := & \sum_{T\in\mathcal{T}_h}\int_T (\mathbf{U}\cdot\nabla)\mathbf{V}\cdot\mathbf{W} + \tfrac{1}{2} div\,\mathbf{U}\mathbf{V}\cdot\mathbf{W}\,dx \\ & - \sum_{F\in\mathcal{F}^i}\int_F (\llbracket\mathbf{V}\rrbracket\cdot\{\!\{\mathbf{W}\}\!\})(\mathbf{U}\cdot\boldsymbol{n}_F)\,dS\,, \end{aligned} \tag{3.54}$$

the bulk integrals are the classical Temam [43] modification of the convective term (1.5), whereas the face integrals are consistency terms. This discretization of convection for discontinuous spaces traces back to [88, 87, 89, 90]. From these references it is known that, provided the first argument ($\mathbf{U}$ in (3.54)) is $\mathbf{H}(div,\Omega)$ conforming and has a vanishing normal trace on the boundary, $b_h^m(\cdot,\cdot,\cdot)$ is skew symmetric, that is (3.40) holds.

The bilinear form $a_h(\cdot,\cdot)$ is obtained with interior penalty techniques

$$a_h(\mathbf{M},\mathbf{Z}) = \langle\mathbf{M},\mathbf{Z}\rangle_{\mathbf{H}(curl_h)} + \langle\mathbf{M},\mathbf{Z}\rangle_{\mathbf{H}(div_h)}, \tag{3.55}$$

where $\langle\cdot,\cdot\rangle_{\mathbf{H}(curl_h)}$ and $\langle\cdot,\cdot\rangle_{\mathbf{H}(div_h)}$ are interior penalty discretizations of $(curl\,\cdot, curl\,\cdot)$ and $(div\,\cdot, div\,\cdot)$, respectively

$$\begin{aligned} \langle\mathbf{M},\mathbf{Z}\rangle_{\mathbf{H}(curl_h)} = & \sum_{T\in\mathcal{T}_h}\int_T curl\,\mathbf{M}\cdot curl\,\mathbf{Z}\,dx \\ & - \sum_{F\in\mathcal{F}^i}\int_F (\{\!\{curl\,\mathbf{M}\}\!\}\times\boldsymbol{n}_F)\cdot\llbracket\mathbf{Z}\rrbracket + (\{\!\{curl\,\mathbf{Z}\}\!\}\times\boldsymbol{n}_F)\cdot\llbracket\mathbf{M}\rrbracket\,dS \\ & + \sum_{F\in\mathcal{F}^i}\tfrac{\eta}{h_F}\int_F (\llbracket\mathbf{M}\rrbracket\times\boldsymbol{n}_F)\cdot(\llbracket\mathbf{Z}\rrbracket\times\boldsymbol{n}_F)\,dS\,, \end{aligned} \tag{3.56}$$

$$\begin{aligned}\langle \mathbf{M}, \mathbf{Z} \rangle_{\mathbf{H}(div_h)} = & \sum_{T \in \mathcal{T}_h} \int_T div\, \mathbf{M}\, div\, \mathbf{Z}\, dx \\ & - \sum_{F \in \mathcal{F}^i} \int_F \{\!\{ div\, \mathbf{M} \}\!\} \left([\![\mathbf{Z}]\!] \cdot \boldsymbol{n}_F \right) + \{\!\{ div\, \mathbf{Z} \}\!\} \left([\![\mathbf{M}]\!] \cdot \boldsymbol{n}_F \right) dS \\ & + \sum_{F \in \mathcal{F}^i} \tfrac{\eta}{h_F} \int_F ([\![\mathbf{M}]\!] \cdot \boldsymbol{n}_F)([\![\mathbf{Z}]\!] \cdot \boldsymbol{n}_F)\, dS\,. \end{aligned} \tag{3.57}$$

As usual, the parameter $\eta > 0$ must be chosen large enough to yield coercivity (3.41) (cf.[87]). In this setting the discrete semi-norm $|\cdot|_a$ is defined as

$$|\mathbf{M}|_a^2 = \sum_{T \in \mathcal{T}_h} \int_T \left(|curl\, \mathbf{M}|^2 + |div\, \mathbf{M}|^2 \right) + \sum_{F \in \mathcal{F}^i} \tfrac{1}{h_F} \int_F \left(|\, [\![\mathbf{M}]\!] \cdot \boldsymbol{n}_F|^2 + |\, [\![\mathbf{M}]\!] \times \boldsymbol{n}_F|^2 \right) ,$$

The choice of the remaining spaces is straightforward. The only restriction (for the scheme (3.44)) is that the pair $\{\mathbb{U}, \mathbb{P}\}$, used to approximate the linear velocity and pressure, must be LBB stable (see (1.14)). Therefore, for $\ell \geq 2$ we set

$$\begin{aligned} \mathbb{U} &= \left\{ \mathbf{U} \in \boldsymbol{\mathcal{C}}^0\big(\overline{\Omega}\big) \mid \mathbf{U}|_T \in [\mathcal{P}_\ell(T)]^d \,, \forall\, T \in \mathcal{T}_h \right\} \cap \mathbf{H}_0^1(\Omega) \\ \mathbb{P} &= \left\{ \mathrm{Q} \in \mathcal{C}^0\big(\overline{\Omega}\big) \mid \mathrm{Q}|_T \in \mathcal{P}_{\ell-1}(T) \,, \forall\, T \in \mathcal{T}_h \right\} \\ \mathbb{W} &= \left\{ \mathbf{W} \in \boldsymbol{\mathcal{C}}^0\big(\overline{\Omega}\big) \mid \mathbf{W}|_T \in [\mathcal{P}_\ell(T)]^d \,, \forall\, T \in \mathcal{T}_h \right\} \cap \mathbf{H}_0^1(\Omega) \\ \mathbb{M} &= \left\{ \mathbf{M} \in \mathbf{L}^2\big(\Omega\big) \mid \mathbf{M}|_T \in [\mathcal{P}_{\ell-1}(T)]^d \,, \forall\, T \in \mathcal{T}_h \right\} \\ \mathbb{X} &= \left\{ \mathrm{X} \in \mathcal{C}^0\big(\overline{\Omega}\big) \mid \mathrm{X}|_T \in \mathcal{P}_\ell(T) \,, \forall\, T \in \mathcal{T}_h \right\} . \end{aligned} \tag{3.58}$$

It is well known that the pair $\{\mathbb{U}, \mathbb{P}\}$ in (3.58) (cf.[42, 53]) is LBB stable for $\ell \geq 2$ under minor restrictions of the mesh $\mathcal{T}_h$. Note also in (3.58), that we are using a continuous finite element space $\mathbb{P}$ for the pressure, which is something we might have to change (the velocity space too) if we want to consider convergence of a numerical scheme under minimal regularity assumptions (the use of discontinuous pressures will be considered for a different model, later in §3.5.3).

In (3.58) we have used polynomials $\mathcal{P}_\ell$ over simplices. However, the fact that the scheme (3.44) is energy-stable is not tightly related to simplices. In (3.52), (3.53) and (3.58), it is possible to replace $\mathcal{P}_\ell$ by $\mathcal{Q}_\ell$ (polynomials of degree at most ℓ in each variable) and use quadrilateral/hexahedral elements. That will only require us to do some minor modifications of the scheme. To simplify our exposition we will always assume that our elements are simplicial and develop our theory under this assumption. We will provide remarks describing the required modifications, if any, when quadrilaterals are to be used. With this choice of spaces, the scheme presents itself as a generalization of those studied in [86, 91].

Remark 3.4.1 (Redefinition of the pressure)**.** Given $\varpi \in \{0,1\}$, let $(\mathbf{u},p) \in \mathbf{H}^1_0(\Omega)\times L^2_0(\Omega)$ solve

$$\begin{aligned}(\nabla\mathbf{u},\nabla\mathbf{v})-(p,div\,\mathbf{v}) &= (\mathbf{f},\mathbf{v})+\varpi(g,div\,\mathbf{v}) \quad \forall\mathbf{v}\in\mathbf{H}^1_0(\Omega)\,,\\ (q,div\,\mathbf{u}) &= 0 \qquad\qquad\qquad\qquad \forall q\in L^2_0(\Omega)\,,\end{aligned}$$

Since the pressure can be redefined as $\widehat{p}=p+\varpi g$, the velocity $\mathbf{u}$ is independent of ϖ. This has been used to devise energy-stable schemes for phase field models [92] and liquid crystals [93]. In the same spirit we have eliminated, from the Kelvin force (in (3.44a)) the term $-\frac{1}{2}(div\,\mathbf{V},\mathbf{M}^k\cdot\mathbf{H}^k)$.

3.4.3 Existence of solutions for $\sigma = 0$

The energy estimate of Proposition 3.4.1 (discrete stability) serves as an a priori estimate of solutions of (3.44). This estimate can be used to establish, with the help of Leray-Schauder theorem (cf.[94, p. 280]), existence of solutions. The core of the

following result is a local in time energy estimate similar to that of Proposition 3.4.1. To avoid repetitions we skip some details.

Theorem 3.4.1 (Existence for $\sigma = 0$)**.** *Let $h, \tau > 0$. For every $k \in \{1, \dots, K\}$ the scheme* (3.44) *has a solution. Moreover, this solution satisfies the estimate of Proposition 3.4.1.*

Proof. We define the linear map $\widehat{x} = \mathcal{L}x$,

$$\left\{\mathbf{U}^k, P^k, \mathbf{W}^k, \mathbf{M}^k, \nabla\Phi^k\right\} \overset{\mathcal{L}}{\mapsto} \left\{\widehat{\mathbf{U}}^k, \widehat{P}^k, \widehat{\mathbf{W}}^k, \widehat{\mathbf{M}}^k, \nabla\widehat{\Phi}^k\right\},$$

where the quantities with hats solve:

$$\begin{aligned}\left(\tfrac{\widehat{\mathbf{U}}^k - \mathbf{U}^{k-1}}{\tau}, \mathbf{V}\right) + b_h\big(\mathbf{U}^k, \widehat{\mathbf{U}}^k, \mathbf{V}\big) + \widehat{\nu}\big(\nabla\widehat{\mathbf{U}}^k, \nabla\mathbf{V}\big) \\ - \big(\widehat{P}^k, div\,\mathbf{V}\big) = 2\nu_r\big(curl\,\widehat{\mathbf{W}}^k, \mathbf{V}\big) + \mu_0\, b_h^m\big(\mathbf{V}, \mathbf{H}^k, \widehat{\mathbf{M}}^k\big),\end{aligned} \tag{3.59a}$$

$$\big(\mathrm{Q}, div\,\widehat{\mathbf{U}}^k\big) = 0, \tag{3.59b}$$

$$\begin{aligned}\jmath\left(\tfrac{\widehat{\mathbf{W}}^k - \mathbf{W}^{k-1}}{\tau}, \mathbf{X}\right) + \jmath\, b_h\big(\mathbf{U}^k, \widehat{\mathbf{W}}^k, \mathbf{X}\big) + c_1\big(\nabla\widehat{\mathbf{W}}^k, \nabla\mathbf{X}\big) + c_2\big(div\,\widehat{\mathbf{W}}^k, div\,\mathbf{X}\big) \\ + 4\nu_r\big(\widehat{\mathbf{W}}^k, \mathbf{X}\big) = 2\nu_r\big(curl\,\mathbf{U}^k, \mathbf{X}\big) + \mu_0\big(\widehat{\mathbf{M}}^k \times \mathbf{H}^k, \mathbf{X}\big),\end{aligned} \tag{3.59c}$$

$$\begin{aligned}\left(\tfrac{\widehat{\mathbf{M}}^k - \mathbf{M}^{k-1}}{\tau}, \mathbf{Z}\right) - b_h^m\big(\mathbf{U}^k, \mathbf{Z}, \widehat{\mathbf{M}}^k\big) + \big(\widehat{\mathbf{M}}^k \times \mathbf{W}^k, \mathbf{Z}\big) + \tfrac{1}{\mathscr{T}}\big(\widehat{\mathbf{M}}^k, \mathbf{Z}\big) \\ = \tfrac{\varkappa_0}{\mathscr{T}}\big(\widehat{\mathbf{H}}^k, \mathbf{Z}\big),\end{aligned} \tag{3.59d}$$

$$(\nabla\widehat{\Phi}^k, \nabla\mathrm{X}) = (\mathbf{h}_a^k - \widehat{\mathbf{M}}^k, \nabla\mathrm{X}), \tag{3.59e}$$

where $\widehat{\mathbf{H}}^k = \nabla\widehat{\Phi}^k$. To assert the existence of a solution we show that the map $\mathcal{L}$ satisfies the requirements of the Leray-Schauder theorem [94, p. 280]:

- ◇ **Well posedness.** The operator $\mathcal{L}$ is clearly well defined. The information follows a bottom-up path, so we start with the coupled system (3.59d)-(3.59e)

on the bottom, which can be conveniently rewritten as follows:

$$\begin{aligned}\Big(\widehat{\mathbf{M}}^k,\mathbf{Z}\Big)-\tau\,b_h^m\big(\mathbf{U}^k,\mathbf{Z},\widehat{\mathbf{M}}^k\big)+\tau\big(\widehat{\mathbf{M}}^k\times\mathbf{W}^k,\mathbf{Z}\big)\\ +\tfrac{\tau}{\mathscr{T}}\big(\widehat{\mathbf{M}}^k,\mathbf{Z}\big)-\tfrac{\tau\varkappa_0}{\mathscr{T}}\big(\widehat{\mathbf{H}}^k,\mathbf{Z}\big)=\big(\mathbf{M}^{k-1},\mathbf{Z}\big)\\ (\widehat{\mathbf{M}}^k,\nabla\mathrm{X})+(\nabla\widehat{\Phi}^k,\nabla\mathrm{X})=(\mathbf{h}_a^k,\nabla\mathrm{X})\,.\end{aligned}$$

Set $\mathbf{Z}=\widehat{\mathbf{M}}^k$ and $\mathrm{X}=\frac{\tau\varkappa_0}{\mathscr{T}}\widehat{\Phi}^k$, to show that this system is positive definite. This yields the functions $\widehat{\mathbf{M}}^k$ and $\widehat{\Phi}^k$, which can be used as data in (3.59c) to obtain $\widehat{\mathbf{W}}^k$. Inserting $\widehat{\mathbf{W}}^k$ and $\widehat{\mathbf{M}}^k$ into (3.59a)–(3.59b) gives rise to the pair $(\widehat{\mathbf{U}^k},\widehat{P^k})$.

◇ **Boundedness.** We must verify that solutions $\widehat{x}=\Big\{\widehat{\mathbf{U}}^k,\widehat{P}^k,\widehat{\mathbf{W}}^k,\widehat{\mathbf{M}}^k,\nabla\widehat{\Phi}^k\Big\}$ of $\frac{1}{\lambda}\widehat{x}=\mathcal{L}\widehat{x}$ with $\lambda\in(0,1]$ can be bounded in terms of the local data $\big\{\mathbf{U}^{k-1},\mathbf{W}^{k-1},\mathbf{M}^{k-1},\nabla\Phi^{k-1},\mathbf{h}_a^k\big\}$ uniformly with respect to λ. In other words, we want to analyze the local boundedness of

$$\begin{aligned}\Big(\tfrac{\lambda^{-1}\widehat{\mathbf{U}^k}-\mathbf{U}^{k-1}}{\tau},\mathbf{V}\Big)+\,b_h\big(\widehat{\mathbf{U}}^k,\lambda^{-1}\,\widehat{\mathbf{U}}^k,\mathbf{V}\big)\\ +\widehat{\nu}\big(\lambda^{-1}\,\nabla\widehat{\mathbf{U}}^k,\nabla\mathbf{V}\big)-\big(\lambda^{-1}\,\widehat{P}^k,div\,\mathbf{V}\big)\\ =2\nu_r\big(\lambda^{-1}\,curl\,\widehat{\mathbf{W}}^k,\mathbf{V}\big)+\mu_0\,b_h^m\big(\mathbf{V},\widehat{\mathbf{H}}^k,\lambda^{-1}\,\widehat{\mathbf{M}}^k\big)\,,\end{aligned}\tag{3.60a}$$

$$\big(\mathrm{Q},div\,\widehat{\mathbf{U}}^k\big)=0\,,\tag{3.60b}$$

$$\begin{aligned}\jmath\,\Big(\tfrac{\lambda^{-1}\widehat{\mathbf{W}}^k-\mathbf{W}^{k-1}}{\tau},\mathbf{X}\Big)+\jmath\,b_h\big(\widehat{\mathbf{U}}^k,\lambda^{-1}\,\widehat{\mathbf{W}}^k,\mathbf{X}\big)+c_1\big(\lambda^{-1}\,\nabla\widehat{\mathbf{W}}^k,\nabla\mathbf{X}\big)\\ +c_2\big(\lambda^{-1}\,div\,\widehat{\mathbf{W}}^k,div\,\mathbf{X}\big)+4\nu_r\big(\lambda^{-1}\,\widehat{\mathbf{W}}^k,\mathbf{X}\big)\\ =2\nu_r\big(curl\,\widehat{\mathbf{U}}^k,\mathbf{X}\big)+\mu_0\big(\lambda^{-1}\,\widehat{\mathbf{M}}^k\times\widehat{\mathbf{H}}^k,\mathbf{X}\big)\,,\end{aligned}\tag{3.60c}$$

$$\begin{aligned}\Big(\tfrac{\lambda^{-1}\widehat{\mathbf{M}}^k-\mathbf{M}^{k-1}}{\tau},\mathbf{Z}\Big)-\,b_h^m\big(\widehat{\mathbf{U}}^k,\mathbf{Z},\lambda^{-1}\,\widehat{\mathbf{M}}^k\big)+\big(\lambda^{-1}\,\widehat{\mathbf{M}}^k\times\widehat{\mathbf{W}}^k,\mathbf{Z}\big)\\ +\tfrac{1}{\mathscr{T}}\big(\lambda^{-1}\,\widehat{\mathbf{M}}^k,\mathbf{Z}\big)=\tfrac{\varkappa_0}{\mathscr{T}}\big(\lambda^{-1}\,\widehat{\mathbf{H}}^k,\mathbf{Z}\big)\end{aligned}\tag{3.60d}$$

$$(\lambda^{-1}\,\nabla\widehat{\Phi}^k,\nabla\mathrm{X})=(\mathbf{h}_a^k-\lambda^{-1}\,\widehat{\mathbf{M}}^k,\nabla\mathrm{X})\,,\tag{3.60e}$$

with $\lambda \in (0,1]$. Set $\mathbf{V} = 2\tau\lambda\widehat{\mathbf{U}}^k$, $\mathbf{X} = 2\tau\lambda\widehat{\mathbf{W}}^k$, $\mathbf{Z} = 2\tau\mu_0\lambda\widehat{\mathbf{M}}^k$, $\mathrm{X} = \frac{2\tau\varkappa_0\mu_0\lambda}{\mathscr{J}}\widehat{\Phi}^k$ in (3.60a)-(3.60e), and use identity (1.11). As we did to obtain (3.47), set $\mathbf{Z} = 2\mu_0\tau\lambda\nabla\widehat{\Phi}^k$ in (3.60d) (to eliminate the trilinear terms). Adding the ensuing equations, and eliminating superfluous positive terms, we obtain:

$$\begin{aligned}
&\|\widehat{\mathbf{U}}^k\|^2_{\mathbf{L}^2} - \|\lambda\mathbf{U}^{k-1}\|^2_{\mathbf{L}^2} + \jmath\|\widehat{\mathbf{W}}^k\|^2_{\mathbf{L}^2} - \jmath\|\lambda\mathbf{W}^{k-1}\|^2_{\mathbf{L}^2} + \mu_0\|\widehat{\mathbf{M}}^k\|^2_{\mathbf{L}^2} \\
&\quad - \mu_0\|\lambda\mathbf{M}^{k-1}\|^2_{\mathbf{L}^2} + 2\left(\nu+\nu_r\right)\tau\,\|\nabla\widehat{\mathbf{U}}^k\|^2_{\mathbf{L}^2} + 2c_1\tau\|\nabla\widehat{\mathbf{W}}^k\|^2_{\mathbf{L}^2} \\
&\quad + 2c_2\tau\|div\,\widehat{\mathbf{W}}^k\|^2_{\mathbf{L}^2} + 8\tau\nu_r\|\widehat{\mathbf{W}}^k\|^2_{\mathbf{L}^2} + \tfrac{2\mu_0\tau}{\mathscr{J}}\|\widehat{\mathbf{M}}^k\|^2_{\mathbf{L}^2} \\
&\quad + \tfrac{4\mu_0\varkappa_0\tau}{\mathscr{J}}\|\nabla\widehat{\Phi}^k\|^2_{\mathbf{L}^2} \leq 4\nu_r\tau(1+\lambda)(curl\,\widehat{\mathbf{U}}^k, \widehat{\mathbf{W}}^k) \\
&\quad + 2\mu_0(\widehat{\mathbf{M}}^k - \lambda\mathbf{M}^{k-1}, \nabla\widehat{\Phi}^k) + \tfrac{2\mu_0\tau}{\mathscr{J}}(\widehat{\mathbf{M}}^k, \nabla\widehat{\Phi}^k) \\
&\quad + \tfrac{2\mu_0\varkappa_0\tau\lambda}{\mathscr{J}}(\mathbf{h}_a^k, \nabla\widehat{\Phi}^k)\,.
\end{aligned} \tag{3.61}$$

Set $\mathrm{X} = \lambda\widehat{\Phi}^k$ in (3.60e) to obtain $\|\nabla\widehat{\Phi}^k\|^2_{\mathbf{L}^2} = (\lambda\mathbf{h}_a^k - \widehat{\mathbf{M}}^k, \nabla\widehat{\Phi}^k)$. Consequently, (3.61) can be rewritten as

$$\begin{aligned}
&\|\widehat{\mathbf{U}}^k\|^2_{\mathbf{L}^2} - \|\lambda\mathbf{U}^{k-1}\|^2_{\mathbf{L}^2} + \jmath\|\widehat{\mathbf{W}}^k\|^2_{\mathbf{L}^2} - \jmath\|\lambda\mathbf{W}^{k-1}\|^2_{\mathbf{L}^2} + \mu_0\|\widehat{\mathbf{M}}^k\|^2_{\mathbf{L}^2} \\
&\quad - \mu_0\|\lambda\mathbf{M}^{k-1}\|^2_{\mathbf{L}^2} + 2\left(\nu+\nu_r\right)\tau\,\|\nabla\widehat{\mathbf{U}}^k\|^2_{\mathbf{L}^2} + 2c_1\tau\|\nabla\widehat{\mathbf{W}}^k\|^2_{\mathbf{L}^2} \\
&\quad + 2c_2\tau\|div\,\widehat{\mathbf{W}}^k\|^2_{\mathbf{L}^2} + 8\tau\nu_r\|\widehat{\mathbf{W}}^k\|^2_{\mathbf{L}^2} + \tfrac{2\mu_0\tau}{\mathscr{J}}\|\widehat{\mathbf{M}}^k\|^2_{\mathbf{L}^2} \\
&\quad + 2\mu_0\left(\tfrac{2\varkappa_0\tau}{\mathscr{J}} + \tfrac{\tau}{\mathscr{J}} + 1\right)\|\nabla\widehat{\Phi}^k\|^2_{\mathbf{L}^2} \leq 4\nu_r\tau(1+\lambda)(curl\,\widehat{\mathbf{U}}^k, \widehat{\mathbf{W}}^k) \\
&\quad - 2\mu_0\lambda(\mathbf{M}^{k-1}, \nabla\widehat{\Phi}^k) + 2\mu_0\lambda\left(\tfrac{\varkappa_0\tau}{\mathscr{J}} + \tfrac{\tau}{\mathscr{J}} + 1\right)(\mathbf{h}_a^k, \nabla\widehat{\Phi}^k)\,.
\end{aligned} \tag{3.62}$$

To conclude it suffices to suitably bound the right-hand side. This can be easily attained by recalling that $\lambda \leq 1$ and using (1.2).

$\diamond$ **Compactness.** Compactness of the linear operator $\mathcal{L}$ is immediate, since we are working in finite dimensions.

□

3.4.4 Lack of stability for $\sigma > 0$

Since $\mathbf{H}^k = \nabla\Phi^k \in \mathbf{H}(curl, \Omega)$ we have that

$$\begin{gathered} curl\,\mathbf{H}^k\Big|_T = 0 \;\; \forall T \in \mathcal{T}_h \;, \quad \Big\{\!\Big\{ curl\,\mathbf{H}^k \Big\}\!\Big\}\Big|_F = 0 \;\; \forall F \in \mathcal{F}^i \;, \\ \Big[\!\Big[\mathbf{H}^k \Big]\!\Big] \times \boldsymbol{n}_F\Big|_F = 0 \;\; \forall F \in \mathcal{F}^i. \end{gathered} \tag{3.63}$$

From these properties and definition (3.56) we deduce that $\langle \mathbf{M}^k, \nabla\Phi\rangle_{\mathbf{H}(curl_h)} = 0$.

If $\sigma > 0$ this result can be used to attempt to obtain an energy estimate for the scheme (3.44). Set $\mathbf{V} = 2\varkappa_0\tau\mathbf{U}^k$, $\mathbf{X} = 2\tau\varkappa_0\mathbf{W}^k$, $\mathbf{Z} = 2\tau\mu_0\mathbf{M}^k$, $\mathrm{X} = \frac{2\tau\varkappa_0\mu_0}{\mathscr{J}}\Phi^k$ and $\mathbf{Z} = \frac{2\tau\varkappa_0\mu_0}{\mathscr{J}}\nabla\Phi^k$. Following Proposition 3.4.1 we get

$$\begin{aligned} &\delta\big(\varkappa_0\|\mathbf{U}^k\|^2_{\mathbf{L}^2} + \varkappa_0\jmath\|\mathbf{W}^k\|^2_{\mathbf{L}^2} + \mu_0\|\mathbf{M}^k\|^2_{\mathbf{L}^2} + \varkappa_0\mu_0\|\nabla\Phi^k\|^2_{\mathbf{L}^2}\big) \\ &\qquad + \varkappa_0\|\delta\mathbf{U}^k\|^2_{\mathbf{L}^2} + \varkappa_0\jmath\|\delta\mathbf{W}^k\|^2_{\mathbf{L}^2} + \mu_0\|\delta\mathbf{M}^k\|^2_{\mathbf{L}^2} + \varkappa_0\mu_0\|\delta\nabla\Phi^k\|^2_{\mathbf{L}^2} \\ &\qquad + 2\varkappa_0\tau\Big(\nu\|\nabla\mathbf{U}^k\|^2_{\mathbf{L}^2} + c_1\|\nabla\mathbf{W}^k\|^2_{\mathbf{L}^2} + \nu_r\|div\,\mathbf{U}^k\|^2_{\mathbf{L}^2} \\ &\qquad + c_2\|div\,\mathbf{W}^k\|^2_{\mathbf{L}^2} + \nu_r\|curl\,\mathbf{U}^k - 2\mathbf{W}^k\|^2_{\mathbf{L}^2} + \tfrac{\mu_0}{\mathscr{J}\varkappa_0}\|\mathbf{M}^k\|^2_{\mathbf{L}^2} \\ &\qquad + \tfrac{\mu_0}{\mathscr{J}}(2+\varkappa_0)\|\nabla\Phi^k\|^2_{\mathbf{L}^2}\Big) + 2\sigma\tau\Big(\mu_0\langle\mathbf{M}^k, \mathbf{M}^k\rangle_{\mathbf{H}(div_h)} \\ &\qquad + \mu_0\langle\mathbf{M}^k, \mathbf{M}^k\rangle_{\mathbf{H}(curl_h)} + \gamma\|(\mathbf{M}^k - \varkappa_0\nabla\Phi^k)\times\boldsymbol{n}\|^2_{\mathbf{L}^2(\Gamma)} \\ &\qquad + \gamma\|(\mathbf{M}^k - \varkappa_0\nabla\Phi^k)\cdot\boldsymbol{n}\|^2_{L^2(\Gamma)}\Big) = 2\mu_0\varkappa_0\left(\delta\mathbf{h}^k_a, \nabla\Phi^k\right) \\ &\qquad + \tfrac{2\varkappa_0\mu_0\tau}{\mathscr{J}}\left(\mathbf{h}^k_a, \nabla\Phi^k\right) + 2\mu_0\sigma\tau\,\langle\mathbf{M}^k, \nabla\Phi^k\rangle_{\mathbf{H}(div_h)}. \end{aligned} \tag{3.64}$$

Notice that we have gained control on the needed boundary terms. However, we have the term $2\mu_0\tau\sigma\,\langle\mathbf{M}^k, \nabla\Phi^k\rangle_{\mathbf{H}(div_h)}$ on the right-hand side, and there is no way to control it, unless one can reproduce identity $(div\,\mathbf{m}, div\,\mathbf{h}) = -\|div\,\mathbf{h}\|^2_{\mathbf{L}^2}$ (used

in §3.3.1 for the identity (3.25)) in a discrete setting (or at least, prove that $\langle \mathbf{M}^k, \nabla\Phi^k \rangle_{\mathbf{H}(div_h)} \leq 0$).

3.5 Simplified ferrohydrodynamics and convergent scheme

3.5.1 Simplification of the model

We can simplify the model defined by (3.1), (3.4), (3.5), (3.18) and $\sigma = 0$ by eliminating the magnetostatics problem (3.18), and setting the effective magnetizing field to be $\mathbf{h} := \mathbf{h}_a$. The purpose of this section is to explain, at least with a heuristic argument, under which circumstances this is a reasonable physical approximation.

As we know from §3.2.1, φ is the sum of two potentials $\varphi = \psi + \phi$ (see Remark 3.2.4), so that $\mathbf{h} = \mathbf{h}_d + \mathbf{h}_a = \nabla\psi + \nabla\phi$. In this context one may ask under which circumstances we can neglect the contribution of the demagnetizing field $\mathbf{h}_d$ and assert that $\mathbf{h} \approx \mathbf{h}_a$ is a good approximation. In other words, we want to assess the difference between $\nabla\varphi$ and $\nabla\phi$. For this purpose we subtract (3.16) from (3.17), set $\chi = \psi$, and use Cauchy-Schwarz inequality to obtain

$$\|\nabla\psi\|_{\mathbf{L}^2} \leq \|\mathbf{m}\|_{\mathbf{L}^2} . \tag{3.65}$$

In conclusion, $\mathbf{h} \approx \mathbf{h}_a$ whenever the magnetization $\mathbf{m}$ is small. On the other hand, as explained in §3.2, the evolution of the magnetization is such that $\mathbf{m} \approx \varkappa_0 \mathbf{h}$ when close to equilibrium. Thus, if $\varkappa_0 << 1$ the magnetization $\mathbf{m}$ will be small, so that we can neglect the contribution of the demagnetizing field to the total magnetic field as suggested by (3.65). Water based ferrofluids subject to slowly varying magnetic

fields could be modeled under these assumptions, since they usually exhibit a small magnetic susceptibility $\varkappa_0$ [95, 96]. It is worth mentioning that the simplification $\mathbf{h} := \mathbf{h}_a$ is not particularly new: it has been used for analytic computations of the Rosensweig model and still retains a significant amount of valid quantitative information as shown for instance in [25, 26, 97]; it has also been suggested in the analysis of stationary configurations of free surfaces of ferrofluids [98].

3.5.2 Ultra weak formulation of simplified ferrohydrodynamics

We will consider the following weak formulation for the model defined by equations (3.1)-(3.5) with $\sigma = 0$: find $(\mathbf{u}, \mathbf{w}, \mathbf{m}) \in L^2([0,t_F); \boldsymbol{\mathcal{V}}) \times L^2([0,t_F); \mathbf{H}_0^1(\Omega)) \times L^2([0,t_F); \mathbf{L}^2(\Omega))$ that satisfy

$$\begin{aligned} \int_0^{t_F} -(\mathbf{u}, \mathbf{v}_t) + b(\mathbf{u}, \mathbf{u}, \mathbf{v}) + \widehat{\nu}(\nabla \mathbf{u}, \nabla \mathbf{v}) \\ = (\mathbf{u}(0), \mathbf{v}(0)) + \int_0^{t_F} \mu_0\, b(\mathbf{m}, \mathbf{h}, \mathbf{v})\,, \end{aligned} \tag{3.66a}$$

$$\begin{aligned} \int_0^{t_F} -\jmath(\mathbf{w}, \mathbf{x}_t) + b(\mathbf{w}, \mathbf{w}, \mathbf{x}) + c_1(\nabla \mathbf{w}, \nabla \mathbf{v}) + c_2(div\,\mathbf{w}, div\,\mathbf{x}) + 4\nu_r(\mathbf{w}, \mathbf{x}) \\ = \jmath(\mathbf{w}(0), \mathbf{x}(0)) + \int_0^{t_F} 2\nu_r(curl\,\mathbf{u}, \mathbf{x}) + \mu_0(\mathbf{m} \times \mathbf{h})\,, \end{aligned} \tag{3.66b}$$

$$-\int_0^{t_F} (\mathbf{m}, \mathbf{z}_t) + b(\mathbf{u}, \mathbf{z}, \mathbf{m}) - \tfrac{1}{\mathscr{T}}(\mathbf{m}, \mathbf{z}) = (\mathbf{m}(0), \mathbf{z}(0)) + \tfrac{\varkappa_0}{\mathscr{T}} \int_0^{t_F} (\mathbf{h}, \mathbf{z})\,, \tag{3.66c}$$

for all $\mathbf{v} \in \{\mathbf{v} \in \boldsymbol{\mathcal{C}}_0^\infty([0,t_F) \times \Omega) \,|\, div\,\mathbf{v} = 0 \text{ in } \Omega\,\}$, $\mathbf{x}, \mathbf{z} \in \boldsymbol{\mathcal{C}}_0^\infty([0,t_F) \times \Omega)$, where now the magnetic field $\mathbf{h}$ is not determined by the Poisson problem (3.18), but rather $\mathbf{h} := \mathbf{h}_a$ is a given harmonic and smooth vector field.

.

We point out that the expressions in (3.66) are obtained from integration by parts in time, and are particularly suitable to prove convergence of discrete solutions, in particular, if the time-integration scheme used is a "Discontinuous Galerkin" (rather than "Continuous Galerkin") scheme (cf.[49]). Most notably, the Backward-Euler method, is a zero-order Discontinuous Galerkin time-integration scheme.

3.5.3 Scheme: Assumptions, Existence and Stability

To discretize the system (3.66), and to avoid technicalities, we will assume that the initial data is smooth and consider an initialization as in (3.43).

For every $k \in \{1, \dots, K\}$ we compute $\{\mathbf{U}^k, P^k, \mathbf{W}^k, \mathbf{M}^k\} \in \mathbb{U} \times \mathbb{P} \times \mathbb{W} \times \mathbb{M}$ that solves

$$\begin{aligned} \Big(\tfrac{\delta \mathbf{U}^k}{\tau}, \mathbf{V}\Big) + b_h\big(\mathbf{U}^k, \mathbf{U}^k, \mathbf{V}\big) + \widehat{\nu}\big(\nabla \mathbf{U}^k, \nabla \mathbf{V}\big) - \big(P^k, div\, \mathbf{V}\big) \\ = 2\nu_r\big(curl\, \mathbf{W}^k, \mathbf{V}\big) + \mu_0\, b_h^m\big(\mathbf{V}, \mathbf{H}^k, \mathbf{M}^k\big)\,, \end{aligned} \tag{3.67a}$$

$$\big(\mathrm{Q}, div\, \mathbf{U}^k\big) = 0\,, \tag{3.67b}$$

$$\begin{aligned} \jmath\Big(\tfrac{\delta \mathbf{W}^k}{\tau}, \mathbf{X}\Big) + \jmath\, b_h\big(\mathbf{U}^k, \mathbf{W}^k, \mathbf{X}\big) + c_1\big(\nabla \mathbf{W}^k, \nabla \mathbf{X}\big) + c_2\big(div\, \mathbf{W}^k, div\, \mathbf{X}\big) \\ + 4\nu_r\big(\mathbf{W}^k, \mathbf{X}\big) = 2\nu_r\big(curl\, \mathbf{U}^k, \mathbf{X}\big) + \mu_0\big(\mathbf{M}^k \times \mathbf{H}^k, \mathbf{X}\big)\,, \end{aligned} \tag{3.67c}$$

$$\begin{aligned} \Big(\tfrac{\delta \mathbf{M}^k}{\tau}, \mathbf{Z}\Big) - b_h^m\big(\mathbf{U}^k, \mathbf{Z}, \mathbf{M}^k\big) + \big(\mathbf{M}^k \times \mathbf{W}^k, \mathbf{Z}\big) + \tfrac{1}{\mathscr{T}}\big(\mathbf{M}^k, \mathbf{Z}\big) \\ = \tfrac{\varkappa_0}{\mathscr{T}}\big(\mathbf{H}^k, \mathbf{Z}\big)\,, \end{aligned} \tag{3.67d}$$

for all $\{\mathbf{V}, \mathrm{Q}, \mathbf{X}, \mathbf{Z}\} \in \mathbb{U} \times \mathbb{P} \times \mathbb{W} \times \mathbb{M}$, where the magnetic field $\mathbf{H}^k$ now is given by

$$\mathbf{H}^k := \mathrm{I}_{\mathbb{M}}[\mathbf{h}_a^k]\,, \tag{3.68}$$

with $\mathrm{I}_{\mathbb{M}}$ defined in (3.42).

The choice of spaces $\mathbb{U}$, $\mathbb{P}$, $\mathbb{W}$ and $\mathbb{M}$ does need to be made precise now, we will provide specific constructions in §3.5.5. Right now we only need to say that the following properties will be required:

- ◇ As usual, we will assume that the domain Ω is a convex polyhedron and that the mesh $\mathcal{T}_h$ is quasi-uniform.

- ◇ In addition to the projector $\Pi_{\mathbb{V}}$ (see (1.21)) and the stability property (1.22), we will also define $\Pi_{\mathbb{W}} : L^2(\Omega) \longrightarrow \mathbb{W}$, the $L^2(\Omega)$ projection onto the space $\mathbb{W}$, and assume that $\Pi_{\mathbb{W}}$ is $\mathbf{H}^1(\Omega)$-stable, namely:

$$\|\nabla \Pi_{\mathbb{W}} \mathbf{v}\|_{\mathbf{L}^2} \leq c \, \|\mathbf{v}\|_{\mathbf{H}^1_0} \quad \forall \, \mathbf{v} \in \mathbf{H}^1_0(\Omega) \,, \tag{3.69}$$

  with c independent of h and $\mathbf{v}$. In the context of quasi-uniform meshes the reader is referred to classical references like [52, 42], and for non quasi-uniform meshes and different norms to [99, 100, 101]. Quasiuniformity is a sufficient condition on $\mathcal{T}_h$ for these properties to hold. More general sufficient conditions can be found in the aforementioned references.

- ◇ For all $\mathbf{Z} \in \mathbb{M}$, we want each space component $\mathbf{Z}^i$ $(i : 1, ..., d)$ to belong to the same finite element space as the pressure, i.e. we will require $\mathbb{M} = [\mathbb{P}]^d$.

- ◇ The pressure space $\mathbb{P}$ should be discontinuous and it should contain a continuous subspace of degree 1 or higher. This assumption, together with the assumption of the previous bullet, implies that $\mathbb{M} \cap \boldsymbol{\mathcal{C}}^0(\Omega) \neq \varnothing$, and that

the construction of an interpolation $\mathrm{I}_{\mathbb{M}}$ satisfying (3.42) and (1.13) is always possible.

Using discontinuous pressures will allow us to localize the incompressibility constraint (3.67b) from the Stokes problem to each element, that is

$$(\mathrm{Q}, div\,\mathbf{U}^k)_T = 0 \quad \forall \mathrm{Q} \in \mathbb{P},\, \forall T \in \mathcal{T}_h\,. \tag{3.70}$$

The constraint $\mathbb{M} = [\mathbb{P}]^d$ together with (3.70) will mean that:

$$\left(\mathbf{Z}^i, div\,\mathbf{U}^k\right)_T = 0 \quad \forall \mathbf{Z} \in \mathbb{M}\,, \forall\, i : 1, ..., d\,,\ \forall T \in \mathcal{T}_h \tag{3.71}$$

The main difference between schemes (3.44) and (3.67), apart from the fact that the Poisson problem for Φ^k was eliminated, are the new requirements on the spaces $\mathbb{P}$ and $\mathbb{M}$.

Note in (3.67), that we are using the definition (3.54) for the trilinear form $b_h^m(\cdot,\cdot,\cdot)$, however, not all the terms are used. In particular, all the jump terms in the Kelvin force $\mu_0\, b_h^m\left(\mathbf{V}, \mathbf{H}^k, \mathbf{M}^k\right)$ disappear, since $\left[\!\left[\mathbf{H}^k\right]\!\right]\Big|_F = 0\ \forall F \in \mathcal{F}^i$, which is a consequence of definition (3.68). This is a very convenient feature which will greatly simplify a priori estimates and consistency analysis. We now present the stability of scheme (3.44).

Proposition 3.5.1 (Existence and stability)**.** *For every $k = 1, \ldots, K$ there is $\left\{\mathbf{U}^k, P^k, \mathbf{W}^k, \mathbf{M}^k\right\} \in \mathbb{U} \times \mathbb{P} \times \mathbb{W} \times \mathbb{M}$ that solves* (3.67)*, with $\mathbf{H}^k$ defined in* (3.68)*. Moreover this solution satisfies the following stability estimate*

$$\begin{aligned} &\tfrac{1}{2}\mathscr{E}_{h,\tau}^K + \tau^{-1}\|\mathscr{I}_{h,\tau}^{\tau}\|_{\ell^1} + \|\mathscr{D}_{h,\tau}^{\tau}\|_{\ell^1} \\ &\qquad \leq \mathscr{F}_{h,\tau}^{\tau} + 2\mathscr{E}_{h,\tau}^0 + \mu_0\|\mathbf{H}^0\|_{\mathbf{L}^2}^2 + 2\mu_0\|\mathbf{H}^K\|_{\mathbf{L}^2}^2 \leq c \end{aligned} \tag{3.72}$$

where

$$\mathscr{E}^k_{h,\tau} := \mathscr{E}^k_{h,\tau}(\mathbf{U}^\tau, \mathbf{W}^\tau, \mathbf{M}^\tau, 0)\,,\ \mathscr{I}^k_{h,\tau} := \mathscr{I}^k_{h,\tau}(\mathbf{U}^\tau, \mathbf{W}^\tau, \mathbf{M}^\tau, 0)\,,$$

$$\mathscr{D}^k_{h,\tau} := \mathscr{D}^k_{h,\tau}(\mathbf{U}^\tau, \mathbf{W}^\tau, \mathbf{M}^\tau, 0)\,,$$

were defined in (3.45)*, and* $\mathscr{F}^k_{h,\tau}$ *is defined as*

$$\mathscr{F}^k_{h,\tau} := \mathscr{F}^k(\mathbf{h}_a) = 3\mu_0\mathscr{T}\sum_{k=1}^{K-1}\tau\left\|\tfrac{\delta\mathbf{H}^{k+1}}{\tau}\right\|^2_{\mathbf{L}^2} + \sum_{k=1}^{K}\tfrac{\mu_0\tau}{\mathscr{T}}(1+3\varkappa_0^2)\|\mathbf{H}^k\|^2_{\mathbf{L}^2}\,.$$

The constant $c<\infty$ *only depends on* $\mathbf{h}_a$*,* $\partial_t\mathbf{h}_a$*, and the initial data* $\mathbf{u}_0$*,* $\mathbf{w}_0$*,* $\mathbf{m}_0$*.*

Proof. Set $\mathbf{V} = 2\tau\mathbf{U}^k$, $\mathbf{X} = 2\tau\mathbf{W}^k$, $\mathbf{Z} = 2\tau\mu_0\mathbf{M}^k$, in (3.67) and add the results. Using (1.2) and identity (1.11), we get

$$\begin{aligned} 2\delta\mathscr{E}^k_{h,\tau} + 2\mathscr{I}^k_{h,\tau} + 2\tau\mathscr{D}^k_{h,\tau} &= 2\mu_0\tau(\mathbf{M}^k\times\mathbf{H}^k, \mathbf{W}^k) \\ &\quad + 2\mu_0\tau\, b^m_h\big(\mathbf{U}^k, \mathbf{H}^k, \mathbf{M}^k\big) + \tfrac{2\tau\mu_0\varkappa_0}{\mathscr{T}}(\mathbf{M}^k, \mathbf{H}^k). \end{aligned} \tag{3.73}$$

As in the proof of Proposition 3.4.1, to deal with the trilinear terms $2\mu_0\tau\, b^m_h\big(\mathbf{U}^k, \mathbf{H}^k, \mathbf{M}^k\big)$ and $2\mu_0\tau(\mathbf{M}^k\times\mathbf{H}^k, \mathbf{W}^k)$ we set $\mathbf{Z} = 2\mu_0\tau\mathbf{H}^k$ in (3.67d). In doing so, we obtain

$$\begin{aligned} \tfrac{2\mu_0\tau\varkappa_0}{\mathscr{T}}\|\mathbf{H}^k\|^2_{\mathbf{L}^2} &= -2\mu_0\tau\big(\mathbf{M}^k\times\mathbf{H}^k, \mathbf{W}^k\big) - 2\mu_0\tau\, b^m_h\big(\mathbf{U}^k, \mathbf{H}^k, \mathbf{M}^k\big) \\ &\quad + 2\mu_0\left(\delta\mathbf{M}^k, \mathbf{H}^k\right) + \tfrac{2\mu_0\tau}{\mathscr{T}}\big(\mathbf{M}^k, \mathbf{H}^k\big). \end{aligned} \tag{3.74}$$

Adding (3.74) to (3.73) we obtain

$$2\delta\mathscr{E}^k_{h,\tau} + 2\mathscr{I}^k_{h,\tau} + 2\tau\mathscr{D}^k_{h,\tau} + \tfrac{2\mu_0\tau\varkappa_0}{\mathscr{T}}\|\mathbf{H}^k\|^2_{\mathbf{L}^2} = \tfrac{2\tau\mu_0}{\mathscr{T}}(1+\varkappa_0)(\mathbf{M}^k, \mathbf{H}^k) + 2\mu_0(\delta\mathbf{M}^k, \mathbf{H}^k).$$

The rest is just a matter of adding over k, using the summation by parts formula (1.12) to $\sum_{k=1}^K\left(\delta\mathbf{M}^k, \mathbf{H}^k\right)$ and applying Cauchy-Schwarz and Young's inequalities with appropriate constants. Finally, existence is guaranteed by an analogous argument to that one used in Theorem 3.4.1, which only requires a local (in time) estimate. This concludes the proof. □

Lemma 3.5.1 (Estimates for the discrete time derivatives)**.** *The following estimates for $\tau^{-1}\delta\mathbf{U}^k$ and $\tau^{-1}\delta\mathbf{W}^k$ hold*

$$\left\|\tfrac{\delta\mathbf{U}^\tau}{\tau}\right\|_{\ell^{4/3}(\boldsymbol{\mathcal{V}}^*)} + \left\|\tfrac{\delta\mathbf{W}^k}{\tau}\right\|_{\ell^{4/3}(\mathbf{H}^{-1})} \leq c\,,$$

where the constant $c < \infty$ only depends on $\mathbf{h}_a$, $\partial_t\mathbf{h}_a$, and the initial data $\mathbf{u}_0$, $\mathbf{w}_0$, $\mathbf{m}_0$.

Proof. Following [102, 103], we use (3.67a), (1.21), (1.22), (3.40), (3.72), and the regularity of the data $\mathbf{h}_a$, to get:

$$\begin{aligned}
\left\|\tfrac{\delta\mathbf{U}^k}{\tau}\right\|_{\boldsymbol{\mathcal{V}}^*} &= \sup_{\mathbf{v}\in\boldsymbol{\mathcal{V}}} \frac{\left(\frac{\delta\mathbf{U}^k}{\tau},\mathbf{v}\right)}{\|\mathbf{v}\|_{\mathbf{H}^1_0}} = \sup_{\mathbf{v}\in\boldsymbol{\mathcal{V}}} \frac{\left(\frac{\delta\mathbf{U}^k}{\tau},\Pi_{\mathbb{V}}[\mathbf{v}]\right)}{\|\mathbf{v}\|_{\mathbf{H}^1_0}} \lesssim \sup_{\mathbf{v}\in\boldsymbol{\mathcal{V}}} \frac{\left(\frac{\delta\mathbf{U}^k}{\tau},\Pi_{\mathbb{V}}[\mathbf{v}]\right)}{\|\Pi_{\mathbb{V}}[\mathbf{v}]\|_{\mathbf{H}^1_0}} \\
&\lesssim \|\mathbf{U}^k\|_{\mathbf{L}^3}\|\mathbf{U}^k\|_{\mathbf{L}^6} + \|div\,\mathbf{U}^k\|_{L^2}\|\mathbf{U}^k\|_{\mathbf{L}^3} + \|\nabla\mathbf{U}^k\|_{\mathbf{L}^2} + \|\mathbf{W}^k\|_{\mathbf{L}^2} \\
&\quad + \|\nabla\mathbf{H}^k\|_{\mathbf{L}^\infty}\|\mathbf{M}^k\|_{\mathbf{L}^2} + \|\mathbf{H}^k\|_{\mathbf{L}^\infty}\|\mathbf{M}^k\|_{\mathbf{L}^2} \\
&\lesssim \|\nabla\mathbf{U}^k\|^{3/2}_{\mathbf{L}^2} + \|\nabla\mathbf{U}^k\|_{\mathbf{L}^2} + \|\nabla\mathbf{W}^k\|_{\mathbf{L}^2} + \|\mathbf{M}^k\|_{\mathbf{L}^2} \\
&\lesssim \left(\|\nabla\mathbf{U}^k\|^2_{\mathbf{L}^2} + \|\nabla\mathbf{U}^k\|^{4/3}_{\mathbf{L}^2} + \|\nabla\mathbf{W}^k\|^{4/3}_{\mathbf{L}^2} + \|\mathbf{M}^k\|^{4/3}_{\mathbf{L}^2}\right)^{3/4},
\end{aligned} \tag{3.75}$$

where we have also used the estimate

$$\|\mathbf{U}^k\|_{\mathbf{L}^3} \leq \|\mathbf{U}^k\|^{1/2}_{\mathbf{L}^2}\|\mathbf{U}^k\|^{1/2}_{\mathbf{L}^6} \lesssim \|\mathbf{U}^k\|^{1/2}_{\mathbf{L}^6} \lesssim \|\nabla\mathbf{U}^k\|^{1/2}_{\mathbf{L}^2}\,,$$

which relies on (3.72), namely $\|\mathbf{U}^k\|_{\mathbf{L}^2} \leq c$ uniformly in k. Raise (3.75) to power $4/3$, multiply by τ, add in time, and use (3.72) to get the desired estimate for $\tau^{-1}\delta\mathbf{U}^k$.

Similarly, for $\frac{\delta\mathbf{W}^k}{\tau}$, we use (3.67c), (3.69), (3.72), and the regularity of the data

$\mathbf{h}_a$:

$$\begin{aligned}
\left\| \tfrac{\delta \mathbf{W}^k}{\tau} \right\|_{\mathbf{H}^{-1}} &= \sup_{\mathbf{x} \in \mathbf{H}_0^1(\Omega)} \frac{\left(\tfrac{\delta \mathbf{W}^k}{\tau}, \mathbf{x} \right)}{\|\mathbf{x}\|_{\mathbf{H}_0^1}} = \sup_{\mathbf{x} \in \mathbf{H}_0^1(\Omega)} \frac{\left(\tfrac{\delta \mathbf{W}^k}{\tau}, \Pi_{\mathbb{W}}[\mathbf{x}] \right)}{\|\mathbf{x}\|_{\mathbf{H}_0^1}} \\
&\lesssim \sup_{\mathbf{x} \in \mathbf{H}_0^1(\Omega)} \frac{\left(\tfrac{\delta \mathbf{W}^k}{\tau}, \Pi_{\mathbb{W}}[\mathbf{x}] \right)}{\|\Pi_{\mathbb{W}}[\mathbf{x}]\|_{\mathbf{H}_0^1}} \lesssim \|\mathbf{U}^k\|_{\mathbf{L}^4} \|\mathbf{W}^k\|_{\mathbf{L}^4} + \|div\, \mathbf{U}^k\|_{L^2} \|\mathbf{W}^k\|_{\mathbf{L}^3} \\
&+ \|\nabla \mathbf{W}^k\|_{\mathbf{L}^2} + \|div\, \mathbf{W}^k\|_{\mathbf{L}^2} + \|\mathbf{W}^k\|_{\mathbf{L}^2} + \|\mathbf{U}^k\|_{\mathbf{L}^2} \\
&+ \|\mathbf{M}^k\|_{\mathbf{L}^2} \|\mathbf{H}^k\|_{\mathbf{L}^\infty} \lesssim \|\nabla \mathbf{U}^k\|_{\mathbf{L}^2}^{3/2} + \|\nabla \mathbf{W}^k\|_{\mathbf{L}^2}^{3/2} + \|\nabla \mathbf{W}^k\|_{\mathbf{L}^2} \\
&+ \|\mathbf{U}^k\|_{\mathbf{L}^2} + \|\mathbf{M}^k\|_{\mathbf{L}^2} \lesssim \Big(\|\nabla \mathbf{U}^k\|_{\mathbf{L}^2}^2 + \|\nabla \mathbf{W}^k\|_{\mathbf{L}^2}^2 + \|\nabla \mathbf{W}^k\|_{\mathbf{L}^2}^{4/3} \\
&+ \|\mathbf{U}^k\|_{\mathbf{L}^2}^{4/3} + \|\mathbf{M}^k\|_{\mathbf{L}^2}^{4/3} \Big)^{3/4},
\end{aligned} \tag{3.76}$$

where we have also used the inequality

$$\|\mathbf{U}^k\|_{\mathbf{L}^4} \leq \|\mathbf{U}^k\|_{\mathbf{L}^2}^{1/4} \|\mathbf{U}^k\|_{\mathbf{L}^6}^{3/4} \lesssim \|\mathbf{U}^k\|_{\mathbf{L}^6}^{3/4} \lesssim \|\nabla \mathbf{U}^k\|_{\mathbf{L}^2}^{3/2},$$

and an analogous estimate for $\mathbf{W}^k$. Raise (3.76) to the power $4/3$, multiply by τ, add in time, and use (3.72) to get the desired estimate for $\tau^{-1}\delta \mathbf{W}^k$. □

3.5.4 Convergence

We want to show that solutions generated by the scheme defined by (3.67), and (3.68), with initial conditions (3.43), converge to the weak solutions defined in (3.66). However, the scheme (3.67) generates a sequence of functions $\left\{ \mathbf{U}^k, \mathbf{P}^k, \mathbf{W}^k, \mathbf{M}^k \right\}_{k=0}^K$ corresponding to the nodes $\left\{ t^k \right\}_{k=0}^K$, rather than space-time functions. In addition, the scheme (3.67) does not have a variational structure in time. In order to reconcile these features we will rewrite scheme (3.67) as a space-time variational formulation.

For this purpose, we start by defining the space-time functions $\mathbf{U}_{h\tau}$, $P_{h\tau}$, $\mathbf{W}_{h\tau}$, $\mathbf{M}_{h\tau}$, such that

$$\mathbf{U}_{h\tau} = \mathbf{U}^k,\ P_{h\tau} = P^k,\ \mathbf{W}_{h\tau} = \mathbf{W}^k,\ \mathbf{M}_{h\tau} = \mathbf{M}^k,\ \mathbf{H}_{h\tau} = \mathbf{H}^k \quad \forall\, t \in (t^{k-1}, t^k]\,, \tag{3.77}$$

which are piecewise constant in time. Even though these functions are not continuous in time, their point values are well defined, in particular they are left-continuous at the nodes $\{t^k\}_{k=0}^K$:

$$\mathbf{U}_{h\tau}(t^k) = \lim_{t \nearrow t^k} \mathbf{U}_{h\tau}(t) \quad \forall\ 0 \le k \le K\,. \tag{3.78}$$

Using the summation by parts formula (1.12), we can rewrite scheme (3.67) in terms of $\{\mathbf{U}_{h\tau}, P_{h\tau}, \mathbf{W}_{h\tau}, \mathbf{M}_{h\tau}\}$ as follows:

$$\begin{aligned}
&(\mathbf{U}_{h\tau}(t_F), \mathbf{V}_{h\tau}(t_F)) - \int_0^{t_F-\tau} \Big(\mathbf{U}_{h\tau}, \tfrac{\mathbf{V}_{h\tau}(\cdot+\tau)-\mathbf{V}_{h\tau}}{\tau}\Big) + b_h\big(\mathbf{U}_{h\tau}, \mathbf{U}_{h\tau}, \mathbf{V}_{h\tau}\big) \\
&\quad + \int_0^{t_F} \big(\widehat{\nu}\nabla\mathbf{U}_{h\tau}, \nabla\mathbf{V}_{h\tau}\big) - \big(P_{h\tau}, div\,\mathbf{V}_{h\tau}\big) = (\mathbf{U}_{h\tau}(0), \mathbf{V}_{h\tau}(0)) \qquad (3.79a)\\
&\quad + \int_0^{t_F} 2\nu_r(curl\,\mathbf{W}_{h\tau}, \mathbf{V}_{h\tau}) + \mu_0\, b_h^m\big(\mathbf{V}_{h\tau}, \mathbf{H}_{h\tau}, \mathbf{M}_{h\tau}\big)\,, \\
&\quad \int_0^{t_F} \big(\mathrm{Q}_{h\tau}, div\,\mathbf{U}_{h\tau}\big) = 0\,, \qquad (3.79b)\\
&\jmath(\mathbf{W}_{h\tau}(t_F), \mathbf{X}_{h\tau}(t_F)) - \int_0^{t_F-\tau} \jmath\,\Big(\mathbf{W}_{h\tau}, \tfrac{\mathbf{X}_{h\tau}(\cdot+\tau)-\mathbf{X}_{h\tau}}{\tau}\Big) \\
&\quad + \int_0^{t_F} \jmath\, b_h\big(\mathbf{U}_{h\tau}, \mathbf{W}_{h\tau}, \mathbf{X}_{h\tau}\big) + c_1(\nabla\mathbf{W}_{h\tau}, \nabla\mathbf{X}_{h\tau}) \\
&\quad + c_2\big(div\,\mathbf{W}_{h\tau}, div\,\mathbf{X}_{h\tau}\big) + 4\nu_r(\mathbf{W}_{h\tau}, \mathbf{X}_{h\tau}) = \jmath(\mathbf{W}_{h\tau}(0), \mathbf{X}_{h\tau}(0)) \qquad (3.79c)\\
&\quad + \int_0^{t_F} 2\nu_r\big(curl\,\mathbf{U}_{h\tau}, \mathbf{X}_{h\tau}\big) + \mu_0(\mathbf{M}_{h\tau} \times \mathbf{H}_{h\tau}, \mathbf{X}_{h\tau})\,, \\
&(\mathbf{M}_{h\tau}(t_F), \mathbf{Z}_{h\tau}(t_F)) - \int_0^{t_F-\tau} \Big(\mathbf{M}_{h\tau}, \tfrac{\mathbf{Z}_{h\tau}(\cdot+\tau)-\mathbf{Z}_{h\tau}}{\tau}\Big) \\
&\quad - \int_0^{t_F} b_h^m\big(\mathbf{U}_{h\tau}, \mathbf{Z}_{h\tau}, \mathbf{M}_{h\tau}\big) + (\mathbf{M}_{h\tau} \times \mathbf{W}_{h\tau}, \mathbf{Z}_{h\tau}) + \tfrac{1}{\mathscr{T}}\big(\mathbf{M}_{h\tau}, \mathbf{Z}_{h\tau}\big) \qquad (3.79d)\\
&\quad = (\mathbf{M}_{h\tau}(0), \mathbf{Z}_{h\tau}(0)) + \tfrac{\varkappa_0}{\mathscr{T}} \int_0^{t_F} \big(\mathbf{H}_{h\tau}, \mathbf{Z}_{h\tau}\big)\,,
\end{aligned}$$

for every $\{\mathbf{V}_{h\tau}, \mathrm{Q}_{h\tau}, \mathbf{X}_{h\tau}, \mathbf{Z}_{h\tau},\} \in \mathbb{U}_{h\tau} \times \mathbb{P}_{h\tau} \times \mathbb{W}_{h\tau} \times \mathbb{M}_{h\tau}$, where

$$\mathbb{U}_{h\tau} = \left\{ \mathbf{V}_{h\tau} \in L^2(0,t_F;\mathbb{U}) \;\middle|\; \mathbf{V}_{h\tau}\big|_{(t^{k-1},t^k]} \in \mathbb{U} \otimes \mathbb{P}_0((t^{k-1},t^k]),\ 0 \le k \le K \right\},$$

$$\mathbb{P}_{h\tau} = \left\{ \mathrm{Q}_{h\tau} \in L^2(0,t_F;\mathbb{P}) \;\middle|\; \mathrm{Q}_{h\tau}\big|_{(t^{k-1},t^k]} \in \mathbb{P} \otimes \mathbb{P}_0((t^{k-1},t^k]),\ 0 \le k \le K \right\},$$

$$\mathbb{W}_{h\tau} = \left\{ \mathbf{X}_{h\tau} \in L^2(0,t_F;\mathbb{W}) \;\middle|\; \mathbf{X}_{h\tau}\big|_{(t^{k-1},t^k]} \in \mathbb{W} \otimes \mathbb{P}_0((t^{k-1},t^k]),\ 0 \le k \le K \right\},$$

$$\mathbb{M}_{h\tau} = \left\{ \mathbf{Z}_{h\tau} \in L^2(0,t_F;\mathbb{M}) \;\middle|\; \mathbf{Z}_{h\tau}\big|_{(t^{k-1},t^k]} \in \mathbb{M} \otimes \mathbb{P}_0((t^{k-1},t^k]),\ 0 \le k \le K \right\},$$

and $\cdot + \tau$ and $\cdot - \tau$ denote positive and negative shifts in time of size τ. Expression (3.79) is the reinterpretation of the Backward-Euler method as a zero-order Discontinuous Galerkin scheme (see for instance [53, 104, 105, 49]). The difference between (3.67) and (3.79) is merely cosmetic, since they are equivalent formulations of the same scheme, but clearly (3.79) has the right structure if we want to compare it with (3.66). Note also that the choice of half-open intervals $(t^{k-1}, t^k]$ in (3.77), leading to the left-continuity (3.78) is consistent with upwinding fluxes — we choose traces from the direction of flow of information, which is also consistent with causality.

Lemma 3.5.2 (Weak convergence)**.** *The family of functions* $\{\mathbf{U}_{h\tau}, \mathbf{W}_{h\tau}, \mathbf{M}_{h\tau}\}_{h,\tau>0}$, *defined in* (3.77) *have the following convergence properties:*

$$\mathbf{U}_{h\tau} \xrightarrow{h,\tau\to 0}_{*} \mathbf{u}^* \text{ in } L^\infty(0,t_F;\mathbf{L}^2(\Omega)),$$

$$\mathbf{U}_{h\tau} \xrightarrow{h,\tau\to 0} \mathbf{u}^* \text{ in } L^2(0,t_F;\mathbf{H}^1(\Omega)),$$

$$\mathbf{W}_{h\tau} \xrightarrow{h,\tau\to 0}_{*} \mathbf{w}^* \text{ in } L^\infty(0,t_F;\mathbf{L}^2(\Omega)),$$

$$\mathbf{W}_{h\tau} \xrightarrow{h,\tau\to 0} \mathbf{w}^* \text{ in } L^2(0,t_F;\mathbf{H}^1(\Omega)),$$

$$\mathbf{M}_{h\tau} \xrightarrow{h,\tau\to 0}_{*} \mathbf{m}^* \text{ in } L^\infty(0,t_F;\mathbf{L}^2(\Omega)),$$

$$\mathbf{M}_{h\tau} \overset{h,\tau\to 0}{\rightharpoonup} \mathbf{m}^* \text{ in } L^2(0,t_F;\mathbf{L}^2(\Omega))\,,$$

for some functions $\mathbf{u}^*$, $\mathbf{w}^*$ *and* $\mathbf{m}^*$. *Here* $\rightharpoonup_*$ *denotes weak-star convergence, and* h *and* τ *tend to zero independently.*

Proof. This is a direct consequence of Proposition 3.5.1 and definition (3.77). □

Note that these modes of convergence are not strong enough to pass to the limit in every term of (3.79), so that the weak limits $\mathbf{u}^*$, $\mathbf{w}^*$ and $\mathbf{m}^*$ of the previous lemma might not necessarily be solutions of (3.66). In order to improve these estimates we will use the classical Aubin-Lions lemma 1.2.1.

Lemma 3.5.3 (strong $L^2(0,t_F;L^2(\Omega))$ convergence)**.** *The families of functions* $\{\mathbf{W}_{h\tau},\mathbf{U}_{h\tau}\}_{h,\tau>0}$ *defined in* (3.77) *have the following additional convergence properties:*

$$\mathbf{U}_{h\tau} \overset{h,\tau\to 0}{\longrightarrow} \mathbf{u}^* \text{ in } L^2(0,t_F;\mathbf{L}^2(\Omega))$$
$$\mathbf{W}_{h\tau} \overset{h,\tau\to 0}{\longrightarrow} \mathbf{w}^* \text{ in } L^2(0,t_F;\mathbf{L}^2(\Omega))$$

for some functions $\mathbf{u}^*$ *and* $\mathbf{w}^*$.

Proof. Using the Aubin-Lions lemma (Lemma 1.2.1) we would like to conclude on the basis of the estimates provided in Proposition 3.5.1 and Lemma 3.5.1. However, this is not possible since the family of functions $\{\mathbf{U}_{h\tau},\mathbf{W}_{h\tau}\}_{h,\tau>0}$ is discontinuous in time — time derivatives are not well defined. This a typical characteristic of discontinuous Galerkin methods for time integration such as the Backward Euler method. To overcome this, we define their Rothe interpolants, that is the piecewise

linear and continuous auxiliary functions $\widehat{\mathbf{U}}_{h\tau}$ and $\widehat{\mathbf{W}}_{h\tau}$:

$$\widehat{\mathbf{U}}_{h\tau} = \ell_{k-1}(t)\mathbf{U}^{k-1} + \ell_k(t)\mathbf{U}^k \ , \quad \widehat{\mathbf{W}}_{h\tau} = \ell_{k-1}(t)\mathbf{W}^{k-1} + \ell_k(t)\mathbf{W}^k \quad \forall\, t \in (t^{k-1}, t^k]$$

where $\ell_{k-1}(t) = (t^k - t)/\tau$ and $\ell_k(t) = (t - t^{k-1})/\tau$. Since

$$\partial_t \widehat{\mathbf{U}}_{h\tau}(t) = \tau^{-1}\delta\mathbf{U}^k, \quad \partial_t \widehat{\mathbf{W}}_{h\tau}(t) = \tau^{-1}\delta\mathbf{W}^k \quad \forall t \in (t^{k-1}, t^k],$$

we have that:

- $\widehat{\mathbf{U}}_{h\tau}$ and $\widehat{\mathbf{W}}_{h\tau}$ converge strongly to some $\mathbf{u}^*$ and $\mathbf{w}^*$ in the $L^2(L^2)$ norm, i.e.

$$\|\widehat{\mathbf{U}}_{h\tau} - \mathbf{u}^*\|_{L^2(0,t_F;\mathbf{L}^2)} + \|\widehat{\mathbf{W}}_{h\tau} - \mathbf{w}^*\|_{L^2(0,t_F;\mathbf{L}^2)} \xrightarrow{h,\tau\to 0} 0\,, \tag{3.80}$$

  which is a consequence of Proposition 3.5.1, the dual norm estimates for the time derivatives of Lemma 3.5.1, and a direct application of Lemma 1.2.1.

- The previous bullet implies that $\mathbf{U}_{h\tau}$ and $\mathbf{W}_{h\tau}$ also converge strongly to the same limits $\mathbf{u}^*$ and $\mathbf{w}^*$ in the $L^2(L^2)$ norm. For the velocity $\mathbf{U}_{h\tau}$ this is easy to show using the triangle inequality

$$\|\mathbf{U}_{h\tau} - \mathbf{u}^*\|_{L^2(0,t_F;\mathbf{L}^2)} \leq \|\mathbf{U}_{h\tau} - \widehat{\mathbf{U}}_{h\tau}\|_{L^2(0,t_F;\mathbf{L}^2)} + \|\widehat{\mathbf{U}}_{h\tau} - \mathbf{u}^*\|_{L^2(0,t_F;\mathbf{L}^2)}\,,$$

  where the term $\|\widehat{\mathbf{U}}_{h\tau} - \mathbf{u}^*\|_{L^2(0,t_F;\mathbf{L}^2)}$ goes to zero because of (3.80), and $\|\mathbf{U}_{h\tau} - \widehat{\mathbf{U}}_{h\tau}\|_{L^2(0,t_F;\mathbf{L}^2)}$ goes to zero because of the identity

$$\|\mathbf{U}_{h\tau} - \widehat{\mathbf{U}}_{h\tau}\|^2_{L^2(0,t_F;\mathbf{L}^2)} = \tfrac{\tau}{3}\sum_{k=1}^{K} \|\delta\mathbf{U}^k\|^2_{\mathbf{L}^2}$$

  and estimate (3.72). For the angular velocity we can use the same argument to show that $\|\mathbf{W}_{h\tau} - \mathbf{w}^*\|_{L^2(0,t_F;\mathbf{L}^2)} \xrightarrow{h,\tau\to 0} 0$.

□

At this point we are in the position to show the main convergence result.

Theorem 3.5.1 (Convergence)**.** *The family of functions* $\{\mathbf{U}_{h\tau}, \mathbf{W}_{h\tau}, \mathbf{M}_{h\tau}\}_{h,\tau>0}$*, defined in* (3.77) *has the following convergence properties*

$$\begin{aligned}
&\mathbf{U}_{h\tau} \xrightarrow{h,\tau\to 0} \mathbf{u}^* \ \textit{in}\ L^2(0,T;\mathbf{L}^2(\Omega)) \\
&\mathbf{U}_{h\tau} \xrightarrow{h,\tau\to 0} \mathbf{u}^* \ \textit{in}\ L^2(0,T;\mathbf{H}^1_0(\Omega)) \\
&\mathbf{W}_{h\tau} \xrightarrow{h,\tau\to 0} \mathbf{w}^* \ \textit{in}\ L^2(0,T;\mathbf{L}^2(\Omega)) \\
&\mathbf{W}_{h\tau} \xrightarrow{h,\tau\to 0} \mathbf{w}^* \ \textit{in}\ L^2(0,T;\mathbf{H}^1_0(\Omega)) \\
&\mathbf{M}_{h\tau} \xrightarrow{h,\tau\to 0} \mathbf{m}^* \ \textit{in}\ L^2(0,T;\mathbf{L}^2(\Omega))
\end{aligned} \tag{3.81}$$

where $\{\mathbf{u}^*, \mathbf{w}^*, \mathbf{m}^*\} \in L^2(0,T;\boldsymbol{\mathcal{V}}) \times L^2(0,T;\mathbf{H}^1_0(\Omega)) \times L^2(0,T;\mathbf{L}^2(\Omega))$ *is a weak solution of* (3.66)*.*

Proof. The modes of convergence (weak or strong and their norm) in (3.81) are a consequence of Lemmas 3.5.2 and 3.5.3. It only remains to show that weak limits $\mathbf{u}^*$, $\mathbf{w}^*$ and $\mathbf{m}^*$ are solutions of the variational problem (3.66). For this purpose we will set $\{\mathbf{V}_{h\tau}, \mathbf{X}_{h\tau}, \mathbf{Z}_{h\tau}\}$ to be the space-time interpolants/projections of the smooth test functions $\{\mathbf{v}, \mathbf{x}, \mathbf{z}\}$ of the variational formulation (3.66):

$$\mathbf{V}_{h\tau} := \Pi_s[\mathbf{v}^k]\,, \quad \mathbf{X}_{h\tau} := \mathrm{I}_{\mathbb{W}}[\mathbf{x}^k]\,, \quad \mathbf{Z}_{h\tau} := \mathrm{I}_{\mathbb{M}}[\mathbf{z}^k] \qquad \forall\, t \in (t^{k-1}, t^k]\,. \tag{3.82}$$

With this definition of discrete test functions we get in (3.79):

$$\begin{aligned}
-\int_0^{t_F-\tau} \Big(\mathbf{U}_{h\tau}, \tfrac{\mathbf{V}_{h\tau}(\cdot+\tau)-\mathbf{V}_{h\tau}}{\tau}\Big) + b_h\big(\mathbf{U}_{h\tau}, \mathbf{U}_{h\tau}, \mathbf{V}_{h\tau}\big) \\
+ \int_0^{t_F} \widehat{\nu}\big(\nabla\mathbf{U}_{h\tau}, \nabla\mathbf{V}_{h\tau}\big) = (\mathbf{U}_{h\tau}(0), \mathbf{V}_{h\tau}(0)) \qquad (3.83a) \\
+ \int_0^{t_F} 2\nu_r(curl\,\mathbf{W}_{h\tau}, \mathbf{V}_{h\tau}) + \mu_0\, b_h^m\big(\mathbf{V}_{h\tau}, \mathbf{H}_{h\tau}, \mathbf{M}_{h\tau}\big)\,,
\end{aligned}$$

$$
\begin{aligned}
&- \int_0^{t_F-\tau} \jmath\left(\mathbf{W}_{h\tau}, \tfrac{\mathbf{X}_{h\tau}(\cdot+\tau)-\mathbf{X}_{h\tau}}{\tau}\right) + \int_0^{t_F} \jmath\, b_h\big(\mathbf{U}_{h\tau}, \mathbf{W}_{h\tau}, \mathbf{X}_{h\tau}\big) \\
&\qquad + c_1(\nabla \mathbf{W}_{h\tau}, \nabla \mathbf{X}_{h\tau}) + c_2\big(div\, \mathbf{W}_{h\tau}, div\, \mathbf{X}_{h\tau}\big) + 4\nu_r(\mathbf{W}_{h\tau}, \mathbf{X}_{h\tau}) \\
&\qquad = \jmath(\mathbf{W}_{h\tau}(0), \mathbf{X}_{h\tau}(0)) + \int_0^{t_F} 2\nu_r\big(curl\, \mathbf{U}_{h\tau}, \mathbf{X}_{h\tau}\big) \\
&\qquad + \mu_0(\mathbf{M}_{h\tau} \times \mathbf{H}_{h\tau}, \mathbf{X}_{h\tau})\,,
\end{aligned}
\tag{3.83b}
$$

$$
\begin{aligned}
&- \int_0^{t_F-\tau} \left(\mathbf{M}_{h\tau}, \tfrac{\mathbf{Z}_{h\tau}(\cdot+\tau)-\mathbf{Z}_{h\tau}}{\tau}\right) - \int_0^{t_F} b_h^m\big(\mathbf{U}_{h\tau}, \mathbf{Z}_{h\tau}, \mathbf{M}_{h\tau}\big) \\
&\qquad + (\mathbf{M}_{h\tau} \times \mathbf{W}_{h\tau}, \mathbf{Z}_{h\tau}) + \tfrac{1}{\mathscr{T}}\big(\mathbf{M}_{h\tau}, \mathbf{Z}_{h\tau}\big) \\
&\qquad = (\mathbf{M}_{h\tau}(0), \mathbf{Z}_{h\tau}(0)) + \tfrac{\varkappa_0}{\mathscr{T}} \int_0^{t_F} \big(\mathbf{H}_{h\tau}, \mathbf{Z}_{h\tau}\big)\,,
\end{aligned}
\tag{3.83c}
$$

where the terms evaluated at time $t = t_F$ have disappeared because of the compact support of the test functions $\{\mathbf{v}, \mathbf{x}, \mathbf{z}\}$. Note also that the pressure term of the Navier Stokes equation has vanished too, which is a consequence of the definition of the discrete test function $\mathbf{V}_{h\tau} := \Pi_s[\mathbf{v}^k] \;\; \forall\, t \in (t^{k-1}, t^k]$, see (3.82), involving the Stokes projector Π_s (1.17) . Now we will pass to the limit term by term in (3.83):

- ◇ We start with the terms with the time derivatives, which are straightforward:

$$
\begin{aligned}
- \int_0^{t_F-\tau} \left(\mathbf{U}_{h\tau}, \tfrac{\mathbf{V}_{h\tau}(\cdot+\tau)-\mathbf{V}_{h\tau}}{\tau}\right) &\xrightarrow{h,\tau\to 0} - \int_0^{t_F} (\mathbf{u}^*, \mathbf{v}_t)\,, \\
- \int_0^{t_F-\tau} \left(\mathbf{W}_{h\tau}, \tfrac{\mathbf{X}_{h\tau}(\cdot+\tau)-\mathbf{X}_{h\tau}}{\tau}\right) &\xrightarrow{h,\tau\to 0} - \int_0^{t_F} (\mathbf{w}^*, \mathbf{x}_t)\,, \\
- \int_0^{t_F-\tau} \left(\mathbf{M}_{h\tau}, \tfrac{\mathbf{Z}_{h\tau}(\cdot+\tau)-\mathbf{Z}_{h\tau}}{\tau}\right) &\xrightarrow{h,\tau\to 0} - \int_0^{t_F} (\mathbf{m}^*, \mathbf{z}_t)\,,
\end{aligned}
$$

  because of the weak $L^2(L^2)$ convergence of $\mathbf{U}_{h\tau}$, $\mathbf{W}_{h\tau}$ and $\mathbf{M}_{h\tau}$, and the strong convergence of the finite differences $\frac{\mathbf{V}_{h\tau}(\cdot+\tau)-\mathbf{V}_{h\tau}}{\tau}$, $\frac{\mathbf{X}_{h\tau}(\cdot+\tau)-\mathbf{X}_{h\tau}}{\tau}$ and $\frac{\mathbf{Z}_{h\tau}(\cdot+\tau)-\mathbf{Z}_{h\tau}}{\tau}$, guaranteed by the regularity of the test functions.

- ◇ We continue with the convective term of (3.83c). Using definition (3.54) we

get

$$\int_0^{t_F} b_h^m\big(\mathbf{U}_{h\tau},\mathbf{M}_{h\tau},\mathbf{Z}_{h\tau}\big) = -\int_0^{t_F} b_h^m\big(\mathbf{U}_{h\tau},\mathbf{Z}_{h\tau},\mathbf{M}_{h\tau}\big)$$
$$= -\int_0^{t_F}\sum_{T\in\mathcal{T}_h}\int_T \big((\mathbf{U}_{h\tau}\cdot\nabla)\mathbf{Z}_{h\tau}\cdot\mathbf{M}_{h\tau} \tag{3.84}$$
$$+\frac{1}{2}div\,\mathbf{U}_{h\tau}\,\mathbf{Z}_{h\tau}\cdot\mathbf{M}_{ht}\big)\,.$$

Note that the consistency terms with the jumps have disappeared since $[\![\mathbf{Z}_{h\tau}]\!]\big|_F = 0$ for all $F\in\mathcal{F}^i$, which is a consequence of definitions (3.42) and (3.82). Passage to the limit of the first part of (3.84), that is

$$-\int_0^{t_F}\sum_{T\in\mathcal{T}_h}\int_T(\mathbf{U}_{h\tau}\cdot\nabla)\mathbf{Z}_{h\tau}\cdot\mathbf{M}_{h\tau} \quad\xrightarrow{h,\tau\to 0}\quad -\int_0^{t_F} b(\mathbf{u}^*,\mathbf{z},\mathbf{m}^*)\,,$$

is carried out using the strong $L^2(L^2)$ convergence of $\mathbf{U}_{h\tau}$, the weak $L^2(L^2)$ convergence of $\mathbf{M}_{h\tau}$ and the strong convergence of $\nabla\mathbf{Z}_{h\tau}$ guaranteed by (1.13). By consistency, we need the second part of (3.84) to vanish when $h,\tau\to 0$:

$$-\int_0^{t_F}\sum_{T\in\mathcal{T}_h}\int_T\frac{1}{2}div\,\mathbf{U}_{h\tau}\,\mathbf{Z}_{h\tau}\cdot\mathbf{M}_{h\tau}$$
$$= -\int_0^{t_F}\sum_{T\in\mathcal{T}_h}\int_T\frac{1}{2}div\,\mathbf{U}_{h\tau}\,(\mathbf{Z}_{h\tau}-\langle\mathbf{Z}_{h\tau}\rangle_T)\cdot\mathbf{M}_{h\tau}\big) \tag{3.85}$$
$$\lesssim \|\nabla\mathbf{U}_{h\tau}\|_{L^2(0,t_F;\mathbf{L}^2)}\; h\|\nabla\mathbf{Z}\|_{L^\infty(0,t_F,\mathbf{L}^\infty)}\;\|\mathbf{M}_{h\tau}\|_{L^2(0,t_F;\mathbf{L}^2)} \xrightarrow{h,\tau\to 0} 0$$

where $\langle\mathbf{Z}_{h\tau}\rangle_T = \frac{1}{|T|}\int_T\mathbf{Z}_{h\tau}$. Estimate (3.85) was obtained using the local orthogonality property (3.71), which is a consequence of the fact that we are using using discontinuous pressures and the choice of the magnetization space $\mathbb{M} = [\mathbb{P}]^d$. In (3.85) we also used the uniform bounds on $\mathbf{U}_{h\tau}$ and $\mathbf{M}_{h\tau}$, and the regularity of the test function $\mathbf{z}$.

Passage to the limit of the remaining convective terms (those in (3.83a) and

(3.83b)) follow standard procedures and their treatment can be found in other works such as [43, 45].

◇ For the Kelvin force in (3.83c), using again definition (3.54) we get

$$\begin{aligned}
&\int_0^{t_F} b_h^m\big(\mathbf{V}_{h\tau}, \mathbf{H}_{h\tau}, \mathbf{M}_{h\tau}\big) \\
&= \int_0^{t_F} \sum_{T\in\mathcal{T}_h} \int_T \big((\mathbf{V}_{h\tau}\cdot\nabla)\mathbf{H}_{h\tau}\cdot\mathbf{M}_{h\tau} + \frac{1}{2} div\,\mathbf{V}_{h\tau}\,\mathbf{H}_{h\tau}\cdot\mathbf{M}_{h\tau}\big) \qquad (3.86)\\
&\xrightarrow{h,\tau\to 0} \int_0^{t_F}\int_\Omega (\mathbf{v}\cdot\nabla)\mathbf{h}\,\mathbf{m}^* = \int_0^{t_F}\int_\Omega (\mathbf{m}^*\cdot\nabla)\mathbf{h}\,\mathbf{v}\,,
\end{aligned}$$

which follows by using an analogous arguments used in to (3.85). To show that the term $\frac{1}{2} div\,\mathbf{V}_{h\tau}\,\mathbf{H}_{h\tau}\cdot\mathbf{M}_{h\tau}$ vanishes in the limit we have to use property (3.71), this time by adding a term of the form $\langle\mathbf{H}_{h\tau}\rangle_T\cdot\mathbf{M}_{h\tau}$. Finally the weak $L^2(L^2)$ convergence of $\mathbf{M}_{h\tau}$, the strong convergence properties of $\mathbf{H}_{h\tau}$ and the test function $\mathbf{V}_{h\tau}$, and the fact that $\nabla\mathbf{h} = \nabla\mathbf{h}^{\mathrm{T}}$ since $curl\,\mathbf{h} = 0$, are all what we need in the passage to the limit.

◇ For the magnetic torque in (3.83b) we have that

$$\int_0^{t_F} \mu_0(\mathbf{M}_{h\tau}\times\mathbf{H}_{h\tau}, \mathbf{X}_{h\tau}) \xrightarrow{h,\tau\to 0} \int_0^{t_F} \mu_0(\mathbf{m}^*\times\mathbf{h}, \mathbf{x})$$

which follows by the weak $L^2(L^2)$ convergence of $\mathbf{M}_{h\tau}$ and the strong convergence of $\mathbf{H}_{h\tau}$ and $\mathbf{X}_{h\tau}$.

Since the remaining terms in (3.83) are linear they require little or no explanation in their passage to the limit. The proof is thus complete. □

3.5.5 Finite element spaces

Now we provide a couple of finite element spaces which satisfy the key assumptions required in the proof of convergence of scheme (3.67).

In space dimension two, the spaces $\mathbb{W}$ and $\mathbb{M}$ can be the same as those defined in (3.58) with $\ell = 2$, while the pair $\{\mathbb{U}, \mathbb{P}\}$ can be chosen as

$$\begin{aligned} \mathbb{U} &= \left\{ \mathbf{U} \in \boldsymbol{\mathcal{C}}^0\left(\overline{\Omega}\right) \,\middle|\, \mathbf{U}|_T \in [\mathcal{P}_\ell(T) \oplus \operatorname{Span} \mathcal{B}(T)]^d \,, \forall\, T \in \mathcal{T}_h \right\} \cap \mathbf{H}_0^1(\Omega) \,, \\ \mathbb{P} &= \left\{ \mathrm{Q} \in L^2\left(\overline{\Omega}\right) \mid \mathrm{Q}|_T \in \mathcal{P}_{\ell-1}(T) \,, \forall\, T \in \mathcal{T}_h \right\} \,, \end{aligned} \tag{3.87}$$

where $\mathcal{B}(T) = \prod_{i=1}^{d+1} \lambda_i$ is the cubic bubble function, and $\{\lambda_i\}_{i=1}^{d+1}$ are the barycentric coordinates. This finite element pair is known as conforming Crouzeix-Raviart (there is a non-conforming version which bears the same name) and it is well known to be LBB stable (cf.[53]) in two dimensions. Approximation (convergence) properties of the Stokes projector in L^∞-norm (more precisely, estimate (1.20)) for this pair were established in [55], which will be required in chapter *Chapter 4*.

In space dimension three the reader could consider using again the finite element spaces $\mathbb{W}$ and $\mathbb{M}$ (with $\ell = 2$) defined in (3.58) and the second-order Bernardi-Raugel element (see [42, p. 148]) which uses $\mathcal{P}_1$ discontinuous elements for the pressure space.

3.6 Numerical validation

Let us computationally explore the convergence properties of the scheme (3.44) using manufactured solutions. The implementation has been carried out with the help of the `deal.II` library; see [70, 71]. Since we must guarantee the inclusion

$\nabla\mathbb{X} \subset \mathbb{M}$ and this library uses quadrilateral/hexahedrons, the finite element spaces defined in (3.52)-(3.53), which are based on simplices, cannot be used. In addition, we cannot use the same polynomial degrees used in (3.52)-(3.53), since the inclusion $\nabla\mathcal{Q}_\ell(T) \subset [\mathcal{Q}_{\ell-1}(T)]^d$ is not true. For this reason we set

$$\begin{aligned} \mathbb{X} &= \left\{ \mathrm{X} \in \mathcal{C}^0\left(\overline{\Omega}\right) \mid \mathrm{X}|_T \in \mathcal{Q}_\ell(T)\,, \forall T \in \mathcal{T}_h \right\} \subset H^1(\Omega)\,, \\ \mathbb{M} &= \left\{ \mathbf{M} \in \mathbf{L}^2(\Omega) \mid \mathbf{M}|_T \in [\mathcal{Q}_\ell(T)]^d\,, \forall\, T \in \mathcal{T}_h \right\}. \end{aligned} \tag{3.88}$$

and since $\nabla\mathcal{Q}_\ell(T) \subset [\mathcal{Q}_\ell(T)]^d$ holds true (3.88) is a valid pair. This choice, however, is suboptimal in terms of approximation. Since $\ell = 2$ we expect

$$\begin{aligned} &\|\mathbf{U}^\tau - \mathbf{u}^\tau\|_{\ell^\infty(\mathbf{L}^2)} + \|\mathbf{W}^\tau - \mathbf{w}^\tau\|_{\ell^\infty(\mathbf{L}^2)} \\ &\qquad + \|\mathbf{M}^\tau - \mathbf{m}^\tau\|_{\ell^\infty(\mathbf{L}^2)} + \|\nabla\Phi^\tau - \nabla\varphi^\tau\|_{\ell^\infty(\mathbf{L}^2)} \lesssim \tau + h^2\,, \end{aligned}$$

which is suboptimal by a power of h for the linear velocity $\mathbf{U}$, angular velocities $\mathbf{W}$ and magnetization $\mathbf{M}$. The reason for this loss of accuracy is the term $\|\nabla\Phi^\tau - \nabla\varphi^\tau\|_{\ell^\infty(\mathbf{L}^2)}$.

The arising linear systems have been solved with the direct solver `UMFPACK`© for validation purposes. The nonlinear system is solved using a fixed point iteration. Let $\Omega = (0,1)^2 \subset \mathbb{R}^2$ and

$$\begin{aligned} \mathbf{u}(x,y,t) &= \sin(t)\big(\sin(\pi x)\sin(\pi(y+0.5)), \cos(\pi x)\cos(\pi(y+0.5))\big)^\intercal\,, \\ p(x,y,t) &= \sin(2\pi(x-y)+t)\,, \\ \mathbf{w}(x,y,t) &= \sin(2\pi x + t)\,\sin(2\pi y + t)\,, \\ \mathbf{m}(x,y,t) &= \big(\sin(2\pi x + t)\cos(2\pi y + t), \cos(2\pi x + t)\sin(2\pi y + t)\big)^\intercal \\ \varphi(x,y,t) &= \sin(\pi x + t)\sin(\pi y + t). \end{aligned}$$

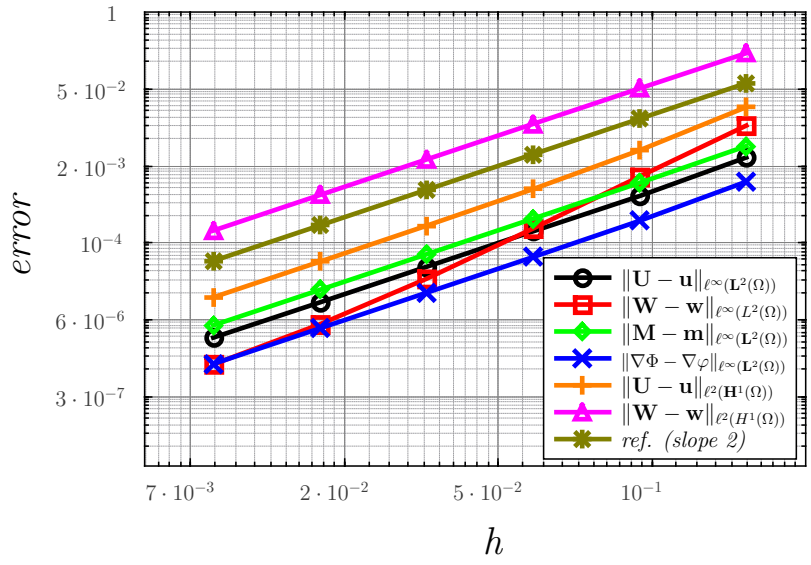

Figure 3.1: **Experimental errors for the Rosensweig's model numerical scheme (log-log scale).** Errors for the linear velocity $\mathbf{u}$, angular velocity $\mathbf{w}$, magnetization $\mathbf{m}$ and magnetic potential φ. Note that the convergence rates in the $\ell^\infty(\mathbf{L}^2)$ norms are suboptimal as expected, because of the choice of finite element spaces (3.88). Note that the angular velocity (square markers) initially converges much faster than it should, and shows the asymptotic rate in the last two points.

The right-hand sides are computed accordingly. To verify the convergence rates we set $\tau = h^2$ and consider a sequence of meshes with $h = 2^{-i}$ for $2 \leq i \leq 7$. Figure 3.1 shows the experimental errors, thereby confirming the predicted convergence rates.

3.7 Numerical experiments with point dipoles

Let us now explore model (3.1) and scheme (3.44) with a series of more realistic examples. In all these experiments we will consider the gradient of the potential of

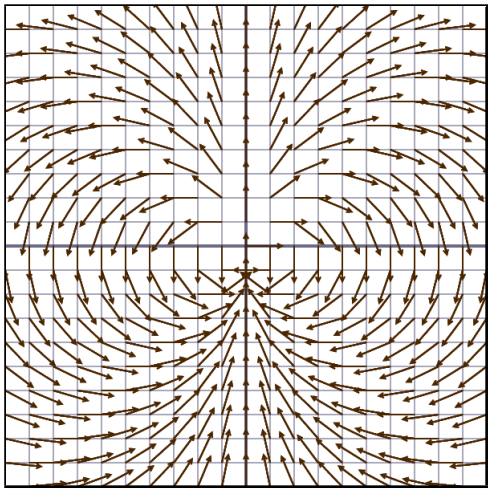

Figure 3.2: Normalized plot of the two dimensional harmonic field $\nabla\phi_s$, with ϕ_s as in (3.90). Here $\mathbf{x}_s = (0,0)$ and $\mathbf{d} = (0,1)$.

a point dipole $\nabla\phi_s$ as a prototype for an applied magnetizing field, where

$$\phi_s(\mathbf{x}) = \frac{\mathbf{d}\cdot(\mathbf{x}_s - \mathbf{x})}{|\mathbf{x}_s - \mathbf{x}|^3}\,, \tag{3.89}$$

$|\mathbf{d}| = 1$ indicates the direction of the dipole, and $\mathbf{x}_s = (x_s, y_s, z_s) \in \mathbb{R}^3$ is its location. It is not difficult to verify that $curl\,\nabla\phi_s = 0$ and $div\,\nabla\phi_s = \Delta\phi_s = 0$ for every $\mathbf{x} \neq \mathbf{x}_s$, so that $\nabla\phi_s$ defines a harmonic vector field. This is a physical requirement in the context of non-conducting media, the magnetic field must satisfy the equations of magnetostatics.

Formula (3.89), however, is intrinsically three dimensional [74]. For this reason, we consider an alternative definition which leads to a two dimensional harmonic vector field:

$$\phi_s(\mathbf{x}) = \frac{\mathbf{d}\cdot(\mathbf{x}_s - \mathbf{x})}{|\mathbf{x}_s - \mathbf{x}|^2}\,, \tag{3.90}$$

where now $\mathbf{x}, \mathbf{x}_s, \mathbf{d} \in \mathbb{R}^2$. Figure 3.2 shows $\nabla\phi_s/|\nabla\phi_s|$ for $\mathbf{d} = (0,1)$ and $\mathbf{x}_s = (0,0)$.

In our numerical experiments we will use linear combinations of dipoles as applied magnetizing field $\mathbf{h}_a$

$$\mathbf{h}_a = \sum_s \alpha_s \nabla \phi_s. \tag{3.91}$$

3.7.1 Experiment 1: Spinning magnet

We consider $\Omega = (0,1)^2 \subset \mathbb{R}^2$ filled with ferrofluid, $t \in [0,4]$, and the applied magnetic field of dipole $\mathbf{h}_a = \alpha_s \nabla \phi_s$, represented in Figure 3.3 as a rectangular permanent magnet. The application of the magnetic field will obey the following sequence:

- ◇ The initial position and orientation of the dipole are $\mathbf{x}_s = (0.5, -0.4)$ and $\mathbf{d} = (0,1)$ respectively.
- ◇ For $t \in [0,1)$ we linearly increase the intensity α_s from $\alpha_s = 0$ to $\alpha_s = 10$ without changing $\mathbf{d}$.
- ◇ We let the fluid rest for $t \in [1,2)$.
- ◇ For $t \in [2,4]$ we make the dipole go through a circular path around the center of the box $(0.5, 0.5)$, with $\mathbf{d}$ pointing to the center of the box at every time as depicted in Figure 3.3.

All the constitutive parameters of the model (ν, ν_r, μ_0, $\jmath$, c_a, c_d, c_0 and $\varkappa_0$) were set to one with the exception of $\mathscr{T}$ which was taken to be 10^{-4} s in order to achieve an almost instantaneous alignment of the magnetization with the magnetic field. The discretization uses a uniform mesh with 100 elements in each space direction

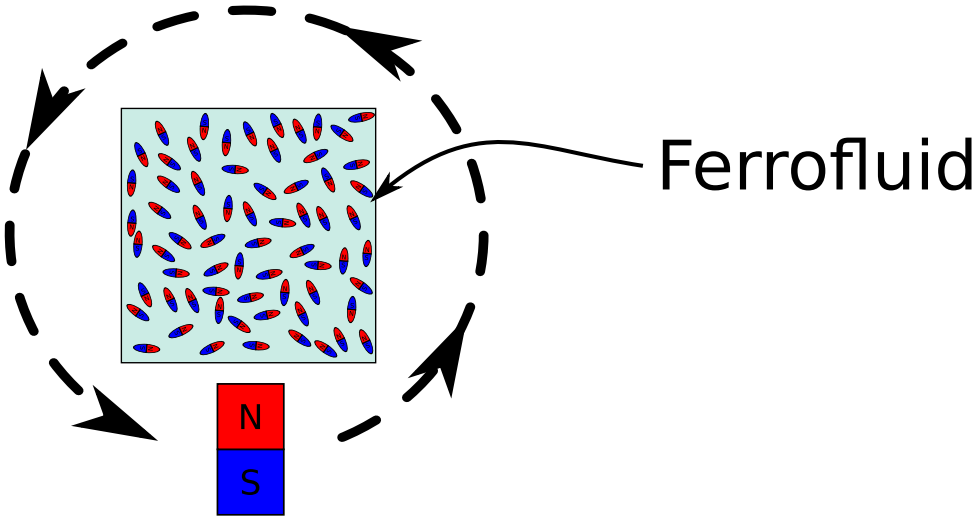

Figure 3.3: **Spinning magnet experiment: setup.** Scheme of the experiment of §3.7.1 (spinning magnet). We make the dipole go through a circular path around the center of the box $(0.5, 0.5)$, with $\mathbf{d}$ pointing to the center of the box at every time.

and 400 time steps. The main goal of this experiment, and the displayed graphical results, is to help the reader form some intuition about the coupling between the linear velocity $\mathbf{u}$, angular velocity $\mathbf{w}$, and the magnetization $\mathbf{m}$. For this reason reference/scales have been omitted. Figures 3.4–3.6 show some graphical results.

3.7.2 Experiment 2: Ferrofluid pumping

This experiment is related to what was the initial motivation for the development of ferrofluids [2], which is pumping by means of magnetic fields without the action of any moving or mechanical device. There are two well known methodologies used to induce pumping in ferrofluids:

- ◇ Using a spatially-uniform but sinusoidal-in-time magnetic field [26].

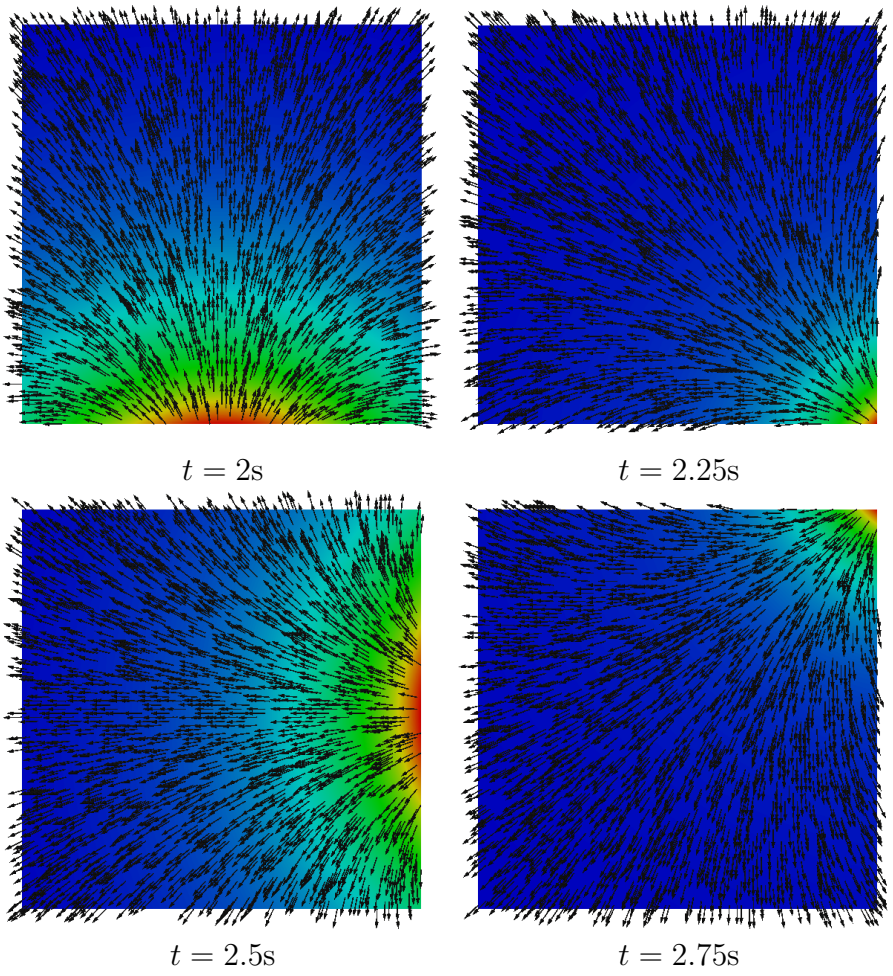

Figure 3.4: **Spinning magnet experiment: magnetization field.** Magnetization at times $t = 2$s, $t = 2.25$s, $t = 2.5$s and $t = 2.75$s for the experiment described in §3.7.1. The magnetization vectors are normalized for visualization, scale has been omitted for brevity. At time $t = 2$ the dipole is at the bottom of the box, at time $t = 2.25$ the dipole is pointing in the $(-1, 1)$ direction, at time $t = 2.5$ the dipole is pointing to $(-1, 0)$, and at $t = 2.75$ the dipole is pointing to $(-1, -1)$.

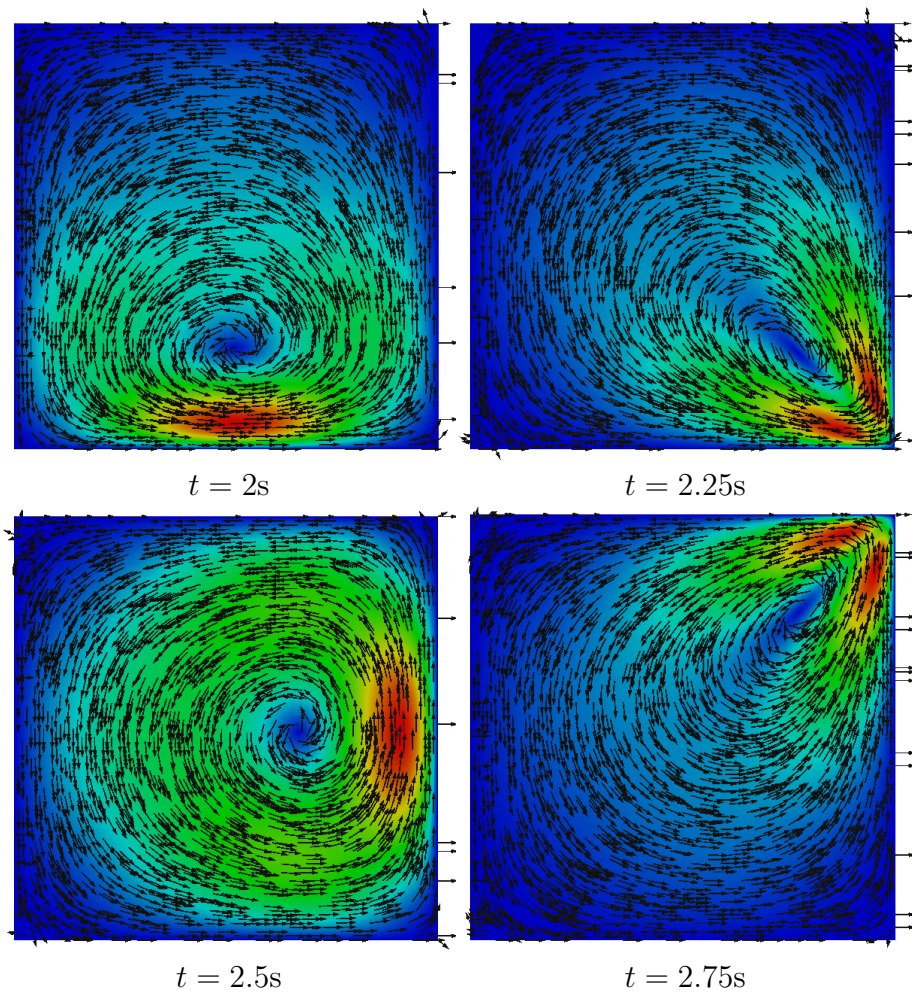

Figure 3.5: **Spinning magnet experiment: velocity field.** Same experiment as in Figure 3.4, but here we have the velocity field at times $t = 2$s, $t = 2.25$s, $t = 2.5$s and $t = 2.75$s. The velocity vectors are normalized to facilitate their visualization. It is easy to see that we have a positive circulation of the velocity field.

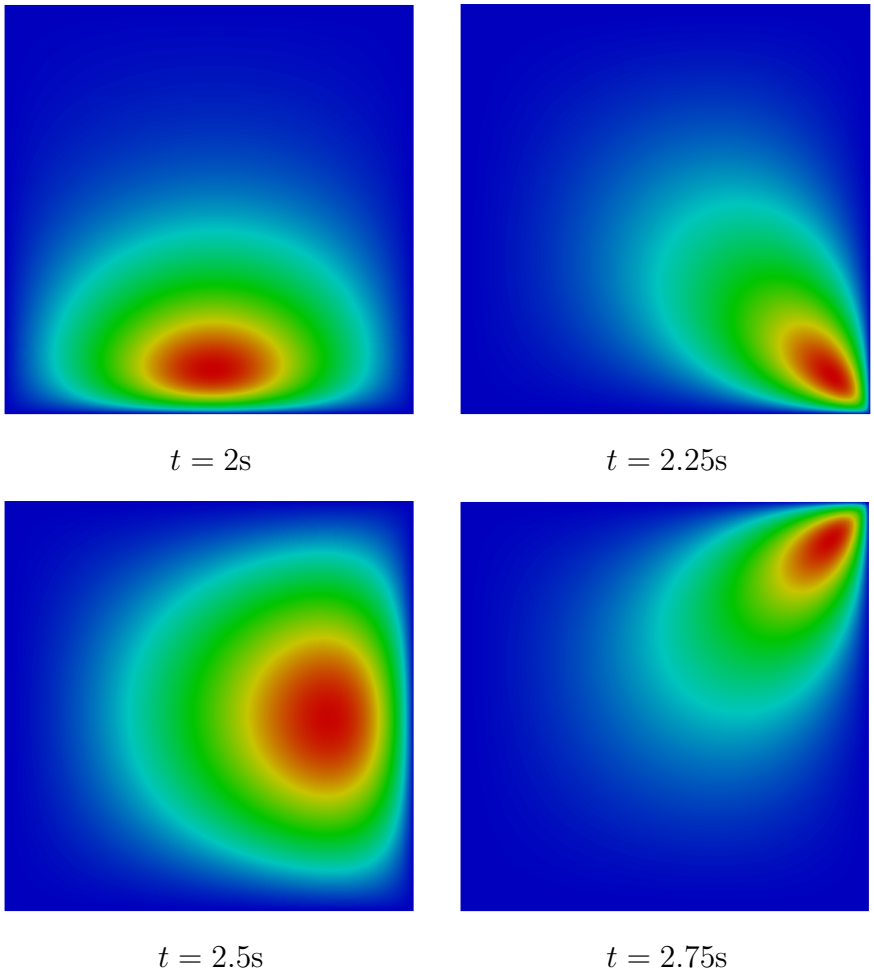

Figure 3.6: **Spinning magnet experiment: angular velocity field.** Angular velocity (spin) at times $t = 2$s, $t = 2.25$s, $t = 2.5$s and $t = 2.75$s for the experiment of §3.7.1. Note that the angular velocity $\mathbf{w}$ takes positive values, i.e., $\mathbf{w} = w\,\hat{k}$ is a vector pointing out of the plane. This is consistent with the velocity field which shows a positive circulation (*curl*) in Figure 3.5 and also with the fact that the magnetic dipole is spinning around the box in counter clockwise direction.

◇ Using a magnetic field that is varying in space and time [65].

Here we will follow the second approach: we will apply a magnetic field which keeps its polarity (sign) constant, but its intensity changes in space, basically a periodic sequence of peaks (pulses) that travel in the direction we want to induce linear momentum. This methodology was chosen because if we assume that we are always close to equilibrium, that is $\mathbf{m} \approx \varkappa_0 \mathbf{h}$, we get the following crude approximation for the Kelvin force:

$$\mu_0(\mathbf{m}\cdot\nabla)\mathbf{h} \approx \mu_0\varkappa_0(\mathbf{h}\cdot\nabla)\mathbf{h} = \tfrac{\mu_0\varkappa_0}{2}\nabla|\mathbf{h}|^2\,.$$

Consequently, if $\nabla\mathbf{h} \approx 0$, then there is no force acting on the ferrofluid, and a methodology based on a spatially uniform magnetic field has very little chances of success. If we want to induce linear momentum in the ferrofluid we need to create steep gradients in the magnetic field. Technical details about the physical implementation of similar ideas, all of them using a magnetic field which resembles traveling pulses or a traveling magnetic wave, can be found in [65, 106, 107].

The idea of a periodic sequence of pulses that travels in the direction we want to induce linear momentum was numerically recreated in a channel of 6 units of length, and one unit of height, using a total of 64 dipoles: 32 on the lower part of the duct and 32 on the upper part, distributed uniformly through 2 units of length in its middle section. The configuration of magnetic dipoles, and the intensities associated to them, in the middle section of the channel is sketched Figure 3.8. The corresponding applied magnetic field is computed as $\mathbf{h}_a = \sum_{s=1}^{64} \alpha_s \nabla\phi_s$, where $\alpha_s = |\sin(\omega t - \kappa x_s)|^{2q}$, $\omega = 2\pi f$ with $f = 10\text{Hz.}$, $q = 5$, $\kappa = 2\pi/\lambda$ with $\lambda = 1.0$,

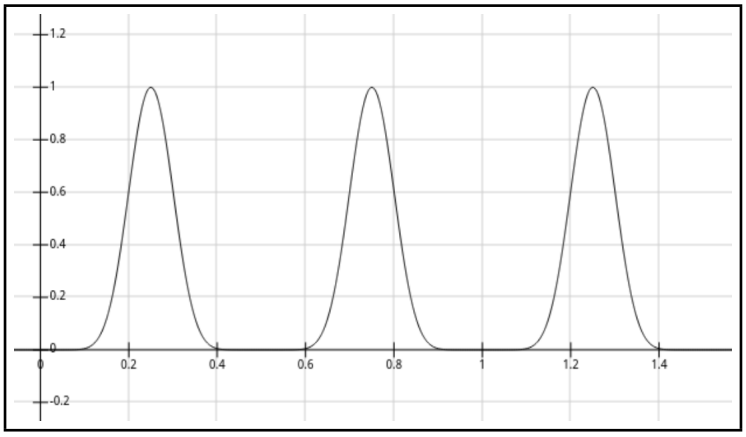

Figure 3.7: **Plot of the function** $\alpha_s = |\mathbf{sin}(\omega t - \kappa x_s)|^{2q}$. Here x_s is the horizontal axis, $t = 0$, $\kappa = 2\pi$, and $q = 5$.

creating the effect of pulses traveling from left to right. In Figure 3.7 we plot the function $\alpha_s = |\sin(\omega t - \kappa x_s)|^{2q}$ in terms of x_s, so that the reader can appreciate the shape of the pulses (intensity of the magnetic field). Some numerical results are depicted in Figures 3.10–3.11.

The magnitude of the magnetization is only relevant in the middle of the channel as it can be appreciated in Figure 3.9. A noteworthy outcome of these experiments is displayed in Figure 3.11: the spin does not seem to help (it induces a flow in the opposite direction), which is a very intriguing result. More precisely, the spin in the upper part of Figure 3.11 is negative and the spin in the lower part of the channel is positive, which will induce flow from right to left as it was shown numerically in [86]. This is an unexpected outcome which requires further investigation.

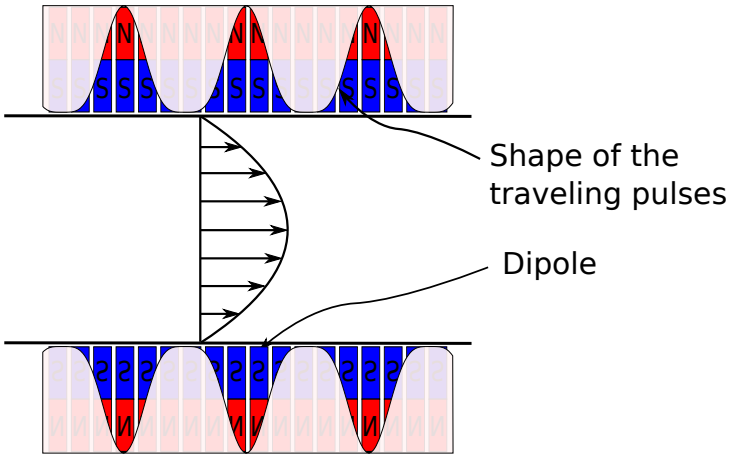

Figure 3.8: **Ferrofluid pumping experiment: setup (sketch) of the experiment**. Sketch of the middle section of the channel showing the setup of the ferrofluid pumping experiment of §3.7.2. The vertical bars represent magnetic dipoles (see formula (3.90)) located in the center of the channel. All the dipoles have the same polarity, which does not change in the x direction, and their intensity is represented by the unshaded region. These dipoles do not move, but their intensity changes in time, reproducing the effect of traveling pulses.

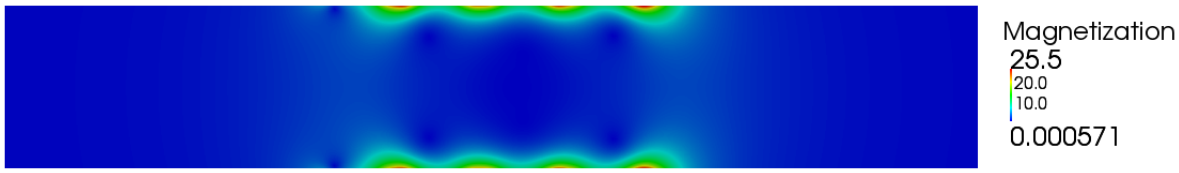

Figure 3.9: **Ferrofluid pumping experiment: detail of the magnetization in the middle section of the channel.** The intensity of the magnetization is relevant close to the upper and lower walls, and is negligible in the center of the channel. This means that most of the force is exerted close to the upper and lower walls.

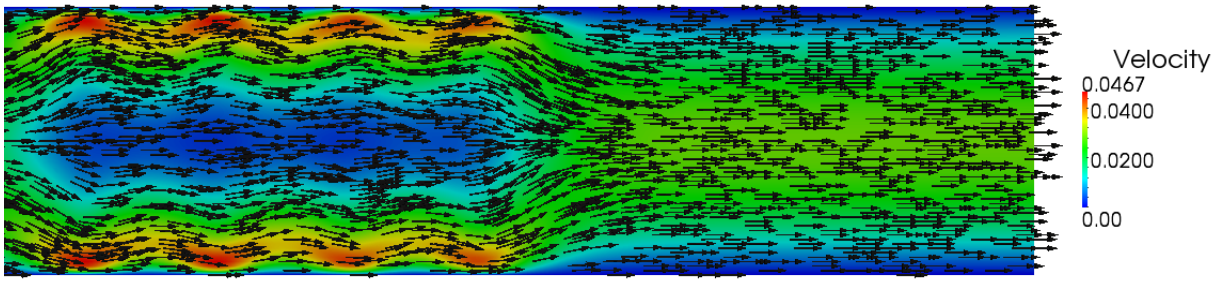

Figure 3.10: **Ferrofluid pumping experiment: detail of the velocity in the middle section of the channel.** It can be appreciated that on the region affected by the external magnetic fields (left) the velocity field is not very aligned, but it becomes much more uniform as we move to the right.

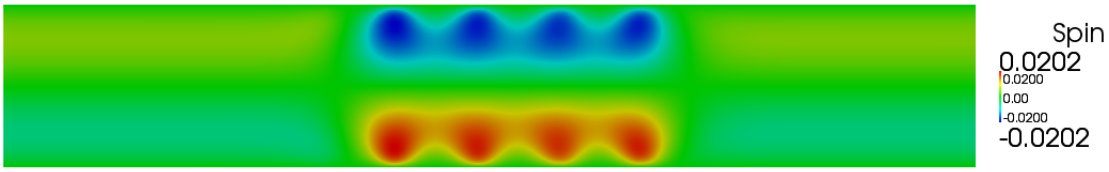

Figure 3.11: **Ferrofluid pumping experiment: angular velocity.** Note that it is positive (counterclockwise) in the lower part of the channel and negative (clockwise) in the upper part. Such profile of angular velocities does not help in the pumping process from left to right. This is a quite intriguing effect.

3.7.3 Experiment 3: Ferromagnetic stirring of a passive scalar

For low Reynolds numbers ($Re \backsimeq 1$) one of the bottlenecks of chemical reactions is mixing, in particular when the effects of diffusion are not strong enough. Slow mixing can lead to very long waiting times or a very poor completion of chemical reactions. Flows inside microfluidic devices (usually called lab-on-chip devices) have quite low Reynolds numbers and there is a growing interest in accelerating the mixing process with the addition of active and passive mixers. Passive mixer designs can range from simple grooved channels and Y-shaped channels to much more sophisticated ideas [108, 109, 110]. Among active mixers we can find mixing by means of ferromagnetic particles [111, 112]. Here we will illustrate the idea of ferrofluid mixing by adding the following convection diffusion equation:

$$c_t + \mathbf{u} \cdot \nabla c - \alpha \Delta c = 0 \tag{3.92}$$

where $\mathbf{u}$ is the velocity from the equations of ferrohydrodynamics (3.1), and $\alpha = 0.001$ for all our experiments. We consider such a small diffusion so that mixing depends mostly on advection. Equation (3.92) is uncoupled from the system (3.1), meaning that no quantity in (3.1) depends on c.

We explore the possibility of designing an active mixer by applying a time-dependent magnetic field to a ferrofluid contained in $\Omega = (0, 1)^2$, and we track the evolution of the concentration c satisfying equation (3.92). As in the previous experiments we make no attempt to use realistic scalings or try to relate the numerical results with any physical situation (as microflows). The main goal is to provide a

proof of concept of some ideas and discard those which have no room for additional improvement. Designing a functional stirrer is a deceptively simple task. For instance, using the setup of Figure 3.3 which involves moving physically the magnet does not work, at least in our experience, even if we relax the viscosity and use values much smaller than unity, or if we make the magnet spin around the box at a much higher angular velocity.

As a first attempt, we let the applied magnetizing field be that of two dipoles with alternating polarity, more precisely

$$\mathbf{h}_a = \sum_{s=1}^{2} \alpha_s \nabla \phi_s \,, \quad \text{where} \quad \alpha_1 = \alpha_0 \sin(\omega t) \,, \quad \alpha_2 = \alpha_0 \sin(\omega t + \pi/2) \,, \tag{3.93}$$

i.e., the two dipoles have a phase mismatch of $\pi/2$; see Figure 3.12 for the sketch of this setup. Here $\omega = 2\pi f$, is the angular velocity of the periodic excitation, f is the frequency, and α_0 is the amplitude. The magnetization and velocity fields induced by this setup are displayed in Figures 3.13 and 3.14. Some results regarding the ability of this setup to actually induce mixing of the passive scalar c can be appreciated in Figure 3.15, where we have used $f = 20$Hz., $\alpha_0 = 5.0$, and $\nu = \nu_r = 0.5$. This setup does indeed shake the fluid as it can be appreciated in Figures 3.14 and 3.15, but the magnitude of the velocity is very small, less than 10^{-2} for most of our experiments, and is not very sensitive to the inputs, meaning that increasing the value of ω and α_0, or using a very small viscosity, does not significantly increase the velocity and as a consequence the mixing will be very poor (at least in this context, which is that of an homogeneous fluid). For instance, the results of setting $f = 40$Hz. and $\nu = \nu_r = 0.1$, are very similar to those of Figure 3.15.

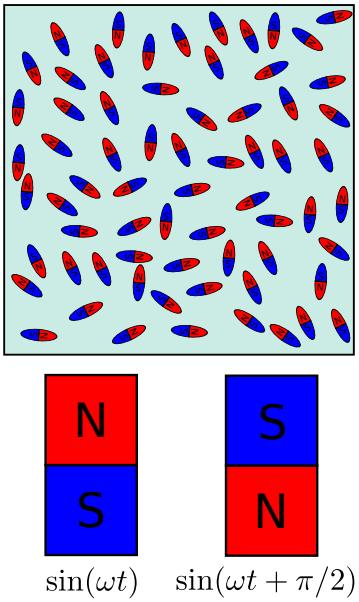

Figure 3.12: **Ferromagnetic stirring (first approach): setup.** The magnetic field satisfies (3.93).

A second, and successful, approach is that of a traveling wave. Consider eight dipoles on the lower edge of the box pointing upwards, much like the setup of Figure 3.12, so that the magnetic field is given by

$$\mathbf{h}_a = \sum_{s=1}^{8} \alpha_s \nabla \phi_s \,, \quad \alpha_s = \alpha_0 \left|\sin(\omega t - \kappa x_s)\right| , \quad \kappa = 2\pi/\lambda \,, \quad \lambda = 0.8 \,. \tag{3.94}$$

Figure 3.16 displays some promising results. There is mixing, even under quite unfavorable conditions: $f = 20\text{Hz.}$, $\alpha_0 = 5.0$, and $\nu = \nu_r = 0.5$. This setting is sensitive to the inputs, as ω and α_0 increase and the viscosity diminishes, the mixing improves. The magnetization and velocity profile for this setting are shown in Figures 3.17 and 3.18, respectively. Much more striking results can be found in Figure 3.19, where we use a higher value for ω, a lower viscosity, a higher intensity α_s, and we also run the simulation for a longer time.

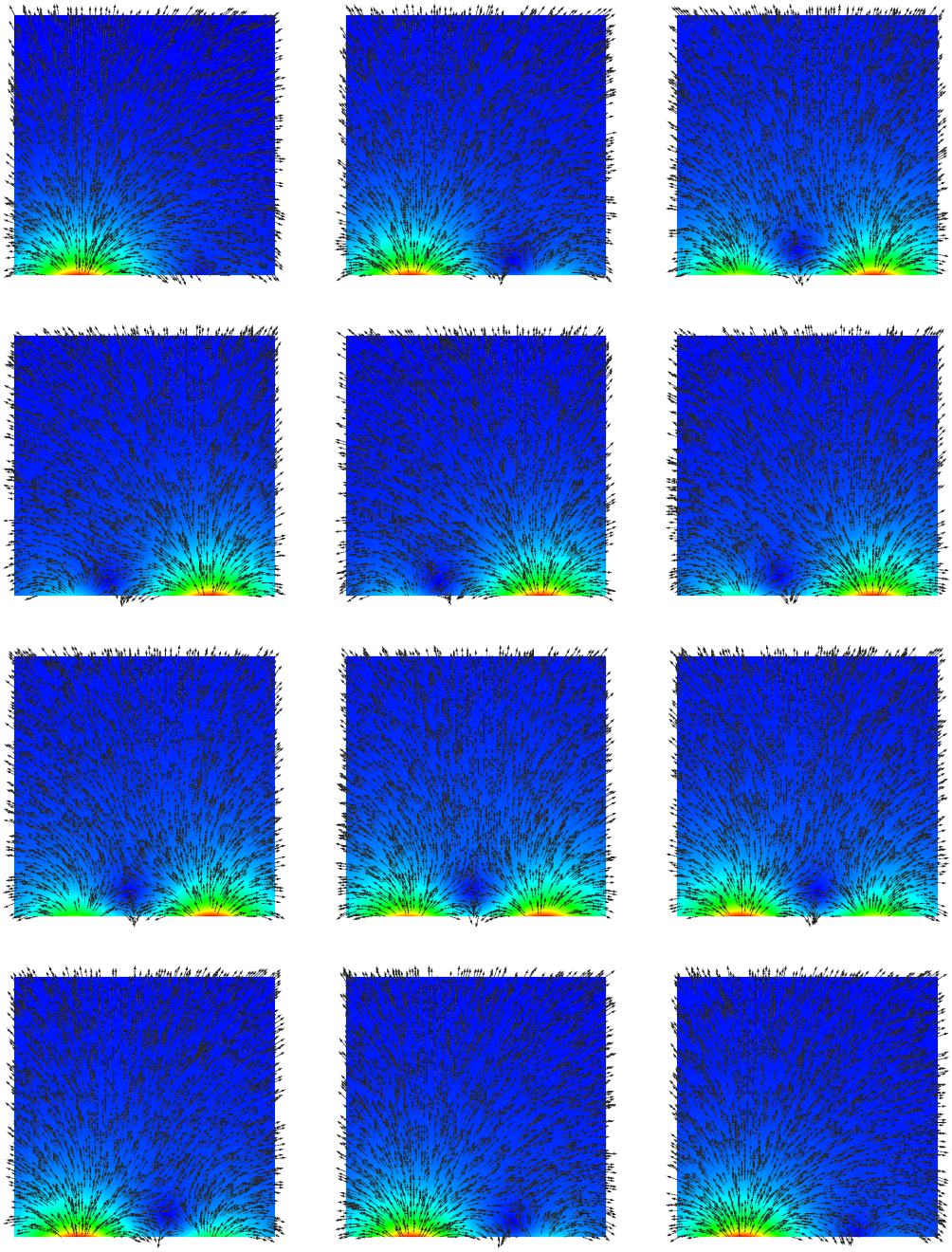

Figure 3.13: **Ferromagnetic stirring (first approach): evolution of the magnetization field.** This corresponds to the setup described in figure 3.12 during a half period $T = \frac{1}{2f}$. The magnetic field satisfies (3.93). The magnets are fixed on the bottom of the container and so is the location where the maximum intensities occur.

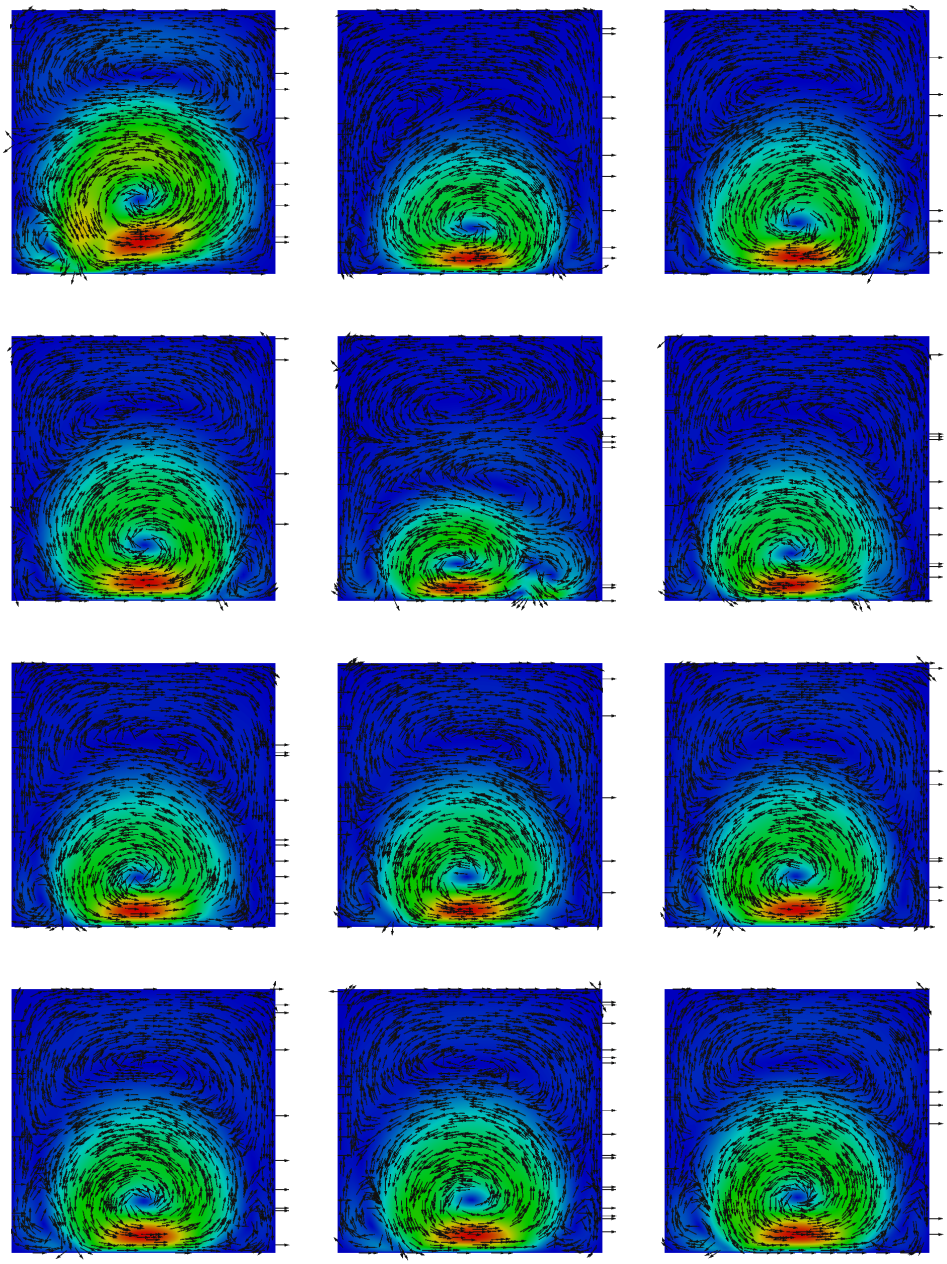

Figure 3.14: **Ferromagnetic stirring (first approach): evolution of velocity.** Evolution of the velocity during a half period $T/2 = \frac{1}{2f}$ for the stirring experiment of §3.7.3 (see figure 3.12 for its setup). The magnetic field satisfies (3.93). Reading from left to right and top to bottom: there is reversal of the circulation (curl) of the flow between the first two figures, and also between the fourth and fifth figure. Here the scale has been omitted, but the maximum velocity is of the order of $\simeq 0.008$, enough to induce some mixing of the passive scalar as it can be appreciated in Figure 3.15, but far from the quality of mixing achieved for instance in Figure 3.19 using the traveling wave approach.

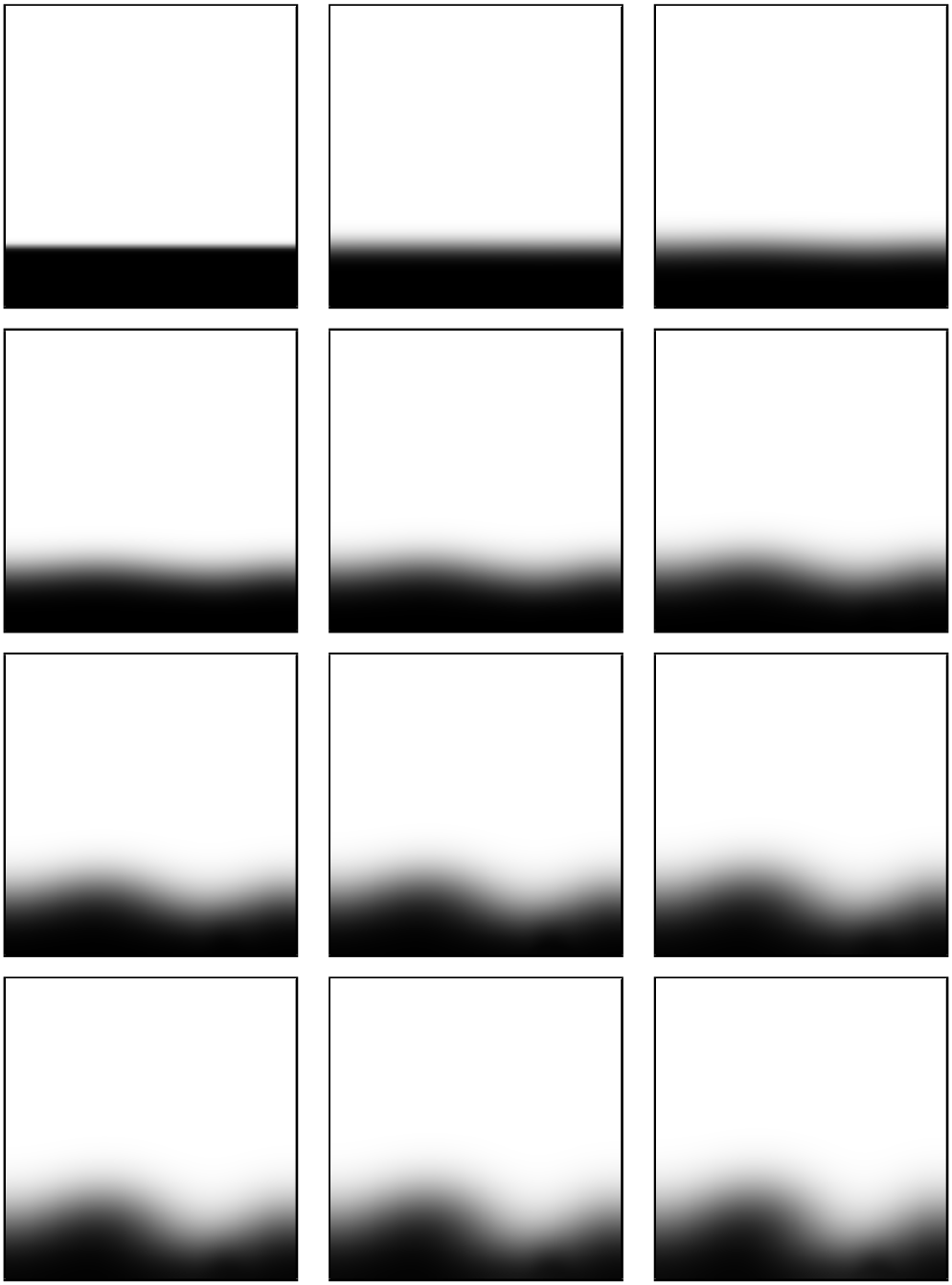

Figure 3.15: **Ferromagnetic stirring (first approach): evolution of the passive scalar.** Evolution of the concentration using the setup described in Figure 3.12, the magnetizing field satisfies (3.93). The sequence of figures shown here was for a total of 4 seconds. We start with concentration equal to one on the bottom of the box (the black region on the bottom). These results were obtained with $f = 20$, and $\nu = \nu_r = 0.5$.

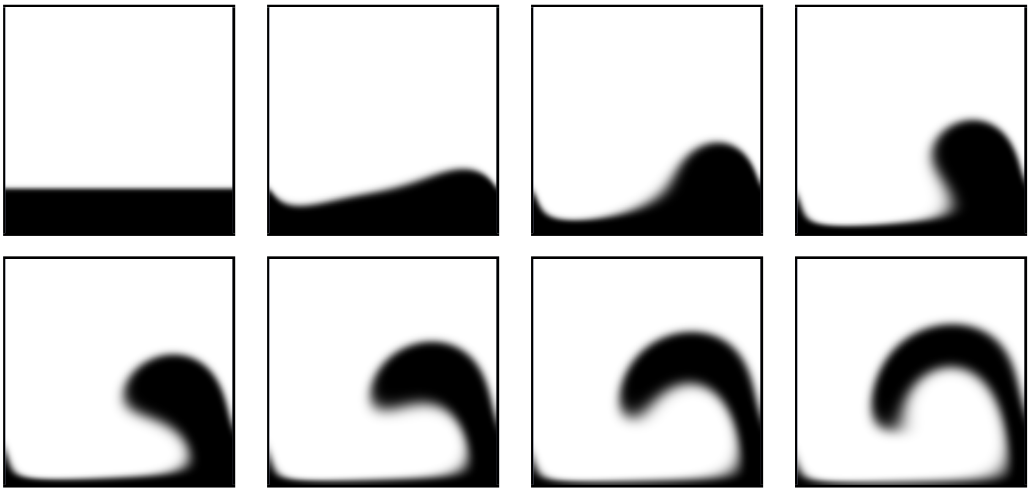

Figure 3.16: **Ferromagnetic stirring (second approach): evolution of the passive scalar.** Contour of the passive scalar satisfying equation (3.92) from time $t = 0$ to $t = 1.0$. The magnetic field satisfies (3.94). We start with concentration equal to one on the bottom of the box, the velocity field induced by the traveling wave of magnetization drags concentration on the bottom and takes it upward. These results were obtained with $f = 20$Hz., $\nu = \nu_r = 0.5$, and $\alpha_0 = 5.0$.

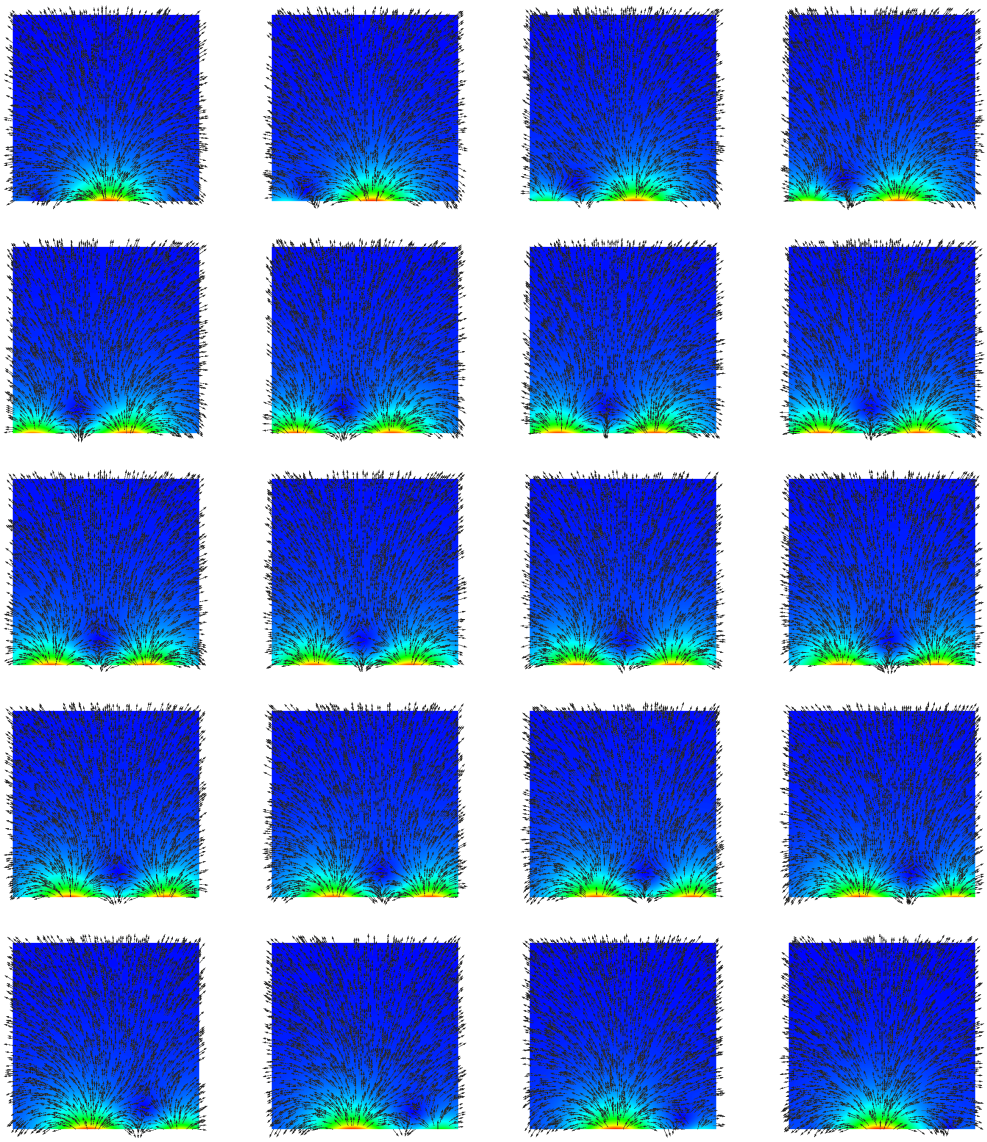

Figure 3.17: **Ferromagnetic stirring (second approach): evolution of the magnetization field.** Magnetization vectors and their intensity when using the magnetic field (3.94). Here we illustrate a half period ($T/2 = \frac{1}{2f}$) of the magnetization profile traveling from left to right. The magnetization is strong in two regions on the lower part of the box. The Kelvin force generated by this magnetization field not only pushes the fluid from left to right, but also creates some effects in the y axis, effectively creating some ripples, which can be appreciated for instance in Figure 3.19 where streamlines go up and down when they are at the bottom of the box.

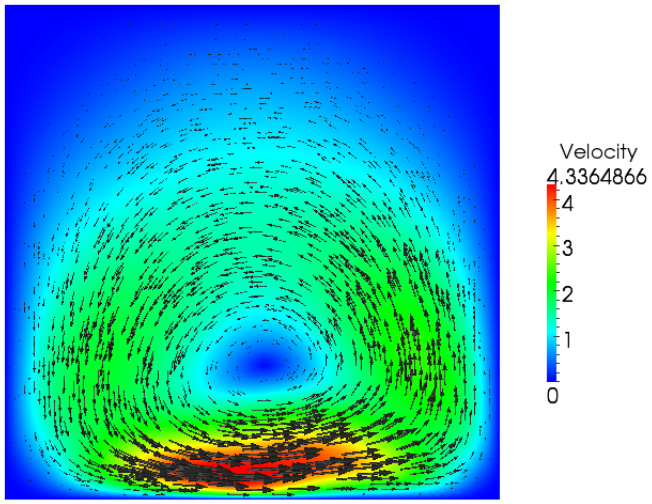

Figure 3.18: **Ferromagnetic stirring (second approach): velocity profile.** Velocity profile induced by the traveling wave of magnetization. This velocity profile shaped the evolution of the concentration c in Figure 3.16.

3.8 Conclusions

In this chapter we proposed and analyzed a numerical scheme for the Rosensweig model of ferrohydrodynamics. The scheme is implicit and we show that, for the magnetic diffusion $\sigma = 0$, it is unconditionally stable and that solutions exist. The use of a discontinuous finite element space for the magnetization $\mathbf{M}$ seems to be mandatory if we want to have a discrete energy law. The scheme delivers the expected convergence rates for smooth solutions. We also showed, under certain additional assumptions, its convergence towards weak solutions.

Although not fully understood in the literature, we considered also $\sigma > 0$. The motivation was twofold: Adding a regularization to the magnetization equa-

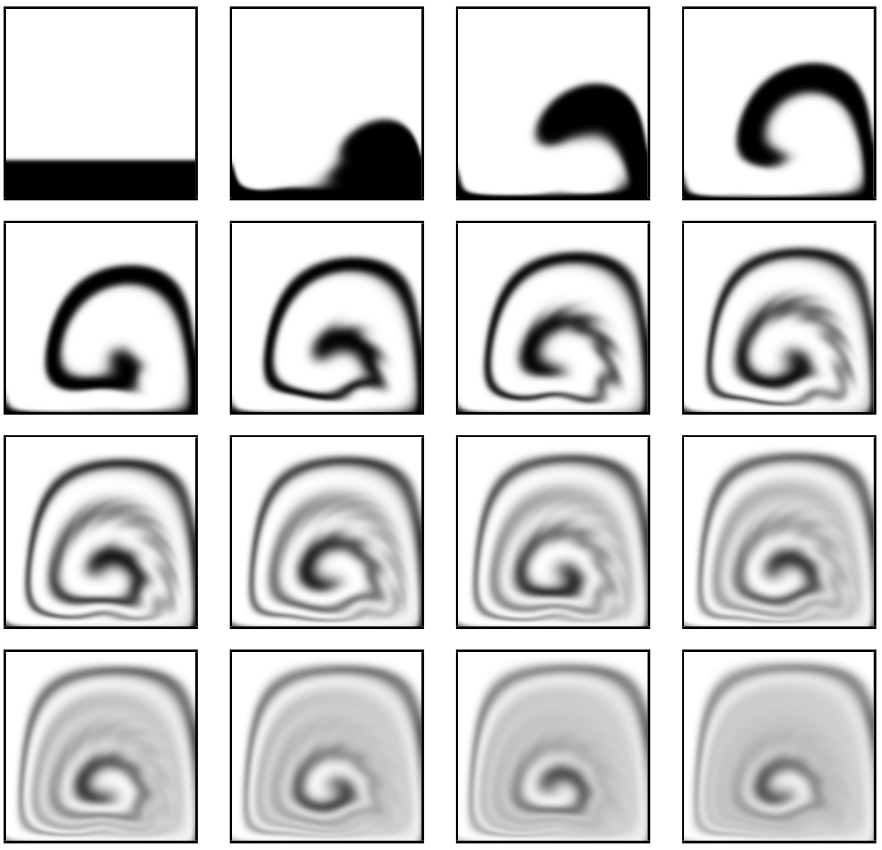

Figure 3.19: **Ferromagnetic stirring (second approach): evolution of the passive scalar.** Contour of the passive scalar from time $t = 0$ to $t = 4.00s$. The magnetizing field satisfies (3.94). These results where obtained with $f = 40$Hz., and $\nu = \nu_r = 0.1$.

tion could be used to obtain global existence of weak solutions. In addition, such regularization enables us to add modeling effects on the boundary. We proposed Robin boundary conditions that agree with the tendency of the magnetization to align with the magnetic field. They yield a formal energy estimate which, however, we were not able to reproduce at the discrete level. The main obstruction is the lack of a methodology capable of computing a magnetic field in $\mathbf{H}(curl, \Omega) \cap \mathbf{H}(div, \Omega)$ compatible with the energy structure of the system.

We also presented some application examples that illustrate the capabilities of the model and the scheme, in particular in the context of ferrofluid pumping and stirring of a passive scalar. These numerical experiments also expose the non-trivial nature of ferrofluids, and how much quantitative tools are needed in order to complement qualitative understanding and experimentation.

Chapter 4: Two-phase model

4.1 Introduction

In the previous chapter we developed and analyzed a numerical scheme for the Rosensweig model. Both the Rosensweig and the (simpler) Shliomis model deal with one-phase flows, which is the case of many technological applications. However, some applications arise naturally in the form of a two-phase flow: one of the phases has magnetic properties and the other one does not (e.g. magnetic manipulation of microchannel flows, microvalves, magnetically guided transport, etc).

The main goal of this *Chapter 4* is to present a simple two-phase PDE model for ferrofluids. The model is not derived, but rather assembled using components of already existing models and high-level (as opposite to deep) understanding of the physics of ferrofluids. The model attempts to retain only the essential features and mathematical difficulties that might appear in much more sophisticated models. To the best of our knowledge this contribution is the first modeling/numerical work in the direction of time-dependent behavior of two-phase ferrofluid flows together with energy-stable and/or convergent schemes.

Regarding pre-existing work, closely related to two-phase flows, it is worth mentioning the interdisciplinary (including physical experiments) work of Tobiska

and collaborators [98, 113, 114] in the context of stationary configurations of free surfaces of ferrofluids using a sharp interface approach. Other models for two-phase ferrofluid flows, this time for non-stationary phenomena, are presented in [115, 116, 117], using either Level-Set or Volume of Fluid method, but very little details are given about their actual numerical implementation, stability or convergence properties.

Our presentation is organized as follows: in §4.2 we select the components of our two-phase model and assemble it. In §4.3 we derive formal energy estimates which will serve as basis for the development of an energy-stable scheme in §4.4. In §4.4.3 we prove that the scheme always has a solution. After that, in §4.5 we propose a simplified model (following the same ideas of §3.5.1) in §4.5, and a corresponding numerical scheme in §4.5.1, for which we prove stability and convergence in §4.5.1 and §4.5.2, respectively. Finally, we show the potential of the model in §4.6 with a series of numerical experiments.

4.2 Heuristic derivation of a two-phase model

We want to develop a simplified model which captures the essence of immiscible, matching density (or almost matching density), two-phase flows, one of them a ferrofluid and the other one a non-magnetic fluid. We aim at a simple mixture like water and an oil based ferrofluid (with, for instance, densities 1000 kg/m^3 and 1050 kg/m^3, respectively), where the dominant body force is the Kelvin force, and the gravitational body force only plays a secondary role, so that we could use a

Boussinesq-like approximation in order to capture gravitational effects.

We will not present a systematic derivation of the model, but rather review existing models and standard assumptions, discard all the non-essential components, and select the right ingredients which could capture the basic phenomenological features of ferrofluids. Our main guidelines are minimalism and symmetry. We want the simplest model, with the smallest number of constitutive parameters and coupled PDEs, that still retains the essential features, and has sufficient symmetries (i.e. cancellations) in order to make possible the development of an energy law.

We consider a two-fluid system (a ferrofluid and a regular one) confined in a bounded and fixed domain $\Omega \subset \mathbb{R}^d$, with $d = 2, 3$. The boundary of Ω is denoted by Γ and is assumed to be Lipschitz continuous. As our model is a diffuse interface one, we will implicitly track the position of each fluid with a phase-field variable θ. The evolution of the system is described by its velocity $\mathbf{u}$ and pressure p. As one of the phases is susceptible to magnetic actuation, we need to keep track of the magnetization $\mathbf{m}$, which is induced by a magnetic field $\mathbf{h}$. To describe the evolution of these quantities we will consider:

- ◇ **Evolution of the phase-field variable θ:** there are very well-known PDE models for this purpose, the Allen-Cahn and the Cahn-Hilliard models. In particular, we will consider the Cahn-Hilliard equation:

$$\begin{cases} \theta_t = -\gamma \Delta \psi & \text{in } \Omega \\ \psi = \varepsilon \Delta \theta - \frac{1}{\varepsilon} f(\theta) & \text{in } \Omega \\ \partial_n \theta = \partial_n \psi = 0 & \text{on } \Gamma \end{cases} \tag{4.1}$$

where $0 < \varepsilon \ll 1$ is related to the interface thickness, γ is the mobility, $f(\theta) = F'(\theta)$ and $F(\theta)$ is the truncated double well potential

$$F(\theta) = \begin{cases} (\theta+1)^2 & \text{if } \theta \in (-\infty, -1] \\ \frac{1}{4}(\theta^2-1)^2 & \text{if } \theta \in [-1, 1] \\ (\theta-1)^2 & \text{if } \theta \in [1, +\infty)\,, \end{cases} \tag{4.2}$$

It is straightforward to check that

$$|f(\theta)| = |F'(\theta)| \leq 2|\theta| + 1 \quad \text{and} \quad |f'(\theta)| = |F''(\theta)| \leq 2 \quad \forall \theta \in \mathbb{R}. \tag{4.3}$$

The reason to choose the Cahn-Hilliard equation is that it is mass conservative, an easy consequence of the divergence theorem:

$$\tfrac{d}{dt}\int_\Omega \theta\, dx = \int_\Omega \theta_t\, dx = -\gamma \int_\Omega \Delta\psi\, dx = -\gamma \int_\Gamma \partial_n \psi\, dS = 0\,. \tag{4.4}$$

◇ **Simplified ferrohydrodynamics:** the Shliomis model (see for instance [19, 18]) is perhaps the simplest well-known PDE model describing the behavior of ferrofluids

$$\mathbf{u}_t + (\mathbf{u}\cdot\nabla)\mathbf{u} - \nu\Delta\mathbf{u} + \nabla p = \mu_0(\mathbf{m}\cdot\nabla)\mathbf{h} + \tfrac{\mu_0}{2}\mathit{curl}\,(\mathbf{m}\times\mathbf{h})\,, \tag{4.5a}$$

$$\mathbf{m}_t + (\mathbf{u}\cdot\nabla)\mathbf{m} - \tfrac{1}{2}\mathit{curl}\,\mathbf{u}\times\mathbf{m} = -\tfrac{1}{\mathscr{T}}(\mathbf{m} - \varkappa_0\mathbf{h}) - \beta\,\mathbf{m}\times(\mathbf{m}\times\mathbf{h})\,, \tag{4.5b}$$

where ν, μ_0, $\mathscr{T}$, β, and $\varkappa_0$ are positive constitutive constants. System (4.5) is the Navier-Stokes equations supplemented with an advection-reaction equation for the magnetization $\mathbf{m}$. Expression (4.5b) can be understood as the $\mathbf{L}^2(\Omega)$ gradient flow of the functional

$$\mathcal{J}(\mathbf{m}) = \tfrac{1}{2\mathscr{T}}\|\mathbf{m} - \varkappa_0\mathbf{h}\|^2_{\mathbf{L}^2} \tag{4.6}$$

augmented with the corresponding kinematics. In other words

$$\langle \mathbf{m}_t, \mathbf{z} \rangle = -\langle \tfrac{\delta \mathcal{J}}{\delta \mathbf{m}}, \mathbf{z} \rangle \quad \Longrightarrow \quad \mathbf{m}_t + \tfrac{1}{\mathscr{T}} \mathbf{m} = \tfrac{\varkappa_0}{\mathscr{T}} \mathbf{h} \tag{4.7}$$

where the symbol δ denotes variational derivative in this context. After that, we can replace the partial derivative $\mathbf{m}_t$ in (4.7) with the co-rotational derivative $\mathbf{m}_t + (\mathbf{u} \cdot \nabla)\mathbf{m} - \frac{1}{2} curl\, \mathbf{u} \times \mathbf{m}$ (see for instance [118]) accounting for the appropriate kinematics. On the other hand, the term $\beta\, \mathbf{m} \times (\mathbf{m} \times \mathbf{h})$ has phenomenological origins which in principle cannot be easily related to kinematic or energy principles (see [72, 18]).

The Shliomis model can be considered to be a limiting case of the more sophisticated Rosensweig model (see for instance [22, 119]), and the core dynamics of the magnetization equation (4.5b) is dominated by the reaction terms for most flows of interest (see for instance [75, 25] for the dimensional analysis of the Rosensweig model). Essentially, this is the case because the relaxation time $\mathscr{T}$ of commercial grade ferrofluids is in the range of 10^{-5} to 10^{-9} seconds (see for instance [75, 18]), which makes $\frac{1}{\mathscr{T}}$ a very large constant. Therefore, a straightforward simplification of (4.5) is:

$$\mathbf{u}_t + (\mathbf{u} \cdot \nabla)\mathbf{u} - \nu \Delta \mathbf{u} + \nabla p = \mu_0 (\mathbf{m} \cdot \nabla)\mathbf{h} \tag{4.8a}$$

$$\mathbf{m}_t + (\mathbf{u} \cdot \nabla)\mathbf{m} + \tfrac{1}{\mathscr{T}} \mathbf{m} = \tfrac{\varkappa_0}{\mathscr{T}} \mathbf{h}. \tag{4.8b}$$

In (4.8) we have dropped the terms $\frac{\mu_0}{2} curl\, (\mathbf{m} \times \mathbf{h})$ and $\beta\, \mathbf{m} \times (\mathbf{m} \times \mathbf{h})$ under the assumption that at every moment the behavior of $\mathbf{m}$ is very close to equilibrium, meaning that $\mathbf{m} \approx \varkappa_0 \mathbf{h}$ and $\mathbf{m} \times \mathbf{h} \approx 0$, so that these terms

are negligible. However, the convective term $(\mathbf{u}\cdot\nabla)\mathbf{m}$ is kept because of symmetry considerations and cannot be dropped if we want to develop an energy stable model. On the other hand, the term $-\frac{1}{2}curl\,\mathbf{u}\times\mathbf{m}$ was dropped under the assumption that convection and reaction are the dominant terms. In a somewhat different context, similar ideas where used in order to simplify liquid-crystal models (see for instance [120]).

◇ **Simplified capillary forces:** the capillary forces are given by $\mathbf{f}_c = -div\,\boldsymbol{\sigma}_{\rm c}$, where $\boldsymbol{\sigma}_{\rm c} = \lambda\nabla\theta\otimes\nabla\theta$ is the so-called capillary stress tensor (see for instance [121, 122]), and λ is the capillary coefficient. Manipulating $\mathbf{f}_c$ we get:

$$\begin{aligned}\mathbf{f}_c = -div\,\boldsymbol{\sigma}_{\rm c} &= -\tfrac{\lambda}{2}\nabla|\nabla\theta|^2 - \lambda\Delta\theta\nabla\theta\\ &= -\tfrac{\lambda}{2}\nabla|\nabla\theta|^2 - \tfrac{\lambda}{\varepsilon^2}f(\theta)\nabla\theta - \tfrac{\lambda}{\varepsilon}\psi\nabla\theta\\ &= -\lambda\nabla\left(\tfrac{1}{2}|\nabla\theta|^2 + \tfrac{\lambda}{\varepsilon^2}F(\theta)\right) - \tfrac{\lambda}{\varepsilon}\psi\nabla\theta\\ &= -\lambda\nabla\left(\tfrac{1}{2}|\nabla\theta|^2 + \tfrac{\lambda}{\varepsilon^2}F(\theta) + \tfrac{\lambda}{\varepsilon}\psi\theta\right) + \tfrac{\lambda}{\varepsilon}\theta\nabla\psi\,.\end{aligned} \tag{4.9}$$

Therefore the term $-\lambda\nabla\left(\frac{1}{2}|\nabla\theta|^2 + \frac{\lambda}{\varepsilon^2}F(\theta) + \frac{\lambda}{\varepsilon}\psi\theta\right)$ only modifies the pressure in the Navier-Stokes system (see Remark 3.4.1 in *Chapter 3*), so that it can be eliminated at the expense of redefining the pressure. Our capillary force will finally be:

$$\mathbf{f}_c := \tfrac{\lambda}{\varepsilon}\theta\nabla\psi. \tag{4.10}$$

This definition of the capillary force traces back to [120, 92] and is not a cosmetic manipulation but rather an essential ingredient in order to have sufficient cancellations allowing the development of an energy law.

◇ **Simplified electromagnetism:** the natural choice in this context are the magnetostatics equations:

$$curl\,\mathbf{h} = 0\ , \quad div\,\mathbf{b} = 0\ ,$$

where

$$\mathbf{b} := \mathbf{h} + \mathbf{m}\ , \quad \mathbf{h} := \mathbf{h}_a + \mathbf{h}_d\,, \tag{4.11}$$

here $\mathbf{h}_a$ is the (given) smooth harmonic (curl-free and div-free) applied magnetizing field, and $\mathbf{h}_d$ is the so-called demagnetizing field (for more details see §3.2.1 in *Chapter 3*). A simplified approach to this problem is by means of the scalar potential (same as in (3.18)):

$$\begin{cases} -\Delta\varphi = div\,\mathbf{m} & \text{in } \Omega \\ \dfrac{\partial\varphi}{\partial\boldsymbol{n}} = (\mathbf{h}_a - \mathbf{m})\cdot\boldsymbol{n} & \text{on } \Gamma \end{cases} \tag{4.12}$$

so that $\mathbf{h} := \nabla\varphi$.

Collecting all these simplifications we propose the following set of equations:

$$\theta_t + div\,(\mathbf{u}\theta) + \gamma\Delta\psi = 0 \tag{4.13a}$$

$$-\varepsilon\Delta\theta + \tfrac{1}{\varepsilon}f(\theta) + \psi = 0 \tag{4.13b}$$

$$\mathbf{m}_t + (\mathbf{u}\cdot\nabla)\mathbf{m} = -\tfrac{1}{\mathscr{T}}(\mathbf{m} - \varkappa_\theta\mathbf{h}) \tag{4.13c}$$

$$-\Delta\varphi = div\,(\mathbf{m} - \mathbf{h}_a) \tag{4.13d}$$

$$\mathbf{u}_t + (\mathbf{u}\cdot\nabla)\mathbf{u} - div\,(\nu_\theta\,\mathbf{T}(\mathbf{u})) + \nabla p = \mu_0(\mathbf{m}\cdot\nabla)\mathbf{h} + \tfrac{\lambda}{\varepsilon}\theta\nabla\psi \tag{4.13e}$$

$$div\,\mathbf{u} = 0 \tag{4.13f}$$

in Ω for every $t \in [0, t_F]$, where $\mathbf{T}(\mathbf{u}) = \frac{1}{2}(\nabla\mathbf{u} + \nabla\mathbf{u}^\intercal)$ denotes the symmetric gradient and

$$\mathbf{h} := \nabla\varphi\,.$$

We supplement this system with the following boundary conditions

$$\partial_n\theta = \partial_n\psi = 0\,, \quad \mathbf{u} = 0\,, \qquad \text{and} \quad \partial_n\varphi = (\mathbf{h}_a - \mathbf{m}) \cdot n \ \text{ on } \ \Gamma. \tag{4.14}$$

Here ν_θ and $\varkappa_\theta$ are viscosities and susceptibilities subordinate to the phase-field variable θ. They are Lipschitz-continuous functions of θ satisfying

$$0 < \nu_w \leq \nu_\theta \leq \nu_f \quad \text{and} \quad 0 \leq \varkappa_\theta \leq \varkappa_0 \tag{4.15}$$

where ν_w is the viscosity of the non-magnetic phase (e.g. water) and ν_f is the viscosity of the ferrofluid (e.g. mineral oil). Here $\varkappa_0 > 0$ is the magnetic susceptibility of the ferrofluid phase, and we set the non-magnetic phase to have zero magnetic susceptibility. For commercial grade ferrofluids we have that $\varkappa_0$ ranges from 0.5 to 4.3 (see for instance [25]). The choice of functions ν_θ and $\varkappa_\theta$ is arbitrary, but essentially they involve a regularized approximation of the Heaviside step function, for instance

$$\nu_\theta = \nu_w + (\nu_f - \nu_w)\mathcal{H}(\theta/\varepsilon) \ \text{ and } \ \varkappa_\theta = \varkappa_0\mathcal{H}(\theta/\varepsilon) \tag{4.16}$$

where $\mathcal{H}(x)$ could be for instance the sigmoid function

$$\mathcal{H}(x) = \frac{1}{1 + e^{-x}} \tag{4.17}$$

Both in theory and practice, the choice of $\mathcal{H}(x)$ and the internal structure of ν_θ and $\varkappa_\theta$ are of very little importance, provided they are Lipschitz-continuous and

satisfy inequalities (4.15). Here (4.16) and (4.17) are just provided as a couple of simple choices, but they are not the only ones; other choices are used for instance in [41, 92].

Since this model is not a genuinely variable-density two-phase model, gravitational forces $\mathbf{f}_g = \rho\mathbf{g}$ can only be included approximately. We will consider supplementing the right hand side of the conservation of linear momentum (4.13e) with a Boussinesq-like approximation in order to include gravitational effects, such as

$$\mathbf{f}_g = (1 + r\,\mathcal{H}(\theta/\varepsilon))\mathbf{g} \tag{4.18}$$

where $r = \frac{|\rho_f - \rho_w|}{min(\rho_f, \rho_w)}$, ρ_f is the density of the ferromagnetic phase, and ρ_w is the density of the non-magnetic phase. Provided $r << 1$ this will be a reasonable approximation.

The development of a complete existence theory for system (4.13) seems unlikely, as it has been the historical case of most systems of PDEs without sufficient regularization mechanisms (e.g. compressible Euler equations of gas dynamics). This is primarily because of the sub-system (4.13c)-(4.13d) and the term $\mu_0(\mathbf{m}\cdot\nabla)\mathbf{h}$ on the right hand side of (4.13e). A first approach to solve this problem would be adding a regularization of the form $-\sigma\Delta\mathbf{m} = curl\,(\sigma\, curl\,\mathbf{m}) - \nabla(\sigma\, div\,\mathbf{m})$ in the equation (4.13c) (as it was considered in §3.2.3, see also reference [22]), or any other second order operator in space. However, most forms of regularization that we could add to this system will introduce new problems, primarily (but not only) related to boundary conditions, and the overall system might not even be formally

energy-stable (see for instance Remark 3.3.2 and also §3.4.4).

These mathematical obstacles, will not interfere with our exploration of the model (4.13), which is a reasonable starting point to understand and develop PDE models for two-phase ferrofluid flows. It is actually possible to develop energy stable numerical methods for system (4.13) and prove local-solvability of the scheme for every time step. With the aid of the developed numerical scheme, we will explore the behavior of this coupled system. Finally, under special circumstances, and with some simplifications, we will obtain a system for which is possible to prove convergence when the discretization parameters h and τ go to zero and, as a by product, global existence of weak solutions.

4.3 Formal energy estimates

Proposition 4.3.1 (Energy estimate)**.** *If $\varkappa_0 \leq 4$, then the following estimate holds for solutions of the system* (4.13)

$$\begin{aligned} \mathscr{E}(\mathbf{u},\mathbf{m},\mathbf{h},\theta;t_F) + \int_0^{t_F} \mathscr{D}(\mathbf{u},\mathbf{m},\mathbf{h},\theta;s)\,ds \\ \leq \int_0^{t_F} \mathscr{F}(\mathbf{h}_a;s)\,ds + \mathscr{E}(\mathbf{u},\mathbf{m},\mathbf{h},\theta;0)\,, \end{aligned} \tag{4.19}$$

where

$$\begin{aligned} \mathscr{E}(\mathbf{u},\mathbf{m},\mathbf{h},\theta;s) &= \tfrac{1}{2}\|\mathbf{u}(s)\|^2_{\mathbf{L}^2} + \tfrac{\mu_0}{2}\|\mathbf{m}(s)\|^2_{\mathbf{L}^2} + \tfrac{\mu_0}{2}\|\mathbf{h}(s)\|^2_{\mathbf{L}^2} \\ &\quad + \tfrac{\lambda}{2}\|\nabla\theta(s)\|^2_{\mathbf{L}^2} + \tfrac{\lambda}{\varepsilon^2}(F(\theta(s)),1)\,, \\ \mathscr{D}(\mathbf{u},\mathbf{m},\mathbf{h},\theta;s) &= \tfrac{\mu_0}{\mathscr{T}}\big(1-\tfrac{\varkappa_0}{4}\big)\|\mathbf{m}(s)\|^2_{\mathbf{L}^2} + \tfrac{\mu_0}{2\mathscr{T}}\|\mathbf{h}(s)\|^2_{\mathbf{L}^2} \\ &\quad + \|\sqrt{\nu_\theta}\,\mathbf{T}(\mathbf{u})(s)\|^2_{\mathbf{L}^2} + \tfrac{\lambda\gamma}{\varepsilon}\|\nabla\psi(s)\|^2_{\mathbf{L}^2}\,, \end{aligned}$$

$$\mathscr{F}(\mathbf{h}_a; s) = \mu_0 \mathscr{T} \|\partial_t \mathbf{h}_a(s)\|^2_{\mathbf{L}^2} + \tfrac{\mu_0}{\mathscr{T}} \|\mathbf{h}_a(s)\|^2_{\mathbf{L}^2}\,,$$

Proof. Multiply (4.13a) by ψ and (4.13b) by θ_t and integrate. Integration by parts yields

$$-(\theta_t, \psi) + \gamma \|\nabla \psi\|^2_{\mathbf{L}^2} = -(\mathbf{u}\theta, \nabla \psi)\,,$$

$$\tfrac{d}{dt}\left(\tfrac{\varepsilon}{2}\|\nabla\theta\|^2_{\mathbf{L}^2} + \tfrac{1}{\varepsilon}(F(\theta), 1)\right) + (\psi, \theta_t) = 0\,,$$

whence, adding both lines and multiplying by $\frac{\lambda}{\varepsilon}$, we get

$$\tfrac{d}{dt}\left(\tfrac{\lambda}{2}\|\nabla\theta\|^2_{\mathbf{L}^2} + \tfrac{\lambda}{\varepsilon^2}(F(\theta), 1)\right) + \tfrac{\lambda\gamma}{\varepsilon}\|\nabla\psi\|^2_{\mathbf{L}^2} = -\tfrac{\lambda}{\varepsilon}(\theta\nabla\psi, \mathbf{u})\,. \tag{4.21}$$

Now we multiply (4.13e) by $\mathbf{u}$, integrate by parts and use (3.26) for the Kelvin force

$$\tfrac{1}{2}\tfrac{d}{dt}\|\mathbf{u}\|^2_{\mathbf{L}^2} + \|\sqrt{\nu_\theta}\,\mathbf{T}(\mathbf{u})\|^2_{\mathbf{L}^2} = -\mu_0\, b(\mathbf{u}, \mathbf{m}, \mathbf{h}) + \tfrac{\lambda}{\varepsilon}(\theta\nabla\psi, \mathbf{u})\,. \tag{4.22}$$

Adding (4.21) and (4.22) we get

$$\begin{aligned}\tfrac{d}{dt}\big(\tfrac{1}{2}\|\mathbf{u}\|^2_{\mathbf{L}^2} + \tfrac{\lambda}{2}\|\nabla\theta\|^2_{\mathbf{L}^2} + \tfrac{\lambda}{\varepsilon^2}(F(\theta), 1)\big)& \\ + \|\sqrt{\nu_\theta}\,\mathbf{T}(\mathbf{u})\|^2_{\mathbf{L}^2} + \tfrac{\lambda\gamma}{\varepsilon}\|\nabla\psi\|^2_{\mathbf{L}^2} = -\mu_0\, b(\mathbf{u}, \mathbf{m}, \mathbf{h})&\end{aligned} \tag{4.23}$$

Finally multiply (4.13c) by $\mu_0\mathbf{m}$ and $\mu_0\mathbf{h}$ and integrate to obtain

$$\tfrac{\mu_0}{2}\tfrac{d}{dt}\|\mathbf{m}\|^2_{\mathbf{L}^2} + \tfrac{\mu_0}{\mathscr{T}}\|\mathbf{m}\|^2_{\mathbf{L}^2} = \tfrac{\mu_0}{\mathscr{T}}(\varkappa_\theta \mathbf{h}, \mathbf{m}) \tag{4.24}$$

$$\mu_0(\mathbf{m}_t, \mathbf{h}) + \mu_0\, b(\mathbf{u}, \mathbf{m}, \mathbf{h}) + \tfrac{\mu_0}{\mathscr{T}}(\mathbf{m}, \mathbf{h}) = \tfrac{\mu_0}{\mathscr{T}}\|\sqrt{\varkappa_\theta}\,\mathbf{h}\|^2_{\mathbf{L}^2}. \tag{4.25}$$

Expression (4.25) requires further manipulation. Using (3.31) and (3.32), we can rewrite (4.25) as follows

$$\begin{aligned}\tfrac{\mu_0}{2}\tfrac{d}{dt}\|\mathbf{h}\|^2_{\mathbf{L}^2} + \tfrac{\mu_0}{\mathscr{T}}\|\mathbf{h}\|^2_{\mathbf{L}^2} + \tfrac{\mu_0}{\mathscr{T}}\|\sqrt{\varkappa_\theta}\,\mathbf{h}\|^2_{\mathbf{L}^2}& \\ = \mu_0(\partial_t \mathbf{h}_a, \mathbf{h}) + \tfrac{\mu_0}{\mathscr{T}}(\mathbf{h}_a, \mathbf{h}) + \mu_0\, b(\mathbf{u}, \mathbf{m}, \mathbf{h}).&\end{aligned} \tag{4.26}$$

Adding (4.23), (4.24) and (4.26), we get

$$\begin{aligned}\tfrac{d}{dt}\mathscr{E}(\mathbf{u},\mathbf{m},\mathbf{h},\theta;t)+\mathscr{D}(\mathbf{u},\mathbf{m},\mathbf{h},\theta;s)+\tfrac{\mu_0\varkappa_0}{4\mathscr{T}}\|\mathbf{m}\|_{\mathbf{L}^2}^2+\tfrac{\mu_0}{2\mathscr{T}}\|\mathbf{h}\|_{\mathbf{L}^2}^2\\ +\tfrac{\mu_0}{\mathscr{T}}\|\sqrt{\varkappa_\theta}\,\mathbf{h}\|_{\mathbf{L}^2}^2=\tfrac{\mu_0}{\mathscr{T}}(\varkappa_\theta\mathbf{h},\mathbf{m})+\mu_0(\partial_t\mathbf{h}_a,\mathbf{h})+\tfrac{\mu_0}{\mathscr{T}}(\mathbf{h}_a,\mathbf{h})\,.\end{aligned}\tag{4.27}$$

Using the bound (4.15), the term $\frac{\mu_0}{\mathscr{T}}(\varkappa_\theta\mathbf{h},\mathbf{m})$ can be estimated as follows:

$$\tfrac{\mu_0}{\mathscr{T}}(\varkappa_\theta\mathbf{h},\mathbf{m})\le\tfrac{\mu_0}{\mathscr{T}}\|\sqrt{\varkappa_\theta}\,\mathbf{h}\|_{\mathbf{L}^2}\|\sqrt{\varkappa_\theta}\,\mathbf{m}\|_{\mathbf{L}^2}\le\tfrac{\mu_0}{\mathscr{T}}\|\sqrt{\varkappa_\theta}\,\mathbf{h}\|_{\mathbf{L}^2}^2+\tfrac{\mu_0\varkappa_0}{4\mathscr{T}}\|\mathbf{m}\|_{\mathbf{L}^2}^2\,,$$

so that using this estimate in (4.27) we finally get

$$\tfrac{d}{dt}\mathscr{E}(\mathbf{u},\mathbf{m},\mathbf{h},\theta;t)+\mathscr{D}(\mathbf{u},\mathbf{m},\mathbf{h},\theta;s)+\tfrac{\mu_0}{2\mathscr{T}}\|\mathbf{h}\|_{\mathbf{L}^2}^2\le\mu_0(\partial_t\mathbf{h}_a,\mathbf{h})+\tfrac{\mu_0}{\mathscr{T}}(\mathbf{h}_a,\mathbf{h})\,.$$

The rest is just a matter of applying Cauchy-Schwarz and Young's inequalities to get the energy estimate (4.19). From the expression for $\mathscr{D}(\mathbf{u},\mathbf{m},\mathbf{h},\theta;s)$ we also get the restriction that we can only consider $\varkappa_0\le 4$. □

Remark 4.3.1 (Range of susceptibility)**.** The restriction $\varkappa_0\le 4$, necessary for Proposition 4.3.1 to hold, covers almost the complete range of commercial grade ferrofluids.

4.4 An energy stable scheme

In this section we present and analyze a discretization of system (4.13a)–(4.13f), its stability, and the existence of solutions. This scheme will be our workhorse: The numerical simulations of §4.6 will use this method, and the existence of solutions for our simplified model will be based on a scheme very similar to the one presented here.

4.4.1 Notation

The space discretization will be based on Galerkin techniques. To this effect, we introduce finite dimensional subspaces $\mathbb{G} \subset H^1(\Omega)$, $\mathbb{Y} \subset H^1(\Omega)$, $\mathbb{M} \subset \mathbf{L}^2(\Omega)$, $\mathbb{X} \subset H^1(\Omega)$, $\mathbb{U} \subset \mathbf{H}_0^1(\Omega)$ and $\mathbb{P} \subset L^2(\Omega)$, where we will approximate the phase-field, chemical potential, magnetization, magnetic potential, linear velocity and pressure respectively. About the pair of spaces $(\mathbb{U}, \mathbb{P})$ we assume that they are LBB stable (see (1.14)). To be able to focus on the fundamental difficulties in the design of an energy stable scheme we will first describe the scheme without being specific on the particular structure of these discrete spaces. As we will see, the choice of discrete spaces shall come naturally from this analysis.

We will consider a discretization of the trilinear form (1.5) associated to the convective term in the Navier-Stokes equation $(\mathbf{u}\cdot\nabla)\mathbf{u}$ analogous to that one defined in (2.16)-(2.17)

Similarly, we also consider a discretization of the trilinear forms associated with the convective term $(\mathbf{u}\cdot\nabla)\mathbf{m}$ and the Kelvin force $\mu_0(\mathbf{m}\cdot\nabla)\mathbf{h}$ analogous to that one defined in (3.39)-(3.40).

Let $\mathrm{I}_{\mathbb{G}}$, $\mathrm{I}_{\mathbb{Y}}$, $\mathrm{I}_{\mathbb{M}}$ and $\mathrm{I}_{\mathbb{U}}$ denote mappings (similar to those defined in (3.42))

$$\begin{aligned} &\mathrm{I}_{\mathbb{G}} : \mathcal{C}^0(\overline{\Omega}) \longrightarrow \mathbb{G}\,, && \mathrm{I}_{\mathbb{Y}} : \mathcal{C}^0(\overline{\Omega}) \longrightarrow \mathbb{Y}\,, \\ &\mathrm{I}_{\mathbb{M}} : \boldsymbol{\mathcal{C}}^0(\overline{\Omega}) \longrightarrow \mathbb{M} \cap \boldsymbol{\mathcal{C}}^0(\overline{\Omega})\,, && \mathrm{I}_{\mathbb{U}} : \boldsymbol{\mathcal{C}}^0(\overline{\Omega}) \longrightarrow \mathbb{U}\,, \end{aligned} \tag{4.28}$$

with optimal approximation properties (see (1.13)).

More notation and details about the space discretization will be provided in §4.4.4. Here we confine ourselves to mention that they can be easily constructed

using finite elements (see for instance [52, 53]).

4.4.2 Description of the scheme and stability

For the Cahn-Hilliard equation we shall use the stabilization methodology proposed by Shen and Yang [123] in order to eliminate the constraint $\tau \lesssim \varepsilon^4$ from the time step. The price paid in this stabilization is the introduction of an error of order $\mathcal{O}(\tau)$ which is consistent with the truncation order of the scheme.

In order to avoid unnecessary technicalities, assume that the initial data is smooth and initialize the scheme as follows

$$\Theta^0 = \mathrm{I}_{\mathbb{G}}[\theta(0)] \ \ , \ \ \mathbf{M}^0 = \mathrm{I}_{\mathbb{M}}[\mathbf{m}(0)] \ \ , \ \ \mathbf{U}^0 = \mathrm{I}_{\mathbb{U}}[\mathbf{u}(0)] \ \ , \tag{4.29}$$

after that, for every $k \in \{1, \dots, K\}$ we compute $\{\Theta^k, \Psi^k, \mathbf{M}^k, \Phi^k, \mathbf{U}^k, P^k\} \in \mathbb{G} \times \mathbb{Y} \times \mathbb{M} \times \mathbb{X} \times \mathbb{U} \times \mathbb{P}$ that solves

$$\Big(\tfrac{\delta\Theta^k}{\tau}, \Lambda\Big) - (\mathbf{U}^k\Theta^{k-1}, \nabla\Lambda) - \gamma(\nabla\Psi^k, \nabla\Lambda) = 0 \tag{4.30a}$$

$$(\Psi^k, \Upsilon) + \tfrac{1}{\eta}(\delta\Theta^k, \Upsilon) + \varepsilon(\nabla\Theta^k, \nabla\Upsilon) + \tfrac{1}{\varepsilon}(f(\Theta^{k-1}), \Upsilon) = 0 \tag{4.30b}$$

$$\Big(\tfrac{\delta\mathbf{M}^k}{\tau}, \mathbf{Z}\Big) - \ b_h^m\big(\mathbf{U}^k, \mathbf{Z}, \mathbf{M}^k\big) + \tfrac{1}{\mathscr{J}}\big(\mathbf{M}^k, \mathbf{Z}\big) = \tfrac{1}{\mathscr{J}}\big(\varkappa_\Theta\mathbf{H}^k, \mathbf{Z}\big) \tag{4.30c}$$

$$(\nabla\Phi^k, \nabla\mathrm{X}) = (\mathbf{h}_a^k - \mathbf{M}^k, \nabla\mathrm{X}) \tag{4.30d}$$

$$\begin{aligned}\Big(\tfrac{\delta\mathbf{U}^k}{\tau}, \mathbf{V}\Big) + \big(\nu_\Theta\mathbf{T}(\mathbf{U}^k), \mathbf{T}(\mathbf{V})\big) + \ b_h\big(\mathbf{U}^{k-1}, \mathbf{U}^k, \mathbf{V}\big) - \big(P^k, \mathit{div}\,\mathbf{V}\big) \\ = \ b_h^m\big(\mathbf{V}, \mathbf{H}^k, \mathbf{M}^k\big) + \tfrac{\lambda}{\varepsilon}(\Theta^{k-1}\nabla\Psi^k, \mathbf{V})\end{aligned} \tag{4.30e}$$

$$\big(\mathrm{Q}, \mathit{div}\,\mathbf{U}^k\big) = 0 \tag{4.30f}$$

for all $\{\Lambda, \Upsilon, \mathbf{Z}, \mathrm{X}, \mathbf{V}, \mathrm{Q}\} \in \mathbb{G} \times \mathbb{Y} \times \mathbb{M} \times \mathbb{X} \times \mathbb{U} \times \mathbb{P}$. Here $\mathbf{H}^k := \nabla\Phi^k$, and $\frac{1}{\eta}(\delta\Theta^k, \Upsilon)$ in (4.30b) is a stabilization term with η sufficiently small.

Remark 4.4.1 (Initialization)**.** The initialization proposed in (4.29) is the simplest choice. From the point of view of convergence to strong solutions (a priori error estimates) it is suboptimal (cf. [86, 49, 53, 87]). However, this choice has no effect on the stability of the scheme, it only affects the regularity assumed on the initial data.

Proposition 4.4.1 (Discrete energy stability)**.** *Let* $\{\Theta^\tau, \Psi^\tau, \mathbf{M}^\tau, \Phi^\tau, \mathbf{U}^\tau, P^\tau\} \subset \mathbb{G} \times \mathbb{Y} \times \mathbb{M} \times \mathbb{X} \times \mathbb{U} \times \mathbb{P}$ *solve* (4.30)*. If* $\nabla\mathbb{X} \subset \mathbb{M}$*,* $\eta \leq \varepsilon$ *and* $\varkappa_0 \leq 4$*, then we have the following stability estimate*

$$\begin{aligned} &\mathscr{E}(\mathbf{U}^\tau, \mathbf{M}^\tau, \Phi^\tau, \Theta^\tau; K) + \sum_{k=1}^{K} \Big(\mathscr{I}(\delta\mathbf{U}^\tau, \delta\mathbf{M}^\tau, \delta\Phi^\tau, \delta\Theta^\tau; k) \\ &\quad + \tau \mathscr{D}(\mathbf{U}^\tau, \mathbf{M}^\tau, \Phi^\tau, \Theta^\tau, \Psi^\tau; k) \Big) \leq \sum_{k=1}^{K} \tau \mathscr{F}(\mathbf{h}_a; k) + \mathscr{E}(\mathbf{U}^\tau, \mathbf{M}^\tau, \Phi^\tau, \Theta^\tau; 0)\,, \end{aligned} \tag{4.31}$$

where

$$\begin{aligned} \mathscr{E}(\mathbf{U}^\tau, \mathbf{M}^\tau, \Phi^\tau, \Theta^\tau; k) &= \tfrac{1}{2}\|\mathbf{U}^k\|_{\mathbf{L}^2}^2 + \tfrac{\mu_0}{2}\|\mathbf{M}^k\|_{\mathbf{L}^2}^2 + \tfrac{\mu_0}{2}\|\nabla\Phi^k\|_{\mathbf{L}^2}^2 \\ &\quad + \tfrac{\lambda}{2}\|\nabla\Theta^k\|_{\mathbf{L}^2}^2 + \tfrac{\lambda}{\varepsilon^2}(F(\Theta^k), 1)\,, \\ \mathscr{I}(\delta\mathbf{U}^\tau, \delta\mathbf{M}^\tau, \delta\Phi^\tau, \delta\Theta^\tau; k) &= \tfrac{1}{2}\|\delta\mathbf{U}^k\|_{\mathbf{L}^2}^2 + \tfrac{\mu_0}{2}\|\delta\mathbf{M}^k\|_{\mathbf{L}^2}^2 \\ &\quad + \tfrac{\mu_0}{2}\|\delta\nabla\Phi^k\|_{\mathbf{L}^2}^2 + \tfrac{\lambda}{2}\|\delta\nabla\Theta^k\|_{\mathbf{L}^2}^2\,, \\ \mathscr{D}(\mathbf{U}^\tau, \mathbf{M}^\tau, \Phi^\tau, \Theta^\tau, \Psi^\tau; k) &= \tfrac{\mu_0}{\mathscr{J}}\big(1 - \tfrac{\varkappa_0}{4}\big)\|\mathbf{M}^k\|_{\mathbf{L}^2}^2 + \tfrac{\mu_0}{2\mathscr{J}}\|\nabla\Phi^k\|_{\mathbf{L}^2}^2 \\ &\quad + \|\sqrt{\nu_\theta}\,\mathbf{T}(\mathbf{U}^k)\|_{\mathbf{L}^2}^2 + \tfrac{\lambda\gamma}{\varepsilon}\|\nabla\Psi^k\|_{\mathbf{L}^2}^2\,, \\ \mathscr{F}(\mathbf{h}_a; k) &= \tfrac{\mu_0\mathscr{J}}{\tau}\int_{t^{k-1}}^{t^k} \|\partial_t \mathbf{h}_a(s)\|_{\mathbf{L}^2}^2\, ds + \tfrac{\mu_0}{\mathscr{J}}\|\mathbf{h}_a^k\|_{\mathbf{L}^2}^2\,. \end{aligned}$$

Proof. We set $\Lambda = \frac{2\lambda\tau}{\varepsilon}\Psi^k$, $\Upsilon = \frac{2\lambda}{\varepsilon}\delta\Theta^k$, $\mathbf{V} = 2\tau\mathbf{U}^k$, $\mathbf{Z} = 2\tau\mu_0\mathbf{M}^k$, $\mathbf{Z} = 2\tau\mu_0\mathbf{H}^k$ and $\mathrm{X} = \frac{2\mu_0\tau}{\mathscr{J}}\Phi^k$ in (4.30) to arrive at:

$$\tfrac{2\lambda\gamma\tau}{\varepsilon}\|\nabla\Psi^k\|_{\mathbf{L}^2}^2 - \tfrac{2\lambda}{\varepsilon}\big(\delta\Theta^k, \Psi^k\big) = -\tfrac{2\lambda\tau}{\varepsilon}(\mathbf{U}^k\Theta^{k-1}, \nabla\Psi^k)\,, \tag{4.32a}$$

$$\tfrac{2\lambda}{\varepsilon}(\Psi^k,\delta\Theta^k)+\tfrac{2\lambda}{\eta\varepsilon}\|\delta\Theta^k\|^2_{\mathbf{L}^2}+2\lambda(\delta\nabla\Theta^k,\nabla\Theta^k)+\tfrac{2\lambda}{\varepsilon^2}(f(\Theta^{k-1}),\delta\Theta^k)=0, \tag{4.32b}$$

$$\begin{aligned}2\left(\delta\mathbf{U}^k,\mathbf{U}^k\right)+2\tau\|\sqrt{\nu_\Theta}\,\mathbf{T}(\mathbf{U}^k)\|^2_{\mathbf{L}^2}&=2\tau\, b_h^m\left(\mathbf{U}^k,\mathbf{H}^k,\mathbf{M}^k\right)\\&\quad+\tfrac{2\lambda\tau}{\varepsilon}(\Theta^{k-1}\nabla\Psi^k,\mathbf{U}^k)\,,\end{aligned} \tag{4.32c}$$

$$2\mu_0\left(\delta\mathbf{M}^k,\mathbf{M}^k\right)+\tfrac{2\mu_0\tau}{\mathscr{J}}\|\mathbf{M}^k\|^2_{\mathbf{L}^2}=\tfrac{2\mu_0\tau}{\mathscr{J}}\left(\varkappa_\Theta\mathbf{H}^k,\mathbf{M}^k\right), \tag{4.32d}$$

$$\begin{aligned}\tfrac{2\mu_0\tau}{\mathscr{J}}\|\sqrt{\varkappa_\Theta}\,\mathbf{H}^k\|^2_{\mathbf{L}^2}&=2\mu_0\left(\delta\mathbf{M}^k,\mathbf{H}^k\right)\\&\quad-2\mu_0\tau\, b_h^m\left(\mathbf{U}^k,\mathbf{H}^k,\mathbf{M}^k\right)+\tfrac{2\mu_0\tau}{\mathscr{J}}\left(\mathbf{M}^k,\mathbf{H}^k\right),\end{aligned} \tag{4.32e}$$

$$\tfrac{2\mu_0\tau}{\mathscr{J}}\|\nabla\Phi^k\|^2_{\mathbf{L}^2}=\tfrac{2\mu_0\tau}{\mathscr{J}}(\mathbf{h}_a^k-\mathbf{M}^k,\nabla\Phi^k)\,, \tag{4.32f}$$

Adding all the previous lines and using (1.11) we get

$$\begin{aligned}&\|\mathbf{U}^k\|^2_{\mathbf{L}^2}-\|\mathbf{U}^{k-1}\|^2_{\mathbf{L}^2}+\mu_0\|\mathbf{M}^k\|^2_{\mathbf{L}^2}-\mu_0\|\mathbf{M}^{k-1}\|^2_{\mathbf{L}^2}+\|\delta\mathbf{U}^k\|^2_{\mathbf{L}^2}+\mu_0\|\delta\mathbf{M}^k\|^2_{\mathbf{L}^2}\\&\quad+2\lambda(\delta\nabla\Theta^k,\nabla\Theta^k)+\tfrac{2\lambda}{\varepsilon^2}(f(\Theta^{k-1}),\delta\Theta^k)+\tfrac{2\lambda}{\eta\varepsilon}\|\delta\Theta^k\|^2_{\mathbf{L}^2}+\tfrac{2\lambda\gamma\tau}{\varepsilon}\|\nabla\Psi^k\|^2_{\mathbf{L}^2}\\&\quad+2\tau\|\sqrt{\nu_\Theta}\,\mathbf{T}(\mathbf{U}^k)\|^2_{\mathbf{L}^2}+\tfrac{2\mu_0\tau}{\mathscr{J}}\|\mathbf{M}^k\|^2_{\mathbf{L}^2}+\tfrac{2\mu_0\tau}{\mathscr{J}}\|\sqrt{\varkappa_\Theta}\,\mathbf{H}^k\|^2_{\mathbf{L}^2}+\tfrac{2\mu_0\tau}{\mathscr{J}}\|\nabla\Phi^k\|^2_{\mathbf{L}^2}\\&\quad=\tfrac{2\mu_0\tau}{\mathscr{J}}\left(\varkappa_\Theta\mathbf{H}^k,\mathbf{M}^k\right)+2\mu_0\left(\delta\mathbf{M}^k,\nabla\Phi^k\right)+\tfrac{2\mu_0\tau}{\mathscr{J}}(\mathbf{h}_a^k,\nabla\Phi^k)\,.\end{aligned} \tag{4.33}$$

Using (3.50), we have that (4.33) can be rewritten as

$$\begin{aligned}&\|\mathbf{U}^k\|^2_{\mathbf{L}^2}-\|\mathbf{U}^{k-1}\|^2_{\mathbf{L}^2}+\mu_0\|\mathbf{M}^k\|^2_{\mathbf{L}^2}-\mu_0\|\mathbf{M}^{k-1}\|^2_{\mathbf{L}^2}+\mu_0\|\nabla\Phi^k\|^2_{\mathbf{L}^2}\\&\quad-\mu_0\|\nabla\Phi^{k-1}\|^2_{\mathbf{L}^2}+\lambda\|\nabla\Theta^k\|^2_{\mathbf{L}^2}-\lambda\|\nabla\Theta^{k-1}\|^2_{\mathbf{L}^2}+\|\delta\mathbf{U}^k\|^2_{\mathbf{L}^2}+\mu_0\|\delta\mathbf{M}^k\|^2_{\mathbf{L}^2}\\&\quad+\mu_0\|\delta\nabla\Phi^k\|^2_{\mathbf{L}^2}+\lambda\|\delta\nabla\Theta^k\|^2_{\mathbf{L}^2}+\tfrac{2\lambda}{\varepsilon^2}(f(\Theta^{k-1}),\delta\Theta^k)+\tfrac{2\lambda}{\eta\varepsilon}\|\delta\Theta^k\|^2_{\mathbf{L}^2}\\&\quad+\tfrac{2\lambda\gamma\tau}{\varepsilon}\|\nabla\Psi^k\|^2_{\mathbf{L}^2}+2\tau\|\sqrt{\nu_\Theta}\,\mathbf{T}(\mathbf{U}^k)\|^2_{\mathbf{L}^2}+\tfrac{2\mu_0\tau}{\mathscr{J}}\|\mathbf{M}^k\|^2_{\mathbf{L}^2}+\tfrac{2\mu_0\tau}{\mathscr{J}}\|\sqrt{\varkappa_\Theta}\,\mathbf{H}^k\|^2_{\mathbf{L}^2}\\&\quad+\tfrac{2\mu_0\tau}{\mathscr{J}}\|\nabla\Phi^k\|^2_{\mathbf{L}^2}=\tfrac{2\mu_0\tau}{\mathscr{J}}\left(\varkappa_\Theta\mathbf{H}^k,\mathbf{M}^k\right)+2\mu_0\left(\delta\mathbf{h}_a^k,\nabla\Phi^k\right)+\tfrac{2\mu_0\tau}{\mathscr{J}}(\mathbf{h}_a^k,\nabla\Phi^k).\end{aligned} \tag{4.34}$$

In only remains to control the terms $\frac{2\lambda}{\varepsilon^2}(f(\Theta^{k-1}),\delta\Theta^k)+\frac{2\lambda}{\eta\varepsilon}\|\delta\Theta^k\|^2_{\mathbf{L}^2}$. This is a standard argument [123], which for the sake of completeness we repeat. Consider Taylor's

formula for $F(\Theta^k)$ around $F(\Theta^{k-1})$

$$F(\Theta^k) = F(\Theta^{k-1}) + f(\Theta^{k-1})\delta\Theta^k + \tfrac{f'(\xi)}{2}(\delta\Theta^k)^2 \tag{4.35}$$

for some ξ, and using the bound (4.3) we get

$$(\delta F(\Theta^k), 1) \leq (f(\Theta^{k-1}), \delta\Theta^k) + \|\delta\Theta^k\|^2_{\mathbf{L}^2} \tag{4.36}$$

Therefore, if we choose $\eta \leq \varepsilon$, we can finally estimate (4.34) as follows

$$\begin{aligned} &2\,\delta\mathscr{E}(\mathbf{U}^\tau, \mathbf{M}^\tau, \Phi^\tau, \Theta^\tau; k) + 2\mathscr{I}(\delta\mathbf{U}^\tau, \delta\mathbf{M}^\tau, \delta\Phi^\tau, \delta\Theta^\tau; k) \\ &\quad + 2\tau\mathscr{D}(\mathbf{U}^\tau, \mathbf{M}^\tau, \Phi^\tau, \Theta^\tau, \Psi^\tau; k) + \tfrac{\mu_0\varkappa_0\tau}{2\mathscr{T}}\|\mathbf{M}^k\|^2_{\mathbf{L}^2} + \tfrac{2\mu_0\tau}{\mathscr{T}}\|\sqrt{\varkappa_\Theta}\,\mathbf{H}^k\|^2_{\mathbf{L}^2} \\ &\quad + \tfrac{\mu_0\tau}{\mathscr{T}}\|\nabla\Phi^k\|^2_{\mathbf{L}^2} \leq \tfrac{2\mu_0\tau}{\mathscr{T}}\big(\varkappa_\Theta\mathbf{H}^k, \mathbf{M}^k\big) + 2\mu_0\left(\delta\mathbf{h}^k_a, \nabla\Phi^k\right) + \tfrac{2\mu_0\tau}{\mathscr{T}}(\mathbf{h}^k_a, \nabla\Phi^k). \end{aligned} \tag{4.37}$$

The rest is a matter of dividing everything by 2, and bounding the right hand side using Chauchy-Schwarz and Young's inequalities with appropriate constants. As in the continuous case, the term $\frac{2\mu_0\tau}{\mathscr{T}}\big(\varkappa_\Theta\mathbf{H}^k, \mathbf{M}^k\big)$ will give us the limitation $\varkappa_0 \leq 4$. Finally, for the term $2\mu_0\left(\delta\mathbf{h}^k_a, \nabla\Phi^k\right)$, we will use the trivial identity $\|\delta\mathbf{h}^k_a\|^2_{\mathbf{L}^2} = \tau^2\left\|\frac{\delta\mathbf{h}^k_a}{\tau}\right\|^2_{\mathbf{L}^2}$ and the estimate

$$\left\|\tfrac{\delta\mathbf{h}^k_a}{\tau}\right\|^2_{\mathbf{L}^2} \leq \tfrac{1}{\tau}\int_{t^{k-1}}^{t^k}\|\partial_t\mathbf{h}_a(s)\|^2_{\mathbf{L}^2}ds.$$

This concludes the proof. Note that (4.31) is consistent with (4.19), except for the term $\mathscr{I}$ of time increments (jumps). The latter is a dissipative term characteristic of the implicit Euler scheme. □

4.4.3 Existence of fixed points (local solvability)

Let us establish the local solvability of the numerical scheme (4.30). To do so we will make use of the well-known Leray-Schauder fixed point theorem. As it is usual

when invoking this result, the core of the proof is a local (in time) a priori estimate, which very much resembles the arguments of §4.4.2. Therefore, a few intermediate steps have been eliminated leaving the details to the reader.

Theorem 4.4.1 (Existence)**.** *Let $h, \tau > 0$, assume that $\varkappa_0 \leq 4$, and that the parameter $\eta \leq \varepsilon$. If $\nabla\mathbb{X} \subset \mathbb{M}$, then for all $k = 1, \dots, K$ there exists $\{\Theta^k, \Psi^k, \mathbf{M}^k, \Phi^k, \mathbf{U}^k, P^k\} \in \mathbb{G}\times\mathbb{Y}\times\mathbb{M}\times\mathbb{X}\times\mathbb{U}\times\mathbb{P}$ that solves* (4.30)*. Moreover, any such sequence of solutions satisfies estimate* (4.31)*.*

Proof. We define the map $\mathcal{L}$ as follows

$$\left\{\Theta^k, \Psi^k, \mathbf{M}^k, \Phi^k, \mathbf{U}^k, P^k\right\} \overset{\mathcal{L}}{\mapsto} \left\{\widehat{\Theta}^k, \widehat{\Psi}^k, \widehat{\mathbf{M}}^k, \widehat{\Phi}^k, \widehat{\mathbf{U}}^k, \widehat{P}^k\right\},$$

where the quantities with the hats solve of the following variational problem:

$$\left(\tfrac{\widehat{\Theta}^k - \Theta^{k-1}}{\tau}, \Lambda\right) - (\mathbf{U}^k\widehat{\Theta}^k, \nabla\Lambda) - \gamma(\nabla\widehat{\Psi}^k, \nabla\Lambda) = 0 \tag{4.38a}$$

$$(\widehat{\Psi}^k, \Upsilon) + \tfrac{1}{\eta}(\widehat{\Theta}^k - \Theta^{k-1}, \Upsilon) + \varepsilon(\nabla\widehat{\Theta}^k, \nabla\Upsilon) + \tfrac{1}{\varepsilon}(f(\Theta^{k-1}), \Upsilon) = 0 \tag{4.38b}$$

$$\left(\tfrac{\widehat{\mathbf{M}}^k - \mathbf{M}^{k-1}}{\tau}, \mathbf{Z}\right) + b_h^m\big(\mathbf{U}^k, \widehat{\mathbf{M}}^k, \mathbf{Z}\big) + \tfrac{1}{\mathscr{T}}\big(\widehat{\mathbf{M}}^k, \mathbf{Z}\big) = \tfrac{1}{\mathscr{T}}\big(\varkappa_\Theta\widehat{\mathbf{H}}^k, \mathbf{Z}\big) \tag{4.38c}$$

$$(\nabla\widehat{\Phi}^k, \nabla\mathrm{X}) = (\mathbf{h}_a^k - \widehat{\mathbf{M}}^k, \nabla\mathrm{X}) \tag{4.38d}$$

$$\begin{aligned}\left(\tfrac{\widehat{\mathbf{U}}^k - \mathbf{U}^{k-1}}{\tau}, \mathbf{V}\right) + \big(\nu_\Theta\mathbf{T}(\widehat{\mathbf{U}}^k), \mathbf{T}(\mathbf{V})\big) + b_h\big(\mathbf{U}^{k-1}, \widehat{\mathbf{U}}^k, \mathbf{V}\big) - \big(\widehat{P}^k, div\,\mathbf{V}\big)& \\ = -\,b_h^m\big(\mathbf{V}, \widehat{\mathbf{M}}^k, \mathbf{H}^k\big) + \tfrac{\lambda}{\varepsilon}(\nabla\widehat{\Psi}^k\Theta^k, \mathbf{V})&\end{aligned} \tag{4.38e}$$

$$\big(div\,\widehat{\mathbf{U}}^k, \mathrm{Q}\big) = 0. \tag{4.38f}$$

for all $\{\Lambda, \Upsilon, \mathbf{Z}, \mathrm{X}, \mathbf{V}, \mathrm{Q}\} \in \mathbb{G}\times\mathbb{Y}\times\mathbb{M}\times\mathbb{X}\times\mathbb{U}\times\mathbb{P}$. Let us now show that the mapping $\mathcal{L}$ satisfies the requirements of the Leray-Schauder theorem (cf.[94], p. 280):

- ⋄ **Well posedness.** The operator $\mathcal{L}$ is clearly well defined. The information follows a top-down path. For a given velocity $\mathbf{U}^k$ the mixed Cahn-Hilliard

system (4.38a)-(4.38b) is well-defined and widely-studied system which can be reduced to a single positive definite system in terms of the phase (see for instance [124] and references therein). System (4.38c)-(4.38d) can be rewritten as follows:

$$\begin{aligned}\Big(\widehat{\mathbf{M}}^k,\mathbf{Z}\Big)+\tau\, b_h^m\big(\mathbf{U}^k,\widehat{\mathbf{M}}^k,\mathbf{Z}\big)+\tfrac{\tau}{\mathscr{T}}\big(\widehat{\mathbf{M}}^k,\mathbf{Z}\big)-\tfrac{\tau}{\mathscr{T}}\big(\varkappa_\Theta\widehat{\mathbf{H}}^k,\mathbf{Z}\big)=\big(\mathbf{M}^{k-1},\mathbf{Z}\big)\\ (\widehat{\mathbf{M}}^k,\nabla \mathrm{X})+(\nabla\widehat{\Phi}^k,\nabla \mathrm{X})=(\mathbf{h}_a^k,\nabla \mathrm{X})\,.\end{aligned}\tag{4.39}$$

Multiply the second line by $\frac{\tau\varkappa_0}{\mathscr{T}}$ and add both lines. The result can be written as a classical variational formulation. Taking $\mathbf{Z}=\widehat{\mathbf{M}}^k$ and $\mathrm{X}=\widehat{\Phi}^k$ one verifies that, provided $\varkappa_0\le 4$, the associated bilinear form is coercive. Once the magnetization problem is solved, we will have the functions $\widehat{\mathbf{M}}^k$ and $\widehat{\Phi}^k$ which can be used as data for the Stokes problem (4.38e)-(4.38f), which is also well posed.

◇ **Boundedness**. Given $\alpha\in[0,1]$, we must verify that all $\widehat{x}=\Big\{\widehat{\Theta}^k,\widehat{\Psi}^k,\widehat{\mathbf{M}}^k,\widehat{\Phi}^k,\widehat{\mathbf{U}}^k,\widehat{P}^k\Big\}$ satisfying $\frac{1}{\alpha}\widehat{x}=\mathcal{L}\widehat{x}$ can be bounded in terms of the local data $\big\{\Theta^{k-1},\mathbf{M}^{k-1},\Phi^{k-1},\mathbf{U}^{k-1},\mathbf{h}_a^k\big\}$ uniformly with respect to α. In other words, we want to analyze the local boundedness of

$$\begin{aligned}&\Big(\tfrac{\alpha^{-1}\,\widehat{\Theta}^k-\Theta^{k-1}}{\tau},\Lambda\Big)-(\widehat{\mathbf{U}}^k\alpha^{-1}\,\widehat{\Theta}^k,\nabla\Lambda)-\gamma(\alpha^{-1}\,\nabla\widehat{\Psi}^k,\nabla\Lambda)=0\,,\\ &(\alpha^{-1}\,\widehat{\Psi}^k,\Upsilon)+\tfrac{1}{\eta}(\alpha^{-1}\,\widehat{\Theta}^k,\Upsilon)\\ &\qquad+\varepsilon(\alpha^{-1}\,\nabla\widehat{\Theta}^k,\nabla\Upsilon)+\tfrac{1}{\varepsilon}(f(\Theta^{k-1}),\Upsilon)=\tfrac{1}{\eta}(\Theta^{k-1},\Upsilon)\,,\\ &\Big(\tfrac{\alpha^{-1}\,\widehat{\mathbf{M}}^k-\mathbf{M}^{k-1}}{\tau},\mathbf{Z}\Big)+\,b_h^m\big(\widehat{\mathbf{U}}^k,\alpha^{-1}\,\widehat{\mathbf{M}}^k,\mathbf{Z}\big)\\ &\qquad+\tfrac{1}{\mathscr{T}}\big(\alpha^{-1}\,\widehat{\mathbf{M}}^k,\mathbf{Z}\big)=\tfrac{1}{\mathscr{T}}\big(\varkappa_\Theta\alpha^{-1}\,\widehat{\mathbf{H}}^k,\mathbf{Z}\big)\,,\\ &\qquad(\alpha^{-1}\,\nabla\widehat{\Phi}^k,\nabla \mathrm{X})=(\mathbf{h}_a^k-\alpha^{-1}\,\widehat{\mathbf{M}}^k,\nabla \mathrm{X})\,,\\ &\Big(\tfrac{\alpha^{-1}\widehat{\mathbf{U}}^k-\mathbf{U}^{k-1}}{\tau},\mathbf{V}\Big)+\big(\nu_\Theta\alpha^{-1}\,\mathbf{T}(\widehat{\mathbf{U}}^k),\mathbf{T}(\mathbf{V})\big)+\,b_h\big(\mathbf{U}^{k-1},\alpha^{-1}\,\widehat{\mathbf{U}}^k,\mathbf{V}\big)\\ &\qquad-\big(\alpha^{-1}\,\widehat{P}^k,div\,\mathbf{V}\big)=-\,b_h^m\big(\mathbf{V},\alpha^{-1}\,\widehat{\mathbf{M}}^k,\widehat{\mathbf{H}}^k\big)+\tfrac{\lambda}{\varepsilon}(\alpha^{-1}\nabla\widehat{\Psi}^k\widehat{\Theta}^k,\mathbf{V})\,,\end{aligned}\tag{4.40}$$

Set $\Lambda = \frac{2\alpha\lambda\tau}{\varepsilon}\widehat{\Psi}^k$, $\Upsilon = \frac{2\alpha\lambda}{\varepsilon}(\widehat{\Theta}^k - \alpha\Theta^{k-1})$, $\mathbf{V} = 2\alpha\tau\widehat{\mathbf{U}}^k$, $\mathbf{Z} = 2\alpha\tau\mu_0\widehat{\mathbf{M}}^k$, and $\mathrm{X} = \frac{2\alpha\mu_0\tau}{\mathscr{T}}\widehat{\Phi}^k$ in (4.40), and use the identity (1.11), to get:

$$\begin{aligned}
&\lambda\|\nabla\widehat{\Theta}^k\|_{\mathbf{L}^2}^2 - \lambda\|\alpha\nabla\Theta^{k-1}\|_{\mathbf{L}^2}^2 + \|\widehat{\mathbf{U}}^k\|_{\mathbf{L}^2}^2 - \|\alpha\mathbf{U}^{k-1}\|_{\mathbf{L}^2}^2 + \mu_0\|\widehat{\mathbf{M}}^k\|_{\mathbf{L}^2}^2 \\
&\quad - \mu_0\|\alpha\mathbf{M}^{k-1}\|_{\mathbf{L}^2}^2 + \|\widehat{\mathbf{U}}^k - \alpha\mathbf{U}^{k-1}\|_{\mathbf{L}^2}^2 + \mu_0\|\widehat{\mathbf{M}}^k - \alpha\mathbf{M}^{k-1}\|_{\mathbf{L}^2}^2 \\
&\quad + \lambda\|\nabla\widehat{\Theta}^k - \alpha\nabla\Theta^{k-1}\|_{\mathbf{L}^2}^2 + \tfrac{2\lambda\gamma\tau}{\varepsilon}\|\nabla\Psi^k\|_{\mathbf{L}^2}^2 + \tfrac{2\lambda}{\eta\varepsilon}\|\widehat{\Theta}^k - \alpha\Theta^{k-1}\|_{\mathbf{L}^2}^2 \\
&\quad + 2\tau\,\|\sqrt{\nu_\Theta}\,\mathbf{T}(\widehat{\mathbf{U}}^k)\|_{\mathbf{L}^2}^2 + \tfrac{2\mu_0\tau}{\mathscr{T}}\|\widehat{\mathbf{M}}^k\|_{\mathbf{L}^2}^2 + \tfrac{2\mu_0\tau}{\mathscr{T}}\|\nabla\Phi^k\|_{\mathbf{L}^2}^2 \\
&\quad = \tfrac{2\mu_0\tau}{\mathscr{T}}\big(\varkappa_\Theta\widehat{\mathbf{H}}^k, \widehat{\mathbf{M}}^k\big) - 2\tau\mu_0\, b_h^m\big(\widehat{\mathbf{U}}^k, \widehat{\mathbf{M}}^k, \nabla\widehat{\Phi}^k\big) \\
&\quad + \tfrac{2\mu_0\tau}{\mathscr{T}}(\alpha\mathbf{h}_a^k - \widehat{\mathbf{M}}^k, \nabla\widehat{\Phi}^k) - \tfrac{2\alpha\lambda}{\varepsilon^2}(f(\Theta^{k-1}), \widehat{\Theta}^k - \alpha\Theta^{k-1})\,.
\end{aligned} \tag{4.41}$$

To gain control over $-2\tau\, b_h^m\big(\widehat{\mathbf{U}}^k, \widehat{\mathbf{M}}^k, \nabla\widehat{\Phi}^k\big)$ we set $\mathbf{Z} = 2\alpha\tau\mu_0\widehat{\mathbf{H}}^k$ in the magnetization equation (note that this requires $\nabla\mathbb{X} \subset \mathbb{M}$ to hold true), so that

$$\begin{aligned}
\tfrac{2\mu_0\tau}{\mathscr{T}}\|\sqrt{\varkappa_\Theta}\,\widehat{\mathbf{H}}^k\|_{\mathbf{L}^2}^2 &= 2\mu_0\left(\widehat{\mathbf{M}}^k - \alpha\mathbf{M}^{k-1}, \widehat{\mathbf{H}}^k\right) \\
&\quad + 2\mu_0\tau\, b_h^m\big(\widehat{\mathbf{U}}^k, \widehat{\mathbf{M}}^k, \widehat{\mathbf{H}}^k\big) + \tfrac{2\mu_0\tau}{\mathscr{T}}\big(\widehat{\mathbf{M}}^k, \widehat{\mathbf{H}}^k\big)\,,
\end{aligned}$$

add it to (4.41) to obtain

$$\begin{aligned}
&\lambda\|\nabla\widehat{\Theta}^k\|_{\mathbf{L}^2}^2 - \lambda\|\alpha\nabla\Theta^{k-1}\|_{\mathbf{L}^2}^2 + \|\widehat{\mathbf{U}}^k\|_{\mathbf{L}^2}^2 - \|\alpha\mathbf{U}^{k-1}\|_{\mathbf{L}^2}^2 + \mu_0\|\widehat{\mathbf{M}}^k\|_{\mathbf{L}^2}^2 \\
&\quad - \mu_0\|\alpha\mathbf{M}^{k-1}\|_{\mathbf{L}^2}^2 + \|\widehat{\mathbf{U}}^k - \alpha\mathbf{U}^{k-1}\|_{\mathbf{L}^2}^2 + \mu_0\|\widehat{\mathbf{M}}^k - \alpha\mathbf{M}^{k-1}\|_{\mathbf{L}^2}^2 \\
&\quad + \lambda\|\nabla\widehat{\Theta}^k - \alpha\nabla\Theta^{k-1}\|_{\mathbf{L}^2}^2 + \tfrac{2\lambda\gamma\tau}{\varepsilon}\|\nabla\Psi^k\|_{\mathbf{L}^2}^2 + \tfrac{2\lambda}{\eta\varepsilon}\|\widehat{\Theta}^k - \alpha\Theta^{k-1}\|_{\mathbf{L}^2}^2 \\
&\quad + 2\tau\,\|\sqrt{\nu_\Theta}\,\mathbf{T}(\widehat{\mathbf{U}}^k)\|_{\mathbf{L}^2}^2 + \tfrac{2\mu_0\tau}{\mathscr{T}}\|\widehat{\mathbf{M}}^k\|_{\mathbf{L}^2}^2 + \tfrac{2\mu_0\tau}{\mathscr{T}}\|\nabla\Phi^k\|_{\mathbf{L}^2}^2 \\
&\quad + \tfrac{2\mu_0\tau}{\mathscr{T}}\|\sqrt{\varkappa_\Theta}\,\widehat{\mathbf{H}}^k\|_{\mathbf{L}^2}^2 = \tfrac{2\mu_0\tau}{\mathscr{T}}\big(\varkappa_\Theta\widehat{\mathbf{H}}^k, \widehat{\mathbf{M}}^k\big) + \tfrac{2\mu_0\alpha\tau}{\mathscr{T}}(\mathbf{h}_a^k, \nabla\widehat{\Phi}^k) \\
&\quad + 2\mu_0\left(\widehat{\mathbf{M}}^k - \alpha\mathbf{M}^{k-1}, \widehat{\mathbf{H}}^k\right) - \tfrac{2\alpha\lambda}{\varepsilon^2}(f(\Theta^{k-1}), \widehat{\Theta}^k - \alpha\Theta^{k-1})\,.
\end{aligned} \tag{4.42}$$

Setting $\mathrm{X} = \alpha\widehat{\Phi}^k$ in the fourth equation of (4.40) yields

$$\|\nabla\widehat{\Phi}^k\|^2_{\mathbf{L}^2} = (\alpha\mathbf{h}_a^k - \widehat{\mathbf{M}}^k, \nabla\widehat{\Phi}^k)\,,$$

whence (4.42) becomes:

$$\begin{aligned}
&\lambda\|\nabla\widehat{\Theta}^k\|^2_{\mathbf{L}^2} - \lambda\|\alpha\nabla\Theta^{k-1}\|^2_{\mathbf{L}^2} + \|\widehat{\mathbf{U}}^k\|^2_{\mathbf{L}^2} - \|\alpha\mathbf{U}^{k-1}\|^2_{\mathbf{L}^2} + \mu_0\|\widehat{\mathbf{M}}^k\|^2_{\mathbf{L}^2} \\
&\quad - \mu_0\|\alpha\mathbf{M}^{k-1}\|^2_{\mathbf{L}^2} + \|\widehat{\mathbf{U}}^k - \alpha\mathbf{U}^{k-1}\|^2_{\mathbf{L}^2} + \mu_0\|\widehat{\mathbf{M}}^k - \alpha\mathbf{M}^{k-1}\|^2_{\mathbf{L}^2} \\
&\quad + \lambda\|\nabla\widehat{\Theta}^k - \alpha\nabla\Theta^{k-1}\|^2_{\mathbf{L}^2} + \tfrac{2\lambda\gamma\tau}{\varepsilon}\|\nabla\Psi^k\|^2_{\mathbf{L}^2} + \tfrac{2\lambda}{\eta\varepsilon}\|\widehat{\Theta}^k - \alpha\Theta^{k-1}\|^2_{\mathbf{L}^2} \\
&\quad + 2\tau\,\|\sqrt{\nu_\Theta}\mathbf{T}(\widehat{\mathbf{U}}^k)\|^2_{\mathbf{L}^2} + \tfrac{2\mu_0\tau}{\mathscr{T}}\|\widehat{\mathbf{M}}^k\|^2_{\mathbf{L}^2} + \tfrac{2\mu_0\tau}{\mathscr{T}}\|\nabla\Phi^k\|^2_{\mathbf{L}^2} \\
&\quad + \tfrac{2\mu_0\tau}{\mathscr{T}}\|\sqrt{\varkappa_\Theta}\,\widehat{\mathbf{H}}^k\|^2_{\mathbf{L}^2} = \tfrac{2\mu_0\tau}{\mathscr{T}}\big(\varkappa_\Theta\nabla\widehat{\Phi}^k, \widehat{\mathbf{M}}^k\big) + \tfrac{2\mu_0\alpha}{\mathscr{T}}(1+\tau)(\mathbf{h}_a^k, \nabla\widehat{\Phi}^k) \\
&\quad - 2\mu_0\alpha\left(\mathbf{M}^{k-1}, \nabla\widehat{\Phi}^k\right) - \tfrac{2\alpha\lambda}{\varepsilon^2}(f(\Theta^{k-1}), \widehat{\Theta}^k - \alpha\Theta^{k-1})\,.
\end{aligned} \tag{4.43}$$

To conclude it remains to bound the right hand side using Cauchy-Schwarz and Young's inequalities with appropriate constants, use that $\alpha \leq 1$, and the bound $\nu_\Theta \geq \nu_w$ of (4.15). We never made explicit if the coefficients ν_Θ and $\varkappa_\Theta$ depend on $\widehat{\Theta}^k$, $\widehat{\Theta}^k/\alpha$ or Θ^{k-1}. This is because, provided that estimates (4.15) hold, the uniform boundedness of the operator $\mathcal{L}$ is independent of ν_Θ and $\varkappa_\Theta$.

- ◇ **Compactness:** this is automatically satisfied since we are working with finite dimensional spaces.

Finally, we apply Leray-Schauder's theorem to prove the assertion. □

4.4.4 Space discretization: definitions and assumptions

Having understood what is required from a Galerkin technique to achieve stability of the scheme (4.30) we will now specify our choices of discrete spaces using finite

elements. We assume that Ω is convex and Γ is polyhedral, and that we have at hand a quasi-uniform mesh $\mathcal{T}_h = \{T\}$ of Ω. As Proposition 4.4.1 shows, to gain stability it is convenient to have $\nabla\mathbb{X} \subset \mathbb{M}$. Since the space $\mathbb{X}$ is used to approximate the solution of an elliptic problem with Neumann boundary conditions, the simplest choice for $\mathbb{X}$ is the same as in (3.52) and (3.53), which entails that $\mathbb{M}$ is a space of discontinuous functions and, consequently, the trilinear form $b_h^m(\cdot,\cdot,\cdot)$ must be defined accordingly. The trilinear form $b_h^m(\cdot,\cdot,\cdot)$ will be defined as in (3.54).

The choice of the remaining spaces is straightforward, for $\ell \geq 2$ we set

$$\begin{aligned}
\mathbb{G} &= \left\{\Lambda \in \mathcal{C}^0\left(\overline{\Omega}\right) \mid \Lambda|_T \in \mathcal{P}_\ell(T)\,, \forall\, T \in \mathcal{T}_h\right\} \\
\mathbb{Y} &= \left\{\Upsilon \in \mathcal{C}^0\left(\overline{\Omega}\right) \mid \Upsilon|_T \in \mathcal{P}_\ell(T)\,, \forall\, T \in \mathcal{T}_h\right\} \\
\mathbb{U} &= \left\{\mathbf{V} \in \boldsymbol{\mathcal{C}}^0\left(\overline{\Omega}\right) \mid \mathbf{V}|_T \in [\mathcal{P}_\ell(T)]^d\,, \forall\, T \in \mathcal{T}_h,\right\} \cap \mathbf{H}_0^1(\Omega) \\
\mathbb{P} &= \left\{\mathrm{Q} \in \mathcal{C}^0\left(\overline{\Omega}\right) \mid \mathrm{Q}|_T \in \mathcal{P}_{\ell-1}(T)\,, \forall\, T \in \mathcal{T}_h\right\}
\end{aligned} \tag{4.44}$$

The finite element spaces $\mathbb{G}$, $\mathbb{Y}$, $\mathbb{M}$, $\mathbb{X}$, $\mathbb{U}$, and $\mathbb{P}$ are defined using polynomial spaces $\mathcal{P}_\ell$, of total degree at most ℓ, usually associated to simplicial elements. However, the fact that the scheme (4.30) is energy stable is independent of whether we choose simplices or quadrilaterals/hexahedrons. If we replace $\mathcal{P}_\ell$ by $\mathcal{Q}_\ell$ (polynomials of degree at most ℓ in each variable) in (3.52), (3.53) and (4.44), we would only need to do minor changes in the choice of polynomial degrees in order to guarantee that the inclusion $\nabla\mathbb{X} \subset \mathbb{M}$ holds true. To simplify our exposition we will always assume that our elements are simplicial and develop our theory under this assumption. We will provide remarks describing the required modifications if quadrilaterals are to be used.

We assume that the pair $\{\mathbb{G}, \mathbb{Y}\}$ is inf-sup stable, meaning that

$$\sup_{\Lambda \in \mathbb{G}} \frac{(\nabla \Lambda, \nabla \Xi)}{\|\Lambda\|_{\mathbf{H}_0^1}} \geq c \|\Xi\|_{L^2} \ \forall \, \Xi \in \mathbb{Y}. \tag{4.45}$$

It is well known that equal-order polynomials spaces for the pair $\{\mathbb{G}, \mathbb{Y}\}$ (as in (4.44)) is enough to satisfy this condition (cf.[44]).

4.5 Simplification of the model

Following §3.5.1, a natural simplification of the model (4.13) is to discard the Poisson problem (4.13d) and set $\mathbf{h} := \mathbf{h}_a$. This will only be physically realistic for ferrofluids with a small susceptibility. Water based ferrofluids subject to slowly varying magnetic fields (and/or small characteristic times $\mathscr{T}$) could be modeled under these assumptions, since they usually exibit a small magnetic susceptibility in the low frequency regime [95, 96].

We will consider the following weak formulation for the model defined by equations (4.13a), (4.13b), (4.13c), (4.13e), (4.13f): Find $(\theta, \psi, \mathbf{m}, \mathbf{u}, p) \in L^2(([0, t_F); H^1(\Omega))$ $\times L^2(([0, t_F); H^1(\Omega)) \times L^2(([0, t_F); \mathbf{L}^2(\Omega)) \times L^2(([0, t_F); \boldsymbol{\mathcal{V}}) \times L^2(([0, t_F); L^2(\Omega))$ that satisfy

$$-\int_0^{t_F} (\theta, \lambda_t) + (\mathbf{u}\theta, \nabla\lambda) + \gamma(\nabla\psi, \nabla\lambda) = (\theta(0), \lambda(0)) \,, \tag{4.46a}$$

$$-\int_0^{t_F} \varepsilon(\nabla\theta, \nabla\upsilon) + \tfrac{1}{\varepsilon}(f(\theta), \upsilon) + (\psi, \upsilon) = 0 \,, \tag{4.46b}$$

$$-\int_0^{t_F} (\mathbf{m}, \mathbf{z}_t) + b(\mathbf{u}, \mathbf{z}, \mathbf{m}) - \tfrac{1}{\mathscr{T}}(\mathbf{m}, \mathbf{z}) = (\mathbf{m}(0), \mathbf{z}(0)) + \tfrac{1}{\mathscr{T}} \int_0^{t_F} (\varkappa_\theta \mathbf{h}, \mathbf{z}) \,, \tag{4.46c}$$

$$\begin{aligned} \int_0^{t_F} -(\mathbf{u}, \mathbf{v}_t) + b(\mathbf{u}, \mathbf{u}, \mathbf{v}) + (\nu_\theta \, \mathbf{T}(\mathbf{u}), \mathbf{T}(\mathbf{v})) &= (\mathbf{u}(0), \mathbf{v}(0)) \\ + \int_0^{t_F} \mu_0 \, b(\mathbf{m}, \mathbf{h}, \mathbf{v}) + \tfrac{\lambda}{\varepsilon}(\theta \nabla\psi, \mathbf{v}) \,, \end{aligned} \tag{4.46d}$$

for all $\lambda, \upsilon \in \mathcal{C}_0^\infty([0,t_F)\times\Omega)$, $\mathbf{z} \in \boldsymbol{\mathcal{C}}_0^\infty([0,t_F)\times\Omega)$, $\mathbf{v} \in \{\mathbf{w} \in \boldsymbol{\mathcal{C}}_{\mathbf{0}}^\infty([0,t_F)\times\Omega)$ $|\, div\, \mathbf{w} = 0 \ \text{ in } \Omega\}$ where now the magnetic field $\mathbf{h}$ is not determined by the Poisson problem (4.13d), but rather $\mathbf{h} := \mathbf{h}_a$ is a given harmonic (curl-free and div-free) smooth vector field.

4.5.1 A convergent scheme

To discretize the system (4.46) we are going to consider an initialization as in (4.29). Then, for every $k \in \{1,\dots,K\}$ we compute $\{\Theta^k, \Psi^k, \mathbf{M}^k, \mathbf{U}^k, P^k\} \in \mathbb{G}\times\mathbb{Y}\times\mathbb{M}\times\mathbb{U}\times\mathbb{P}$ that solve

$$\Big(\tfrac{\delta\Theta^k}{\tau}, \Lambda\Big) - (\mathbf{U}^k\Theta^{k-1}, \nabla\Lambda) - \gamma(\nabla\Psi^k, \nabla\Lambda) = 0\,, \tag{4.47a}$$

$$(\Psi^k, \Upsilon) + \tfrac{1}{\eta}(\delta\Theta^k, \Upsilon) + \varepsilon(\nabla\Theta^k, \nabla\Upsilon) + \tfrac{1}{\varepsilon}(f(\Theta^{k-1}), \Upsilon) = 0\,, \tag{4.47b}$$

$$\Big(\tfrac{\delta\mathbf{M}^k}{\tau}, \mathbf{Z}\Big) - b_h^m\big(\mathbf{U}^k, \mathbf{Z}, \mathbf{M}^k\big) + \tfrac{1}{\mathscr{T}}\big(\mathbf{M}^k, \mathbf{Z}\big) = \tfrac{1}{\mathscr{T}}\big(\varkappa_\Theta \mathbf{H}^k, \mathbf{Z}\big)\,, \tag{4.47c}$$

$$\begin{aligned}\Big(\tfrac{\delta\mathbf{U}^k}{\tau}, \mathbf{V}\Big) + \big(\nu_\Theta \mathbf{T}(\mathbf{U}^k), \mathbf{T}(\mathbf{V})\big) + b_h\big(\mathbf{U}^{k-1}, \mathbf{U}^k, \mathbf{V}\big) - \big(P^k, div\,\mathbf{V}\big)\\ = b_h^m\big(\mathbf{V}, \mathbf{H}^k, \mathbf{M}^k\big) + \tfrac{\lambda}{\varepsilon}(\Theta^{k-1}\nabla\Psi^k, \mathbf{V})\,,\end{aligned} \tag{4.47d}$$

$$\big(\mathrm{Q}, div\,\mathbf{U}^k\big) = 0\,, \tag{4.47e}$$

for all $\{\Lambda, \Upsilon, \mathbf{Z}, \mathbf{V}, \mathrm{Q}\} \in \mathbb{G}\times\mathbb{Y}\times\mathbb{M}\times\mathbb{U}\times\mathbb{P}$. Here, the magnetic field $\mathbf{H}^k$ is given by

$$\mathbf{H}^k := \mathrm{I}_{\mathbb{M}}[\mathbf{h}_a^k]\,, \tag{4.48}$$

where $\mathrm{I}_{\mathbb{M}}$ was defined in (4.28).

The choice of spaces $\mathbb{G}$, $\mathbb{Y}$, $\mathbb{M}$, $\mathbb{U}$ and $\mathbb{P}$ does need to be made precise now, we will provide a specific construction in Remark 4.5.2. Right now we only need to say

that, in order for (4.47) to be convergent, in addition to the requirements (4.45) for the spaces $\mathbb{G}$ and $\mathbb{Y}$, and the LBB compatibility condition for the spaces $\{\mathbb{U}, \mathbb{P}\}$, we will also require that:

1. The pressure space $\mathbb{P}$ should be discontinuous and it should contain a continuous subspace of degree 1 or higher.

2. For all $\mathbf{Z} \in \mathbb{M}$, we want each space component $\mathbf{Z}^i$ $(i : 1, ..., d)$ to belong to the same finite element space as the pressure, i.e. we will require $\mathbb{M} = [\mathbb{P}]^d$.

3. The L^∞ estimates (1.20) of the Stokes projector should hold true.

4. Let $\Pi_{\mathbb{G}} : L^2(\Omega) \longrightarrow \mathbb{G}$ denote the $L^2(\Omega)$ projection onto the space $\mathbb{G}$. We will assume that the projector $\Pi_{\mathbb{G}}$ is $H^1(\Omega)$-stable, namely

$$\|\nabla \Pi_{\mathbb{G}} \lambda\|_{L^2} \leq c \, \|\lambda\|_{H^1} \quad \forall \, \lambda \in H^1(\Omega) \,, \tag{4.49}$$

   with c independent of h and λ. In the context of quasi-uniform meshes the reader can check the classical references [52, 42], and for non quasi-uniform meshes and different norms [99, 100, 101].

The motivations behind assumptions 1 and 2 were explained in §3.5.3, and they are primarily to related to the consistency of the convective term of the magnetization equation. The motivation for assumption 3, will be made clear in §4.5.2. To the best of the author's knowledge, at the time of this writing, there are no finite element pairs $\{\mathbb{U}, \mathbb{P}\}$ for the three-dimensional case satisfying assumptions 1 and 3. Therefore, we can only provide a specific (realizable) finite element construction of scheme (4.47) for the two-dimensional case.

Adapting the arguments of Propostion 4.4.1 we can show that the scheme (4.47) is stable, and proceeding as in Theorem 4.4.1 existence of solutions can be established. We do this next.

Proposition 4.5.1 (Properties of the scheme)**.** *Assume that* $\varkappa_0 \leq 4$ *and* $\eta \leq \varepsilon$*. In this setting, for every* $k = 1, \dots, K$ *there is* $\left\{\Theta^k, \Psi^k, \mathbf{M}^k, \mathbf{U}^k, P^k\right\} \in \mathbb{G}\times\mathbb{Y}\times\mathbb{M}\times\mathbb{U}\times\mathbb{P}$ *that solves* (4.47)*, with* $\mathbf{H}^k$ *defined in* (4.48)*. Moreover this solution satisfies the following stability estimate*

$$
\begin{aligned}
&\|\mathbf{U}^K\|_{\mathbf{L}^2}^2 + \tfrac{\mu_0}{2}\|\mathbf{M}^K\|_{\mathbf{L}^2}^2 + \lambda\|\nabla\Theta^K\|_{\mathbf{L}^2}^2 + \tfrac{2\lambda}{\varepsilon^2}(F(\Theta^K),1) \\
&\quad + \sum_{k=1}^{K}\Big(\|\delta\mathbf{U}^k\|_{\mathbf{L}^2}^2 + \mu_0\|\delta\mathbf{M}^k\|_{\mathbf{L}^2}^2 + \lambda\|\delta\nabla\Theta^k\|_{\mathbf{L}^2}^2 + \tfrac{2\lambda\gamma\tau}{\varepsilon}\|\nabla\Psi^k\|_{\mathbf{L}^2}^2 \\
&\quad + 2\tau\|\sqrt{\nu_\Theta}\,\mathbf{T}(\mathbf{U}^k)\|_{\mathbf{L}^2}^2 + \tfrac{\mu_0\tau}{\mathscr{T}}\|\mathbf{M}^k\|_{\mathbf{L}^2}^2 + \tfrac{2\mu_0\tau}{\mathscr{T}}\|\sqrt{\varkappa_\Theta}\,\mathbf{H}^k\|_{\mathbf{L}^2}\Big) \\
&\quad \leq \sum_{k=1}^{K}\tfrac{3\mu_0\tau}{\mathscr{T}}(1+\varkappa_0^2)\|\mathbf{H}^k\|_{\mathbf{L}^2}^2 + 3\mu_0\mathscr{T}\sum_{k=1}^{K-1}\tau\left\|\tfrac{\delta\mathbf{H}^{k+1}}{\tau}\right\|_{\mathbf{L}^2}^2 \\
&\quad + \|\mathbf{U}^0\|_{\mathbf{L}^2}^2 + 2\mu_0\|\mathbf{M}^0\|_{\mathbf{L}^2}^2 + \lambda\|\nabla\Theta^0\|_{\mathbf{L}^2}^2 + \tfrac{2\lambda}{\varepsilon^2}(F(\Theta^0),1) \\
&\quad + 2\mu_0\|\mathbf{H}^K\|_{\mathbf{L}^2}^2 + \mu_0\|\mathbf{H}^0\|_{\mathbf{L}^2}^2 \leq c < \infty\,.
\end{aligned}
\tag{4.50}
$$

The scheme is mass preserving

$$
(\Theta^k, 1) = (\Theta^0, 1) \quad \forall\, 1 \leq k \leq K\,, \tag{4.51}
$$

and the following additional estimate holds

$$
\|\Psi^\tau\|_{\ell^2(H^1(\Omega))} \leq c < \infty\,. \tag{4.52}
$$

Proof. Set $\Lambda = \frac{2\lambda\tau}{\varepsilon}\Psi^k$, $\Upsilon = \frac{2\lambda}{\varepsilon}\delta\Theta^k$, $\mathbf{V} = 2\tau\mathbf{U}^k$, $\mathbf{Z} = 2\tau\mu_0\mathbf{M}^k$, and $\mathbf{Z} = 2\tau\mu_0\mathbf{H}^k$ (now, with $\mathbf{H}^k$ defined as in (4.48)) in (4.47) and add the result. We treat the double

well potential as in (4.35)-(4.36) and add in time to get

$$
\begin{aligned}
&\|\mathbf{U}^k\|^2_{\mathbf{L}^2} + \mu_0\|\mathbf{M}^k\|^2_{\mathbf{L}^2} + \lambda\|\nabla\Theta^k\|^2_{\mathbf{L}^2} + \tfrac{2\lambda}{\varepsilon^2}(F(\Theta^k),1) \\
&\quad + \sum_{k=1}^{K}\Big(\|\delta\mathbf{U}^k\|^2_{\mathbf{L}^2} + \mu_0\|\delta\mathbf{M}^k\|^2_{\mathbf{L}^2} + \lambda\|\delta\nabla\Theta^k\|^2_{\mathbf{L}^2} + \tfrac{2\lambda\gamma\tau}{\varepsilon}\|\nabla\Psi^k\|^2_{\mathbf{L}^2} \\
&\quad + 2\tau\|\sqrt{\nu_\Theta}\,\mathbf{T}(\mathbf{U}^k)\|^2_{\mathbf{L}^2} + \tfrac{2\mu_0\tau}{\mathscr{T}}\|\mathbf{M}^k\|^2_{\mathbf{L}^2} + \tfrac{2\mu_0\tau}{\mathscr{T}}\|\sqrt{\varkappa_\Theta}\,\mathbf{H}^k\|_{\mathbf{L}^2}\Big) \\
&\quad \leq \sum_{k=1}^{K}\Big(\tfrac{2\mu_0\tau}{\mathscr{T}}\big(\varkappa_\Theta\mathbf{H}^k,\mathbf{M}^k\big) + 2\mu_0\left(\delta\mathbf{M}^k,\mathbf{H}^k\right) + \tfrac{2\mu_0\tau}{\mathscr{T}}\big(\mathbf{M}^k,\mathbf{H}^k\big)\Big) \\
&\quad + \|\mathbf{U}^{k-1}\|^2_{\mathbf{L}^2} + \mu_0\|\mathbf{M}^{k-1}\|^2_{\mathbf{L}^2} + \lambda\|\nabla\Theta^{k-1}\|^2_{\mathbf{L}^2} + \tfrac{2\lambda}{\varepsilon^2}(F(\Theta^0),1)\,.
\end{aligned}
\tag{4.53}
$$

The rest is just a matter of applying summation by parts formula (1.12) to the term $\sum_{k=1}^{K}\left(\delta\mathbf{M}^k,\mathbf{H}^k\right)$, and applying Cauchy-Schwarz and Young's inequalities with appropriate constants. Estimate (4.50) and analogous arguments to those of Theorem 4.4.1 yield local existence of solutions via Leray-Schauder's theorem.

The mass preserving property (4.51) can be easily verified by taking $\Lambda = 1$ in (4.47a). Notice that (4.51) also implies the following Poincaré-type inequality

$$
\|\Theta^k\|_{L^2} \leq c\left(\|\nabla\Theta^k\|_{\mathbf{L}^2} + \Big|\int_\Omega \Theta^k\Big|\right) = c\left(\|\nabla\Theta^k\|_{\mathbf{L}^2} + \Big|\int_\Omega \Theta^0\Big|\right). \tag{4.54}
$$

Estimate (4.52) follows by taking $\Upsilon = 1$ in (4.47b), using the bounds on $\|\nabla\Theta^\tau\|_{\ell^\infty(\mathbf{L}^2)}$ provided by the estimate (4.50) and Poincaré inequality (4.54) to get

$$
\Big|\int_\Omega \Psi^k\Big| \lesssim \int_\Omega |\delta\Theta^k| + |\nabla\Theta^k| + |f(\Theta^{k-1})|\,. \tag{4.55}
$$

To control $\int_\Omega |f(\Theta^{k-1})|$, we use (4.3). From this we conclude that

$$
\max_k \Big|\int_\Omega \Psi^k\Big| \leq c < \infty\,. \tag{4.56}
$$

Finally, (4.52) follows by combining (4.56) with (4.50). □

Remark 4.5.1 (Technical assumption)**.** From now on we will assume that $\int_\Omega \Theta^0 = 0$ in order to simplify the presentation.

Lemma 4.5.1 (Estimates for the discrete time derivatives)**.** *The following estimates for* $\frac{\delta\nabla\Theta^k}{\tau}$ *and* $\frac{\delta\mathbf{U}^k}{\tau}$ *hold*

$$\left\|\tfrac{\delta\nabla\Theta^\tau}{\tau}\right\|_{\ell^2(\mathbf{H}^{-1}(\Omega))} + \left\|\tfrac{\delta\mathbf{U}^\tau}{\tau}\right\|_{\ell^{4/3}(\boldsymbol{\mathcal{V}}^*)} \leq c < \infty\,,$$

with c *independent of* h *and* τ*, depending only on* $\mathbf{h}_a$*.*

Proof. Following [102] we first use (1.21) and (1.22)

$$\left\|\tfrac{\delta\mathbf{U}^k}{\tau}\right\|_{\boldsymbol{\mathcal{V}}^*} = \sup_{\mathbf{v}\in\boldsymbol{\mathcal{V}}} \frac{\left(\frac{\delta\mathbf{U}^k}{\tau}, \mathbf{v}\right)}{\|\mathbf{v}\|_{\mathbf{H}^1_0}} = \sup_{\mathbf{v}\in\boldsymbol{\mathcal{V}}} \frac{\left(\frac{\delta\mathbf{U}^k}{\tau}, \Pi_{\mathbb{V}}[\mathbf{v}]\right)}{\|\mathbf{v}\|_{\mathbf{H}^1_0}} \lesssim \sup_{\mathbf{v}\in\boldsymbol{\mathcal{V}}} \frac{\left(\frac{\delta\mathbf{U}^k}{\tau}, \Pi_{\mathbb{V}}[\mathbf{v}]\right)}{\|\Pi_{\mathbb{V}}[\mathbf{v}]\|_{\mathbf{H}^1_0}}\,.$$

We next utilize (4.47d) and (3.40) to get:

$$\begin{aligned}\left\|\tfrac{\delta\mathbf{U}^k}{\tau}\right\|_{\boldsymbol{\mathcal{V}}^*} &\lesssim \|\nabla\mathbf{U}^k\|_{\mathbf{L}^2} + \|\mathbf{U}^{k-1}\|_{\mathbf{L}^3}\|\mathbf{U}^k\|_{\mathbf{L}^6} + \|div\,\mathbf{U}^{k-1}\|_{L^2}\|\mathbf{U}^k\|_{\mathbf{L}^3} \\ &\quad + \|\nabla\mathbf{H}^k\|_{\mathbf{L}^\infty}\|\mathbf{M}^k\|_{\mathbf{L}^2} + \|\mathbf{H}^k\|_{\mathbf{L}^\infty}\|\mathbf{M}^k\|_{\mathbf{L}^2} + \|\Theta^{k-1}\|_{L^3}\|\nabla\Psi^k\|_{\mathbf{L}^2}\,.\end{aligned}$$

We employ the estimate (4.50) and inequality

$$\|\mathbf{U}^k\|_{\mathbf{L}^3} \leq \|\mathbf{U}^k\|^{1/2}_{\mathbf{L}^2}\|\mathbf{U}^k\|^{1/2}_{\mathbf{L}^6} \lesssim \|\mathbf{U}^k\|^{1/2}_{\mathbf{L}^6} \lesssim \|\nabla\mathbf{U}^k\|^{1/2}_{\mathbf{L}^2}\,, \tag{4.57}$$

to deduce that

$$\begin{aligned}\left\|\tfrac{\delta\mathbf{U}^k}{\tau}\right\|_{\boldsymbol{\mathcal{V}}^*} &\lesssim \|\nabla\mathbf{U}^k\|_{\mathbf{L}^2} + \|\nabla\mathbf{U}^{k-1}\|^{3/2}_{\mathbf{L}^2} + \|\nabla\mathbf{U}^k\|^{3/2}_{\mathbf{L}^2} + \|\mathbf{M}^k\|_{\mathbf{L}^2} + \|\nabla\Psi^k\|_{\mathbf{L}^2} \\ &\lesssim \left(\|\nabla\mathbf{U}^k\|^{4/3}_{\mathbf{L}^2} + \|\nabla\mathbf{U}^{k-1}\|^2_{\mathbf{L}^2} + \|\nabla\mathbf{U}^k\|^2_{\mathbf{L}^2}\|\mathbf{M}^k\|^{4/3}_{\mathbf{L}^2} + \|\nabla\Psi^k\|^{4/3}_{\mathbf{L}^2}\right)^{\frac{3}{4}}.\end{aligned} \tag{4.58}$$

Raise (4.58) to the power 4/3, multiply by τ, and add in time to get the desired estimate on $\tau^{-1}\delta\mathbf{U}^k$. For the term $\left\|\frac{\delta\nabla\Theta^k}{\tau}\right\|_{\ell^2(\mathbf{H}^{-1}(\Omega))}$ we proceed analogously using (4.47a) and (4.49):

$$\left\|\tfrac{\delta\nabla\Theta^k}{\tau}\right\|_{\mathbf{H}^{-1}(\Omega)} = \sup_{\Lambda\in H^1(\Omega)} \frac{\left(\frac{\delta\Theta^k}{\tau}, \Lambda\right)}{\|\Lambda\|_{H^1}} \lesssim \sup_{\Lambda\in H^1(\Omega)} \frac{\left(\frac{\delta\Theta^k}{\tau}, \Pi_{\mathbb{G}}[\Lambda]\right)}{\|\Pi_{\mathbb{G}}[\Lambda]\|_{H^1}}\,,$$

whence

$$\left\| \frac{\delta \nabla \Theta^k}{\tau} \right\|_{\mathbf{H}^{-1}(\Omega)} \lesssim \|\mathbf{U}^k\|_{\mathbf{L}^4} \|\Theta^k\|_{\mathbf{L}^4} + \|\nabla \Psi^k\|_{\mathbf{L}^2} \lesssim \|\nabla \mathbf{U}^k\|_{\mathbf{L}^2} + \|\nabla \Psi^k\|_{\mathbf{L}^2}, \tag{4.59}$$

where we have used the Sobolev embedding inequality in three dimensions, the equivalence between $\|\Theta^k\|_{H^1}$ and $\|\nabla \Theta^k\|_{\mathbf{L}^2}$ given by the Poincaré inequality (4.54), and the fact that $\|\nabla \Theta^\tau\|_{\ell^\infty(\mathbf{L}^2(\Omega))} \leq c < \infty$ given by estimate (4.50). Square (4.59) and add over k to get the desired estimate on $\tau^{-1} \delta \nabla \Theta^k$. □

4.5.2 Convergence

The outline of this subsection is similar to that one of §3.5.4. We want to show that solutions generated by the scheme (4.47) converge to the weak solutions of (4.46). The proof relies on classical compactness arguments. We first need the basic energy estimates, and then the estimates on the time derivatives in dual norms. Applying Aubin's lemma we can establish existence of strongly convergent subsequences in $L^2(L^2)$ norms, which is enough to pass to the limit in each term. Finally, we show that weak limits are solutions of (4.46). The construction combines some elements from both [102] and the "discrete transport" theory developed in [104].

The scheme (4.47) generates a sequence of functions $\{\Theta^\tau, \Psi^\tau, \mathbf{M}^\tau, \mathbf{U}^\tau, \mathbf{P}^\tau\}$ corresponding to the nodes $\left\{t^k\right\}_{k=0}^K$, rather than space-time functions. In addition, the scheme (4.47) does not have a variational structure in time. As in §3.5.4, in order to reconcile these differences, we will rewrite scheme (4.47) as a space-time variational formulation. For this purpose, we start by defining the functions $\Theta_{h\tau}$,

$\Psi_{h\tau}$, $\mathbf{M}_{h\tau}$, $\mathbf{U}_{h\tau}$, $P_{h\tau}$ such that

$$\begin{aligned} \Theta_{h\tau} = \Theta^k,\ \Psi_{h\tau} = \Psi^k,\ \mathbf{M}_{h\tau} = \mathbf{M}^k, \\ \mathbf{U}_{h\tau} = \mathbf{U}^k,\ P_{h\tau} = P^k \quad \forall\, t \in (t_{k-1}, t_k],\ k = 1, \ldots, K\,, \end{aligned} \tag{4.60}$$

which are piecewise constant in time.

From scheme (4.47) and using (1.12) we have that $\{\Theta_{h\tau}, \Psi_{h\tau}, \mathbf{M}_{h\tau}, \mathbf{U}_{h\tau}, P_{h\tau}\}$ satisfies

$$\begin{aligned} &(\Theta_{h\tau}(t_F), \Lambda_{h\tau}(t_F)) - \int_0^{t_F-\tau} \Big(\Theta_{h\tau}, \tfrac{\Lambda_{h\tau}(\cdot+\tau)-\Lambda_{h\tau}}{\tau}\Big) \\ &\quad - \int_0^{t_F} (\mathbf{U}_{h\tau}\Theta_{h\tau}(\cdot-\tau), \nabla\Lambda_{h\tau}) + \gamma(\nabla\Psi_{h\tau}, \nabla\Lambda_{h\tau}) = (\Theta_{h\tau}(0), \Lambda_{h\tau}(0))\,, \end{aligned} \tag{4.61a}$$

$$\begin{aligned} &\int_0^{t_F} (\Psi_{h\tau}, \Upsilon_{h\tau}) + \tfrac{1}{\eta}(\Theta_{h\tau} - \Theta_{h\tau}(\cdot-\tau), \Upsilon_{h\tau}) \\ &\quad + \varepsilon(\nabla\Theta_{h\tau}, \nabla\Upsilon_{h\tau}) + \tfrac{1}{\varepsilon}(f(\Theta_{h\tau}(\cdot-\tau)), \Upsilon_{h\tau}) = 0\,, \end{aligned} \tag{4.61b}$$

$$\begin{aligned} &(\mathbf{M}_{h\tau}(t_F), \mathbf{Z}_{h\tau}(t_F)) - \int_0^{t_F-\tau} \Big(\mathbf{M}_{h\tau}, \tfrac{\mathbf{Z}_{h\tau}(\cdot+\tau)-\mathbf{Z}_{h\tau}}{\tau}\Big) \\ &\quad - \int_0^{t_F} b_h^m\big(\mathbf{U}_{h\tau}, \mathbf{Z}_{h\tau}, \mathbf{M}_{h\tau}\big) + \tfrac{1}{\mathscr{T}}\big(\mathbf{M}_{h\tau}, \mathbf{Z}_{h\tau}\big) \\ &\quad = (\mathbf{M}_{h\tau}(0), \mathbf{Z}_{h\tau}(0)) + \tfrac{1}{\mathscr{T}}\int_0^{t_F} \big(\varkappa_\Theta \mathbf{H}_{h\tau}, \mathbf{Z}_{h\tau}\big)\,, \end{aligned} \tag{4.61c}$$

$$\begin{aligned} &(\mathbf{U}_{h\tau}(t_F), \mathbf{V}_{h\tau}(t_F)) - \int_0^{t_F-\tau} \Big(\mathbf{U}_{h\tau}, \tfrac{\mathbf{V}_{h\tau}(\cdot+\tau)-\mathbf{V}_{h\tau}}{\tau}\Big) \\ &\quad + \int_0^{t_F} \big(\nu_\Theta \mathbf{T}(\mathbf{U}_{h\tau}), \mathbf{T}(\mathbf{V}_{h\tau})\big) + b_h\big(\mathbf{U}_{h\tau}, \mathbf{U}_{h\tau}, \mathbf{V}_{h\tau}\big) - \big(P_{h\tau}, div\, \mathbf{V}_{h\tau}\big) \\ &\quad = (\mathbf{U}_{h\tau}(0), \mathbf{V}_{h\tau}(0)) + \int_0^{t_F} b_h^m\big(\mathbf{V}_{h\tau}, \mathbf{H}_{h\tau}, \mathbf{M}_{h\tau}\big) \\ &\quad + \tfrac{\lambda}{\varepsilon}(\Theta_{h\tau}(\cdot-\tau)\nabla\Psi_{h\tau}, \mathbf{V}_{h\tau})\,, \end{aligned} \tag{4.61d}$$

$$\int_0^{t_F} \big(\mathrm{Q}_{h\tau}, div\, \mathbf{U}_{h\tau}\big) = 0\,, \tag{4.61e}$$

for every $\{\Upsilon_{h\tau}, \Lambda_{h\tau}, \mathbf{Z}_{h\tau}, \mathbf{V}_{h\tau}, \mathrm{Q}_{h\tau}\} \in \mathbb{G}_{h\tau} \times \mathbb{Y}_{h\tau} \times \mathbb{M}_{h\tau} \times \mathbb{U}_{h\tau} \times \mathbb{P}_{h\tau}$, where

$$
\begin{aligned}
\mathbb{G}_{h\tau} &= \left\{ \Lambda_{h\tau} \in L^2(0,t_F;\mathbb{G}) \;\middle|\; \Lambda_{h\tau}\big|_{(t_{k-1},t_k]} \in \mathbb{G} \otimes \mathbb{P}_0((t_{k-1},t_k]),\, 1 \le k \le K \right\}, \\
\mathbb{Y}_{h\tau} &= \left\{ \Upsilon_{h\tau} \in L^2(0,t_F;\mathbb{Y}) \;\middle|\; \Upsilon_{h\tau}\big|_{(t_{k-1},t_k]} \in \mathbb{Y} \otimes \mathbb{P}_0((t_{k-1},t_k]),\, 1 \le k \le K \right\}, \\
\mathbb{M}_{h\tau} &= \left\{ \mathbf{Z}_{h\tau} \in L^2(0,t_F;\mathbb{M}) \;\middle|\; \mathbf{Z}_{h\tau}\big|_{(t_{k-1},t_k]} \in \mathbb{M} \otimes \mathbb{P}_0((t_{k-1},t_k]),\, 1 \le k \le K \right\}, \\
\mathbb{U}_{h\tau} &= \left\{ \mathbf{V}_{h\tau} \in L^2(0,t_F;\mathbb{U}) \;\middle|\; \mathbf{V}_{h\tau}\big|_{(t_{k-1},t_k]} \in \mathbb{U} \otimes \mathbb{P}_0((t_{k-1},t_k]),\, 1 \le k \le K \right\}, \\
\mathbb{P}_{h\tau} &= \left\{ \mathrm{Q}_{h\tau} \in L^2(0,t_F;\mathbb{P}) \;\middle|\; \mathrm{Q}_{h\tau}\big|_{(t_{k-1},t_k]} \in \mathbb{P} \otimes \mathbb{P}_0((t_{k-1},t_k]),\, 1 \le k \le K \right\},
\end{aligned}
\tag{4.62}
$$

where $\cdot + \tau$ and $\cdot - \tau$ denote positive and negative shifts in time of size τ.

Expressions (4.60)-(4.62) are the reinterpretation of the Backward-Euler method as a zero-order Discontinuous Galerkin scheme (see for instance [53, 104, 105, 49]). The difference between (4.47) and (4.61) is merely cosmetic, since they are equivalent formulations of the same scheme, but clearly (4.61) has the right structure if we want to compare it with (4.46).

Lemma 4.5.2 (Weak convergence)**.** *The family of functions* $\{\Theta_{h\tau}, \Psi_{h\tau}, \mathbf{M}_{h\tau}, \mathbf{U}_{h\tau}\}_{h,\tau>0}$*, defined in* (4.60) *have the following convergence properties:*

$$
\begin{aligned}
&\Theta_{h\tau} \xrightarrow{h,\tau\to 0}_{*} \theta^* \;\; \textit{in } L^\infty(0,t_F;H^1(\Omega)), \\
&\Psi_{h\tau} \xrightarrow{h,\tau\to 0} \psi^* \;\; \textit{in } L^2(0,t_F;H^1(\Omega)), \\
&\mathbf{M}_{h\tau} \xrightarrow{h,\tau\to 0}_{*} \mathbf{m}^* \;\; \textit{in } L^\infty(0,t_F;\mathbf{L}^2(\Omega)), \\
&\mathbf{U}_{h\tau} \xrightarrow{h,\tau\to 0}_{*} \mathbf{u}^* \;\; \textit{in } L^\infty(0,t_F;\mathbf{L}^2(\Omega)), \\
&\mathbf{U}_{h\tau} \xrightarrow{h,\tau\to 0} \mathbf{u}^* \;\; \textit{in } L^2(0,t_F;\mathbf{H}^1(\Omega)),
\end{aligned}
$$

for some functions θ^**,* ψ^**,* $\mathbf{m}^*$ *and* $\mathbf{u}^*$*. Here* $\rightharpoonup_*$ *denotes weak-star convergence.*

Proof. It is a direct consequence of Proposition 4.5.1 and definition (4.60). □

Note that these modes of convergence are not strong enough to pass to the limit in every term of (4.61), so that the weak limits θ^*, ψ^*, $\mathbf{m}^*$ and $\mathbf{u}^*$ of the previous lemma might not necessarily be solutions of (4.46). In order to improve these estimates we will use the classical Aubin-Lions Lemma 1.2.1.

Lemma 4.5.3 (Strong $L^2(0,t_F;L^2(\Omega))$ convergence)**.** *The family of functions* $\{\Theta_{h\tau},\mathbf{U}_{h\tau}\}_{h,\tau>0}$ *defined in* (4.60) *has the following additional convergence properties:*

$$\Theta_{h\tau} \xrightarrow{h,\tau\to 0} \theta^* \text{ in } L^2(0,t_F;L^2(\Omega))\,,$$

$$\mathbf{U}_{h\tau} \xrightarrow{h,\tau\to 0} \mathbf{u}^* \text{ in } L^2(0,t_F;\mathbf{L}^2(\Omega))\,,$$

for some functions θ^* *and* $\mathbf{u}^*$.

Proof. We would like to apply the estimates from Proposition 4.5.1 and Lemmas 4.5.1 and 1.2.1 directly to the family of functions $\{\Theta_{h\tau},\mathbf{U}_{h\tau}\}_{h,\tau>0}$. However, that is not possible since they are functions which are discontinuous in time. Therefore, we define the following auxiliary functions $\widehat{\Theta}_{h\tau}$ and $\widehat{\mathbf{U}}_{h\tau}$ by:

$$\widehat{\Theta}_{h\tau} = \ell_{k-1}(t)\Theta^{k-1} + \ell_k(t)\Theta^k \quad \forall\, t\in(t_{k-1},t_k]\,,$$

$$\widehat{\mathbf{U}}_{h\tau} = \ell_{k-1}(t)\mathbf{U}^{k-1} + \ell_k(t)\mathbf{U}^k \quad \forall\, t\in(t_{k-1},t_k]\,,$$

where $\ell_{k-1}(t) = (t_k - t)/\tau$ and $\ell_k(t) = (t - t_{k-1})/\tau$. We have that $\widehat{\Theta}_{h\tau}$ and $\widehat{\mathbf{U}}_{h\tau}$ are continuous functions in time, so that:

- $\widehat{\mathbf{U}}_{h\tau}$ and $\widehat{\Theta}_{h\tau}$ converge strongly to some $\mathbf{u}^*$ and θ^* in the $L^2(L^2)$ norm, i.e.

$$\|\widehat{\mathbf{U}}_{h\tau}-\mathbf{u}^*\|_{L^2(0,t_F;\mathbf{L}^2(\Omega))} + \|\widehat{\Theta}_{h\tau}-\theta^*\|_{L^2(0,t_F;L^2(\Omega))} \xrightarrow{h,\tau\to 0} 0\,, \tag{4.63}$$

which is a direct consequence Proposition 4.5.1, the dual norm estimates for the time derivatives of Lemma 4.5.1, and an application of Lemma 1.2.1.

◇ The previous bullet implies that $\mathbf{U}_{h\tau}$ and $\Theta_{h\tau}$ also converge strongly to the same limits $\mathbf{u}^*$ and θ^* in the $L^2(L^2)$ norm. For the velocity $\mathbf{U}_{h\tau}$ this is easy to show using the triangle inequality

$$\|\mathbf{U}_{h\tau} - \mathbf{u}^*\|_{L^2(0,t_F;\mathbf{L}^2(\Omega))} \leq \|\mathbf{U}_{h\tau} - \widehat{\mathbf{U}}_{h\tau}\|_{L^2(0,t_F;\mathbf{L}^2(\Omega))} + \|\widehat{\mathbf{U}}_{h\tau} - \mathbf{u}^*\|_{L^2(0,t_F;\mathbf{L}^2(\Omega))},$$

where clearly the term $\|\widehat{\mathbf{U}}_{h\tau} - \mathbf{u}^*\|_{L^2(0,t_F;\mathbf{L}^2(\Omega))}$ goes to zero because of (4.63), and the term $\|\mathbf{U}_{h\tau} - \widehat{\mathbf{U}}_{h\tau}\|_{L^2(0,t_F;\mathbf{L}^2(\Omega))}$ goes to zero because of the following identity

$$\|\mathbf{U}_{h\tau} - \widehat{\mathbf{U}}_{h\tau}\|^2_{L^2(0,t_F;\mathbf{L}^2(\Omega))} = \tfrac{\tau}{3} \sum_{k=1}^{K} \|\delta\mathbf{U}^k\|^2_{\mathbf{L}^2}$$

and estimate (4.50) for $\sum_{k=1}^{K} \|\delta\mathbf{U}^k\|^2_{\mathbf{L}^2}$. For the phase-field we can show that $\|\Theta_{h\tau} - \theta^*\|_{L^2(0,t_F;L^2(\Omega))} \xrightarrow{h,\tau\to 0} 0$ using the same argument.

This concludes the proof. □

At this point we are in the position to show the main convergence result.

Theorem 4.5.1 (Convergence)**.** *The family of functions* $\{\Theta_{h\tau}, \Psi_{h\tau}, \mathbf{M}_{h\tau}, \mathbf{U}_{h\tau}\}_{h,\tau>0}$,

defined in (4.60) *has the following convergence properties*

$$
\begin{aligned}
&\Theta_{h\tau} \xrightarrow{h,\tau\to 0} \theta^* \ \textit{in}\ L^2(0,t_F;L^2(\Omega))\\
&\Theta_{h\tau} \xrightarrow{h,\tau\to 0}\!\!\!\!\searrow\ \theta^* \ \textit{in}\ L^2(0,t_F;H^1(\Omega))\\
&\Psi_{h\tau} \xrightarrow{h,\tau\to 0}\!\!\!\!\searrow\ \psi^* \ \textit{in}\ L^2(0,t_F;H^1(\Omega))\\
&\mathbf{M}_{h\tau} \xrightarrow{h,\tau\to 0}\!\!\!\!\searrow\ \mathbf{m}^* \ \textit{in}\ L^2(0,t_F;\mathbf{L}^2(\Omega))\\
&\mathbf{U}_{h\tau} \xrightarrow{h,\tau\to 0} \mathbf{u}^* \ \textit{in}\ L^2(0,t_F;\mathbf{L}^2(\Omega))\\
&\mathbf{U}_{h\tau} \xrightarrow{h,\tau\to 0}\!\!\!\!\searrow\ \mathbf{u}^* \ \textit{in}\ L^2(0,t_F;\mathbf{H}^1(\Omega))
\end{aligned}
\tag{4.64}
$$

where $\{\theta^*,\psi^*,\mathbf{m}^*,\mathbf{u}^*\} \in L^2(0,t_F;H^1(\Omega)) \times L^2(0,t_F;H^1(\Omega)) \times L^2(0,t_F;\mathbf{L}^2(\Omega)) \times L^2(0,t_F;\mathbf{H}^1(\Omega))$ *is a weak solution of* (4.46).

Proof. The modes of convergence (weak or strong and their norm) in (4.64) are a consequence of Lemmas 4.5.2 and 4.5.3. It only remains to show that weak limits θ^*, ψ^*, $\mathbf{m}^*$ and $\mathbf{u}^*$ are solutions of the variational problem (4.46). For this purpose we set $\{\Lambda_{h\tau},\Upsilon_{h\tau},\mathbf{Z}_{h\tau},\mathbf{V}_{h\tau}\}$ to be the space-time interpolants/projections of the smooth test functions $\{\lambda,\upsilon,\mathbf{z},\mathbf{v}\}$ of the variational formulation (4.46):

$$
\Lambda_{h\tau} := \mathrm{I}_{\mathbb{G}}\lambda^k,\ \Upsilon_{h\tau} := \mathrm{I}_{\mathbb{Y}}\upsilon^k,\ \mathbf{Z}_{h\tau} := \mathrm{I}_{\mathbb{M}}\mathbf{z}^k,\ \mathbf{V}_{h\tau} := \Pi_s\mathbf{v}^k,\ \forall\, t\in(t_{k-1},t_k]\,. \tag{4.65}
$$

Note that we are using the Stokes projector $\Pi_s\mathbf{v}^k$ (see (1.17) for the definition of the Stokes projector) of the test function $\mathbf{v}^k$ as a discrete test function $\mathbf{V}_{h\tau}$, which means that we are only going to test with discretely divergence-free functions. With

this definition of discrete test functions we get in (4.61):

$$
\begin{aligned}
&-\int_0^{t_F-\tau}\Big(\Theta_{h\tau},\tfrac{\Lambda_{h\tau}(\cdot+\tau)-\Lambda_{h\tau}}{\tau}\Big)-\int_0^{t_F}(\mathbf{U}_{h\tau}\Theta_{h\tau}(\cdot-\tau),\nabla\Lambda_{h\tau})\\
&\quad+\gamma(\nabla\Psi_{h\tau},\nabla\Lambda_{h\tau})=(\Theta_{h\tau}(0),\Lambda_{h\tau}(0))\,,
\end{aligned}
\tag{4.66a}
$$

$$
\begin{aligned}
&\int_0^{t_F}(\Psi_{h\tau},\Upsilon_{h\tau})+\tfrac{1}{\eta}(\Theta_{h\tau}-\Theta_{h\tau}(\cdot-\tau),\Upsilon_{h\tau})\\
&\quad+\varepsilon(\nabla\Theta_{h\tau},\nabla\Upsilon_{h\tau})+\tfrac{1}{\varepsilon}(f(\Theta_{h\tau}(\cdot-\tau)),\Upsilon_{h\tau})=0\,,
\end{aligned}
\tag{4.66b}
$$

$$
\begin{aligned}
&-\int_0^{t_F-\tau}\Big(\mathbf{M}_{h\tau},\tfrac{\mathbf{Z}_{h\tau}(\cdot+\tau)-\mathbf{Z}_{h\tau}}{\tau}\Big)-\int_0^{t_F}b_h^m\big(\mathbf{U}_{h\tau},\mathbf{Z}_{h\tau},\mathbf{M}_{h\tau},\big)\\
&\quad+\tfrac{1}{\mathscr{J}}\big(\mathbf{M}_{h\tau},\mathbf{Z}_{h\tau}\big)=(\mathbf{M}_{h\tau}(0),\mathbf{Z}_{h\tau}(0))+\tfrac{1}{\mathscr{J}}\int_0^{t_F}\big(\varkappa_\Theta\mathbf{H}_{h\tau},\mathbf{Z}_{h\tau}\big)\,,
\end{aligned}
\tag{4.66c}
$$

$$
\begin{aligned}
&-\int_0^{t_F-\tau}\Big(\mathbf{U}_{h\tau},\tfrac{\mathbf{V}_{h\tau}(\cdot+\tau)-\mathbf{V}_{h\tau}}{\tau}\Big)+\int_0^{t_F}\big(\nu_\Theta\mathbf{T}(\mathbf{U}_{h\tau}),\mathbf{T}(\mathbf{V}_{h\tau})\big)\\
&\quad+b_h\big(\mathbf{U}_{h\tau},\mathbf{U}_{h\tau},\mathbf{V}_{h\tau}\big)-\big(P_{h\tau},div\,\mathbf{V}_{h\tau}\big)=(\mathbf{U}_{h\tau}(0),\mathbf{V}_{h\tau}(0))\\
&\quad+\int_0^{t_F}b_h^m\big(\mathbf{V}_{h\tau},\mathbf{H}_{h\tau},\mathbf{M}_{h\tau}\big)+\tfrac{\lambda}{\varepsilon}(\Theta_{h\tau}(\cdot-\tau)\nabla\Psi_{h\tau},\mathbf{V}_{h\tau})\,,
\end{aligned}
\tag{4.66d}
$$

$$
\int_0^{t_F}\big(\mathrm{Q}_{h\tau},div\,\mathbf{U}_{h\tau}\big)=0\,,
$$

where the terms evaluated at time $t=t_F$ have disappeared because of the compact support of the test functions $\{\lambda,\upsilon,\mathbf{z},\mathbf{v}\}$ and their discrete counterparts $\{\Lambda_{h\tau},\Upsilon_{h\tau},\mathbf{Z}_{h\tau},\mathbf{V}_{h\tau}\}$. Now we will pass to the limit term by term in (4.66):

◇ We start with the terms with the time derivatives, which are straightforward:

$$
\begin{aligned}
-\int_0^{t_F-\tau}\Big(\Theta_{h\tau},\tfrac{\Lambda_{h\tau}(\cdot+\tau)-\Lambda_{h\tau}}{\tau}\Big)\quad&\xrightarrow{h,\tau\to0}\quad-\int_0^{t_F}(\theta^*,\lambda_t)\,,\\
-\int_0^{t_F-\tau}\Big(\mathbf{M}_{h\tau},\tfrac{\mathbf{Z}_{h\tau}(\cdot+\tau)-\mathbf{Z}_{h\tau}}{\tau}\Big)\quad&\xrightarrow{h,\tau\to0}\quad-\int_0^{t_F}(\mathbf{m}^*,\mathbf{z}_t)\,,\\
-\int_0^{t_F-\tau}\Big(\mathbf{U}_{h\tau},\tfrac{\mathbf{V}_{h\tau}(\cdot+\tau)-\mathbf{V}_{h\tau}}{\tau}\Big)\quad&\xrightarrow{h,\tau\to0}\quad-\int_0^{t_F}(\mathbf{u}^*,\mathbf{v}_t)\,,
\end{aligned}
$$

because of the weak $L^2(L^2)$ convergence of $\Theta_{h\tau}$, $\mathbf{M}_{h\tau}$ and $\mathbf{U}_{h\tau}$, and the strong convergence of the finite differences $\frac{\Lambda_{h\tau}(\cdot+\tau)-\Lambda_{h\tau}}{\tau}$, $\frac{\mathbf{Z}_{h\tau}(\cdot+\tau)-\mathbf{Z}_{h\tau}}{\tau}$ and $\frac{\mathbf{V}_{h\tau}(\cdot+\tau)-\mathbf{V}_{h\tau}}{\tau}$

guaranteed by the regularity of the test functions.

◇ We continue with the convective terms. We start with the convective term of (4.66a)

$$-\int_0^{t_F}(\mathbf{U}_{h\tau}\Theta_{h\tau}(\cdot-\tau),\nabla\Lambda_{h\tau}) \quad \xrightarrow{h,\tau\to 0} \quad -\int_0^{t_F}(\mathbf{u}^*\theta^*,\nabla\lambda)$$

for which the convergence modes in (4.64) are more than we need: for $\mathbf{U}_{h\tau}$ and $\Theta_{h\tau}$ we just need them to converge one weak and one strong in $L^2(L^2)$, and the strong convergence of $\nabla\Lambda_{h\tau}$ guaranteed by (1.13) and the regularity of the test function λ.

◇ For the convective term of (4.66c), we proceed as in (3.84)-(3.85). For the Kelvin force in (4.66c) we proceed as in (3.86). Here is where the use of a discontinuous pressure space, and the choice $\mathbb{M}=[\mathbb{P}]^d$, play a critical role.

◇ We have to show that the stabilization term in (4.66b) vanishes in the limit:

$$\int_0^{t_F}\tfrac{1}{\eta}(\Theta_{h\tau}-\Theta_{h\tau}(\cdot-\tau),\Upsilon_{h\tau})=\tfrac{1}{\eta}\sum_{k=1}^{K}\tau(\delta\Theta^k,\Upsilon^k)\leq$$
$$\leq\tfrac{1}{\eta}\left(\sum_{k=1}^{K}\tau\|\delta\Theta^k\|_{L^2}^2\right)^{1/2}\left(\sum_{k=1}^{K}\tau\|\Upsilon^k\|_{L^2}^2\right)^{1/2}\lesssim\tau^{1/2}\,,$$

which follows by the stability estimate (4.50).

◇ Finally, the only critical term is $\int_0^{t_F}\big(\nu_\Theta\mathbf{T}(\mathbf{U}_{h\tau}),\mathbf{T}(\mathbf{V}_{h\tau})\big)$ in (4.66d), passage to the limit

$$\int_0^{t_F}\big(\nu_\Theta\mathbf{T}(\mathbf{U}_{h\tau}),\mathbf{T}(\mathbf{V}_{h\tau})\big) \quad \xrightarrow{h,\tau\to 0} \quad \int_0^{t_F}\big(\nu_{\theta^*}\mathbf{T}(\mathbf{u}^*),\mathbf{T}(\mathbf{v})\big) \tag{4.67}$$

uses strong $L^2(L^2)$ convergence of θ^*, the Lipschitz continuity property of ν_θ, the weak $L^2(L^2)$ convergence of $\nabla \mathbf{U}_{h\tau}$, and strong convergence of $\nabla \mathbf{V}_{h\tau}$ from estimate (1.20) (see assumption 3 at the beginning of §4.5.1).

The remaining terms require little or no explanation, or the passage to the limit can be found in other works such as [102, 105, 103]. □

Remark 4.5.2 (Choice of finite element spaces)**.** For the two dimensional case, the choice of finite element spaces for scheme (4.47) can be the following one: $\mathbb{M}$ will be the same as that one defined in (3.53), the spaces $\mathbb{G}$ and $\mathbb{Y}$ will be the same as in (4.44), while the Stokes pair $\{\mathbb{U}, \mathbb{P}\}$ will be the Crouzeix-Raviart pair defined in (3.87), which uses $\mathcal{P}_1$ discontinuous pressures. These choices of finite element spaces are far from arbitrary, part of the motivations (constraints) in this construction where explained in §3.4.2 and are also motivated by consistency analysis carried out in §3.5.4.

Remark 4.5.3 (Stabilization)**.** For the sake of simplicity, we have presented the numerical scheme (4.47) without any form of stabilization (upwinding). Unlike Continuous Galerkin methods, DG schemes do not need any form of additional numerical stabilization in order to work. However, without some form of linear stabilization they will deliver sub-optimal convergence rates to smooth solutions (see for instance [125, 87]). Numerical stabilization can be incorporated by adding the term

$$s_h^{\text{up}}(\mathbf{U}^k, \mathbf{M}^k, \mathbf{Z}) = \tfrac{1}{2} \sum_{F \in \mathcal{F}^i} \int_F |\mathbf{U}^k \cdot n_F| \left[\!\left[\mathbf{M}^k\right]\!\right] \cdot [\![\mathbf{Z}]\!] \, dS \tag{4.68}$$

to the left-hand side of (4.47c). With such a modification all the results presented above remain unchanged.

4.6 Numerical Experiments

4.6.1 General considerations

Let us now explore model (4.13) and scheme (4.30) with a series of examples. The main goal of these experiments is to assess the robustness of scheme (4.30) and to show the reader the ability of the model to capture some well-known phenomena observed in real ferrofluids. In all these experiments we will use the magnetic field due to 2d point dipoles already discussed in §3.7 (see (3.90) and (3.91)).

On the other hand, in order to carry out meaningful computations of phase-field models it is crucial to resolve the transition layer, otherwise artificial spurious oscillations will arise (cf.[126, 127, 128]). Even in the context of two dimensional simulations, using for instance $\varepsilon = 0.01$, and resolving the transition layer by means of uniform meshes can turn out to be prohibitively expensive and slow. If we want to obtain results in a timely fashion, computations of phase-field models claiming to have any practical value will invariably need some form of adaptivity. Our work is no exception, and for that reason we will use adaptivity in space, which entails using numerical schemes which are not covered by the theory developed in this paper.

The implementation has been carried out with the help of the `deal.II` library, see [70, 71]. In particular the parallel-adaptive framework discussed in [129, 130] was extensively used in this work. Regarding error indicators we have used the simplest

indicator, basically

$$\eta_T^2 = h_T \int_{\partial T} \left| \left[\!\left[\frac{\partial \Theta}{\partial n} \right]\!\right] \right|^2 dS \tag{4.69}$$

widely attributed to [131]. Computationally, it is well-known that (4.69) performs reasonably well for second order elliptic and parabolic problems. This error indicator is already implemented in the library `deal.II`, being that the main reason for its selection. From a mathematical point of view, using (4.69) is questionable, since residual a posteriori error indicators for phase-field models (Allen-Cahn and Cahn-Hilliard) have been an area of major research; the interested reader can check [132, 133] and references therein. The marking strategy follows the Dörfler (or bulk chasing) approach, requiring in this time dependent context, marking for refinement, and in addition, marking for coarsening (a judiciously small fraction). The mesh will be refined-coarsened once every 5 time steps.

4.6.2 Parametric study of the Rosensweig instability

The purpose of this section is to run a series of parametric studies with respect to h and τ in order to assess the robustness of scheme (4.30) with respect to these two parameters. In order to run such studies, we have chosen to use the Rosensweig instability (also called normal-field instability) as an example. We will start by explaining the setup of the parameters of the model. Then we will explain what the Rosensweig instability is, provide some well-known analytic results, and point to some background references for the interested reader. Finally, we will use these analytic results to tweak the numerical experiment, and run the parametric study.

Regarding inertial scalings, we will work in a rectangular domain of 1 unit of width and 0.6 units of height, with vertices at $(0,0)$, $(0,0.6)$, $(1,0.6)$ and $(1,0)$. So that $diam\,\Omega \approx 1$, together with the following parameters

$$\nu_w = 1.0 \text{ and } \nu_f = 2.0\,,$$

and the density ρ implicitly taken (from the very beginning of the paper) to be unitary, we have that $Re = \mathcal{O}(\|\mathbf{u}\|_{\mathbf{L}^\infty(\Omega\times(0,t_F))})$. On the other hand, we will use $\mu_0 = 1$, $\varkappa_0 = 0.5$, $\gamma = 0.0002$, $\lambda = 0.05$, and we will set the coefficient r of (4.18) equal to 0.1. The main goal of such an arbitrary choice of parameters (ν_w, ν_f, ρ, μ_0, $\varkappa_0$, γ and λ) is to have a very stable PDE system. Note that in (4.19) and (4.31) all the natural estimates for the phase-field and chemical potential depend on λ, thus for small values of λ, we should expect the stability of the interfaces (and the whole PDE system (4.13) in general) to deteriorate severely. With such a deliberate choice of parameters we will have a very stable system of equations, paradoxically, now we will try to come up with a smart scaling of the forces in order to get an interesting (unstable) behavior as it will be detailed in the following paragraphs.

The Rosensweig instability (also called normal field instability) is perhaps the simplest nontrivial phenomena observed in ferrofluids. Basically, if we have a pool of ferrofluid lying horizontally, subject to the force of gravity, and also subject to a uniform magnetic field $\mathbf{h}_a$ pointing upwards, it is well known that a flat profile will not be stable for all values of the magnetic field and a regular pattern of peaks and valleys will form. The formation of these patterns is the result of competing forces: both gravity and surface tension favor a flat surface, but above a critical

magnetic field strength, the flat profile will not be the most stable configuration. A sufficiently strong magnetic field will trigger the instability and the pattern will form. We give some references in the following paragraph.

There are analytical expressions for the distance between the peaks and for the critical magnetic field strength that triggers the instability. There is a vast literature on this topic and it is impossible to do justice to all possible references, here we will just comment on a few of them as background for the interested reader. The work of Cowley and Rosensweig [134] is most probably the first one to provide analytical results based on linear stability analysis (dependence of the most unstable modes on the constitutive parameters) valid only in the asymptotic limit of vanishing magnetic susceptibility $\varkappa_0$:

$$\ell_c = 2\pi \left(\frac{\sigma}{g\Delta\rho} \right)^{1/2} \quad , \quad m_c^2 = \tfrac{2}{\mu_0} \left(\tfrac{2+\varkappa_0}{1+\varkappa_0} \right) \left(g\Delta\rho\sigma \right)^{1/2} \, , \tag{4.70}$$

where ℓ_c is the critical spacing between the peaks, m_c is the critical magnetization, σ is the surface tension coefficient in the sharp interface limit, $g = |\mathbf{g}|$ is the magnitude of the gravity, and $\Delta\rho$ is the jump of the density across the interface. The work of Gailitis [135] using an energetic approach (minimization of a functional), considered to be the first attempt to include nonlinear effects, was able describe the shape of the patterns (hexagons, squares, etc), but still suffers from the same limitations of the work of Cowley and Rosensweig (small susceptibilities, finite depth, etc). The work [136] overcomes, to some degree, the deficiencies of the work of Gailitis. Validation of all these analytical results is far from complete, requiring carefully crafted experiments which mimic ideal conditions, some efforts in this direction can

be found in [137, 113].

Most of these results are useful for their qualitative value, but they are far from accurate for any realistic context which could include finite magnetic susceptibilities, finite depth of the ferrofluid pool, nonlinear effects (large displacements of the interface between both phases), and diffusive effects (partial mixture). In particular, to the best of the author's knowledge, there are not analytical results for highly paramagnetic ferrofluids ($\varkappa_0 > 1$), and the treatment (or inclusion) of effects related to the demagnetizing field is quite poor.

For instance, we cannot expect the linear stability result (4.70) to accurately predict the behavior of system (4.13) in the context of bounded domains (with non-periodic boundary conditions), finite depth, finite magnetic susceptibility ($\varkappa_0 = \mathcal{O}(1)$), highly deformed transition layer (not a straight line), and finite interaction length (layer thickness ε) involving additional diffusive effects. We also have that our phase-field model is not a genuine variable density model, so that the term $\Delta\rho$ has very little meaning in the context of the model (4.13), and gravitational effects are only included approximately via (4.18). Finally, the relationship between the capillary coefficient λ and the surface tension σ (see for instance [122, 138]) is only known approximately

$$\lambda \sim \sigma\varepsilon\,, \tag{4.71}$$

where the constant involved in this relationship is unknown but of $\mathcal{O}(1)$. Yet, it can be proved that the linear relationship (4.71) is particularly accurate for small mobilities γ (see [139]), being that the reason why we chose $\gamma = 0.0002$.

Taking a giant leap of faith, we can only expect (4.70) to be able to deliver the right order of magnitude for the relationship between the gravity g and the surface tension coefficient σ which could yield a predetermined number of peaks. Let's consider that we want four peaks inside our unit length box, that is $\ell_c = 0.25$, combining (4.70) and (4.71), and inserting our choice of parameters ($\varepsilon = 0.01$, $\lambda = 0.05$, $\Delta\rho \approx 0.1$, $\ell_c = 0.25$) we get:

$$g = \frac{4\pi^2\sigma}{\ell_c^2\Delta\rho} \sim \frac{4\pi^2\lambda}{\ell_c^2\Delta\rho\varepsilon} \approx 3 \cdot 10^4 \tag{4.72}$$

This number is just telling us that, if we want to obtain four peaks inside our unit-size box, the appropriate order of magnitude for the gravity is 10^4. We will use (4.72) as an educated guess and load $\mathbf{g} = (0, -30000)^T$ in the computer code.

In order to generate a pseudo-uniform magnetic field, we will place 5 dipoles pointing upwards, that is $\mathbf{d} = (0, 1)^T$ (see formula (3.90)), sufficiently far away from our rectangular box, so that for most practical purposes the magnetic field is uniform, having only a slight gradient (decay) in the y direction. The coordinates $\mathbf{x}_s$ of the dipoles will be $(-0.5, -15)$, $(0, -15)$, $(0.5, -15)$, $(1, -15)$ and $(1.5, -15)$. The intensity α_s (see expression (3.91)) will be the same for each dipole but will evolve in time. More precisely, α_s will be ramp-loaded starting from $\alpha_s = 0$ at time $t = 0$ to its maximum value $\alpha_s = 6000$ at time $t = 1.6$, and from time $t = 1.6$ to $t = 2.0$ the intensity of the dipoles will be kept constant in order to let the system rest and develop a stable configuration.

Regarding the space discretization, the initial mesh will have 10 elements in the x direction and 6 units in the y direction, and allow for a maximum refinement

of 4, 5, 6 and 7 levels. On the other hand, regarding time discretization we will use 1000, 2000, 4000, and 8000 time steps for a total of 2 units of simulation time.

With this non-trivial setup, involving a choice of coefficients, a specific configuration of the external magnetic field $\mathbf{h}_a$, and space adaptivity, the reader can visualize some numerical results in Figure 4.1. The simulation starts with a ferrofluid pool of 0.2 units of depth at rest at time $t = 0$, and at time $t = 2.0$ we have not obtained exactly four peaks inside the box as we desired, but clearly (4.72) was able to deliver a very reasonable initial guess. In Figure 4.2 we show a sample finite element mesh corresponding to the simulation of Figure 4.1. In Figure 4.1 we can see that most of the interesting dynamics happens from times $t = 0.7$ to $t = 1.4$. Therefore, we will focus on the interval of time $[0.7, 1.4]$ for a parametric study in order to show the robustness of this simulation with respect to the discretization parameters h and τ. Figures 4.3 and 4.4 show the results of the parametric study with respect to the space and time discretization respectively. The results from Figure 4.1 correspond to the third column of Figures 4.3 and 4.4 which, as it can be appreciated, is a meaningful (well-resolved) solution.

The Rosensweig instability considered in this section, in practice, can only be reproduced under carefully controlled laboratory conditions. That is, this instability is not the most common form of ferrofluid instability we can find in everyday experiments (such as commercial ferrofluid toys) since in practice most magnetic fields are by no means uniform nor have magnetic field lines very aligned. This is the reason why in §4.6.3 we will consider a much more mundane (common) form of the Rosensweig instability, involving non-uniform magnetic fields with relatively

poor alignment of the magnetic field lines.

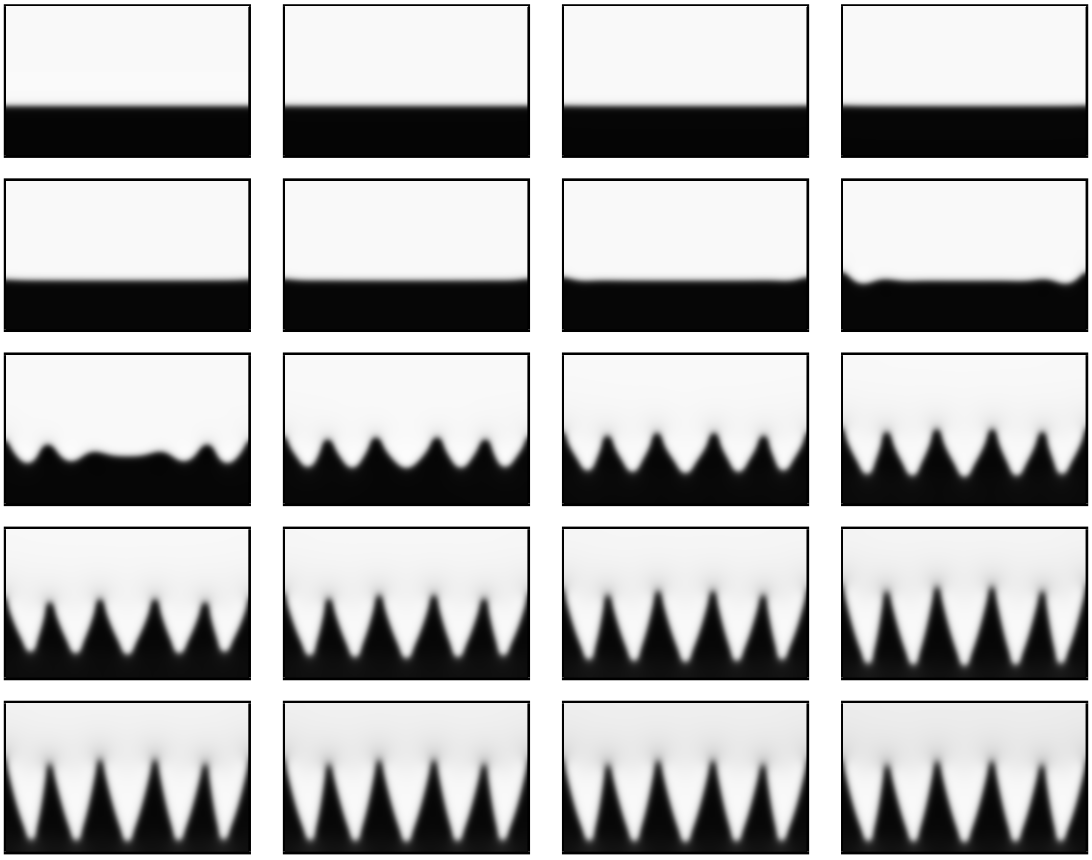

Figure 4.1: **Rosensweig instability: evolution screenshots.** Sequence of screen shots from time $t = 0.1$ to $t = 2.0$ in regular intervals of 0.1 showing the evolution of the phase-field variable Θ (read from left-to-right and top-to-bottom). As it can be appreciated, we obtained in the order of 4 peaks inside the box, showing us that the crude estimate (4.72) was a very good initial guess for the scaling between the capillary coefficient λ and the gravity g. Note that diffusive effects are quite noticeable as we are using $\varepsilon = 0.01$. Most of the interesting transient behavior happens from time $t = 0.7$ to $t = 1.3$ (reading from left-to-right and top-to-bottom: boxes 7 to 13), so we will focus on this interval for a parametric study. This simulation was obtained using 6 levels of refinement in space, and 4000 times steps for a total of 2 seconds of simulation.

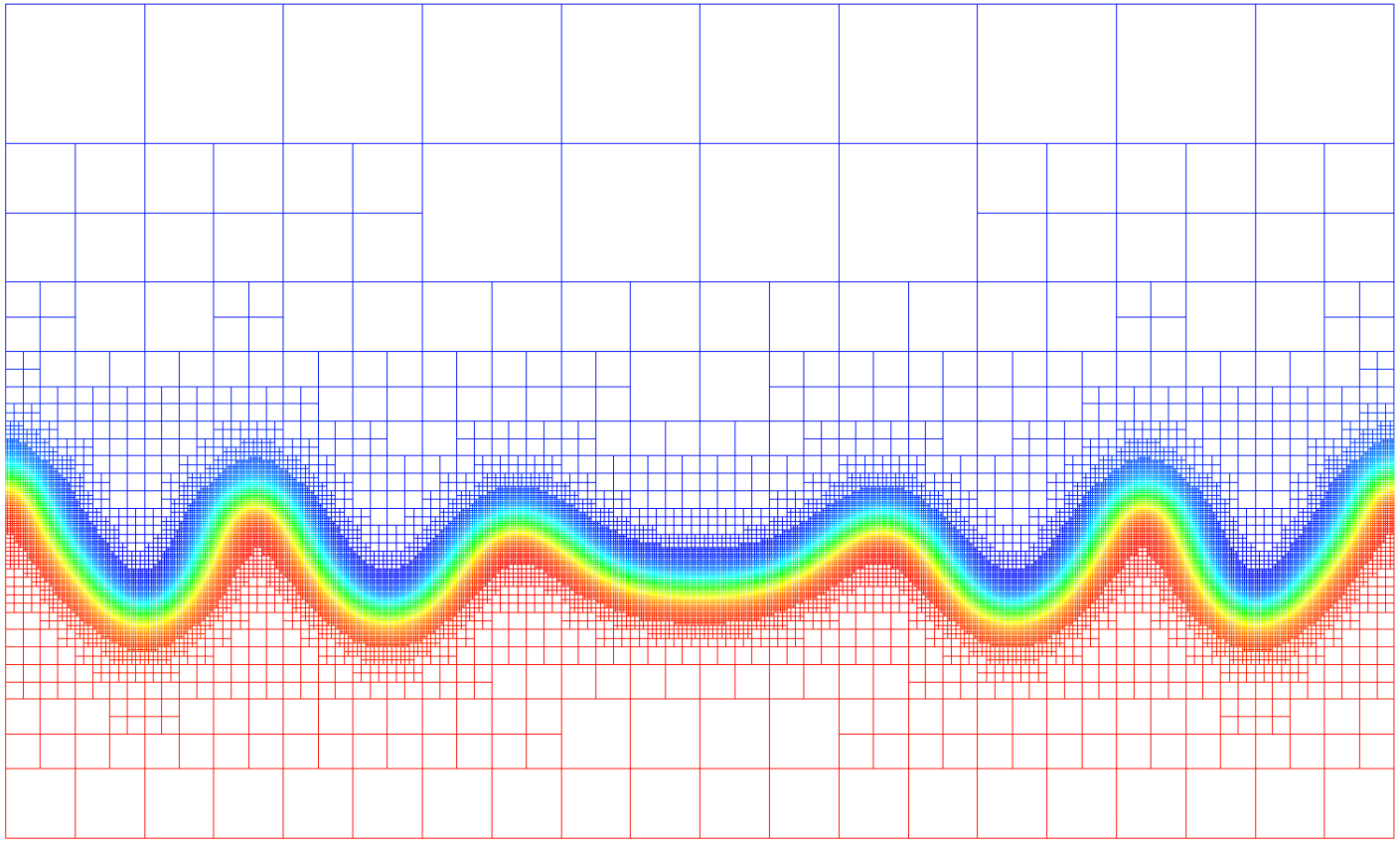

Figure 4.2: **Rosensweig instability: sample mesh.** Finite element mesh with 6 levels of refinement at time $t = 0.92$, corresponding with the simulation of Figure 4.1. In order to have meaningful (well-resolved) simulation we need approx. 20 elements of the finest level resolving the transition layer.

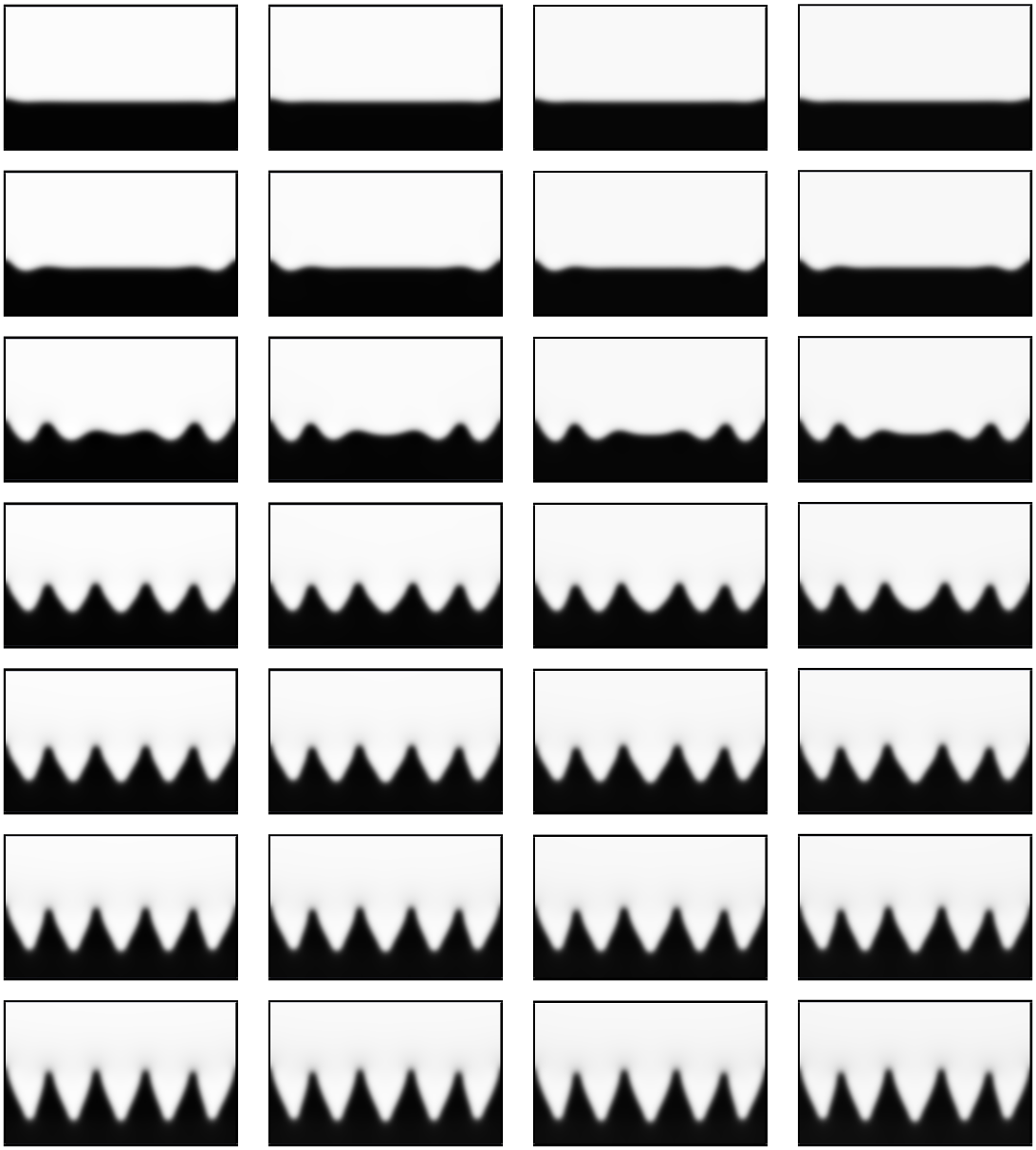

Figure 4.4: **Parametric study: time discretization.** This figure shows the results obtained from time $t = 0.7$ (uppermost row) to time $t = 1.3$ (lowermost row) using 6 levels of refinement is space and four different time discretizations: the coarsest time discretization uses 1000 times steps (first column), 2000 time steps (second column), 4000 time steps (third column), and the finest discretization 8000 time steps (fourth column). The reader can appreciate that even the coarsest time discretization does not generate artificial or spurious features in the numerical solution.

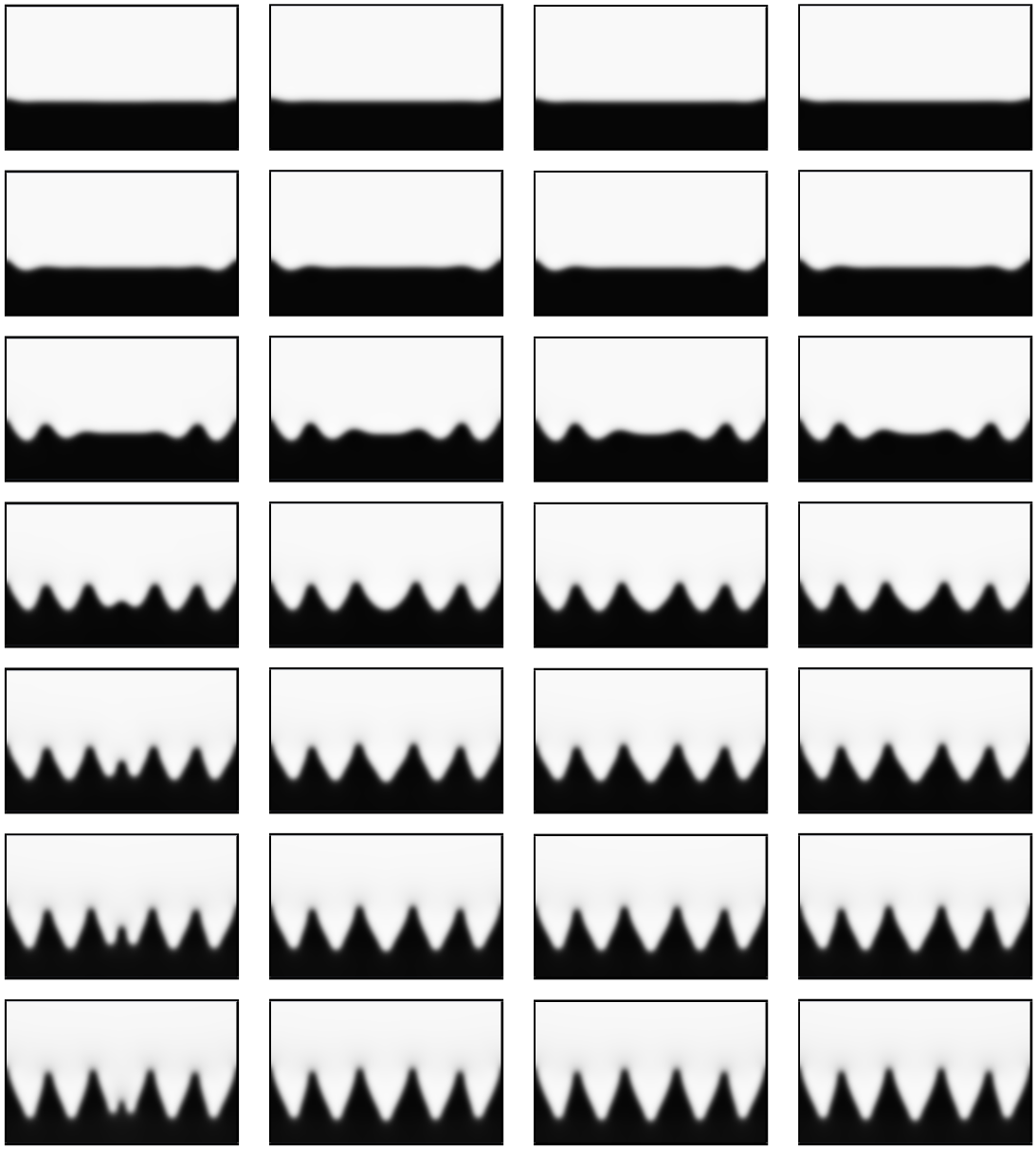

Figure 4.3: **Parametric study: space discretization.** This figure shows the results obtained from time $t = 0.7$ (uppermost row) to time $t = 1.3$ (lowermost row) using 4000 time steps and four different levels of refinement in space: the coarsest mesh uses 4 levels of refinement (first column), 5 levels (second column), 6 levels (third column), and the finest mesh uses 7 levels (fourth column). The reader can appreciate that with the coarsest mesh (leftmost column) the numerical solution exhibits artificial features which do not survive additional refinement. In particular, we have an additional spike in the middle for the case of the coarsest mesh (first column) which is not present in the second, third and fourth columns. This simple examples illustrates the importance of parametric studies in the context of phase-field methods.

4.6.3 The ferrofluid hedgehog

In this section we will carry out two numerical experiments in order to explore the effects of a different kind of magnetic field (not uniform), depth of the ferrofluid pool, and the effects of the demagnetizing field. For these experiments we will use the same constitutive constants that we used for Experiment 4.6.2, with exception of the magnetic susceptibility which we will set to be $\varkappa_0 = 0.9$, the layer thickness ε will be set to $\varepsilon = 0.005$ to reduce diffusive effects and get sharper interfaces, and $\lambda = 0.025$ to get slightly more unstable interfaces (easier to perturb). The depth of the ferrofluid pool will be now of 0.11 units. We will still use 6 levels of refinement, but the initial mesh will have 15 elements in the x direction and 9 elements in the y direction. Regarding temporal discretization we will use a total of 24000 times steps for 6 units of simulation time.

It is clear that we are changing many parameters at the same time (magnetic susceptibility, pool depth, capillarity coefficient, and layer thickness), in such a way that we will not be able to understand the separate influence of each of them on the behavior of the system. Doing a parametric/sensitivity study of all these variables (modifying only one variable at a time) would be highly desirable, but that would involve an ambitious separate analysis. By now, the purpose of this section is just to showcase other interesting phenomena (another instance of the Rosensweig instability) that we can obtain with this simple PDE model. We will call the instability obtained in these experiments the "ferrofluid hedgehog", because of its natural resemblance with the spiny mammal.

The main reason to use a higher magnetic susceptibility $\varkappa_0$ is making the effects of the demagnetizing field $\mathbf{h}_d$ much more pronounced than those of Experiment 4.6.3. As it will be shown later, the demagnetizing field $\mathbf{h}_d$ plays a fundamental role in the instability.

The experiments will be carried out in the same rectangular domain used for Experiment 4.6.2 (with vertices at $(0,0)$, $(0,0.6)$, $(1,0.6)$ and $(1,0)$). The magnetic field $\mathbf{h}_a = \sum_s \alpha_s \nabla\phi_s$ will be generated by a set of 42 dipoles. More precisely, we want to create a crude "discrete" approximation of what would be the magnetic field due to a bar magnet of 0.4 units of width and 0.5 units of height pointing upwards (i.e. $\mathbf{d} = (0,1)^T$ again). The dipoles will be located in three rows (each row will have 14 dipoles): one at $y = -0.5$, $y = -0.75$ and $y = -1.0$, and the 14 dipoles will be equi-distributed in the x direction as shown in Figure 4.5. The main idea of this setup is to create a non-uniform magnetic field, with an open pattern of magnetic field lines (as sketched in Figure 4.5) rather than aligned magnetic field lines (as it was the case of Experiment 4.6.2).

The intensity α_s will be the same for each dipole, but it will evolve in time. More precisely, α_s will be ramp-loaded starting from $\alpha_s = 0$ at time $t = 0$, to its maximum value $\alpha_s = 4.3$ at time $t = 4.2$, and from time $t = 4.2$ to $t = 6.0$ the intensity of the dipoles will be kept constant in order to let the system rest and develop a stable configuration. The motivation behind a longer simulation time (6 units) and the maximum intensity $\alpha_s = 4.3$, it to push the system to a barely stable configuration at the brink of a second transition, so that allowing more simulation time, the system could evolve and capture more non-trivial evolution.

Numerical results using the complete (effective) magnetizing field defined in (4.11) and (4.12) (same as (3.2) and (3.18) respectively) are displayed in Figure 4.6. Numerical results using the definition $\mathbf{h} := \mathbf{h}_a$ can be found in Figure 4.7. Simulations 4.6 and 4.7 are strikingly different, highlighting the importance of using a physically reasonable definition for effective magnetizing field $\mathbf{h}$, and the influence of the demagnetizing field $\mathbf{h}_d$ (see (3.9)-(3.10) for the exact definition of the demagnetizing field $\mathbf{h}_d$, and (3.15) for the crude approximation used in these simulations) in the overall behavior of the system.

Even though (4.12), used in Figures (4.1)-(4.6), is a questionable approach to compute an approximation of $\mathbf{h} = \mathbf{h}_a + \mathbf{h}_d$, it keeps the influence of $\mathbf{h}_d$ alive, and is able to deliver the classical Rosensweig instability (even able to respect the scaling (4.72) reasonably well) in the context of uniform magnetic fields (see Figure 4.1), and the more common version of the Rosensweig instability in the context of non-uniform magnetic fields, as shown for instance in Figure 4.6.

Many attempts to model and explain the Rosensweig instability (and ferrofluid behavior in general) found in the literature (cf.[137, 136, 116, 117, 115, 23]), pay special attention to the modeling of non-linear susceptibilities and saturation effects (usually carried out with the Langevin function). However, they rarely ever elaborate on the effective magnetizing field, the demagnetizing field (also called stray field), and their approximation/computation. They are sometimes not even mentioned in the entire text.

Saturation is indeed an important component in the physical behavior of magnetic materials, specially if we are working past the saturation limit, however it is

the opinion of the author that current emphasis on the modeling of saturation effects is somehow not commensurate with its actual impact in the physical behavior of ferrofluids. Preliminary computational experiments carried out by the author (not reported) seem to indicate that the modeling of saturation effects add almost imperceptible nuances in the overall behavior of the system, while proper computation of the effective field (using (4.12) or a better approximation if possible) has much more striking consequences in the global behavior of the system (particularly relevant for the study of the Rosensweig instability). Those consequences can be as noticeable as the difference between Figures 4.6 and 4.7.

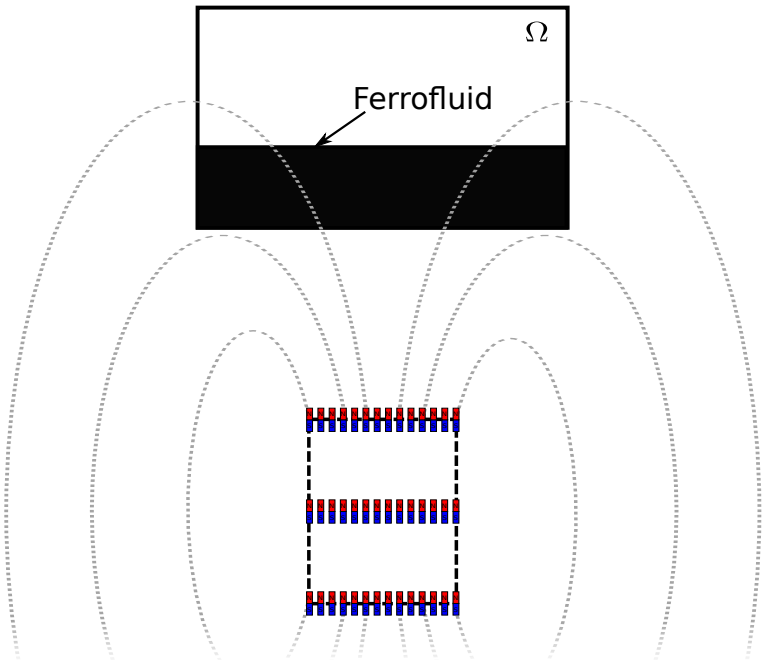

Figure 4.5: **The ferrofluid hedgehog: setup of the dipoles.** Setup of the dipoles for the Experiment 4.6.3, showing our rectangular domain Ω with the ferrofluid (dark region) in the bottom of the box, and the arrangement of the dipoles below Ω. The 42 dipoles are located in three rows in the lower part of the picture, here represented like small bar magnets, delivering a coarse approximation of what would be the magnetic field due to a bar magnet. The idea of such a configuration is to obtain an open pattern of magnetic field lines and steeper gradients than those of Experiment 4.6.2.

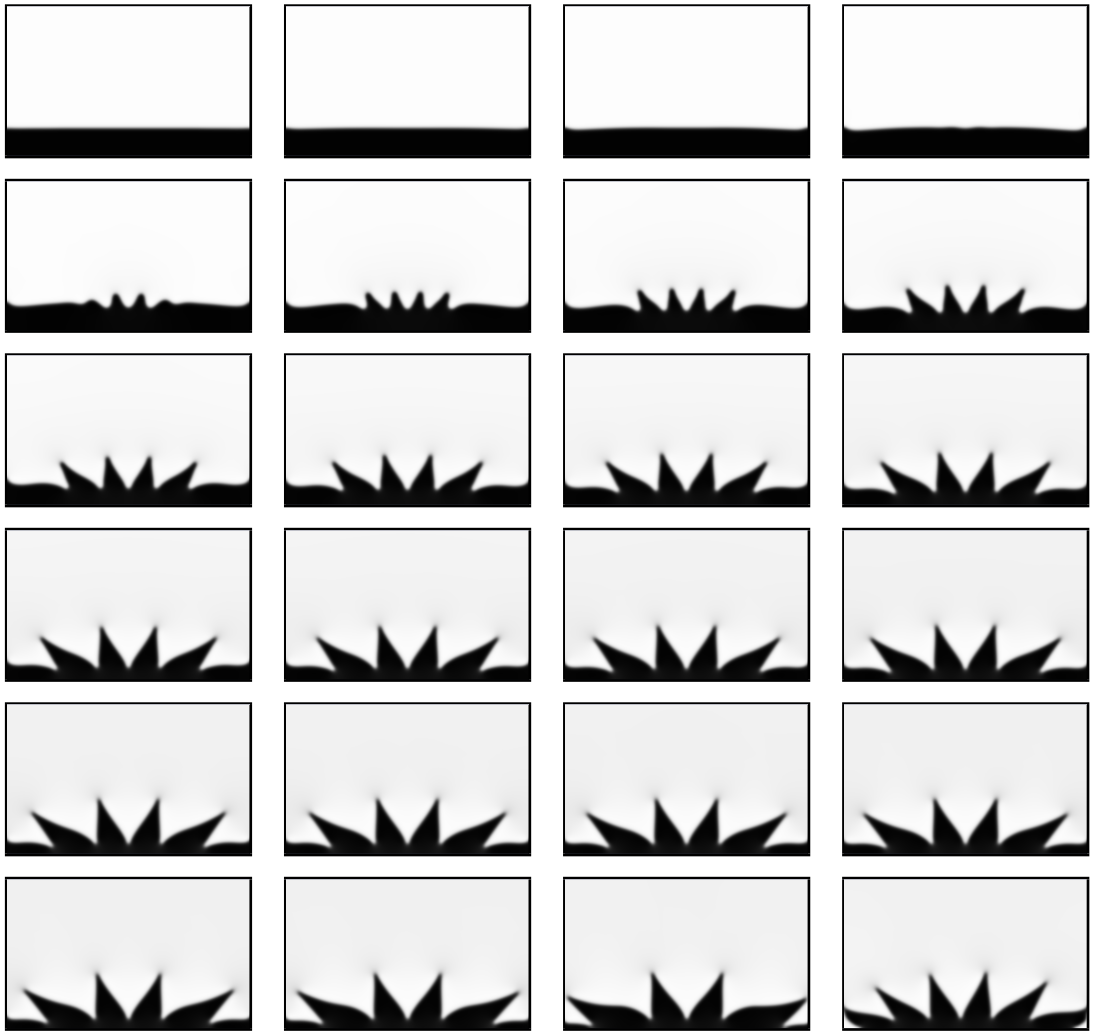

Figure 4.6: **The ferrofluid hedgehog: using the complete magnetizing field**. This figure shows another instance of the Rosensweig instability, this time with a non-uniform magnetic field (see Figure 4.5 for details regarding the source of magnetic field). This computation was carried out using the definition (4.11)-(4.12) (same as (3.2) and (3.18) respectively in *Chapter 3*) for the effective magnetizing field. The instability manifests, but not in the same way it did in Experiment 4.6.2, see Figure 4.1. Now the ferrofluid spikes exhibit an open pattern, just like the magnetic field $\mathbf{h}_a$ driving the system. In addition, note that the interface starts flat, it develops four spikes in the middle region (where there is a narrow band of quasi-uniform magnetic field pointing upwards), the configuration with four spikes remains quite stable throughout most of the simulation time, but finally it has a second (much faster) transition from four to six spikes which can be appreciated in the last two frames. This numerical experiment clearly exhibits a resemblance with physical experiments shown in Figures 4.8 and 4.9.

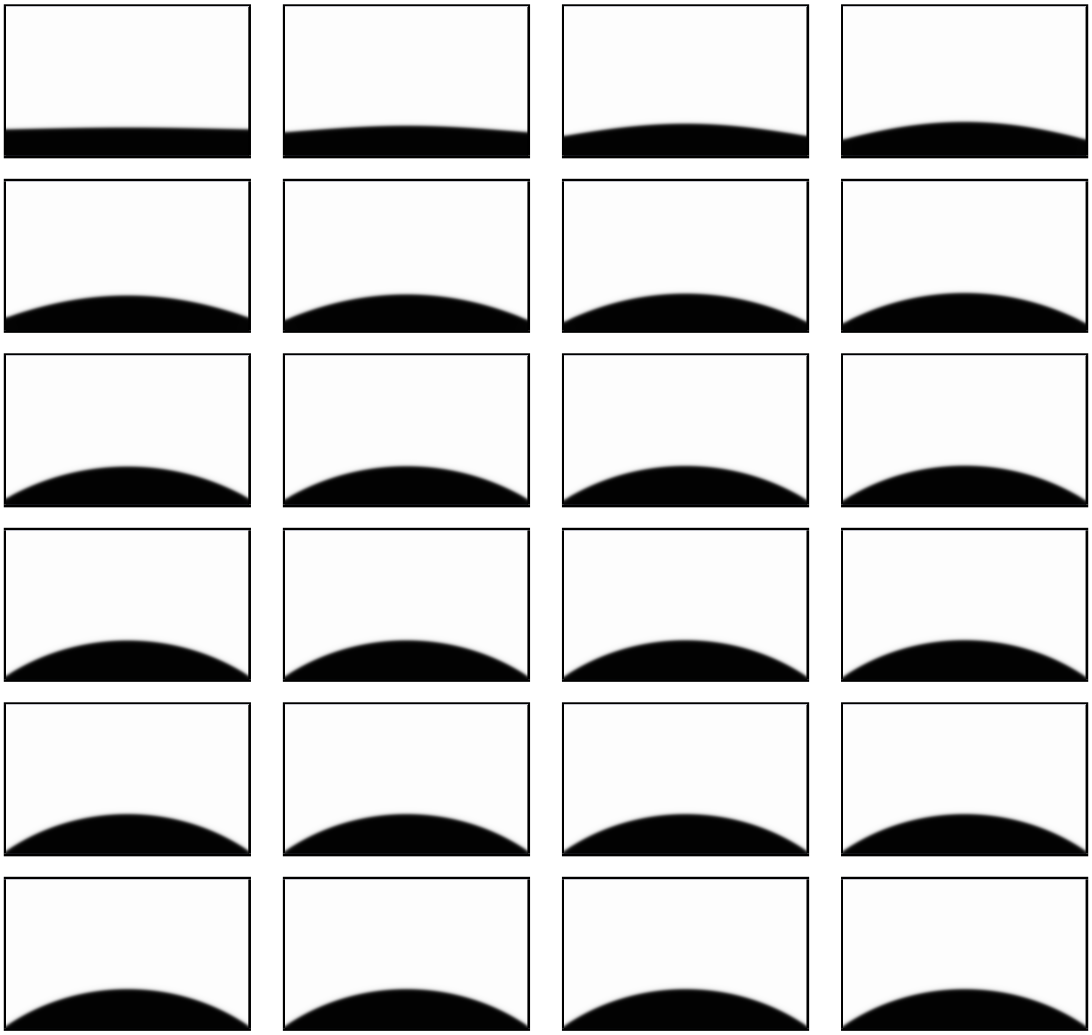

Figure 4.7: **The ferrofluid hedgehog (attempt): using only $\mathbf{h}_a$.** This figure shows a computation carried out using the same setup of Figure 4.6, but this time, with the definition $\mathbf{h} := \mathbf{h}_a$ for the effective magnetizing field (at discrete level we use (4.48)), which ignores completely the effects of the demagnetizing field $\mathbf{h}_d$. Clearly the evolution of the phase variable is totally different to that one of Figure 4.6, and there is no manifestation of the Rosensweig instability (there is no Hedgehog). The final configuration adopted by the system does not even resemble what would hapen in a real life experiment (see for instance Figures 4.8 and 4.9).

Figure 4.8: **Real experiment of a ferrofluid subject to a non-uniform magnetic field**. Courtesy (reproduced with permission, see Appendix) of [140].

Figure 4.9: **Another real experiment of a ferrofluid subject to a non-uniform magnetic field**. Courtesy of [140].

4.7 Conclusions

In this chapter we proposed a simple PDE model describing the behavior of two-phase ferrofluid flows. The model was assembled by choosing components from the one-phase Shliomis model of ferrofluids, simplified magnetostatics, and well-known assumptions and simplifications from phase-field techniques. The model satisfies a formal energy law and we were able to devise a numerical scheme that mimics it. The use of a discontinuous finite element space for the magnetization $\mathbf{M}^k$ seems to be mandatory if we want to have a discrete energy law, hence, numerical stability. We were also able to prove that the scheme always has a solution.

We also presented a simplified version of this model, which has a somewhat more restrictive scope of physical validity, its use would be primarily oriented to ferrofluids with small magnetic susceptibilities, such as those found in biomedical applications. For this simplified model we were able to develop a convergent numerical scheme. Convergence of the scheme relies on classical compactness arguments. The fact that the limits for $h, \tau \longrightarrow 0$ are weak solutions of (4.46) (consistency in the limit) required a special choice of finite element spaces, requiring in particular the use of discontinuous pressures.

We showed a series of numerical experiments which illustrate the robustness of the numerical schemes, the potential of these models, and their ability to capture basic phenomenological features of ferrofluids. In particular, we showed the ability of the model in the context of the classical Rosensweig instability (uniform magnetic fields), and the more common case of the Rosensweig instability (using non-uniform

magnetic field) when the ferrofluid forms and open pattern of spikes (hedgehog-like). We also carried out a simulation using the definition $\mathbf{h} := \mathbf{h}_a$ for the effective magnetizing field which ignores completely the effects of the demagnetizing field $\mathbf{h}_d$. This simulation highlights the importance of using a physically reasonable (sensible) approximation to the exact demagnetizing field.

Finally, we must comment that many important issues were not discussed. Among them we have to mention how to regularize the model (4.13) (laying the path to a successful global existence theory) is very much an open problem, how to actually solve the system posed by the numerical schemes proposed in this work, modeling of saturation effects (which is an important physical feature of ferrofluids), and the derivation of energy-variational ferrofluid models.

Appendix : Reproduction Authorizations

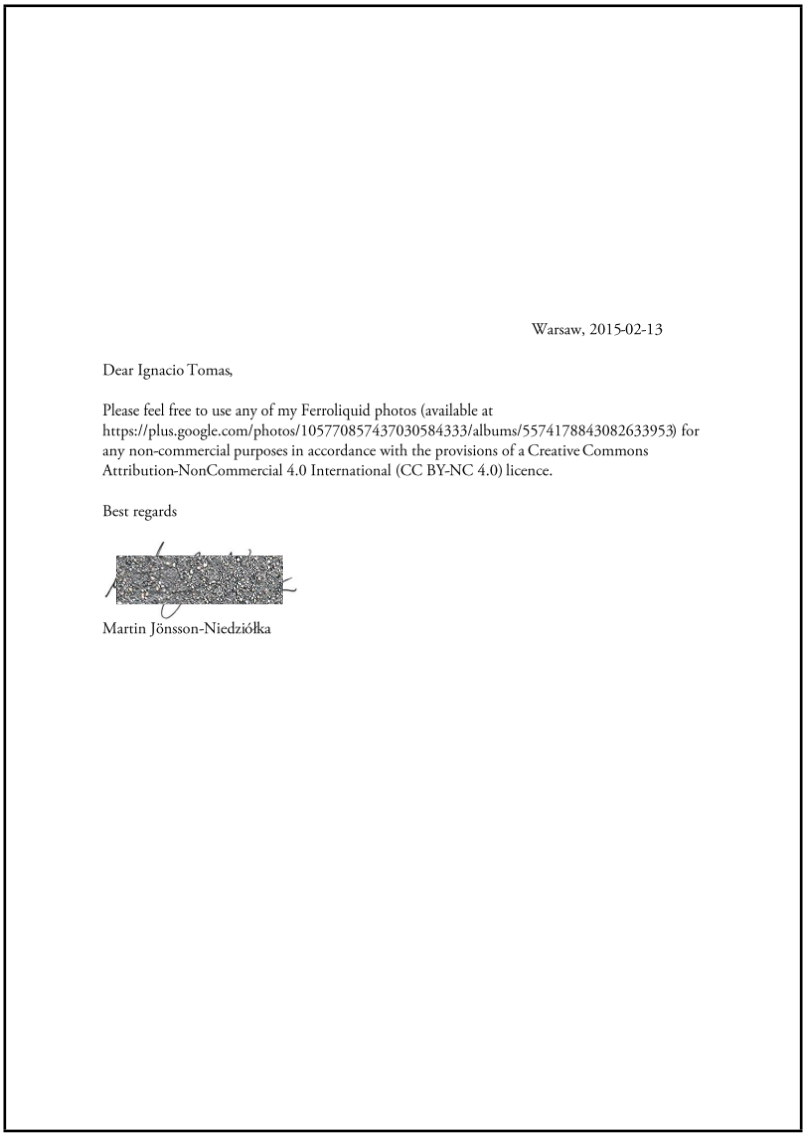

Warsaw, 2015-02-13

Dear Ignacio Tomas,

Please feel free to use any of my Ferroliquid photos (available at https://plus.google.com/photos/105770857437030584333/albums/5574178843082633953) for any non-commercial purposes in accordance with the provisions of a Creative Commons Attribution-NonCommercial 4.0 International (CC BY-NC 4.0) licence.

Best regards

Martin Jönsson-Niedziółka

Bibliography

[1] S. Behrens and H. Bonemann. Synthesis and characterization. In Stefan Odenbach, editor, *Colloidal Magnetic Fluids. Basics, Development and Application of Ferrofluids.*, Lecture Notes in Physics, pages 1–69. Springer-Verlag, 2009.

[2] Papell Solomon Stephen. Low viscosity magnetic fluid obtained by the colloidal suspension of magnetic particles, November 2 1965. US Patent 3,215,572.

[3] M. Miwa, H. Harita, T. Nishigami, R. Kaneko, and H. Unozawa. Frequency characteristics of stiffness and damping effect of a ferrofluid bearing. *Tribology Letters*, 15(2):97–105, 2003.

[4] K. Raj, B. Moskowitz, and R. Casciari. Advances in ferrofluid technology. *Journal of Magnetism and Magnetic Materials*, 149(12):174 – 180, 1995. Proceedings of the Seventh International Conference on Magnetic Fluids.

[5] K. J. Vinoy and R. M. Jha. *Radar Absorbing Materials: From Theory to Design and Characterization*. Springer, Kluwer Academic Publishers, 2011.

[6] Yuichi Shibata, Taiga Takamine, and Masahiro Kawaji. Emission of liquid droplets from an interface of bidrops pulled by a ferrofluid in a microchannel. *International Journal of Thermal Sciences*, 50(3):233 – 238, 2011.

[7] Herb Hartshorne, Christopher J Backhouse, and William E Lee. Ferrofluid-based microchip pump and valve. *Sensors and Actuators B: Chemical*, 99(23):592 – 600, 2004.

[8] C. Yamahata, M. Chastellain, V.K. Parashar, A. Petri, H. Hofmann, and M. A M Gijs. Plastic micropump with ferrofluidic actuation. *Microelectromechanical Systems, Journal of*, 14(1):96–102, 2005.

[9] Markus Zahn. Magnetic fluid and nanoparticle applications to nanotechnology. *Journal of Nanoparticle Research*, (3):73 – 78, 2001.

[10] Jian Zeng, Yanxiang Deng, Pallavi Vedantam, Tzuen-Rong Tzeng, and Xiangchun Xuan. Magnetic separation of particles and cells in ferrofluid flow through a straight microchannel using two offset magnets. *Journal of Magnetism and Magnetic Materials*, 346(0):118 – 123, 2013.

[11] Magda Latorre and Carlos Rinaldi. Applications of magnetic nanoparticles in medicine: magnetic fluid hyperthermia. *PR Health Sciences Journal*, 28(3), 2009.

[12] Q. Q. A. Pankhurst, J. Connolly, S. K. Jones, and J. Dobson. Applications of magnetic nanoparticles in biomedicine. (36):R167–R181, 2003.

[13] A. Sarwar, R. Lee, D.A. Depireux, and B. Shapiro. Magnetic injection of nanoparticles into rat inner ears at a human head working distance. *Magnetics, IEEE Transactions on*, 49(1):440–452, 2013.

[14] Phil R. Laird, Ermanno F. Borra, Rosangela Bergamasco, Julie Gingras, Long Truong, and Anna Ritcey. Deformable mirrors based on magnetic liquids. *Proc. SPIE*, 5490:1493–1501, 2004.

[15] P. Laird, N. Caron, M. Rioux, E. F. Borra, and A. Ritcey. Ferrofluidic adaptive mirrors. *Appl. Opt.*, 45(15):3495–3500, May 2006.

[16] Denis Brousseau, Ermanno F. Borra, and Simon Thibault. Wavefront correction with a 37-actuator ferrofluid deformable mirror. *Opt. Express*, 15(26):18190–18199, Dec 2007.

[17] Ronald E. Rosensweig. *Ferrohydrodynamics*. Dover Publications, 1997.

[18] Mark I. Shliomis. Ferrohydrodynamics: Retrospective and issues. In Stefan Odenbach, editor, *Ferrofluids: Magnetically controllable fluids and their applications*, Lecture Notes in Physics, pages 85–111. Springer-Verlag, 2002.

[19] Youcef Amirat and Kamel Hamdache. Global weak solutions to a ferrofluid flow model. *Math. Methods Appl. Sci.*, 31(2):123–151, 2008.

[20] Youcef Amirat and Kamel Hamdache. Strong solutions to the equations of a ferrofluid flow model. *J. Math. Anal. Appl.*, 353(1):271–294, 2009.

[21] Youcef Amirat and Kamel Hamdache. Unique solvability of equations of motion for ferrofluids. *Nonlinear Anal.*, 73(2):471–494, 2010.

[22] Youcef Amirat, Kamel Hamdache, and François Murat. Global weak solutions to equations of motion for magnetic fluids. *J. Math. Fluid Mech.*, 10(3):326–351, 2008.

[23] Stefan Odenbach, editor. *Ferrofluids: Magnetically Controllable Fluids and Their Applications (Lecture Notes in Physics)*. Springer, 2002.

[24] Stefan Odenbach, editor. *Colloidal Magnetic Fluids: Basics, Development and Application of Ferrofluids (Lecture Notes in Physics)*. Springer, 2009.

[25] Carlos Rinaldi and Markus Zahn. Effects of spin viscosity on ferrofluid flow profiles in alternating and rotating magnetic fields. *Physics of Fluids*, 14(8):2847–2870, 2002.

[26] Markus Zahn and Donald R. Greer. Ferrohydrodynamic pumping in spatially uniform sinusoidally time-varying magnetic fields. *Journal of Magnetism and Magnetic Materials*, 149(12):165 – 173, 1995.

[27] Arlex Chaves, Markus Zahn, and Carlos Rinaldi. Spin-up flow of ferrofluids: Asymptotic theory and experimental measurements. *Physics of Fluids*, 20(5), 2008.

[28] J. S. Dahler and L. E. Scriven. Angular momentum of continua. *Nature*, 192:36–37, 1961.

[29] J. S. Dahler and L. E. Scriven. Theory of structured continua. I. General consideration of angular momentum and polarization. *Proc. Roy. Soc.*, vol. 275 no. 1363:504–527, 1963.

[30] A. Cemal Eringen. Theory of micropolar fluids. *J. Math. Mech.*, 16:1–18, 1966.

[31] A. Cemal Eringen. *Microcontinuum field theories. I. Foundations and solids*. Springer-Verlag, New York, 1999.

[32] A. Cemal Eringen. *Microcontinuum field theories. II. Fluent Media*. Springer-Verlag, New York, 2001.

[33] A.C. Eringen and G.A. Maugin. *Electrodynamics of Continua: Foundations and solid media*. Electrodynamics of Continua. Springer-Verlag, 1990.

[34] A.C. Eringen and G.A. Maugin. *Electrodynamics of Continua II: Fluids and Complex Media*. Electrodynamics of Continua. Springer New York, 2011.

[35] Ronald E. Rosensweig. Stress boundary-conditions in ferrohydrodynamics. *Industrial & Engineering Chemistry Research*, 46(19):6113–6117, 2007.

[36] Arlex Chaves and Carlos Rinaldi. Interfacial stress balances in structured continua and free surface flows in ferrofluids. *Physics of Fluids (1994-present)*, 26(4), 2014.

[37] C. Liu. An introduction of elastic complex fluids: an energetic variational approach. In *Multi-scale phenomena in complex fluids*, volume 12 of *Ser. Contemp. Appl. Math. CAM*, pages 286–337. World Sci. Publishing, Singapore, 2009.

[38] Huan Sun and Chun Liu. On energetic variational approaches in modeling the nematic liquid crystal flows. *Discrete Contin. Dyn. Syst.*, 23(1-2):455–475, 2009.

[39] Yunkyong Hyon, Do Young Kwak, and Chun Liu. Energetic variational approach in complex fluids: maximum dissipation principle. *Discrete Contin. Dyn. Syst.*, 26(4):1291–1304, 2010.

[40] Helmut Abels, Harald Garcke, and Günther Grün. Thermodynamically consistent, frame indifferent diffuse interface models for incompressible two-phase flows with different densities. *Math. Models Methods Appl. Sci.*, 22(3):1150013, 40, 2012.

[41] Ricardo H. Nochetto, Abner J. Salgado, and Shawn W. Walker. A diffuse interface model for electrowetting with moving contact lines. *Mathematical Models and Methods in Applied Sciences*, 24(01):67–111, 2014.

[42] Vivette Girault and Pierre-Arnaud Raviart. *Finite element methods for Navier-Stokes equations*, volume 5 of *Springer Series in Computational Mathematics*. Springer-Verlag, Berlin, 1986. Theory and algorithms.

[43] Roger Temam. *Navier-Stokes equations*, volume 2 of *Studies in Mathematics and its Applications*. North-Holland Publishing Co., Amsterdam, third edition, 1984. Theory and numerical analysis, With an appendix by F. Thomasset.

[44] Daniele Boffi, Franco Brezzi, and Michel Fortin. *Mixed finite element methods and applications*, volume 44 of *Springer Series in Computational Mathematics*. Springer, Heidelberg, 2013.

[45] Martine Marion and Roger Temam. Navier-Stokes equations: theory and approximation. In *Handbook of numerical analysis, Vol. VI*, Handb. Numer. Anal., VI, pages 503–688. North-Holland, Amsterdam, 1998.

[46] J.-L. Lions. *Quelques méthodes de résolution des problèmes aux limites non linéaires*. Dunod; Gauthier-Villars, Paris, 1969.

[47] Luc Tartar. *An introduction to Navier-Stokes equation and oceanography*, volume 1 of *Lecture Notes of the Unione Matematica Italiana*. Springer-Verlag, Berlin; UMI, Bologna, 2006.

[48] Franck Boyer and Pierre Fabrie. *Mathematical tools for the study of the incompressible Navier-Stokes equations and related models*, volume 183 of *Applied Mathematical Sciences*. Springer, New York, 2013.

[49] Vidar Thomée. *Galerkin finite element methods for parabolic problems*, volume 25 of *Springer Series in Computational Mathematics*. Springer-Verlag, Berlin, second edition, 2006.

[50] John G. Heywood and Rolf Rannacher. Finite-element approximation of the nonstationary Navier-Stokes problem. IV. Error analysis for second-order time discretization. *SIAM J. Numer. Anal.*, 27(2):353–384, 1990.

[51] Susanne C. Brenner and L. Ridgway Scott. *The mathematical theory of finite element methods*, volume 15 of *Texts in Applied Mathematics*. Springer-Verlag, New York, 1994.

[52] Philippe G. Ciarlet. *The finite element method for elliptic problems*. North-Holland Publishing Co., Amsterdam-New York-Oxford, 1978. Studies in Mathematics and its Applications, Vol. 4.

[53] Alexandre Ern and Jean-Luc Guermond. *Theory and practice of finite elements*, volume 159 of *Applied Mathematical Sciences*. Springer-Verlag, New York, 2004.

[54] J.-L. Guermond and L. Quartapelle. On the approximation of the unsteady Navier-Stokes equations by finite element projection methods. *Numer. Math.*, 80(2):207–238, 1998.

[55] Ricardo G. Durán and Ricardo H. Nochetto. Weighted inf-sup condition and pointwise error estimates for the Stokes problem. *Math. Comp.*, 54(189):63–79, 1990.

[56] V. Girault and L. R. Scott. A quasi-local interpolation operator preserving the discrete divergence. *Calcolo*, 40(1):1–19, 2003.

[57] Johnny Guzman, AbnerJ. Salgado, and Francisco-Javier Sayas. A note on the Ladyženskaja-Babuška-Brezzi condition. *Journal of Scientific Computing*, 56(2):219–229, 2013.

[58] V. Girault, R. H. Nochetto, and R. Scott. Maximum-norm stability of the finite element Stokes projection. *J. Math. Pures Appl. (9)*, 84(3):279–330, 2005.

[59] J. Guzmán and D. Leykekhman. Pointwise error estimates of finite element approximations to the Stokes problem on convex polyhedra. *Math. Comp.*, 81(280):1879–1902, 2012.

[60] Alan Demlow and Stig Larsson. Local pointwise a posteriori gradient error bounds for the Stokes equations. *Math. Comp.*, 82(282):625–649, 2013.

[61] Johnny Guzmn and ManuelA. Snchez. Max-norm stability of low order taylorhood elements in three dimensions. *Journal of Scientific Computing*, pages 1–24, 2015.

[62] Grzegorz Łukaszewicz. *Micropolar fluids*. Modeling and Simulation in Science, Engineering and Technology. Birkhäuser Boston Inc., Boston, MA, 1999. Theory and applications.

[63] Namiko Mitarai, Hisao Hayakawa, and Hiizu Nakanishi. Collisional granular flow as a micropolar fluid. *Phys. Rev. Lett.*, 88:174301, Apr 2002.

[64] Ian Papautsky, John Brazzle, Timothy Ameel, and A.Bruno Frazier. Laminar fluid behavior in microchannels using micropolar fluid theory. *Sensors and Actuators A: Physical*, 73(12):101 – 108, 1999.

[65] Leidong Mao and Hur Koser. Ferrohydrodynamic pumping in spatially traveling sinusoidally time-varying magnetic fields. *Journal of Magnetism and Magnetic Materials*, 289:199 – 202, 2005. Proceedings of the 10th International Conference on Magnetic Fluids.

[66] Ricardo G. Durán and Maria Amelia Muschietti. An explicit right inverse of the divergence operator which is continuous in weighted norms. *Studia Math.*, 148(3):207–219, 2001.

[67] Elva Ortega-Torres and Marko Rojas-Medar. Optimal error estimate of the penalty finite element method for the micropolar fluid equations. *Numerical Functional Analysis and Optimization*, 29(5-6):612–637, 2008.

[68] Howard C. Elman, David J. Silvester, and Andrew J. Wathen. *Finite elements and fast iterative solvers: with applications in incompressible fluid dynamics*. Numerical Mathematics and Scientific Computation. Oxford University Press, New York, 2005.

[69] J.-L. Guermond and A.J. Salgado. Error analysis of a fractional time-stepping technique for incompressible flows with variable density. *SIAM J. Numer. Anal.*, 49(3):917–944, 2011.

[70] W. Bangerth, R. Hartmann, and G. Kanschat. deal.II – a general purpose object oriented finite element library. *ACM Trans. Math. Softw.*, 33(4):24/1–24/27, 2007.

[71] W. Bangerth, T. Heister, and G. Kanschat. `deal.II` *Differential Equations Analysis Library, Technical Reference*. `http://www.dealii.org`.

[72] Ronald E. Rosensweig. Basic equations for magnetic fluids with internal rotations. In Stefan Odenbach, editor, *Ferrofluids: Magnetically controllable fluids and their applications*, Lecture Notes in Physics, pages 61–84. Springer-Verlag, 2002.

[73] Carlos Rinaldi. Personal communication. 2013.

[74] J.D. Jackson. *Classical Electrodynamics*. Wiley, 1998.

[75] C.M.R.R. Rinaldi. *Continuum Modeling of Polarizable Systems*. PhD thesis, Massachusetts Institute of Technology, Department of Chemical Engineering, June 2002.

[76] Giorgio Bertotti, Isaak D. Mayergoyz, and Claudio Serpico. *Nonlinear magnetization dynamics in nanosystems*. Elsevier Series in Electromagnetism. Elsevier B. V., Amsterdam, 2009.

[77] T.R. Koehler. Hybrid fem-bem method for fast micromagnetic calculations. *Physica B: Condensed Matter*, 233(4):302 – 307, 1997.

[78] Sören Bartels, Mario Bebendorf, and Michael Bratsch. A fast and accurate numerical method for the computation of unstable micromagnetic configurations. In Michael Griebel, editor, *Singular Phenomena and Scaling in Mathematical Models*, pages 413–434. Springer International Publishing, 2014.

[79] L'ubomír Baňas, Sören Bartels, and Andreas Prohl. A convergent implicit finite element discretization of the Maxwell-Landau-Lifshitz-Gilbert equation. *SIAM J. Numer. Anal.*, 46(3):1399–1422, 2008.

[80] Alain Bossavit. *Computational electromagnetism*. Electromagnetism. Academic Press Inc., San Diego, CA, 1998.

[81] Jacques Rappaz and Rachid Touzani. *Mathematical and numerical models for eddy currents and magnetostatics: with selected applications*. Scientific Computation. Springer, Dordrecht, 2013.

[82] P. P. Silvester and R. L. Ferrari. *Finite Elements for Electrical Engineers*. Springer, Kluwer Academic Publishers, 2011.

[83] Pekka Neittaanmäki, A Savini, and M Rudnicki. *Inverse problems and optimal design in electricity and magnetism*. Clarendon press, 1996.

[84] Douglas N. Arnold, Richard S. Falk, and Ragnar Winther. Finite element exterior calculus: from Hodge theory to numerical stability. *Bull. Amer. Math. Soc. (N.S.)*, 47(2):281–354, 2010.

[85] S. Venkatasubramanian and P. N. Kaloni. Stability and uniqueness of magnetic fluid motions. *R. Soc. Lond. Proc. Ser. A Math. Phys. Eng. Sci.*, 458(2021):1189–1204, 2002.

[86] R.H. Nochetto, A.J. Salgado, and I. Tomas. The micropolar Navier-Stokes equations: *a priori* error analysis. *Math. Models Methods Appl. Sci.*, 24(7):1237–1264, 2014.

[87] Daniele A. Di Pietro and Alexandre Ern. Discrete functional analysis tools for discontinuous Galerkin methods with application to the incompressible Navier-Stokes equations. *Math. Comp.*, 79(271):1303–1330, 2010.

[88] D.A. Di Pietro and A. Ern. *Mathematical Aspects of Discontinuous Galerkin Methods*. Mathematiques Et Applications. Springer, 2012.

[89] Vivette Girault, Béatrice Rivière, and Mary F. Wheeler. A discontinuous Galerkin method with nonoverlapping domain decomposition for the Stokes and Navier-Stokes problems. *Math. Comp.*, 74(249):53–84 (electronic), 2005.

[90] P. Lasaint and P.-A. Raviart. On a finite element method for solving the neutron transport equation. In *Mathematical aspects of finite elements in partial differential equations (Proc. Sympos., Math. Res. Center, Univ. Wisconsin, Madison, Wis., 1974)*, pages 89–123. Publication No. 33. Math. Res. Center, Univ. of Wisconsin-Madison, Academic Press, New York, 1974.

[91] A.J. Salgado. Convergence analysis of fractional time-stepping techniques for incompressible fluids with microstructure. *J. Sci. Comp.*, 2014. DOI 10.1007/s10915-014-9926-x.

[92] Chun Liu and Jie Shen. A phase field model for the mixture of two incompressible fluids and its approximation by a Fourier-spectral method. *Phys. D*, 179(3-4):211–228, 2003.

[93] Ping Lin, Chun Liu, and Hui Zhang. An energy law preserving C^0 finite element scheme for simulating the kinematic effects in liquid crystal dynamics. *J. Comput. Phys.*, 227(2):1411–1427, 2007.

[94] David Gilbarg and Neil S. Trudinger. *Elliptic partial differential equations of second order*. Classics in Mathematics. Springer-Verlag, Berlin, 2001. Reprint of the 1998 edition.

[95] Y. Bao, A. B. Pakhomov, and Kannan M. Krishnan. Brownian magnetic relaxation of water-based cobalt nanoparticle ferrofluids. *Journal of Applied Physics*, 99(8), 2006.

[96] Ferrotec. https://www.ferrotec.com/products/ferrofluid/emg/water/, 2014.

[97] Sunil, Prakash Chand, and Pavan Kumar Bharti. Double-diffusive convection in a micropolar ferromagnetic fluid. *Applied Mathematics and Computation*, 189(2):1648 – 1661, 2007.

[98] O Lavrova, G Matthies, T Mitkova, V Polevikov, and L Tobiska. Numerical treatment of free surface problems in ferrohydrodynamics. *Journal of Physics: Condensed Matter*, 18(38):S2657, 2006.

[99] James H. Bramble, Joseph E. Pasciak, and Olaf Steinbach. On the stability of the L^2 projection in $H^1(\Omega)$. *Math. Comp.*, 71(237):147–156 (electronic), 2002.

[100] M. Crouzeix and V. Thomée. The stability in L_p and W_p^1 of the L_2-projection onto finite element function spaces. *Math. Comp.*, 48(178):521–532, 1987.

[101] R.E. Bank and H. Yserentant. On the H^1-stability of the L_2-projection onto finite element spaces. *Numer. Math.*, 126(2):361–381, 2014.

[102] Xiaobing Feng. Fully discrete finite element approximations of the Navier-Stokes-Cahn-Hilliard diffuse interface model for two-phase fluid flows. *SIAM J. Numer. Anal.*, 44(3):1049–1072 (electronic), 2006.

[103] G. Grün. On convergent schemes for diffuse interface models for two-phase flow of incompressible fluids with general mass densities. *SIAM Journal on Numerical Analysis*, 51(6):3036–3061, 2013.

[104] Noel J. Walkington. Convergence of the discontinuous Galerkin method for discontinuous solutions. *SIAM J. Numer. Anal.*, 42(5):1801–1817 (electronic), 2005.

[105] Chun Liu and Noel J. Walkington. Convergence of numerical approximations of the incompressible Navier-Stokes equations with variable density and viscosity. *SIAM J. Numer. Anal.*, 45(3):1287–1304 (electronic), 2007.

[106] Leidong Mao, Shihab Elborai, Xiaowei He, Markus Zahn, and Hur Koser. Direct observation of closed-loop ferrohydrodynamic pumping under traveling magnetic fields. *Phys. Rev. B*, 84:104431, September 2011.

[107] C.J. Crowley and W.D. Stacy. Magnetic pump for ferrofluids, February 28 1989. US Patent 4,808,079.

[108] Seck Hoe Wong, Patrick Bryant, Michael Ward, and Christopher Wharton. Investigation of mixing in a cross-shaped micromixer with static mixing elements for reaction kinetics studies. *Sensors and Actuators B: Chemical*, 95(1–3):414 – 424, 2003.

[109] Jongkwang Lee and Sejin Kwon. Mixing efficiency of a multilamination micromixer with consecutive recirculation zones. *Chemical Engineering Science*, 64(6):1223 – 1231, 2009.

[110] Ying Lin, Xinhai Yu, Zhenyu Wang, Shan-Tung Tu, and Zhengdong Wang. Design and evaluation of an easily fabricated micromixer with three-dimensional periodic perturbation. *Chemical Engineering Journal*, 171(1):291 – 300, 2011.

[111] L.M. Fu, C.H. Tsai, K.P. Leong, and C.Y. Wen. Rapid micromixer via ferrofluids. *Physics Procedia*, 9(0):270 – 273, 2010. 12th International Conference on Magnetic Fluids (ICMF12).

[112] Tsung-Han Tsai, Dar-Sun Liou, Long-Sheng Kuo, and Ping-Hei Chen. Rapid mixing between ferro-nanofluid and water in a semi-active y-type micromixer. *Sensors and Actuators A: Physical*, 153(2):267 – 273, 2009.

[113] Christian Gollwitzer, Gunar Matthies, Reinard Richter, Ingo Rehberg, and Lutz Tobiska. The surface topography of a magnetic fluid: a quantitative comparison between experiment and numerical simulation. *Journal of Fluid Mechanics*, 571:455–474, 1 2007.

[114] Olga Lavrova, Gunar Matthies, and Lutz Tobiska. Numerical study of soliton-like surface configurations on a magnetic fluid layer in the Rosensweig instability. *Communications in Nonlinear Science and Numerical Simulation*, 13(7):1302 – 1310, 2008.

[115] Jing Liu, Say-Hwa Tan, YitFatt Yap, MinYuan Ng, and Nam-Trung Nguyen. Numerical and experimental investigations of the formation process of ferrofluid droplets. *Microfluidics and Nanofluidics*, 11(2):177–187, 2011.

[116] S. Afkhami, Y. Renardy, M. Renardy, J. S. Riffle, and T. St Pierre. Field-induced motion of ferrofluid droplets through immiscible viscous media. *Journal of Fluid Mechanics*, 610:363–380, 9 2008.

[117] S. Afkhami, A. J. Tyler, Y. Renardy, M. Renardy, T. G. St. Pierre, R. C. Woodward, and J. S. Riffle. Deformation of a hydrophobic ferrofluid droplet suspended in a viscous medium under uniform magnetic fields. *Journal of Fluid Mechanics*, 663:358–384, 11 2010.

[118] André M. Sonnet and Epifanio G. Virga. *Dissipative ordered fluids*. Springer, New York, 2012. Theories for liquid crystals.

[119] Yanjin Wang and Zhong Tan. Global existence and asymptotic analysis of weak solutions to the equations of ferrohydrodynamics. *Nonlinear Anal. Real World Appl.*, 11(5):4254–4268, 2010.

[120] Fang-Hua Lin and Chun Liu. Nonparabolic dissipative systems modeling the flow of liquid crystals. *Comm. Pure Appl. Math.*, 48(5):501–537, 1995.

[121] D. M. Anderson, G. B. McFadden, and A. A. Wheeler. Diffuse-interface methods in fluid mechanics. In *Annual review of fluid mechanics, Vol. 30*, volume 30 of *Annu. Rev. Fluid Mech.*, pages 139–165. Annual Reviews, Palo Alto, CA, 1998.

[122] J. Lowengrub and L. Truskinovsky. Quasi-incompressible Cahn-Hilliard fluids and topological transitions. *R. Soc. Lond. Proc. Ser. A Math. Phys. Eng. Sci.*, 454(1978):2617–2654, 1998.

[123] Jie Shen and Xiaofeng Yang. Energy stable schemes for Cahn-Hilliard phase-field model of two-phase incompressible flows. *Chinese Annals of Mathematics, Series B*, 31(5):743–758, 2010.

[124] Jie Shen. Modeling and numerical approximation of two-phase incompressible flows by a phase-field approach. In *Multiscale modeling and analysis for materials simulation*, volume 22 of *Lect. Notes Ser. Inst. Math. Sci. Natl. Univ. Singap.*, pages 147–195. World Sci. Publ., Hackensack, NJ, 2012.

[125] Claes Johnson. *Numerical solution of partial differential equations by the finite element method*. Cambridge University Press, Cambridge, 1987.

[126] Giovanni Bellettini, Maurizio Paolini, and Claudio Verdi. Γ-convergence of discrete approximations to interfaces with prescribed mean curvature. *Atti Accad. Naz. Lincei Cl. Sci. Fis. Mat. Natur. Rend. Lincei (9) Mat. Appl.*, 1(4):317–328, 1990.

[127] C. M. Elliott and A. M. Stuart. The global dynamics of discrete semilinear parabolic equations. *SIAM J. Numer. Anal.*, 30(6):1622–1663, 1993.

[128] Andrea Braides and Nung Kwan Yip. A quantitative description of mesh dependence for the discretization of singularly perturbed nonconvex problems. *SIAM J. Numer. Anal.*, 50(4):1883–1898, 2012.

[129] Wolfgang Bangerth, Carsten Burstedde, Timo Heister, and Martin Kronbichler. Algorithms and data structures for massively parallel generic adaptive finite element codes. *ACM Trans. Math. Software*, 38(2):Art. 14, 28, 2011.

[130] Timo Heister. *A Massively Parallel Finite Element Framework with Application to Incompressible Flows*. PhD thesis, Georg-August-Universität at Göttingen, Mathematisch-Naturwissenschaftlichen Fakultäten, June 2011.

[131] D. W. Kelly, J. P. De S. R. Gago, O. C. Zienkiewicz, and I. Babuska. A posteriori error analysis and adaptive processes in the finite element method: Part ierror analysis. *International Journal for Numerical Methods in Engineering*, 19(11):1593–1619, 1983.

[132] Daniel Kessler, Ricardo H. Nochetto, and Alfred Schmidt. A posteriori error control for the allencahn problem: circumventing gronwall's inequality. *ESAIM: Mathematical Modelling and Numerical Analysis*, 38:129–142, 1 2004.

[133] Sören Bartels and Rüdiger Müller. A posteriori error controlled local resolution of evolving interfaces for generalized cahn–hilliard equations. *Interfaces and Free Boundaries*, 12(1):45–74, 2010.

[134] M. D. Cowley and R. E. Rosensweig. The interfacial stability of a ferromagnetic fluid. *Journal of Fluid Mechanics*, 30:671–688, 12 1967.

[135] A. Gailitis. Formation of the hexagonal pattern on the surface of a ferromagnetic fluid in an applied magnetic field. *Journal of Fluid Mechanics*, 82:401–413, 9 1977.

[136] René Friedrichs and Andreas Engel. Pattern and wave number selection in magnetic fluids. *Phys. Rev. E*, 64:021406, Jul 2001.

[137] Bérengère Abou, Jose-Eduardo Wesfreid, and Stéphane Roux. The normal field instability in ferrofluids: hexagonsquare transition mechanism and wavenumber selection. *Journal of Fluid Mechanics*, 416:217–237, 8 2000.

[138] David Jacqmin. Calculation of two-phase navierstokes flows using phase-field modeling. *Journal of Computational Physics*, 155(1):96 – 127, 1999.

[139] Chun Liu and Noel J. Walkington. An Eulerian description of fluids containing visco-elastic particles. *Arch. Ration. Mech. Anal.*, 159(3):229–252, 2001.

[140] Martin Jönsson-Niedziólka
. http://ekorrbilden.blogspot.com/2011/02/ferrofluid.html, 2011.